Modulation of basal ganglia local field potentials by deep brain stimulation in Parkinson's disease and dystonia



Christoph Wiest

Doctoral Thesis

Nuffield Department of Clinical Neurosciences

MRC Brain Network Dynamics Unit

University of Oxford & Wolfson College

December 2022

Word count: 57,944

i) Declaration

I, Christoph Wiest, confirm that the work presented in this thesis is my own. Where information has been derived from other sources, I confirm that this has been indicated in this thesis.

Signed: 

Date: 12 December 2022

ii) Abstract

Subthalamic (STN) deep brain stimulation (DBS) is an effective treatment option in advanced Parkinson's disease, however, its underlying mechanism remains largely speculative. Continuous DBS may come with side effects such as speech impairment, paraesthesia and mood changes, which necessitates research into adaptive DBS. Adaptive DBS requires feedback signals reflecting pathological activity to guide stimulation. Previous studies have focused on beta oscillations in the STN as a potential biomarker for parkinsonian symptoms and beta power suppression has been suggested as a potential action mechanism of DBS.

In this thesis, we sought to investigate mechanisms underlying STN stimulation beyond beta power suppression and studied other potential feedback markers to improve current frameworks of adaptive DBS.

In the first part, we performed local field potential (LFP) recordings from Parkinson's disease patients and studied evoked and induced changes with DBS. DBS-evoked resonant neural activity (ERNA) consists of a high-frequency, high-amplitude activity focal to dorsolateral STN that has fast and slow components. Furthermore, the ERNA is highly adjustable and varies with different DBS frequencies, intensities, medication states and stimulation modes. DBS also induced instantaneous power suppression in the beta and gamma frequency range and *de-novo* finely-tuned gamma (FTG) oscillations that are modulated during and after DBS.

In the second part, we demonstrate in rodent data that aperiodic exponents of subthalamic LFPs reflect excitatory and inhibitory input to STN and report higher aperiodic exponents ON levodopa and stimulation, in keeping with more inhibition. Subsequently, we found aperiodic exponent changes with levodopa and DBS in Parkinson's disease patients, consistent with more inhibition of STN when symptoms are alleviated.

In the third part, we recorded subthalamic and thalamic LFPs from cervical dystonia patients and found that neither ERNA, FTG, power suppression or aperiodic exponent changes with DBS are specific to Parkinson's disease.

Overall, this thesis extends the knowledge on existing feedback signals for adaptive DBS and supports the inactivation hypothesis of subthalamic DBS.

iii) Table of Contents

i) Declaration ii
ii) Abstract iii
iii) Table of Contents v
iv) List of Figures vi
v) List of Supplementary Figures viii
vi) List of Tables ix
vii) Acknowledgements x
viii) Abbreviations xi
ix) Publications included in this thesis xiv
1. General Introduction 1
2. Methods and Materials 49
3. Project 1: Local field potential activity dynamics in response to deep brain stimulation of the subthalamic nucleus in Parkinson's disease 62
4. Project 2: Evoked Resonant Neural Activity in subthalamic local field potentials reflects basal ganglia network dynamics 96
5. Project 3: Subthalamic deep brain stimulation induces finely-tuned gamma oscillations in the absence of levodopa 128
6. Project 4: Finely-tuned gamma oscillations: Spectral characteristics and links to dyskinesia 155
7. Project 5: The aperiodic exponent of subthalamic field potentials reflects excitation/inhibition balance in Parkinsonism: a cross-species study *in vivo* 177
8. Project 6: Subthalamic stimulation-induced local field potential changes in dystonia 202
9. General Discussion 224
10. References 237
11. Supplementary Figures and Tables 289

iv) List of Figures

Figure 1.1. Functional Connectivity of the BG Network. 13
Figure 1.2. Schematic of adaptive deep brain stimulation. 28
Figure 2.1. Recording Setup. 53
Figure 2.2. Saline Tank Recordings. 59
Figure 3.1. Stimulation settings and experimental conditions. 70
Figure 3.2. ERNA during long stimulation blocks (condition 1) characterised in the spectral domain. 76
Figure 3.3. ERNA during long stimulation blocks (condition 1) in the temporal domain. 78
Figure 3.4. ERNA after DBS. 80
Figure 3.5. Modulation of beta power induced by DBS. 82
Figure 3.6. DBS modulation of LFP in other frequency bands. 84
Figure 3.7. Modulation of HFO by DBS. 86
Figure 3.8. Clinical correlations. 87
Figure 4.1. Recording setup and experimental paradigm. 103
Figure 4.2. Time series and FFT-based ERNA represent the same activity. 105
Figure 4.3. ERNA dynamics are relatively slow. 109
Figure 4.4. Fast ERNA dynamics. 110
Figure 4.5. ERNA dynamics are modulated by different DBS frequencies. 112
Figure 4.6. ERNA dynamics are modulated by different DBS intensity. 114
Figure 4.7. ERNA dynamics are modulated by levodopa. 116
Figure 4.8. ERNA parameters differ between continuous and adaptive DBS. 117
Figure 4.9. ERNA as a feedback marker for aDBS. 127
Figure 5.1. Stimulation settings and experimental paradigm. 139
Figure 5.2. 130 Hz DBS induces finely-tuned gamma (FTG) oscillations in the absence of levodopa and dyskinesia. 141
Figure 5.3. FTG dynamics during DBS blocks. 144
Figure 5.4. FTG dynamics after DBS blocks. 147
Figure 5.5. Different DBS frequencies do not change FTG frequency. 148
Figure 5.6. FTG in short DBS blocks. 149
Figure 5.7. LFP-EEG coherence at FTG frequencies. 152
Figure 6.1. Comparison of different gamma rhythms. 158
Figure 6.2. Levodopa-induced finely-tuned gamma (FTG) oscillations are modulated by movement. 160
Figure 6.3. FTG as a feedback marker for aDBS. 176
Figure 7.1. Aperiodic exponents and power of STN-LFPs between 30 and 100 Hz reflect STN excitation and inhibition in lesioned animals. 190

Figure 7.2. Aperiodic exponents between 40-90 Hz of STN-LFPs distinguish medication states in externalised recordings from Parkinson's patients. 192
Figure 7.3. The aperiodic exponent between 10-50 Hz of STN-LFP distinguishes stimulation states in externalised recordings from PD patients. 194
Figure 7.4. Aperiodic Exponents as a feedback marker for aDBS. 201
Figure 8.1. Recording Setup. 206
Figure 8.2. Subthalamic and thalamic power spectra in dystonia. 210
Figure 8.3. DBS-induced power suppression in STN-LFPs of dystonic patients. 212
Figure 8.4. Evoked Resonant Neural Activity (ERNA) can be elicited by STN-DBS in dystonia. 214
Figure 8.5. Single pulse STN stimulation elicits Evoked Neural Activity (ENA). 216
Figure 8.6. DBS-induced finely-tuned gamma (FTG) oscillations occur in the STN of dystonic patients when stimulation is switched off. 218

v) List of Supplementary Figures

Figure 3.S1. STNs showing absence of an ERNA in response to 130 Hz stimulation in three cases. 289
Figure 3.S2. Comparison of spectral and time domain analysis in group data. 290
Figure 5.S1. Promotion of FTG during DBS is greater than the promotion of broadband gamma activity. 290
Figure 7.S1. Signal processing of the electrophysiological data recorded in animals. 291
Figure 7.S2. Sensitivity analysis of FoooF parameterisation. 292
Figure 7.S3. Spectral changes with levodopa and STN-DBS. 293
Figure 7.S4. Goodness of FoooF parameterisation. 294
Figure 7.S5. Knee parameterisation of animal data. 294
Figure 9.S1. ERNA fluctuations during steady state. 300
Figure 9.S2. ERNA is entrained when it crosses a harmonic of stimulation. 300

vi) List of Tables

Table 1.1. Other motor and non-motor features of PD. 8
Table 1.2. Potential DBS mechanisms. 25
Table 1.3. Beta as a feedback signal for aDBS. 47
Table 3.1. Patients clinical details. 66
Table 3.2. Patients surgical and recordings details. 68
Table 4.1. Clinical and recording details. 99
Table 4.2. ERNA as a feedback marker for aDBS. 126
Table 5.1. Patients clinical and recording details. 132
Table 5.2. Details of the finely-tuned gamma. 133
Table 6.1. FTG as a feedback marker for aDBS. 176
Table 7.1. Aperiodic Exponents as a feedback marker for aDBS. 201
Table 8.1. Clinical and recording details. 205
Table 6.S1. Levodopa-induced FTG in humans. 295
Table 6.S2. Levodopa-induced FTG in animal studies. 296
Table 6.S3. Comparison of different gamma activities. 296
Table 6.S4. DBS-induced FTG in humans. 297
Table 6.S5. Broad movement-related gamma ERS. 298
Table 9.S1. Advantages and disadvantages of biomarkers for aDBS. 299

vii) Acknowledgements

I would like to thank Huiling Tan, Andrew Sharott, Flavie Torrecillos and Peter Brown for bearing with me over the past three odd years and for being the best supervisors I could have wished for. I am incredibly grateful for the fast and high-quality feedback I received from you over the years. You taught me all I know about neural time series data analysis, local field potentials and the basal ganglia. The world needs more supervisors like you.

I am incredibly grateful for the friendly and constructive lab environment and want to thank Alek Pogosyan, Shenghong He and all other members of the Brown/Tan Lab over the past years. You consistently challenged me to be more meticulous and made my work better. This thesis would not be the same without you and I am proud to be part of the academic Brown/Tan family. My gratitude extends to the MRC BNDU, in which our lab was embedded. I fondly remember all the Unit Science Days and Trainings Events. From the first day in summer 2018 when I visited the unit you gave me the feeling of being accepted and at home.

I would like to thank all collaborators at St. George's University Hospital, London, King's College Hospital, London, University Medical Centre Mainz and University Medical Centre Cologne. Beyond this, I am grateful to all participants of the studies included in this thesis. We spent many hours during the recording sessions together and you really enabled this work.

My appreciation extends to Nuffield Department of Clinical Neurosciences, the University of Oxford, Wolfson College and my funding bodies. I am proud to graduate from this prestigious institution. Oxford will always stay my intellectual home.

Finally, I would never have been able to pursue research within this unique environment if my family had not supported me all the way through and thank you Rupi for your patience and encouragement.

viii) Abbreviations

aDBS	adaptive deep brain stimulation
ALIC	anterior limb of the internal capsule
BCI	brain computer interface
BG	basal ganglia
BNST	bed nucleus of stria terminalis
CBT	cognitive behavioural therapy
CD	cervical dystonia
cDBS	continuous/conventional deep brain stimulation
CSAI	continuous subcutaneous apomorphine infusion
DA	dopamine agonist
DBS	deep brain stimulation
ECoG	electrocorticography
EEG	electroencephalography
EMG	electromyography
ERD	event related desynchronisation
ERNA	evoked resonant neural activity
ERS	event related synchronisation
ET	essential tremor
FDA	Food and Drug Administration
FFT	Fast Fourier Transform
fMRI	functional magnetic resonance imaging
FTG	finely-tuned gamma
GABA	gamma aminobutyric acid
GPe	external globus pallidus

GPi	internal globus pallidus
HFO	high frequency oscillation
HFS	high frequency stimulation
ICD	impulse control disorder
ION	inferior olivary nucleus
IPG	internal pulse generator
IPSP	inhibitory postsynaptic potential
ITP	inferior thalamic peduncle
LCIG	levodopa-carbidopa intestinal gel infusion
LFP	local field potential
MER	microelectrode recording
MFB	medial forebrain bundle
MDD	major depressive disorder
MPTP	1-methyl-4-phenyl-1,2,3,6-tetrahydropyridine
MRI	magnetic resonance imaging
MRIgFUS	MRI-guided focused ultrasound
MSN	medium spiny neurons
MUA	multi unit activity
NAc	nucleus accumbens
NHP	non-human primate
OCD	obsessive compulsive disorder
PAC	phase amplitude coupling
PET	positron emission tomography
PSA	posterior subthalamic area
PD	Parkinson’s disease
SCC	subcallosal cingulate

SMA	supplementary motor area
SNc	substantia nigra pars compacta
SNr	substantia nigra pars reticulata
SSRI	selective serotonine reuptake inhibitor
STN	subthalamic nucleus
SUA	single unit activity
TACS	transcranial alternating current stimulation
VC	ventral capsule
VIM	ventral intermediate nucleus of the thalamus
VL	ventrolateral thalamus
VLp	posterior ventrolateral thalamus
VS	ventral striatum
ZI	zona incerta

ix) Publications included in this thesis

Wiest, C., Tinkhauser, G., Pogosyan, A., Bange, M., Muthuraman, M., Groppa, S., Baig, F., Mostofi, A., Pereira, E.A., Tan, H., Brown, P., Torrecillos, F., 2020. Local field potential activity dynamics in response to deep brain stimulation of the subthalamic nucleus in Parkinson's disease. Neurobiol. Dis. 143, 105019. https://doi.org/10.1016/j.nbd.2020.105019

Wiest, C., Tinkhauser, G., Pogosyan, A., He, S., Baig, F., Morgante, F., Mostofi, A., Pereira, E.A., Tan, H., Brown, P., Torrecillos, F., 2021. Subthalamic deep brain stimulation induces finely-tuned gamma oscillations in the absence of levodopa. Neurobiol. Dis. 152, 105287. https://doi.org/10.1016/j.nbd.2021.105287

Wiest, C., Torrecillos, F., Tinkhauser, G., Pogosyan, A., Morgante, F., Pereira, E.A., Tan, H., 2022. Finely-tuned gamma oscillations: Spectral characteristics and links to dyskinesia. Exp. Neurol. 351, 113999. https://doi.org/10.1016/j.expneurol.2022.113999

Wiest, C., He, S., Duchet, B., Pogosyan, A., Benjaber, M., Denison, T., Hasegawa, H., Ashkan, K., Baig, F., Bertaina, I., Morgante, F., Pereira, E.A., Torrecillos, F., Tan, H., 2023a. Evoked resonant neural activity in subthalamic local field potentials reflects basal ganglia network dynamics, Neurobiol. Dis. 106019. https://doi.org/10.1016/j.nbd.2023.106019

Wiest, C., Morgante, F., Torrecillos, F., Pogosyan, A., He, S., Baig, F., Bertaina, I., Hart, M.G., Edwards, M.J., Pereira, E.A., Tan, H., 2022. Subthalamic Nucleus Stimulation-Induced Local Field Potential Changes in Dystonia. Mov. Disord. https://doi.org/10.1002/mds.29302

Wiest, C., Torrecillos, F., Pogosyan, A., Bange, M., Muthuraman, M., Groppa, S., Hulse, N., Hasegawa, H., Ashkan, K., Baig, F., Morgante, F., Pereira, E.A., Mallet, N., Magill, P.J., Brown, P., Sharott, A., Tan, H., 2023b. The aperiodic exponent of subthalamic field potentials reflects excitation/inhibition balance in Parkinsonism. Elife 12, e82467. https://doi.org/10.7554.eLife.82467

Other publications during the PhD:

He, S., Deli, A., Fischer, P., Wiest, C., Huang, Y., Martin, S., Khawaldeh, S., Aziz, T.Z., Green, A.L., Brown, P., Tan, H., 2021. Gait-Phase Modulates Alpha and Beta Oscillations in the Pedunculopontine Nucleus. J. Neurosci. Off. J. Soc. Neurosci. 41, 8390–8402. https://doi.org/10.1523/JNEUROSCI.0770-21.2021

Kermen, F., Darnet, L., Wiest, C., Palumbo, F., Bechert, J., Uslu, O., Yaksi, E., 2020. Stimulus-specific behavioral responses of zebrafish to a large range of odors exhibit individual variability. BMC Biol. 18, 66. https://doi.org/10.1186/s12915-020-00801-8

1. General Introduction

1.1. History of deep brain stimulation (DBS) 2
1.2. Lesioning methods for movement disorders 3
1.3. DBS applications 5
1.3.1. DBS for Parkinson's disease 5
1.3.1.1. Epidemiology and aetiology 5
1.3.1.2. Motor symptoms 7
1.3.1.3. Non - motor symptoms 8
1.3.1.4. Pathophysiology 10
1.3.1.4.1. Cellular pathology 10
1.3.1.4.2. Basal ganglia networks 11
1.3.1.4.3. Network pathology 13
1.3.1.5. Pharmacological and advanced treatments 15
1.3.1.6. Role of DBS 16
1.3.2. DBS for Dystonia 18
1.3.2.1. Epidemiology, classification and pathogenesis 18
1.3.2.2. Clinical manifestations 19
1.3.2.3. Medical management 20
1.3.2.4. Role of DBS 21
1.4. Action mechanism of DBS 22
1.5. Closed-loop stimulation methods 27
1.5.1. Approaches to closed-loop neuromodulation 28
1.5.2. Feedback signals 30
1.5.2.1. Local field potentials 31
1.5.2.1.1. Beta oscillations 31
1.5.2.1.2. Gamma and high frequency oscillations (HFO) 34
1.5.2.1.3. Evoked resonant neural activity (ERNA) 35
1.5.2.1.4. Phase-amplitude coupling (PAC) 36
1.5.2.2. Cortical signals 38
1.5.2.3. Single- and multi-unit activity (SUA & MUA) 39
1.5.2.4. Peripheral signals 40
1.5.2.5. Non-electrical signals 40
1.5.3. Existing technology 41
1.5.4. Current limitations of closed-loop DBS 42
1.5.5. Machine-learning based stimulation paradigms 45
1.6. Thesis Roadmap 46

The overarching goal of this thesis was to explore mechanisms underlying deep brain stimulation (DBS) and to investigate candidate biomarkers for adaptive DBS (aDBS). To provide context, we will first introduce the history of DBS and lesioning methods that preceded modern DBS. Next we are going to elaborate on the two clinical conditions that were studied in this thesis: Parkinson's disease (PD) and dystonia. Towards the end of chapter 1, we will introduce common hypotheses on the action mechanism of DBS and the current state of adaptive DBS.

1.1. History of deep brain stimulation (DBS)

The birth of modern DBS is widely attributed to Alim-Louis Benabid in 1987. Benabid's group in Grenoble used thalamic DBS to alleviate medically-refractory tremor (Benabid et al., 1987), but the use of electricity in medicine goes back many centuries. In Greek medicine the torpedo fish (electric ray) was used to numb pain during childbirth and operations (Schwalb and Hamani, 2008). In the 18th century, Galvani discovered muscle contraction upon contact with electrical current (Bresadola, 2008). Over the following centuries, electrical stimulation further helped to map the brain. Gustav Fritsch and Eduard Hitzig stimulated the cerebral cortex in dogs and mapped motor functions (Kerr et al., 2005). David Ferrier localised hearing and visual attention in monkeys (Ferrier, 1874); Paul Broca mapped speech to brain regions (Broca, 1861). Roberts Barthelow performed the first parietal lobe stimulation in 1874 producing contralateral movements and seizures (Morgan, 1982) and Sir Victor Horsley started using cortical stimulation for functional mapping (Vilensky and Gilman, 2002).

Similarly, accidental or intentional lesion studies and animal experiments helped to link behaviours and tasks to specific brain regions. Phineas Gage displayed behavioural changes after a frontal lobe disconnection but miraculously survived his accident (Harlow, 1993). Russell Meyers found that basal ganglia lesions could effectively treat tremor, although this

was accompanied by high mortality rates (Meyers, 1942) and Irving Cooper noticed tremor release after ligation of the anterior choroidal artery with infarction of the neighbouring tissue (Cooper, 1953).

Functional neurosurgery became safer and more precise after stereotactic frames were introduced by Horsley and Clarke (Horsley and Clarke, 1908) and later refined by Ernest A. Spiegel and Henry T. Wycis (Spiegel et al., 1947) and Lars Leksell (Leksell, 1951). These frames allowed the precise targeting of brain regions using a three dimensional system of Cartesian coordinates. Apart from movement disorders, stereotactic surgery was performed in psychiatric patients. Leksell treated patients with obsessive compulsive disorder (OCD) using an anterior capsulotomy (Leksell and Backlund, 1978). Functional neurosurgery based on lesioning faced transient setbacks after the advent of levodopa (1968) and chlorpromazine (1950). However, best medical therapy was still proved inadequate in the long-run, and DBS underwent a renaissance under Benabid. In 1997, the US Food and Drug Administration (FDA) approved thalamic DBS for Essential Tremor (ET) and Parkinson's disease (PD) followed by pallidal and subthalamic nucleus (STN) DBS for PD in 2002. In 2003, DBS was approved for dystonia, in 2009 for OCD and in 2018 for epilepsy and so far ~160.000 patients with different indications have been treated with DBS (Lozano et al., 2019). While DBS is successful, in its fledgling stages it relied on a period of unrivalled empirical human experimentation with numerous unethical interventions (Oliveria, 2018).

1.2. Lesioning methods for movement disorders

The use of lesioning procedures dwindled after advances in DBS due to their irreversibility and generally more serious adverse effects, but still has its place in developing countries, or after recurrent infections of DBS systems. Lesioning procedures in PD and ET include thalamotomies, pallidotomies and subthalamotomies which may be conducted conventionally

(using stereotactic and electrophysiological techniques to locate the target and radiofrequency thermal ablation to create a lesion) or more recent procedures. The latter include MRI-guided focused ultrasound (MRIgFUS) which utilises high-energy ultrasound beams to generate thermal brain lesions. Although MRIgFUS does not require surgery, it constitutes an invasive and irreversible procedure causing a permanent lesion without the help of electrophysiological guidance (Ghanouni et al., 2015).

Conventional unilateral thalamotomies may control medication-resistant tremor in PD but do not help reduce bradykinesia, dyskinesia or motor fluctuations and have been largely replaced by DBS. In ET, unilateral thalamotomy reduces tremor severity in 80-90% of patients over the long-term but with transient side-effects in 14-47% of cases (Zesiewicz et al., 2005). Conventional unilateral pallidotomies may be effective for contralateral dopamine-related motor complications, improve all cardinal symptoms long-term and also partially improve ipsilateral symptoms (Lai et al., 2000; Vitek et al., 2003). However, 14% of patients report permanent adverse effects (4% infarction/haemorrhage, 1% mortality) and bilateral pallidotomies may cause permanent speech impairment (de Bie et al., 2002). Effectiveness of conventional unilateral subthalamotomies in PD has so far only been shown in uncontrolled and unblinded studies (Tarsy, 2009). Unilateral subthalamotomy is as effective as unilateral DBS (same for bilateral lesions and DBS) after 12 months (Merello et al., 2008) and unilateral subthalamotomy has similar clinical benefits as bilateral subthalamotomy but fewer adverse effects although it is predominantly unilateral in its benefits (Alvarez et al., 2009). Adverse effects of subthalamotomy are common and include transient or persistent dyskinesia in 58% of cases (Alvarez et al., 2009). MRIgFUS thalamotomy was FDA approved for tremor in PD in 2018, but treats only tremor and may only be performed unilaterally since bilateral application has a high risk of speech impairment. In ET, unilateral MRIgFUS thalamotomy was reported to display a gradual loss of efficacy (Louis, 2016).

Furthermore, Gamma Knife surgery may be used in the treatment of refractory movement disorders. It comprises stereotactic radiosurgery in the form of a single high radiation dose delivered to a highly focused MRI-defined target. 75-90% show clinical improvement (Zesiewicz et al., 2005), however, it appears delayed by weeks to months following the procedure (Niranjan et al., 2000). While it is incisionless, complications include delayed radiation side effects (e.g. necrosis), risk of secondary tumours, hemiparesis, facial sensory loss, and visual field cuts. Finally, laser interstitial thermal therapy (LITT) with MRI thermography allows to monitor thermal lesioning temperatures and temperatures in surrounding structures. However, in a study including two dystonic patients one participant experienced one-sided worsening of hypertonicity following LITT (Gross and Stern, 2018).

1.3. DBS applications

1.3.1. DBS for Parkinson's disease

1.3.1.1. Epidemiology and aetiology

James Parkinson first described parkinsonism in 'An Essay on the Shaking Palsy' in 1817 (Parkinson, 1817), however, there is evidence in the ancient Indian medical system, Ayurveda, of a disorder called 'kampavata' (kampa = shaking; vata = lack of muscular movement) (Manyam, 1990). Kampavata is responsive to the *Mucuna pruriens* plant which was later found to contain levodopa (Katzenschlager et al., 2004). PD is a progressive neurodegenerative disease and the fastest growing neurologic disorder mostly owing to an ageing society. Given the caveats of inconsistent diagnostic criteria and study populations, a meta-analysis of 47 studies reports a worldwide prevalence of 0.3% in the general population aged 40 or above (Pringsheim et al., 2014). The prevalence rises with age: 1% of people in their 60s and 3% in their 80s are affected (Tanner, 1992). Between 1990 and 2016 the global prevalence increased from 2.5 million to 6.1 million (GBD 2016 PD Collaborators, 2018) and a male preponderance

(3:2) is consistently reported. Several studies identified an inverse relationship between PD and cigarette smoking (Chen et al., 2010; Liu et al., 2012; Noyce et al., 2012). Less well examined protective factors include caffeine intake (Liu et al., 2012), physical activity (Logroscino et al., 2006), ibuprofen (Samii et al., 2009) and statins (Bai et al., 2016). A positive family history is considered an important risk factor for PD (Noyce et al., 2012). A number of reports debate depression and constipation as either risk factors or prodromal symptoms (Gustafsson et al., 2015; Noyce et al., 2012). Apart from this, pesticides (Ascherio et al., 2006), heavy metals (Willis et al., 2010), dairy products (Jiang et al., 2014) and in keeping with this farming and rural living have been considered possible risk factors. Suspicion that an environmental toxin might be important was increased when a commercially available chemical MPTP (1-methyl-4-phenyl-1,2,3,6-tetrahydropyridine) sold as synthetic heroin was self-injected by a college student (Davis et al., 1979) and IV drug abusers in California in 1983 (Langston et al., 1983). MPTP is oxidised to MPP+ after crossing the blood brain barrier and constitutes a potent neurotoxin for dopaminergic neurons (Langston et al., 1999). All subjects became profoundly parkinsonian after MPTP exposure which was later exploited in animal studies. Other risk factors include amongst others a history of traumatic brain injury (Jafari et al., 2013), vitamin D deficiency (Lv et al., 2014) and type 2 diabetes (De Pablo-Fernandez et al., 2018). Interestingly, mortality from PD increases with higher socioeconomic status. Literature reports substantial ethnic differences with lowest prevalence in Asia and Africa and highest levels in western Caucasians (Zhang and Román, 1993).

The cause of PD is yet unknown. In 1912 Frederick Lewy reported neuronal cytoplasmic inclusions in several brain regions. Seven years later Konstantin Tretiakoff described dopaminergic neuron loss in the substantia nigra pars compacta (SNc) as the most critical abnormality in PD. Eventually in the 1950s, the importance of dopamine depletion for basal ganglia function was uncovered (Hornykiewicz, 2006).

1.3.1.2. Motor symptoms

Idiopathic PD is diagnosed clinically by the cardinal symptoms of tremor, rigidity, bradykinesia and postural instability, and divided into three subtypes: tremor-dominant, akinetic-rigid and not-determined (mixed symptoms). Of these the tremor-dominant subtype is associated with slower progression and less neuropsychological impairment (Zetusky et al., 1985). Cardinal symptoms begin unilaterally and remain asymmetric throughout.

PD tremor is described as a pill-rolling rest tremor and can be present during postural manoeuvres but is usually more severe at rest. At first tremor is intermittent and is decreased with purposeful action which is why it is often the least disabling cardinal manifestation. Rest tremor accentuates with mental calculations, repetitive movements of the contralateral limb, anxiety, excitement and stress. PD tremor is low-frequency (3-7 Hz) (Findley et al., 1981), present in 70-80% of cases at disease onset (Hoehn and Yahr, 1967) and can involve legs, lips, jaw and tongue.

Bradykinesia, slowness of movement, is often considered the major cause of disability and present in 80% of PD patients at onset (Pagano et al., 2016). In the arms, it starts distally with decreased manual dexterity e.g. difficulty buttoning clothes, tying shoelaces, double clicking a computer mouse or lifting coins. In the legs, it presents as dragging of the foot, shorter steps, difficulty standing up, freezing of gait and festination. Rigidity, increased resistance to passive movements, is present in 75-90% of all PD patients (Hoehn and Yahr, 1967). It presents as cogwheel rigidity, a jerky pattern of resistance and relaxation (Deuschl et al., 1998), or in some cases as lead-pipe rigidity, a smooth tonic resistance. Moreover, rigidity manifests as decreased arm swing while walking, stooped posture and a striatal hand. Postural instability, the impairment of centrally mediated postural reflexes, becomes apparent during later stages of PD mostly as an increased tendency to fall. It is less responsive to dopaminergic therapies (Koller

et al., 1989), assessed using the pull-test and over time can render patients wheelchair-bound. Several further features of PD are summarised in **Table 1.1**.

Craniofacial	Visual	Musculoskeletal	Gait
hypomimia	blurred vision	micrographia	shuffling, short-stepped gait
decreased eye blinking	impaired contrast sensitivity	dystonia	freezing
speech disturbances (dysarthria, hypophonia)	hypometric saccades	myoclonus	festinations
dysphagia	impaired vestibuloocular reflex	stooped posture	
sialorrhea	lid apraxia	camptocormia	
		pisa syndrome	
		kyphosis	
		scoliosis	
		difficulty turning in bed	

Table 1.1. Other motor and non-motor features of PD

1.3.1.3. Non - motor symptoms

97% of PD patients report non-motor symptoms of which psychiatric symptoms are most common (Barone et al., 2009). Non-motor disorders may become more troublesome than cardinal symptoms and some such as olfactory dysfunction, depression, constipation and REM sleep behaviour disorder (RBD) may even present long before motor symptoms (Langston, 2006).

Cognitive dysfunction and dementia are prevalent in 41% of PD patients, increasing with age, severity of motor symptoms and presence of psychiatric disorders (Svenningsson et al., 2012). In PD, a subcortical dementia with psychomotor retardation, memory loss, altered personality and problems in executive function presents at later stages. In contrast, dementia with Lewy bodies (DLB) strikes primarily as dementia with parkinsonian features on the side. Neuropathologically, cortical Lewy bodies filled with alpha-synuclein coexist with amyloid plaques and neurofibrillary tangles. 20-40% of cases are diagnosed with psychotic symptoms

while visual hallucinations are most common and become more prevalent and severe over time (Fénelon et al., 2000). It is unclear if the underlying Lewy body disease or antiparkinsonian therapy, mostly dopamine agonists, cause hallucinations. Less common are paranoid delusions such as spousal infidelity or fantasies of theft and intruders. Mood disorders and above all depression (50% of cases) are highly prevalent. In addition, sadness and anhedonia are difficult to disentangle from bradykinesia. 30% PD cases display anxiety and social phobias which are associated with "on-off" fluctuations (Broen et al., 2016). Furthermore, apathy, loss of motivation, abulia, loss of impulse, and fatigue (33-58% (van Hilten et al., 1993)) are worth a note. Sleep disorders (55-80% (Tandberg et al., 1998)) such as insomnia, daytime sleep attacks, restless leg syndrome (RLS) and RBD are disabling symptoms. Insomnia can present as sleep fragmentation and early morning awaking which is in part due to nocturia, difficulty turning in bed, cramps, nightmares and pain. RBD presents as vigorous movements (e.g. kicking) with increased muscle tone during REM sleep and vocalisations. Several autonomic dysfunctions are described in relation to PD such as orthostasis, constipation, dysphagia, diaphoresis, urinary dysfunction and sexual dysfunction. At times, differentiation from multiple system atrophy (MSA) which presents with more severe autonomic symptoms and which is less levodopa responsive can be challenging. Often unnoticed but very common is the prodromal olfactory dysfunction in PD. Pain in PD correlates with motor fluctuations, can be caused by dystonia and may present as lancinating, burning or tingling. Eventually, seborrheic dermatitis (20-60%) is common in PD and presents as scaly erythematous patches on the scalp, face or chest (Fischer et al., 2001). Additionally, PD patients have a 2-fold increased risk for melanomas. Disease progression is variable in PD. On average 25% are severely disabled or dead after 5 years. This number increases to 80% after 10-14 years (Hoehn and Yahr, 1967).

1.3.1.4. Pathophysiology

1.3.1.4.1. Cellular pathology

Idiopathic PD is characterised by depigmentation, neuronal loss and gliosis in the SNc. At disease presentation, 60% of dopaminergic neurons mostly in the ventrolateral portion of SNc which project to the putamen are believed to be lost (Hornykiewicz, 2006; Porritt et al., 2005). However, the cholinergic, serotonergic, glutamatergic and GABA-ergic systems are affected in PD, as well, in keeping with neural loss in the locus ceruleus and dorsal nucleus of the vagus (Barone, 2010).

Lewy bodies constitute the pathologic hallmark of PD. These round, eosinophilic, intracytoplasmic neuronal inclusions are made up of a dense granular core surrounded by a 'halo' and consist mostly of alpha-synuclein and ubiquitin (Murakami et al., 2004). Lewy bodies arise from pale bodies and are prevalent in the SNc, basal nucleus of Meynert, locus ceruleus, cortex, sympathic ganglia, dorsal vagal nucleus and the myenteric plexus (Wakabayashi et al., 2007). They are not specific to PD since they appear in 10% of healthy old adults and in ataxia-teleangiectasia, progressive supranuclear palsy, corticobasal degeneration and Alzheimer's disease. It is controversial if Lewy bodies are toxic or if they represent a failed neuroprotective attempt (Bodner et al., 2006; Wakabayashi et al., 2007). According to Braak staging, pathological processes are first observed in the medulla oblongata and olfactory bulb (stage 1 + 2) while patients are presymptomatic, followed by rostral migration to SNc, midbrain and basal forebrain (stage 3 + 4) with onset of motor symptoms and involvement of the temporal and frontal cortex (stage 5 + 6) (Goedert et al., 2013).

Different processes of cell degeneration are discussed which all lead to apoptosis. Mutations in the SNCA gene cause alpha-synuclein to alter its secondary structure, self-aggregate and become neurotoxic after being fused with ubiquitin (Feany, 2004). In health, PINK1, DJ-1 and parkin form a complex which promotes the ubiquitin-proteasome system (Xiong et al., 2009).

Disruption of these genes causes defective proteolysis. MPTP is metabolised to MPP+ and ingested by dopaminergic terminals where it inhibits the mitochondrial complex I of the respiratory chain (Przedborski et al., 2004). Mitochondrial dysfunction consequently triggers apoptosis. Rotenone, also a complex I inhibitor, has been used to create a rodent PD model (Sherer et al., 2003). Furthermore, reactive oxygen species, formed during dopamine metabolisation, cause neurotoxicity (Ahlskog, 2005). Since elemental iron is increased by 50% in PD SNc (Oakley et al., 2007) as well as TNF-alpha, interleukin-1 beta and interferon-gamma (Hirsch and Hunot, 2009), the iron metabolism and immunologic mechanisms are believed to be involved in PD, too.

1.3.1.4.2. Basal ganglia networks

The basal ganglia (BG) are composed of subcortical nuclei that are involved in motor, associative, cognitive and mnemonic functions (Nelson and Kreitzer, 2014). 99% of BG neurons are GABAergic; the STN consists of glutamatergic neurons, SNc of dopaminergic neurons and a minority of striatal neurons are cholinergic (Bolam et al., 2009). The major afferents to the BG are glutamatergic, coming from cortex and thalamus with the striatum functioning as the entry point. However, the hyperdirect pathway consists of corticosubthalamic projections which make STN another point of entry (Nambu et al., 2002). Traditionally, the rate model is used to explain BG function. It posits a duality of pathways with opposing effects regarding locomotion (Albin et al., 1989; DeLong, 1990 and **Figure 1.1**). In the direct pathway, GABAergic striatal neurons project directly to the BG output structures (internal globus pallidus (GPi) and substantia nigra pars reticulata (SNr)) which results in disinhibition of the thalamus (Bolam et al., 2009; Smith et al., 1998). In the indirect pathway, relays (external globus pallidus (GPe) and STN) are interposed between striatum and SNr/GPi (Bolam et al., 2009; Smith et al., 1998). What is more, GPe and STN go beyond simple relay

stations and constitute a highly interconnected network (Bolam et al., 2009). Several feedback mechanisms fine tune these pathways such as dopaminergic SNc neurons projecting to striatum, STN and GPe (Bolam et al., 2009). The components of the dorsal division of the BG are reviewed below. The striatum, consisting of the caudate nucleus and putamen, is made up of 97% GABAergic medium spiny neurons (MSN) (Bolam et al., 2009) and has a filtering function for cortical and nigral inputs (Calabresi et al., 2014). It is subdivided into MSNs expressing D_1-receptors (G_s-protein coupled), substance P and dynorphin which belong to the direct pathway and MSNs expressing D_2-receptors (G_i-protein coupled) and enkephalin which are part of the indirect pathway (Bolam et al., 2009). The GPe consists of GABAergic neurons also expressing calbindin and parvalbumin. It receives striatal and STN afferents and electrophysiological properties allow division of GPe neurons into prototypic neurons (66%) that project to the STN and arkypallidal neurons (25%) that project to the striatum (Abdi et al., 2015b; Mallet et al., 2012a). Striatal feedback control places GPe in a powerful position (Deffains et al., 2016). The STN is a grey, lens-shaped nucleus surrounded by thalamus, ZI, SN and the internal capsule (Yelnik and Percheron, 1979). It receives afferents from GPe, cortex and thalamus, can be divided in a large dorsolateral motor area and small limbic area and has somatotopic organisation. STN neurons are active with a tonic rate of 5-30 Hz and owing to this are sometimes considered the BG's pacemaker (Bevan et al., 2007; Fujimoto and Kita, 1993). The SNr and GPi consist of GABAergic neurons and project mainly to thalamus and thus influence the cortex. They also provide efferents to the superior colliculus, the reticular formation, the pedunculopontine nucleus and lateral habenula (Bolam et al., 2009).

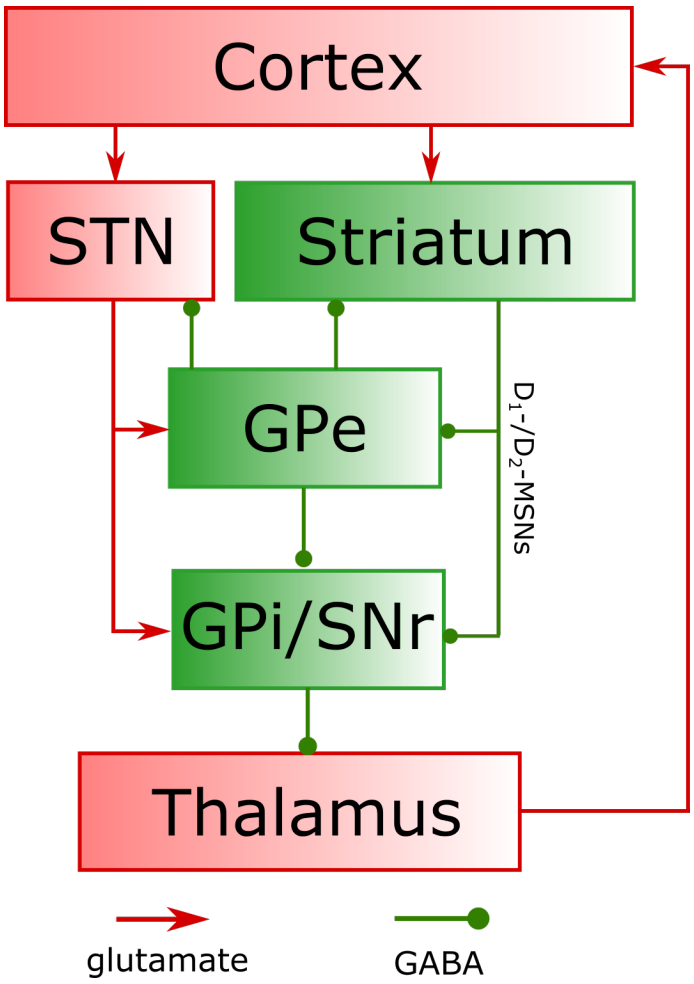


Figure 1.1. Functional Connectivity of the BG Network. Striatum and STN (hyperdirect pathway) are input structures of the BG. STN sends glutamatergic efferents to GPi/SNr as well as GPe from which it receives GABAergic inputs. Glutamatergic and GABAergic projections are colour-coded as shown. Abbreviations: BG, basal ganglia; D_1-/D_2-MSMs, striatal medium spiny neurons expressing D_1/D_2 dopamine receptors; GPe and GPi, external and internal segment of the globus pallidus; STN, subthalamic nucleus; SNr, substantia nigra pars reticulata (reproduced and modified from Deffains et al. 2016)

1.3.1.4.3. Network pathology

Normally, the SNc consists of ~ 450.000 dopaminergic neurons (German et al., 1983). Once the critical level of 100.000 neurons is undercut, the rate model postulates an imbalance of two pathways. The indirect pathway – which in health inhibits movements – becomes overactive, disinhibiting the STN, and MSNs of the direct pathway – which usually promote movement – become less active resulting in additional disinhibition of SNr and GPi. Both mechanisms lead to increased thalamic inhibition and cortical underfacilitation, purported to lead to

bradykinesia. During the early stages of PD several compensatory mechanisms mask disease progression: expression of tyrosine hydroxylase is increased in surviving neurons increasing dopamine synthesis (Bezard et al., 2003; Huot and Parent, 2007), increased afferents to dendrites of dopaminergic neurons (Calabresi et al., 2000), proliferation and hypersensitivity of dopamine receptors (Bamford et al., 2004), gap junctions increasing intrastriatal communication (Moore and Grace, 2002) and downregulation of dopamine reuptake transporters (Adams et al., 2005). The classical rate model also helps explain symptoms of Huntington's chorea (with underlying striatal atrophy) and levodopa-induced dyskinesia which both result in cortical overfacilitation. However, the rate model constitutes an oversimplification of the complex BG network. Relevant criticisms include the fact that both pathways are structurally and functionally intertwined at the striatal (communication via interneurons and biochemical) and GPe levels (collaterals bridge both pathways) (Calabresi et al., 2014). Furthermore, the non-selective dopamine agonist apomorphine attenuates Parkinsonian symptoms without altering STN firing rates (Levy et al., 2001). Moreover, corticospinal neurons project both to direct and indirect MSNs (Kress et al., 2013) and, calcium imaging studies reveal activation of the direct and indirect pathway in an operant task in mice (Cui et al., 2013). Finally, levodopa is an activator of D_1 and D_2 receptors alike and prokinetic effects of the direct pathway should be balanced by antikinetic effects of indirect pathway activation (Calabresi et al., 2014).

While the rate model aids understanding of the BG, it fails to explain why functional neurosurgery is successful in PD (Brown and Eusebio, 2008; Marsden and Obeso, 1994). Thalamotomy and pallidotomy improve PD symptoms but the rate model suggests that these two lesions should obliterate BG output to cortex completely. Further paradoxes of the rate model exist: how may pallidotomy improve opposing symptoms such as akinesia and dyskinesia? While the rate model suggests that STN lesioning should improve PD symptoms,

it is still unclear if DBS effects may be best explained as a virtual lesion or stimulation. Marsden and Obeso summarised these paradoxes and suggested that in addition to firing rate, firing pattern may be crucial for BG function (Marsden and Obeso, 1994). Abnormal patterns could perturb BG function. This may explain how multiple functional and dysfunctional circuits characterised by firing patterns may occupy the same anatomical structures. Moreover, different patterns may be associated with different PD symptoms. Bergman et al. established the pathological patterning of neuronal firing in STN and pallidum in an MPTP-induced non-human primate (NHP) model of PD (Bergman et al., 1994). Since then there is growing evidence for abnormal patterning as a characteristic feature of PD.

1.3.1.5. Pharmacological and advanced treatments

All pharmacological treatments for PD are symptomatic and depend on the degree of which symptoms interfere with quality of life. While there is no text book scheme that applies to all cases, symptoms can be clustered according to severity. Mild symptoms may be controlled with substances of low dopaminergic potency such as monoamine oxidase type B (MAO-B) inhibitors (e.g. selegiline, rasagiline), amantadine or anticholinergics. The latter are reserved for patients $\leq$ 65 years that are primarily tremor-dominant. Moderate symptoms that affect daily living are best controlled by either levodopa or dopamine agonists (DA). While levodopa is recommended for patients $\geq$ 65 years, both levodopa and DAs may be considered for patients $\leq$ 65. Levodopa, a dopamine precursor which is taken along with a peripheral decarboxylase inhibitor (e.g. carbidopa), has the greatest antiparkinsonian potency but 30-40% of patients develop motor fluctuations or dyskinesias within 5 years of treatment (increased risk for younger patients) (Ahlskog and Muenter, 2001). Motor fluctuations include a “wearing off” effect 3-4 hours after levodopa intake, unpredictable “off” periods, freezing of gait, failure of “on” response and acute akinesia. Dyskinesias encompass abnormal, involuntary movements

after levodopa intake including chorea, dystonia, ballism and myoclonus and present as peak-dose dyskinesia (30-90 min after intake), diphasic dyskinesia or wearing off dystonia. On the other hand, DAs (mostly nonergot DAs e.g. pramipexole, ropinirole, rotigotine) come in once daily formulations but may induce oedema, somnolence (e.g. sleep attacks), nausea, hallucinations and impulse control disorders (ICD). ICDs appear in 50% of patients on DAs and include pathologic gambling, compulsive sexual behaviour and compulsive buying (Corvol et al., 2018). Ergot DAs (bromocriptine, cabergoline) have a limited role today since they were associated with cardiac, pulmonary and peritoneal fibrosis and valvular heart disease (Van Camp et al., 2004). If symptoms become severe, levodopa is the drug of choice. It is titrated up and spaced out over every 4-6 waking hours. If patients are irresponsive to levodopa, differential diagnoses such as MSA, progressive supranuclear palsy and vascular parkinsonism need to be considered. Levodopa-induced motor fluctuations and dyskinesias are caused by progressive degeneration of nigrostriatal dopaminergic terminals which limits the presynaptic dopamine storage capacity and symptoms align with levodopa pharmacodynamics (90 min half-life) (Olanow et al., 2001).

Ultimately, DBS, continuous levodopa-carbidopa intestinal gel infusion (LCIG) and continuous subcutaneous apomorphine infusion (CSAI) may become necessary. LCIG requires a percutaneous gastrojejunostomy tube and a battery-powered pump and minimises motor fluctuations due to more consistent drug delivery. CSAI is less invasive and was shown to reduce “off” and increase “on” time compared to placebo in the TOLEDO trial (Katzenschlager et al., 2018).

1.3.1.6. Role of DBS

If motor complications persist despite optimal medical care, DBS becomes an option. Eligible patients have a clear response to levodopa (> 30% reduction of UPDRS motor score (Bronstein

et al., 2011)) since DBS outcome is hardly ever better than the best preoperative levodopa response except for levodopa-resistant tremor. Similar to pharmacotherapy, DBS has only symptomatic benefit and does not alter progression. However, in many cases it allows a reduction in the use of medication postoperatively. DBS results in improvement of all cardinal symptoms with sustained long-term benefits except in the case of postural instability, speech and swallowing problems. Also, non-motor symptoms are not well mitigated by DBS. Exclusion criteria for DBS surgery include cognitive impairment, psychiatric disorders and atypical or secondary parkinsonism. The two primary target nuclei in PD are STN and GPi which are comparable in terms of outcome. STN-DBS appears to be linked with greater reduction of dopaminergic medication (Follett et al., 2010) while GPi-DBS is associated with greater dyskinesia reduction (Odekerken et al., 2013). In the case of tremor-dominant PD, DBS to VIM, ZI or the posterior subthalamic area are viable options. DBS constitutes a reversible and non-destructive procedure which may be modified later on. Frame-based or frameless stereotactic brain surgery is required for unilateral or bilateral electrode placement. Leads are anchored to the burr hole site and tunnelled under the skin to a pulse generator in the chest wall. While DBS used to be exclusive for advanced PD, the EARLYSTIM trial showed significant improvement with moderate PD and early motor complications (Lhommée et al., 2018). Adverse effects from DBS include surgical complications (e.g. infection, intracerebral haemorrhage, confusion, seizures, CSF leak), hardware complications, stimulation-related complications (e.g. paraesthesia, dysarthria, dyskinesia), cognitive and behavioural complications (e.g. decline in verbal fluency, psychosis, hypomania) and increased risk of suicide.

1.3.2. DBS for Dystonia

1.3.2.1. Epidemiology, classification and pathogenesis

Dystonia is defined as a syndrome complex of hyperkinetic movement disorders with sustained or intermittent involuntary muscle contractions (simultaneous contractions of agonists and antagonists) causing abnormal or repetitive movements or postures (Albanese et al., 2013). Dystonic movements may be patterned, twisting or tremulous and may be initiated or worsened by voluntary action. Isolated dystonia is a heterogeneous syndrome complex encompassing early-onset (≤ 21) dystonia with symptoms primarily in the legs which generalise in 50% of cases (Greene et al., 1995) and late-onset (>21) dystonia which begins in the neck, arm or face and remains focal. A two-axial system is used to categorise dystonia. Axis 1 consists of clinical characteristics such as age of onset, body distribution (focal, segmental, multifocal, hemidystonia, generalised), temporal pattern and associated features (isolated or combined with additional neurologic signs). Axis 2 comprises aetiology such as nervous system pathology (degeneration or structural lesions), inherited (proven genetic origin with autosomal-dominant, recessive, mitochondrial and X-linked mutations having been discovered), acquired (perinatal brain injury, cerebrovascular, infection, medication, poisoning, neoplastic) or idiopathic. The DYT-TOR1A dystonia (mutation in ATP-binding protein) accounts for a high percentage of early-onset generalised dystonias (Bressman et al., 1994). Another genetic variant – DYT-THAP1 dystonia – originally found in Amish-Mennonite families, is an adolescent-onset cranial-cervical dystonia leading to dysarthria and dysphonia (Saunders-Pullman et al., 2007).

Owing to the phenotypic and genetic heterogeneity, neuropathological findings of isolated dystonia are inconsistent. PET and fMRI studies have registered abnormal activity in the motor cortex, basal ganglia, SMA and the cerebellum (Carbon et al., 2004; Eidelberg et al., 1998). MER during DBS surgery show decreased discharge rates in the globus pallidus in dystonic patients consistent with predictions based on the rate model for movement disorders (Vitek,

2002a). However, the reduced discharge rates in GPi are confounded by the use of propofol in this study (Lozano et al., 1997). The dopaminergic system seems to be implicated given that dopamine receptor antagonists may induce dystonic symptoms and dystonia is often associated with PD. The success of anticholinergic therapy also makes an involvement of the cholinergic system likely (Pisani et al., 2007). Several hypotheses about the pathogenesis of dystonia include a decrease of central inhibition, increased plasticity and sensory impairment (Hallett, 2006; Phukan et al., 2011). The overall prevalence of isolated dystonia is 16.4 in 100 000 cases (Steeves et al., 2012). Prevalence increases with age and focal dystonia (above all cervical dystonia) is about 10 times more frequent than generalised dystonia.

1.3.2.2. Clinical manifestations

Sustained movements are a hallmark of dystonia but tremor may also occur. Dystonic tremor is directional, task specific and less rhythmic than ET. Strikingly, many dystonic symptoms may be alleviated by a 'geste antagoniste' (sensory trick). Voluntary light touching of the affected body part reduces symptoms in 60% of cases and even an imaginary touch may prove effective (Greene and Bressman, 1998).

Early-onset dystonia typically begins with an inversion of the foot. Initially this abnormal posture is triggered during physical activity (e.g. running) but later occurs while standing or at rest. Early-onset isolated dystonias generalise in 50-90% within 5 years and are not associated with cognitive impairment (Albanese et al., 2013). Adult-onset focal or segmental isolated dystonia typically begins in the upper body, are mostly sporadic and rarely generalise. Its most common form, cervical dystonia (spasmodic torticollis), involves neck and shoulders and is painful in 50% (Chan et al., 1991). Cervical dystonia may appear as a torticollis (horizontal head turning), laterocollis (lateral tilt), anterocollis (flexion) or retrocollis (extension). Blepharospasm involves the orbicularis oculi muscles and presents as bilateral and

synchronous blinking or spasms of involuntary eye closure (Defazio et al., 2013). It is commonly increased during stress or in brightly lit areas and may be associated with facial dystonia (Meige syndrome). Oromandibular and facial dystonia include involuntary masticatory, lingual or pharyngeal movements and often appear with dystonia in adjacent body parts. It results in difficulty speaking and swallowing and may be disfiguring. Spasmodic dysphonia consists of voice breaks during normal speech. The adductor type results in a strained pattern of vocalisations since vocal cords are forcefully adducted while the abductor type results in a whispering and breathy voice. Task-specific dystonias (writer's dystonia, typist's dystonia, golfer's dystonia, musician's dystonia) are selective for given tasks and epitomise that dystonias may be a dynamic disorder. Further isolated forms include vocal tremor and arm dystonia.

Combined dystonias comprise dystonia-parkinsonism (many variants), myoclonus-dystonia (myoclonic jerks in conjunction with dystonia, improves after alcohol intake) and paroxysmal dyskinesia with dystonia. The most common dystonia-parkinsonism is dopa-responsive dystonia (DRD) which presents as a generalised, early-onset dystonia with parkinsonism which improves after levodopa intake and is usually not susceptible to dopamine-related motor complications (Nygaard et al., 1990).

1.3.2.3. Medical management

No treatment option for dystonia is curative; the following agents may provide symptomatic mitigation. Levodopa proved to be a potent cure in DRD and virtually eliminates symptoms without inducing motor complications (Rajput et al., 1994). In other dystonias, levodopa has a 15% response rate (Greene et al., 1988). Some studies suggest anticholinergics may be beneficial in focal and generalised dystonia. While one study suggests trihexyphenidyl may be effective in torsion dystonia (Burke et al., 1986), another study failed to demonstrate a benefit

(Nutt et al., 1984). Other anticholinergics only have questionable effectiveness and come along with typical anticholinergic side-effects. Tetrabenazine (VMAT2 inhibitor) was reported to induce a sustained benefit over 6 years but bears the risk of severe depression (Jankovic and Beach, 1997). The evidence of effectiveness is scant for clonazepam, baclofen, zolpidem and dopamine receptor blockers.

BoNT injection has proved advantageous for cervical dystonia (Castelão et al., 2017), blepharospasm (Bilyk et al., 2018), spasmodic dysphonia (Troung et al., 1991), limb dystonia and oromandibular dystonia. The Clostridium botulinum neurotoxin inhibits vesicular fusion which results in regional muscle weakness. In cervical dystonia, BoNT-A is the first-line option, and improves posture and pain and yields continued effects over 1-10 years (Truong et al., 2010). If unsuccessful, BoNT-B may be beneficial. Side-effects include diffuse weakness, dysphagia, neck weakness, dry mouth and hoarseness. It is controversial if neutralising antibodies are responsible for a lack of response in some cases (Lange et al., 2009).

1.3.2.4. Role of DBS

Patients with severe dystonia who fail best medical therapy, including BoNT injections, become candidates for DBS. DBS of the GPi has a proven long-term benefit for primary generalised and cervical dystonia (Alterman et al., 2007; Kiss et al., 2007; Parr et al., 2007). In one study, 75% of cases show a positive response to GPi-DBS (Kupsch et al., 2006) and benefits persisted between 3-10 years (Cif et al., 2010). Side effects, apart from typical surgery-related ones, include dysarthria and a newly developed bradykinetic movement disorder after GPi-DBS (Berman et al., 2009). In another study, 8% developed a new gait disorder (Schrader et al., 2011). Since GPi is somatotopically organised, focal and segmental symptoms are best targeted in the respective body subregions (Vayssiere et al., 2004). While GPi-DBS has questionable benefits for secondary dystonia (Eltahawy et al., 2004), STN-DBS seems to be

beneficial in dystonia secondary to PD. The STN has also been suggested as an alternative target for primary dystonia, however, its effectiveness is less well studied (Ostrem et al., 2011). Furthermore, thalamic targets (VIM and posterior region of VL) have been stimulated (and lesioned) for dystonic symptoms with a heavy tremor component (Kuncel et al., 2009). Similarly, PSA or ZI have been proposed (Blomstedt et al., 2009; Plaha et al., 2008). So far there is no proven superiority of one target for all dystonic patients.

1.4. Action mechanism of DBS

The time course of therapeutic benefits of DBS differs; STN-DBS provides relief of tremor over seconds (Blahak et al., 2009), rigidity and bradykinesia over minutes to hours (Temperli et al., 2003) and axial symptoms over hours to days (Fasano et al., 2015). This is similar to other disorders treated by DBS and alludes to different mechanisms of action involved (Herrington et al., 2016). Fast effects may be explained by immediate desynchronisation of pathological network rhythms; slow effects by synaptic plasticity and anatomical remodelling (Herrington et al., 2016). While the exact mechanism of action of DBS remains elusive it is unlikely that only one mechanism is involved (see **Table 1.2**).

Initially, DBS was thought to induce functional lesioning since STN-DBS and STN lesions had similar beneficial effects on symptom alleviation (Aziz et al., 1991; Benabid et al., 1994; Bergman et al., 1990; Limousin et al., 1995). The inhibition hypothesis was corroborated when suppression of neuronal activity was recorded surrounding STN-DBS leads in patients, NHP and rodents (Filali et al., 2004; Meissner et al., 2005; Shi et al., 2006). Some neurons ceased firing completely while others displayed residual activity. Similarly, suppression of neuronal activity was recorded around GPi-DBS sites in patients and NHP (Chiken and Nambu, 2013; Dostrovsky et al., 2000). The inhibition hypothesis fits well with the rate model and pattern model of movement disorders. Possible underlying mechanisms include depolarisation block,

inactivation of voltage-gated currents (Magariños-Ascone et al., 2002; Shin et al., 2007) and activation of inhibitory afferents (Chiken and Nambu, 2016). It is believed that DBS activates GABAergic and glutamatergic afferents but GABAergic inhibition probably overwhelms glutamatergic excitation and the net effect varies depending on the composition of inhibitory and excitatory axon terminals.

In contrast, the excitation hypothesis suggests that direct excitation of neuronal elements is possible. GPi-DBS was shown to induce evoked spikes in GPi neurons (Johnson and McIntyre, 2008) and consequently GPi-DBS inhibits thalamic neurons via GABAergic projections in monkeys (Anderson et al., 2003) and dystonic patients (Pralong et al., 2003). Consistent with the hypothesis that electrical stimulation increases output from the stimulated structure in humans, Montgomery and colleagues reported inhibition of thalamic neurons during HFS of GPi (Montgomery, 2006). In analogy to this, STN-DBS excites GPi and GPe neurons in parkinsonian rhesus monkeys (Hashimoto et al., 2003) and SNr neurons in PD patients (Galati et al., 2006) via glutamatergic projections and a microdialysis study in rats found increased levels of glutamate in GPi during STN stimulation (Windels et al., 2000). Further corroboration of the excitation hypothesis comes from human studies where GPe stimulation improved PD motor signs (Vitek et al., 2004, 1998; Yelnik et al., 2000). This clinical effect may be mediated by the activation of striato-pallidal fibers (direct pathway) and/or activation of GPe output either by increasing neuronal activity or activation of axons from GPe neurons (Vitek, 2002b).

While stimulation may fail to activate cell bodies, it may excite efferent axons and elicit spikes at target neurons (McIntyre et al., 2004). Axons can be excited orthodromically and antidromically. Low-intensity STN-DBS antidromically activated GPe neurons and induced SNr inhibition (Deniau et al., 2010; Maurice et al., 2003). Conversely, high-intensity STN-DBS induced glutamatergic SNr excitation (Deniau et al., 2010; Maurice et al., 2003). STN-DBS was also shown to activate cortical neurons likely via the hyperdirect pathway (Degos et

al., 2013; Miocinovic et al., 2018a; Walker et al., 2012). If HFS-driven antidromic spikes collide with spontaneous orthodromic ones, this may lead to a blockade of ongoing pathological activity in subpopulations of the basal ganglia (Hammond et al., 2008). Nevertheless, the excitation hypothesis does not fit with the firing rate model.

Potential action mechanism	Details	Reference
Inhibition Hypothesis		
Depolarisation block	HFS causes sustained depolarisation inactivating voltage-dependent Na+ channels and increases of extracellular K+	Magariños-Ascone et al., 2002 Shin et al., 2007
Activation of inhibitory presynaptic afferent terminals	HFS leads GABA release from presynaptic terminals of afferent GPe projections causing STN to be hyperpolarised	Milosevic et al., 2018
Excitation Hypothesis		
Direct excitation	HFS excites local neural elements inducing evoked spikes	Johnson and McIntyre, 2008 McCairn and Turner, 2009
Antidromic activation	low-intensity STN-DBS activates GPe neurons and inhibts SNr; STN-DBS activates cortical neurons	Deniau et al., 2010 Maurice et al., 2003 Walker et al., 2012 Miocinovic et al., 2018
Disruption Hypothesis		
Information block	DBS activates glutamatergic and GABAergic axon terminals in the stimulated nucleus and dissociates inputs and outputs; disruption of abnormal information flow	Chiken and Nambu, 2013
Cellular mechanisms		
Synaptic depletion	HFS does not afford the synapse enough time to replenish its vesicle pools; HFS decreases presynaptic Ca2+ conductance and inhibits neurotransmitter release	Zucker, 1989 Denker and Rizzoli, 2010 Rizzoli and Betz, 2005
Network mechanisms		
Network desynchronisation	STN-DBS suppresses beta oscillations (in STN and GPi) phase-amplitude coupling and STN-cortical beta coherence; STN-DBS at beta frequency worsens bradykinesia	Bronte-Stewart et al., 2009 Eusebio et al., 2011 Giannicola et al., 2010 Kühn et al., 2008 Brown et al., 2004
Anatomic changes mediated by neuroprotection and neurogenesis	DBS leads to increased neuronal precursor cell proliferation in the subventricular zone of the lateral ventricles, the third ventricle and tissue surrounding DBS leads; STN-DBS improves survival of SNc neurons	Vedam-Mai et al., 2014 Temel et al., 2006 Wallace et al., 2007
Synaptic plasticity-mediated connectivity changes	STN-DBS in rat brain slices induces LTP and LTD; STN-DBS evoked potentials in SNr showed LTP-like potentiaion under levodopa	Shen et al., 2013 Prescott et al., 2009
Network reorganisation	STN-DBS and GPi-DBS decrease the PD-related metabolic pattern (PDRP) in FDG-PET imaging	Fukuda et al., 2001 Asanuma et al., 2006 Trost et al., 2006

Table 1.2. Potential DBS mechanisms. Abbreviations: HFS, high frequency stimulation; Na^{+}, sodium; K^{+}, potassium; Ca^{2+}, calcium; GABA, gamma-aminobutyric acid; STN, subthalamic nucleus; DBS, deep brain stimulation; GPe and GPi, external and internal globus pallidus; SNr, substantia nigra pars reticulata; LTP and LTD, long-term potentiation and depression; FDG-PET, fluorodeoxyglucose-positron emission tomography; PDRP, Parkinson disease-related metabolic pattern.

The disruption hypothesis assumes that information transmission is blocked at a relay station of a circuit. DBS activates axon terminals, induces extensive GABA and glutamate release and dissociates inputs and outputs. GPi-DBS was shown to inhibit cortically evoked responses and spontaneous GPi discharges by strong GABAergic inhibition suggesting that it blocks information flow (Chiken and Nambu, 2013). Since GPi is an output nucleus of the BG GPi-DBS disrupts information outflow from the BG. STN-DBS may similarly block transmission through STN and disrupt abnormal firing patterns produced by reciprocal GPe-STN connections (Maurice et al., 2003).

Other potential action mechanisms include the modulation of neural networks via rapid desynchronisation of abnormal oscillatory activity (improving information coding capacity) (Chiken and Nambu, 2016), network reorganisation, synaptic plasticity-mediated changes in connectivity akin to neuronal changes seen during learning and anatomic changes mediated by neuroprotection or neurogenesis (Herrington et al., 2016).

On a cellular level, continuous HFS may cause synaptic depletion (Milosevic et al., 2018). Either HFS does not afford the synapse enough time to replenish its releasable vesicle pools (Zucker, 1989) or HFS decreases presynaptic Ca^{2+} conductance and therefore inhibits neurotransmitter release. Milosevic et al. showed that the evoked field potential after the first pulse was potentiated (synaptic facilitation) whereas the evoked potential after the last pulse of a train was attenuated. This depression after initial potentiation is presumably due to vesicle depletion. This effect was previously shown in hippocampal slice preparations where GABAergic IPSPs were attenuated after repetitive stimulation (Thompson and Gähwiler, 1989) and is frequency dependent.

DBS may work in part through modulation of remote brain regions connected to the site of stimulation; network modulation (Montgomery and Gale, 2008). The concept of

neuromodulation to target distributed networks is not new since Talairach and Leksell lesioned the ALIC in patients with psychiatric disorders to disrupt limbic input to the prefrontal cortex (Feldman and Goodrich, 2001). Focal brain lesions that lead to the same clinical symptom are often scattered in different brain regions across patients. DWI sequences allow to visualise fibre tracts and despite methodological limitations normative connectomes can be used to test if heterogeneous lesion locations map to a single circuit (Fox, 2018). Using this approach, lesions inducing amnesia were found to map to a network defined by connectivity to the subiculum (Ferguson et al., 2019) and lesions inducing depression mapped to a circuit connected to the left dorsolateral prefrontal cortex (Padmanabhan et al., 2019). Transferring this principle to DBS, VTAs and normative connectomes can be used to identify brain regions that are anatomically or functionally connected to the stimulation site. This approach was used to identify connections that co-varied with clinical improvement in PD (Horn et al., 2017b), ET (Al-Fatly et al., 2019), dystonia (Corp et al., 2019), OCD (Li et al., 2020) and epilepsy (Middlebrooks et al., 2018).

1.5. Closed-loop stimulation methods

Closed-loop stimulation is not the only potential advance in DBS. The ability to shape electrical fields is being explored, as are new stimulation patterns. For example, coordinated reset – brief, high-frequency pulse trains that are believed to reset pathological activity – described in model-based stimulations is being explored in clinical studies (Tass, 2003). However, in this thesis I will focus on adaptive DBS.

1.5.1. Approaches to closed-loop neuromodulation

The current state-of-the-art in DBS therapy is continuous DBS (cDBS, also known as open-loop DBS) which consists of permanent high-frequency DBS regardless of the presence or severity of pathological symptoms. Given partial efficacy, side effects and costs (£42,100 over 5 years (NICE, 2006)) of stimulation, there is a need for improvement. Side effects include speech impairment, neuropsychiatric symptoms (Chiung Chu Chen et al., 2006a; Okun, 2012; Parsons et al., 2006) and paradoxical worsening of movement as shown by slower manual tapping (Chiung Chu Chen et al., 2006a) or longer response times during DBS (Ray et al., 2009). In dystonic patients, DBS can even worsen bradykinesia in the non-dystonic limb (Berman et al., 2009; Schrader et al., 2011) and STN-DBS has been shown to impair swimming ability (Waldvogel et al., 2020). Side effects are believed to be partly caused by perturbation of physiological circuits, which is why tailored stimulation regimens based on LFP biomarkers or wearables measuring physical activity might circumvent adverse effects, as they might deliver less stimulation. In adaptive DBS (aDBS, also known as closed-loop DBS) stimulation is titrated according to biomarkers indicative of the severity of clinical symptoms or is only switched on when such biomarkers are present (see **Figure 1.2.**).

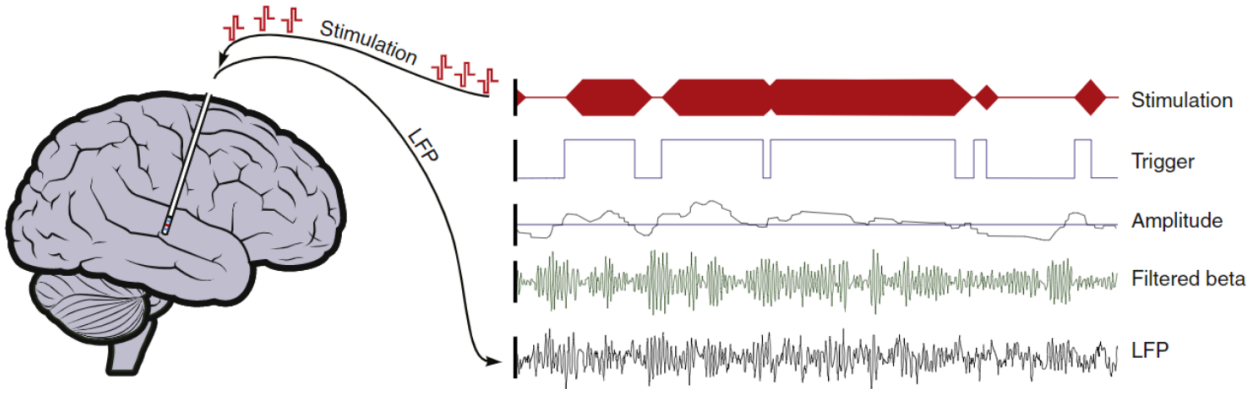


Figure 1.2. Schematic of adaptive deep brain stimulation. Local field potentials (LFPs) are recorded from the depth electrode. The LFP is subsequently band-pass filtered around a beta peak and smoothed. A threshold is defined that determines when stimulation is switched ON and OFF.

In acute trials in PD this may result in less total electrical energy delivered, fewer side effects (e.g. dysarthria and dyskinesia) and possibly improved clinical outcomes (Herz et al., 2018; Iturrate et al., 2019; Little et al., 2013, 2016b; Piña-Fuentes et al., 2019). The intermittent nature of aDBS has not caused significant paraesthesia. The overall efficacy of aDBS over the unstimulated off medication state in PD lies at about 35% (Little and Brown, 2020). Acute trials of adaptive DBS have also been successful in essential tremor (He et al., 2021; Opri et al., 2020), where there is the potential for reduced habituation to DBS over time (continuous VIM-DBS loses its effects on tremor (Barbe et al., 2011)). Chronic closed-loop DBS is effective in epilepsy (Fisher et al., 2010; Jobst et al., 2010). Using the Responsive Neurostimulation System (RNS, NeuroPace, Inc., Mountain View, CA) seizures could be reduced by 40% with closed-loop therapeutic stimulation compared to 17% reduction with sham stimulation (Morrell, 2011). The benefit of reduced power consumption only holds up provided that adaptive sensing capabilities do not require more energy and rechargeable batteries have lessened the relevance of this action. Nevertheless, some patients are unsuitable for rechargeable IPG systems (Timmermann et al., 2013) and reduced battery size might pave the way to skull-mounted IPGs (e.g. Picostim from Bioinduction).

Two different paradigms were suggested to increase specificity and widen the therapeutic window in aDBS: amplitude-responsive and phase-responsive aDBS (Meidahl et al., 2017). Amplitude-responsive algorithms rely on a threshold of filtered beta activity in which DBS is triggered once a critical power value is surpassed or stimulation is increased in proportion to filtered beta. Little and colleagues applied this method in parkinsonian humans after a previous study in NHPs (Rosin et al., 2011) and showed that unilateral aDBS at 130 Hz resulted in 50% reduction of contralateral UPDRS III and 56% reduction of time on stimulation (Little et al., 2013). Importantly, random stimulation did not deliver this clinical improvement.

Rosin and colleagues probed phase-responsive aDBS in MPTP-induced NHP and found that bursts of high-frequency GPi-DBS 80 ms after spikes in a single neuron recording from the ipsilateral M1 evoked better clinical improvement than cDBS (Rosin et al., 2011). Phase-responsive aDBS was subsequently applied in ET and the phase at which stimulation is delivered shown to determine whether the amplitude of oscillations and clinical symptoms increase or decrease (Cagnan et al., 2017).

1.5.2. Feedback signals

In aDBS, the clinical state determines when to stimulate. Peripheral measures of motor state, signals directly recorded from brain activity or a combination of both may be sources of promising biomarkers. Peripheral measures of motor state may be particularly valuable in tremor, but in patients with PD peripheral measurement of rigidity and bradykinesia in each limb may not be tractable. Furthermore, peripheral measures of motor state might be too late to allow anticipation and prevention of falls. So the search is on for brain signals that faithfully reflect clinical state and therapeutic effect with reasonable time resolution and may be measured with minimal additional intervention. Several requirements need to be met by prospective markers: signals need to be sensitive and specific to the pathological state, reliable over time and localise to the respective target nucleus (Steiner et al., 2019), they must be calculable with low computational requirements to minimise power consumption and provide rapid feedback. Markers with a causal link to pathological symptoms allow DBS to be specifically patterned to maximally disrupt causal circuit dynamics (Little et al., 2016b). However, secondary activities with good correlation to clinical state may still prove to be helpful as feedback. So far, no single biomarker has been identified that fulfils all requirements and the best clinical improvement achievable may only be accomplished integrating several biomarkers.

1.5.2.1. Local field potentials

LFPs comprise oscillatory activity of neuronal populations around the recording electrode which carry information on the state of synchrony in neural ensembles. Synaptic currents are generally slow and more likely to overlap and sum up in the population average (Buzsáki et al., 2012). The LFP captures predominantly postsynaptic membrane potential fluctuations resulting from excitatory and inhibitory presynaptic input (Haider et al., 2016) but also any type of transmembrane currents resulting from synchronised spiking or afterhyperpolarisation. The LFP reflects spatially averaged activity of many neurons as random activity would cancel itself out. Although subcortical nuclei lack the structure of cortical columns the STN-LFP appears to capture synchronous population activity (Magill et al., 2004). LFPs are recorded from large-surface, low-impedance cylindrical platinum-iridium contacts which allow stable recordings and do not require additional hardware or changes in DBS surgery (Arlotti et al., 2016). The LFP signal can be clustered into frequency bands from delta to high-frequency oscillations and band specific changes are detectable in response to clinical state, movement execution and cognitive or behavioural stimuli. The correlations between LFP and clinical state form the basis for its use in aDBS. Furthermore, the LFP signal is preferred over MER due to its long-term stability over several years, which makes it an attractive feedback control parameter. Given the composite nature of the LFP, there may be a limit to its capacity to accurately represent complex state dynamics.

1.5.2.1.1. Beta oscillations

In PD, multiple studies have demonstrated a correlation between a high level of synchronised activity in the beta range (13-30 Hz) in STN and GPi averaged over seconds or minutes and bradykinesia and rigidity. Similarly, correlations have been shown between treatment-induced

(levodopa, STN-DBS) reduction in mean beta activity and improvement in bradykinesia and rigidity (Beudel et al., 2017; Bronte-Stewart et al., 2009; Cassidy et al., 2002; Kuhn et al., 2008; Andrea A Kühn et al., 2006; Kühn et al., 2009; Neumann et al., 2016a; Oswal et al., 2016; Özkurt et al., 2011; Ray et al., 2008; Whitmer et al., 2012). Moreover, beta activity and its correlation with bradykinesia-rigidity remains consistent over many years (Abosch et al., 2012; Neumann et al., 2017b). However, not all studies show correlations between UPDRS III improvement and beta activity and some cases fail to display a beta peak off medication. Reasons for these discrepancies include the bursting nature of beta oscillations and hence optimal time resolution might have been missed in some correlative studies (Deffains et al., 2018; Tinkhauser et al., 2017a), the stun effect and variability in lead positioning. Correlations between beta bursts and motor state have been reported even if correlations are absent with overall beta power (Lofredi et al., 2019; Torrecillos et al., 2018). Apart from this, beta oscillations appeared to be reduced during slow wave sleep which might allow for aDBS to be turned off at night (Urrestarazu et al., 2009). Beta suppression occurs prior to onset of resting tremor, challenging its use as a feedback marker in tremulous PD patients (Wang et al., 2007). However, in practice aDBS improves tremor in 75% of cases (Piña-Fuentes et al., 2019; Velisar et al., 2019). To overcome the confound of the stun effect LFPs were recorded and used in acute trials of adaptive DBS at battery change (Piña-Fuentes et al., 2019). A clinical trial to demonstrate the safety and effectiveness of adaptive DBS in PD chronically implanted patients has started in 2020 (ADAPT-PD trial, Medtronic).

Several aDBS algorithms have been trialled. The first works as follows: beta activity is extracted from the STN-LFP, rectified and smoothed using a moving average of 400-500 ms (Little et al., 2013; Little and Brown, 2020). A heuristic threshold is set and if exceeded high-frequency DBS is triggered and aborted once beta levels fall below the cut-off. The threshold is set so that DBS is delivered about half the time in the off drug state. This procedure

selectively targets long bursts (> 500 ms) which reinforces that these bursts may play a crucial role in perturbing motor function in PD. Another control algorithm uses two thresholds; beta levels falling below the lower trigger incremental decrease in DBS and beta levels exceeding the upper threshold trigger incremental DBS increase (Velisar et al., 2019). Beta levels are computed over a similarly brief time period (800 ms) and this approach has shown efficacy through objective kinematic measures in chronically implanted patients. Another algorithm uses beta amplitudes in a fundamentally different manner. Instead of tracking bursts, the beta signal is exponentially smoothed over ~ 50 s, and a proportional control policy used in which DBS voltage linearly scales with the feedback signal. Given the markedly slower dynamics it is possible that this approach primarily tracks on-off drug states (Arlotti et al., 2018; Rosa et al., 2017). In the off drug state, this approach affords 50% less DBS voltage usage but only a modest clinical improvement (27% UPDRS III improvement relative to no DBS) compared to 66% improvement with the more dynamic burst triggered control (Little et al., 2013). On the other hand this approach is less susceptible to artefacts and ameliorates dyskinesias on medication. In theory, the slow dynamics may compromise mobility during night-time arousal from deep sleep.

Concerns have been raised that beta control algorithms might fail during voluntary movement given the prominent beta suppression during movement planning, execution and repetitive tasks in healthy subjects (Johnson et al., 2016). Beta bursts occur less frequently after movement cues or during self-paced upper limb movements in PD, but when they do occur movements have slower peak velocities (Tinkhauser et al., 2020; Torrecillos et al., 2018). This indicates that beta burst triggered algorithms may potentially improve bradykinetic movements but spare those with normal speed. Still, beta responsive aDBS may compromise the beta rebound and possibly delay movement termination (Iturrate et al., 2019; Wang et al., 2005). Another concern is that beta power is physiologically increased in the face of conflicting

evidence (Herz et al., 2018). Thus adaptive DBS, like cDBS, may compromise this beta power increase in situations of conflict and lead to motor impulsivity.

1.5.2.1.2. Gamma and high frequency oscillations (HFO)

Decreased gamma power (35-90 Hz) in the basal ganglia LFP correlates with akinesia and inversely, low gamma power (35-55 Hz) is emphasised during periods of stronger tremor (Weinberger et al., 2009). Similarly, where two LFPs were recorded coherence between sites in the gamma range increased with tremor (Weinberger et al., 2009). Previously, gamma oscillations were purported to contribute to movement generation (Brown, 2003; Brown and Williams, 2005) and their prokinetic features led researchers to believe gamma might in part mediate some of the effects of DBS. Power increase in the gamma range during voluntary movement correlates positively with movement velocity in PD (Lofredi et al., 2018) and is related to response vigour (Jenkinson et al., 2013). However, gamma is not only prokinetic. Fischer et al. demonstrated a gamma increase linked to successful stopping of movements (Fischer et al., 2017). Apart from this, gamma is increased following levodopa intake (Androulidakis et al., 2007a; Cassidy et al., 2002; Williams et al., 2002) and it is thought of as a key rhythm for coordinating spatially separate but functionally related neural assemblies (Fries, 2015). There is hence good evidence for gamma rhythms reflecting medication state and movement changes which make them potential biomarkers in aDBS.

HFO (> 200 Hz) are observed in the STN- (López-Azcárate et al., 2010a; Wang et al., 2014) and GPi-LFP (Connolly et al., 2015) and are not disease specific since they are present in PD and non-PD patients (Danish et al., 2007). HFO are modulated by levodopa and voluntary movement. Levodopa leads to a power shift within the HFO band with more power peaks above 300 Hz (Özkurt et al., 2011), hence the ratio between slow (200-300 Hz) and fast (300-400 Hz) HFO power might be an electrophysiological marker of clinical state. Hirschmann et al. found

that tremor shifts the balance of HFO sub-bands in the opposite direction to levodopa (LFP spectrum during tremor resembles that of the dopamine-depleted state) (Hirschmann et al., 2016). They also described that the ratio between slow and fast HFO increased during rest tremor, which occurred on and off PD medication and they suggested that the HFO ratio is a better identifier of tremor than power in lower frequency bands. Additionally, fast HFO power increases at the onset of voluntary movements (Foffani et al., 2003; Litvak et al., 2012) and coincides with low motor impairment (Wang et al., 2014). Put together, slow and fast HFO sub-bands may possess antagonistic functional roles similar to beta and gamma (Oswal et al., 2013). The HFO power ratio may become a potential marker in aDBS owing to its sensitivity to tremor and dopamine states, which would allow triggering of DBS whenever tremor is present or medication wears off. However, the very low amplitude of HFOs will make them challenging for implanted ultra-low power amplifier circuits to detect.

1.5.2.1.3. Evoked resonant neural activity (ERNA)

The ERNA is not a spontaneous signal but needs to be evoked by DBS pulses applied in proximity to STN and is characterised by an under-damped oscillation with the first peak occurring around 4 ms after the DBS pulse (Thevathasan et al., 2020). The ERNA is modulated by consecutive pulses at a therapeutic frequency (Sinclair et al., 2018a, 2019b). During DBS, the ERNA can be visualised by periodically omitting a pulse – with negligible impact on therapy – to create a window larger than 7.7 ms between two pulses. When DBS is off, the ERNA must be probed with a pulse burst to study its amplitude and frequency. The ERNA is of neural origin – ERNA waveform is not inverted by reversing pulse polarity and ERNA amplitudes increase with proximity to the dorsolateral STN – and occupies a similar frequency band as the HFO (Sinclair et al., 2019a). Its key benefit is the large amplitude compared to

spontaneous LFP signals and similar evoked potentials have been employed for use in cochlear implants (Shallop et al., 1999).

Since the ERNA localises to STN and is absent in adjacent white matter tracts, Vim and PSA it was suggested as a marker for electrode implantation guidance (Sinclair et al., 2018a). ERNA amplitude varies within STN and is greatest in the dorsolateral sensorimotor subregion. Furthermore, the ERNA is discernible under general anaesthesia which sets it apart from MER as an accurate marker during asleep surgery (Sinclair et al., 2019b).

The ERNA might also aid selection of the optimal electrode configuration for chronic DBS. Lead contacts with larger ERNA amplitudes produced greater clinical benefit from DBS and factoring in further ERNA features (e.g. natural frequency, decay rate) may further improve contact selection (Sinclair et al., 2018a). Finally, the ERNA was hypothesised to become a potential feedback signal for aDBS due to modulation of ERNA frequency and amplitude with DBS. In preliminary intraoperative clinical assessments, relief of upper limb bradykinesia and rigidity coincided with DBS levels where ERNA frequency plateaued (Sinclair et al., 2019b). Moreover, ERNA frequency correlates with the amplitude of beta activity (Sinclair et al., 2019b) which is considered a reliable surrogate for bradykinesia and rigidity.

1.5.2.1.4. Phase-amplitude coupling (PAC)

Interactions between oscillations of different frequencies are computationally important (Buzsáki and Wang, 2012). PAC is an example of such cross-frequency-coupling where the phase of a low rhythm is statistically coupled to the amplitude of a high frequency and PAC plays a role in a variety of brain functions including cognition, motor control, sensory processing and memory consolidation (Canolty and Knight, 2010; de Hemptinne et al., 2015; Seymour et al., 2017; Tort et al., 2009). Beta-HFO PAC in STN (López-Azcárate et al., 2010a;

van Wijk et al., 2016) and beta-gamma PAC in motor cortex (de Hemptinne et al., 2015; Shimamoto et al., 2013) have been shown to correlate with motor symptom severity (bradykinesia and rigidity) in PD and developed *de-novo* in GPe and cortex of an MPTP-NHP model (Escobar Sanabria et al., 2017). However, it remains unclear if these correlations reflect a mechanistic relationship with PD symptoms. PAC in STN was shown to be attenuated by dopamine replacement (López-Azcárate et al., 2010a; van Wijk et al., 2016) and PAC in the motor cortex was reduced by STN-DBS (de Hemptinne et al., 2015).

Three hypotheses have been put forward for the genesis of PAC. Firstly, PAC might underlie functional coupling between neural populations at different frequencies and origin (Buzsáki and Wang, 2012). Secondly, the lower frequency may be dominated by synaptic input and the higher frequency arises from background spiking locked to this input (Sanders, 2016). Thirdly, the shape of the low frequency carrier signal might create a high frequency spectral component with consistent phase (Aru et al., 2015).

Given its relation to PD symptom severity, PAC was proposed as a biomarker for aDBS. In STN in PD, PAC was shown to reflect the locking of local spiking activity to beta oscillations (Meidahl et al., 2019) as suggested in a computational model (Sanders, 2016). Furthermore, PAC increased with beta burst duration and the HFO amplitude was synchronised to spiking at beta frequencies in the presence of PAC (Meidahl et al., 2019). If PAC is to become a useful biomarker may depend on whether HFO locking provides information that cannot be extracted from beta oscillations alone. Apart from this, PAC may potentially be masked by DBS which will impede its use (Sanders, 2016).

1.5.2.2. Cortical signals

Cortical electrocorticographic (ECoG) signal can be recorded over the motor cortex to steer aDBS in PD. ECoG narrowband gamma activity (60-90 Hz) is related to brittle dyskinesias and in one closed-loop application STN-DBS voltage was decreased when cortical gamma activity was high or increased when low (Swann et al., 2016). In 2 PD patients, this procedure yielded energy savings between 38-45% while therapeutic benefits were maintained (Swann et al., 2018). However, the primary objective of such closed-loop DBS is to avoid dyskinesias and this has not been demonstrated thus far.

Using STN-LFP for aDBS comes with certain challenges. STN-LFP is a low amplitude signal which is difficult to recover from the large amplitude of the DBS artefact especially if a contact close to the recording site is stimulated. In contrast, a permanent subdural paddle lead over the ipsilateral motor cortex is further away from the source of stimulation which results in reduced contamination by DBS artefact. Cortical gamma has a larger amplitude and can be more reliably recorded than STN gamma and taking the ECoG signal as a feedback does not limit the choice of DBS contacts given the inability to stimulate and record from the same contact. This is important since the STN contact that most faithfully signals clinical state may also correspond to the STN contact which is best targeted in DBS (Trottenberg et al., 2007). Cortical gamma was suggested to be not strongly modulated by voluntary movement (Swann et al., 2016) which distinguishes it from canonical broadband gamma changes in the motor cortex during voluntary movement and makes it a promising candidate for aDBS (Crone et al., 1998; Miller et al., 2007). Insertion of ECoG leads is technically simple, can be done at the same time as STN lead implantation through the same burr hole and is not associated with negative outcomes (Panov et al., 2017; Swann et al., 2018). However, using cortical gamma as the single feedback parameter does not modulate DBS outside of dyskinetic periods unless beta activity

is also evaluated at the cortical level. Moreover, an ECoG signal for adaptive feedback requires two IPGs for bilateral therapy since conventional IPGs only allow inputs from two leads.

1.5.2.3. Single- and multi-unit activity (SUA & MUA)

SUA and MUA rely on extracellular action potentials which allow high spatial and temporal precision. Individual neurons are tuned to specific behaviours and MUA allows the decoding of task-specific neuronal patterns. This technique requires high-impedance electrodes as implemented in multielectrode arrays such as the Utah array in excess of 100 microelectrodes, Michigan probes or prototypes from MIT's media lab or Neuralink with arrays of thousands of contacts for chronic recording. Intracortical microelectrode arrays are used for human brain-computer-interfaces (BCI) including systems controlling neuroprosthetics (Hochberg et al., 2012), graphic user interfaces (Jarosiewicz et al., 2015) and functional electrical stimulation (Ajiboye et al., 2017). Bouton et al. restored cortical control of limited functional forearm movements in a patient with quadriplegia in real-time (Bouton et al., 2016). To this end, machine-learning algorithms were used to decode the intracortically recorded signal (from the 'hand knob' region in M1) and to extract information related to activation of forearm muscles. The advantages of these highly discrete input signals are offset by several drawbacks. Only small areas of the brain can be sampled and recordings are limited to the cortical surface. Further roadblocks include finite recording quality of SUA due to mismatch in material properties between brain and electrodes, small shifts of electrode position, build-up of impedance over time and loss of individual neurons. Chronic applications require either simplified decoding algorithms that are robust to neuron loss (Chestek et al., 2011) or frequent recalibrations.

1.5.2.4. Peripheral signals

Surface EMG and multi-axis accelerometers can be used to monitor tremor amplitude and feed the information back into an aDBS system which stimulates at a predetermined frequency and intensity when onset of tremor is predicted from limb movement (Basu et al., 2013; Herron and Chizeck, 2014; Yamamoto et al., 2013). Such aDBS systems reduce the total stimulation energy by 50% (Graupe et al., 2010) and tremor severity can be used to fine-tune DBS amplitude (Herron and Chizeck, 2014). Inertial sensors are nowadays integrated in smart watches and smart phones but wireless data fidelity and security may still be problematic. Prediction algorithms decompose EMG and accelerometer data into different frequency bands. Power changes and regularity of muscle contractions are used to distinguish tremor from voluntary movement and allow estimation of tremor onset with 80-85% accuracy (Basu et al., 2013, 2011; Graupe et al., 2010). Stimulation at certain parts of the tremor cycle may either enhance or disrupt periodic neural activity driving tremor and peripheral tremor amplitude (Cagnan et al., 2014, 2013). Both Vim-DBS and tACS over the motor cortex at fixed phase relationship can achieve significant tremor suppression (Brittain et al., 2013; Cagnan et al., 2017). These effects are accumulative which may be explained by short-term synaptic plasticity (Cagnan et al., 2015). This aDBS method requires significantly lower stimulation frequencies (4-8 Hz) which may reduce side effects. Finally, out-of-phase stimulation to tremorgenic muscles aimed at mechanically occluding tremor was shown to significantly suppress tremor (Javidan et al., 1992).

1.5.2.5. Non-electrical signals

Since DBS may increase striatal dopamine release, dopamine metabolite concentration may serve as a biomarker for DBS efficacy (Lee et al., 2009). Intracranial microdialysis may be used to assess extracellular neurotransmitter levels during lead placement or for real-time

monitoring of cerebral metabolites during post-traumatic head injury (Kilpatrick et al., 2010). Microdialysis tubules could be integrated into DBS electrodes (Schwartz et al., 2006) and such a system could operate similar to an insulin pump that monitors blood glucose. However, tube blockage, miniaturisation of chemical analysers and temporal resolution may pose barriers. Alternatively, carbon fibre electrodes detect electroactive molecules such as dopamine in real-time using fast-scanning cyclic voltammetry or amperometry techniques on a sub-second temporal scale (Grahn et al., 2014). This technique has been applied in animal models (Grahn et al., 2014) and humans (Kishida et al., 2011) and shows that DBS elicits a time-locked release of dopamine which is intensity and frequency dependent (Shon et al., 2010).

1.5.3. Existing technology

Initially to implement aDBS, Medtronic's conventional DBS neurostimulator Activa PC was equipped with a sensing feature (Activa PC+S). This tool was initially approved for investigational purposes and allowed the same therapeutic stimulation variables as the Activa PC. The Activa PC+S accommodates two quadripolar leads (8 channels) for concurrent stimulating and sensing (up to two contacts per lead can record voltage time series with 2.5-500 Hz sampling rate (Stanslaski et al., 2009)). Recording can be initiated either with an external trigger or via auto-detection once the real-time computed power spectrum meets a predetermined condition (Ryapolova-Webb et al., 2014). The Activa PC+S stores up to 8 min of data at 800 Hz (Swann et al., 2018). Algorithms to analyse sensed data in real-time can be programmed on an external PC that communicates with the Activa PC+S via the Nexus D system (a bidirectional port). Several studies have exploited this tool to record LFP signals from STN and GPi in NHP and humans (Neumann et al., 2016b; Quinn et al., 2015; Swann et al., 2016; Trager et al., 2016). Since the Activa PC+S is optimised for stimulation, frequent recording leads to rapid battery depletion. Its successor, the rechargeable Activa RC+S, may provide up to 15 years of continuous therapy. Recently, Medtronic's Percept neurostimulator

got FDA approval. This device is equipped with the BrainSense technology which allows it to chronically capture and record brain signals while delivering therapeutic stimulation. The Percept is also smaller and thinner than the Activa PC, has 15% increased longevity and is 1.5 T and 3 T MRI compatible. Finally, a skull-mounted stimulator, Bioinduction's Picostim, is under active investigation. This device can be implanted in a single-incision one-stage procedure which reduces anaesthetic risk, surgery time, costs and risk of infection, lead breakage and side-effects related to tunnelling along the neck. The Picostim also promises a better cosmetic result. Being 1/3 the size of current IPGs, it can be recessed into the skull bone like a cochlear implant and can be recharged (weekly for 2 hours) via an external inductive coil fitted into a baseball cap. The Picostim's monitoring function allows recording of LFPs in real-time. One major advantage of skull-mounted sensing is the reduced ECG artefact compared to chest-mounted IPGs. However, initial designs only allow closed-loop feedback using accelerometer signals, as the circuitry for LFP sensing is not finalised.

1.5.4. Current limitations of closed-loop DBS

aDBS is applied through standard quadripolar DBS electrodes and faces constraints. Given the immense voltage difference between a stimulation pulse and pathological LFP activity, common mode rejection is necessary to recover spontaneous LFP (Meidahl et al., 2017). In doing so, DBS can only be applied to either of the two middle ring contacts to allow bipolar recordings from the contacts flanking the stimulation contact. This method reduces the amount of available contact pairs, but octopolar directional and non-directional electrodes and thin-film probe technology (enabling high-density, high-resolution multi-contact electrodes (Connolly et al., 2016)) might help overcome this.

So far, it is difficult to assess aDBS efficacy unambiguously. LFP recordings are commonly conducted from externalised electrodes 2-7 days postoperatively. During this period,

substantial symptom relief may be observed due to stun effect (Mestre et al., 2016) which may last for up to 6 months (Mestre et al., 2016) and which is why postoperative programming is delayed (Deuschl et al., 2006). Also, changes in impedance and LFP occur during the stun period and are most prominent within 24 hours of surgery (Rosa et al., 2010). Apart from this, limited time available for recordings and postoperative fatigue pose limits for LFP recordings and analysis. Especially due to time constraints postoperative cDBS cannot be optimised and comparing postoperative cDBS and aDBS may be misleading. Since this is not representative of the chronic state, comparing symptom improvement due to cDBS and aDBS at the time of battery change when the stun effect is absent and knowledge of clinically optimised parameters is available may be more informative. Furthermore, it is challenging to assess side effects of stimulation. The reduced side-effects of aDBS in acute recordings may be unrepresentative of the chronic state. Dyskinesia under cDBS and levodopa may be less once the stun effect abates and medication is titrated over time (Rosa et al., 2017a). Speech impairment in postoperative cDBS which is absent in aDBS may also disappear once stimulation parameters are optimised (Little et al., 2016b). Other chronic features, like the habituation to the effects of DBS over time in ET cannot be assessed acutely (Barbe et al., 2011).

Since most aDBS trials were performed acutely, there is insufficient time for adaptive effects to unfold. While the action mechanism of DBS is unclear it likely includes time dependent mechanisms such as acute local neuromodulation, changes in synaptic plasticity and long-term functional reorganisation, and the potential long-term adaptive effects cannot be studied in a postoperative setting (Herrington et al., 2016). Interestingly, time on stimulation during aDBS has been reported to decrease suggestive of short-term plasticity (Little et al., 2013) which was also noted in a computational study (Hauptmann and Tass, 2007) and may contribute to carry-over effects of high-frequency stimulation by automated seizure detection in epilepsy.

So far, only one dimensional feedback markers were suggested for aDBS such as beta oscillations which correlate with bradykinesia and rigidity but not tremor. Interestingly, aDBS using filtered and smoothed beta amplitudes as a feedback parameter also controlled tremor in the majority of cases, possibly owing to tremor being more susceptible to the stun effect or a lower stimulation threshold for tremor suppression. Combining LFP activity and inertial motion sensors may allow for a dual feedback control loop that also consistently controls tremor, but this may come with problems of redundancy and tractability (Meidahl et al., 2017). For example, PAC correlates with bradykinesia and rigidity but the detection of the very low-amplitude HFO signal from the STN which is required for PAC is very power demanding (López-Azcárate et al., 2010a; van Wijk et al., 2016). Moreover, an amplitude-responsive aDBS algorithm simply distinguishes on and off depending on a fixed threshold but lacks information on continuous evolution. Imagine the room temperature dropping swiftly, it may make sense to switch on the heating earlier and higher even before a fixed value is undercut. Such considerations are incorporated in continuous time control strategies in which for example the intensity of DBS depends proportionally on beta amplitude at all times (Rosa et al., 2017a). Alternatively, a proportional-integral-derivative control as in automated insulin delivery may be a further improvement which allows anticipation of changes in feedback signals rapidly and efficiently (Ly et al., 2017). Continuous-time evolved control may further allow multivariable control using beta and peripheral sensors or different spectral features. Two caveats should be mentioned with respect to continuous-time controlled algorithms: DBS effects have a threshold and sub-threshold amplitudes and frequencies may be superfluous; multivariable sensing may require more computing power and therefore limit battery life.

aDBS is far from optimal so far. The threshold for amplitude-responsive algorithms is determined heuristically and may still not be optimised. An automated, online comprehensive optimisation may suggest best parameters for contact selection, pulse width, DBS frequency

and amplitude. In amplitude-responsive control further parameters may be optimised including the frequency band of interest, smoothing of the signal, thresholds, steepness of the ramp and duration of the lock out period after a DBS burst. In phase-responsive control the number and frequency of pulses has to be optimised. There is also a need for optimal patient selection to best profit of chronic aDBS. While only ET and not dystonic tremor was responsive to phase-responsive aDBS, even within ET patients those with tight tuning of tremor and presence of single dominant limb oscillations favoured a good response (Cagnan et al., 2017). aDBS has other unresolved questions: what if aDBS parameters change over time especially with medication or disease progression? Monitoring the stability of the control loop or even better auto-identification and auto-tuning may help overcome this. A performance index (e.g. time-weighted absolute error) may be used and if it exceeds a threshold aDBS may be reverted to cDBS and vice versa.

1.5.5. Machine-learning based stimulation paradigms

Programming of DBS parameters constitutes a time-consuming and in part subjective process of trial and error. Particularly after the introduction of octopolar leads, clinicians require many visits to find the optimal combination of stimulation settings. This appears to become even more complex for aDBS since more parameters need to be set and certain biomarkers may disappear over time. Programming is further complicated by disease progression and loss of therapeutic efficacy which require recalibration of DBS parameters (Shih et al., 2013). Machine-learning algorithms may help tackle the increasing complexity in aDBS programming, integrate inputs from multiple biomarkers and facilitate personal medicine approaches. Under supervised frameworks, algorithms are trained on a data set to identify patterns of neuronal activity that correlate with a particular behaviour or pathological state (Deo, 2015). In contrast, unsupervised frameworks enable algorithms to be applied naively to

neuronal data with minimal assumptions about what biomarkers may be most relevant or what DBS settings most effective (Deo, 2015). Machine-learning algorithms usually comprise three parts: feature extraction, dimensionality reduction and pattern classification. Khawaldeh et al. used naïve Bayes conditional probability models for classification to show that LFP dynamics allow for accurate prediction of intended movements ahead of their execution and for discrimination of upper and lower limb movements (Khawaldeh et al., 2020). This suggests that the STN-LFP could serve as a potential signal source in restorative BCIs. Tan et al. used a logistic regression model to show that voluntary movements and postural tremor can be decoded from thalamic LFPs with an average sensitivity of 0.8 (Tan et al., 2019). Furthermore, ECoG signals may prove useful for machine learning-based decoding of tremor (Opri et al., 2020) and may even be superior to subcortical LFPs (Merk et al., 2022). To be applied machine-learning based algorithms will need high accuracy and computational efficiency to allow for real-time detection and miniaturisation (Mohammed et al., 2017). In addition, the ground truth against which they optimise has to be determined; in tremor peripheral kinematic measures may be suitable but the issue is less clear cut in the case of bradykinesia-rigidity.

1.6. Thesis Roadmap

For clarity, we are going to outline the structure of this thesis here. In chapter 2, we are going to briefly introduce our experimental setup and analysis methods that are common to all experimental chapters. Then we are focusing on potential feedback signals for adaptive DBS in the subsequent experimental chapters. Over the past two decades, beta activity was extensively studied as a feedback signal for bradykinesia and rigidity in PD, but as it is not correlated with resting tremor, freezing of gait and dyskinesia it is not an all exhaustive feedback signal. Hence, our goal was to study further candidate feedback signals for aDBS in PD and namely evoked resonant neural activity (ERNA), finely-tuned gamma (FTG)

oscillations and the slope of the subthalamic power spectrum (aperiodic exponent). Below, we review the characteristics of beta activity as a feedback marker for aDBS (**Table 1.3**) and a circuit schematic of how beta activity may be used in an aDBS algorithm is provided in **Figure 2.1B**. We will revisit this table to provide the same details for other candidate feedback signals after the respective chapters.

	Beta
Sensitive and specific to the pathological state	Yes, beta reflects bradykinesia and rigidity.
Reliable over time	Yes, beta based aDBS was confirmed at IPG change several years post implantation.
Localise to stimulation sweet spot	Yes
Calculable with low computational requirements	Yes, a beta filter and smoothing are computationally cheap.
Provide rapid feedback	Yes, in a beta burst-triggered aDBS paradigm when the beta signal is smoothed over ~ 400 ms.

Table 1.3. Beta as a feedback signal for aDBS.

Previously, beta activity and ERNA have been suggested as potential feedback markers for aDBS as both are modulated by DBS (Little and Brown, 2020; Sinclair et al., 2019b). In chapter 3 we studied beta and low gamma activity and ERNA during and after blocks of continuous STN-DBS and compared the temporal dynamics of their modulation/suppression during DBS. In chapter 4 we scrutinised the ERNA further and probed it using different stimulation intensities and frequencies to extract as much information on the ERNA and its potential usefulness as a feedback signal in aDBS as possible.

Then we focused on the FTG, which had previously been suggested as a feedback marker for dyskinesia in PD. In chapter 5 we showed that FTG can also be induced by deep brain stimulation while patients are OFF medication and not dyskinetic at all. In chapter 6, we further

elaborated on the FTG and parsed it from movement-related gamma synchronisation. We further speculated on its potential usefulness in an adaptive feedback algorithm.

In previous studies, the slope of the power spectrum (aperiodic exponent) was suggested as a marker of excitation/inhibition (E/I) balance. We confirmed this in chapter 7 in parkinsonian rats during slow-wave sleep when STN firing is rhythmic and synaptic inputs are relatively controlled. In keeping with the hypothesis that parkinsonian STN is overactive, we showed that aperiodic exponents separated medication and stimulation states in PD.

In our last experimental chapter 8, we had the unique opportunity to record thalamic and subthalamic LFPs from cervical dystonia patients and found that several spectral fingerprints that were only reported in PD before such as the ERNA, DBS-induced FTG and beta/gamma power suppression are also present in the STN of dystonic patients and hence not disease-specific.

2. Methods and Materials

2.1. Patients and operative procedure 49
2.1.1. Ethics 49
2.1.2. Surgical procedure 50
2.1.3. Clinical assessment 51
2.2. Electrophysiological data acquisition 52
2.3. Pre-processing 55
2.4. General data analysis 56
2.4.1. Time-frequency decomposition 56
2.4.2. Recording artefacts 58
2.5. Statistical analysis 61

2.1. Patients and operative procedure

All participants had a clinical indication for DBS and were evaluated by a multidisciplinary team of movement disorder neurologists, functional neurosurgeons and neuropsychologists. Participants were either diagnosed with advanced idiopathic PD or dystonia refractory to standard medical therapy. Experiments took place in the early post-operative period 2-7 days following electrode implantation and externalisation. PD patients were recorded on the morning following overnight withdrawal of antiparkinsonian medication to achieve a relatively dopamine deficient state (dopamine agonists have an extended half-life and therefore will not have been completely eliminated). In a subset of PD patients, recordings could be repeated in the afternoon on medication after levodopa intake. LFPs were recorded from STN or ventrolateral thalamus depending on the respective disorder and symptom preponderance.

2.1.1. Ethics

All human data were acquired from participants who gave their informed written consent in accordance with the latest version of the Declaration of Helsinki. All experimental protocols had been approved by the local ethics committees.

2.1.2. Surgical procedure

Electrodes implanted were either of the following: the quadripolar Medtronic leads (model 3389) with 1.5 mm measuring cylindrical platinum-iridium contacts with a centre-to-centre separation of 2 mm; the octopolar (1-3-3-1 configuration) directional Vercise system by Boston Scientific (model DB-2202) with 6 segmented (each 1.5 mm^2), 1 ring and 1 dome tip (each 6 mm^2) contact made of platinum-iridium; the octopolar directional Infinity system by St. Jude Medical (now Abbott; model 6170) with 0.5 mm spacing. In our recordings, segmented contacts of the two middle levels that normally allow steering of the electrical field towards desired areas were connected to give one "cylindrical ring contact". By convention, the lowermost contact is labelled 0 increasing to the uppermost contact labelled 3. When targeting STN in PD, placement aims for location of contact 0 just below or at the lower border of the STN and for contact 3 superior to or at the uppermost border of the dorsolateral STN. Trajectory planning is based on fusion images of preoperative MRI with CT while the stereotactic frame is in place using commercial navigation software. Trajectories usually have a frontal inclination with an entry point designed to avoid blood vessels, sulci, ventricles and the caudate nuclei (Foltynie and Hariz, 2010). Following electrode placement, leads are anchored at the burr hole site and connected to a lead extension which is externalised and serves to record LFPs. Immediate post-operative imaging is performed to ensure the correct location of electrodes. Despite efforts during surgery to point the lead in a certain direction large deviations from the intended orientation are frequently observed (Dembek et al., 2019). However, once leads are inserted orientation remains stable for more than two years (Dembek et al., 2020). Critically, lead migration (> 3 mm) was shown in one study in 12% of cases (Morishita et al., 2017) while earlier studies report lower numbers (Blomstedt and Hariz, 2005; Oh et al., 2002; Voges et al., 2006). Factors affecting lead position and direction include the

fixation technique at the burr hole, lead tension and patient-specific factors such as brain atrophy. Changes in DBS settings including contact selection and steering may reflect changes due to disease progression or possibly lead migration and rotation. 3-7 days post-implantation, a second surgery is performed in which the externalised extensions are removed and intracranial electrodes are reconnected to new sterile extensions which are positioned subcutaneously and tunnelled towards the subclavicular area where they are connected to a pulse generator and battery pack. Externalisation of DBS leads is not associated with increased risk of infection (Bojanic et al., 2004; Rosa et al., 2017b). In most centres, however, DBS surgery is a one-stage procedure but may become two-stage for clinical indications (e.g. uncertainty of lead position and need for a trial response, service reasons like theatre time) or research.

2.1.3. Clinical assessment

The most commonly used grading system for clinical evaluation in PD is the Unified Parkinson's Disease Rating Scale (UPDRS) with part III explicitly for motor evaluation (Goetz et al., 2008). Of the multiple available scales for PD, the UPDRS has a high internal consistency and inter-rater reliability (Ramaker et al., 2002). Nevertheless, the UPDRS comes with a certain redundancy and strong emphasis on bradykinesia which contributes 40% to the total score. The UPDRS consists of a qualitative scale with in part subjective rating between 0 and 4 indicating absent, slight, moderate or severe presence of symptoms. This was improved in 2007 by adding more formal descriptions (Goetz et al., 2008). In some studies half points were used to improve sensitivity (Kuhn et al., 2006) which makes it a useful tool for monitoring disease progression and quantifying symptom changes. In the usual preoperative work up before DBS UPDRS scores are taken following 12 hours of dopamine withdrawal and after levodopa intake. Given UPDRS is a partly subjective, ordinal scale it is not perfectly suited for unequivocal symptom

assessment. More objective measures employ kinematic devices that track movement such as tremor directly (Weinberger et al., 2009). However, this is more difficult for bradykinesia defined as slowness of movement with progressive decrement of speed and amplitude. A number of metrics were developed to better assess bradykinesia such as tapping time and rapid alternating movements (Jobbágy et al., 2005; Kim et al., 2011). Likewise, precise assessment of rigidity is more complex necessitating measurement of force and angle during passive limb displacement (Endo et al., 2009; Park et al., 2011).

2.2. Electrophysiological data acquisition

Externalised lead extensions can be connected to an amplifier to record LFPs against a ground electrode at the inside of the wrist. The Saga/Porti Amplifier (TMS international, Netherlands) has the capability to record in a monopolar mode with additional bipolar and auxiliary channels for bipolar electrodes (e.g. EMG) or sensors such as accelerometers. It employs common average rejection on all monopolar inputs to remove mains artefacts whereby signal common to all electrodes is assumed to be artefactual and removed. Nevertheless, strong diffuse physiological signal may fall victim to common mode rejection and may also be suppressed which can be avoided by adding extra electrodes distant to the measured signal. The Saga/Porti amplifier also includes TMSi's True Active Signal Shielding technology which results in a clean signal with low mains interference. Data recorded with the TMSi Porti is sampled at 2048 Hz (TMSi Saga at 4096 Hz), acquired using in-house software, high-pass (> 1 Hz) filtered, notch (50 Hz) filtered and low-pass anti-aliasing (< 1000 Hz) filtered, saved and exported to Spike2 (Cambridge Electronic Design, UK) for further visualisation and analysis. Either of two options for common reference removal were applied: signals recorded from monopolar channels with common average reference were re-referenced offline to bipolar montages resulting in spatially focal voltage deflections by subtracting neighbouring channels of the

same lead (Schiff, 2005) or, alternatively, a bipolar electrode was used to record time series from two contacts via a bipolar channel which is exempt from common average referencing. For an example of the electrophysiological recording setup see **Figure 2.1A**.

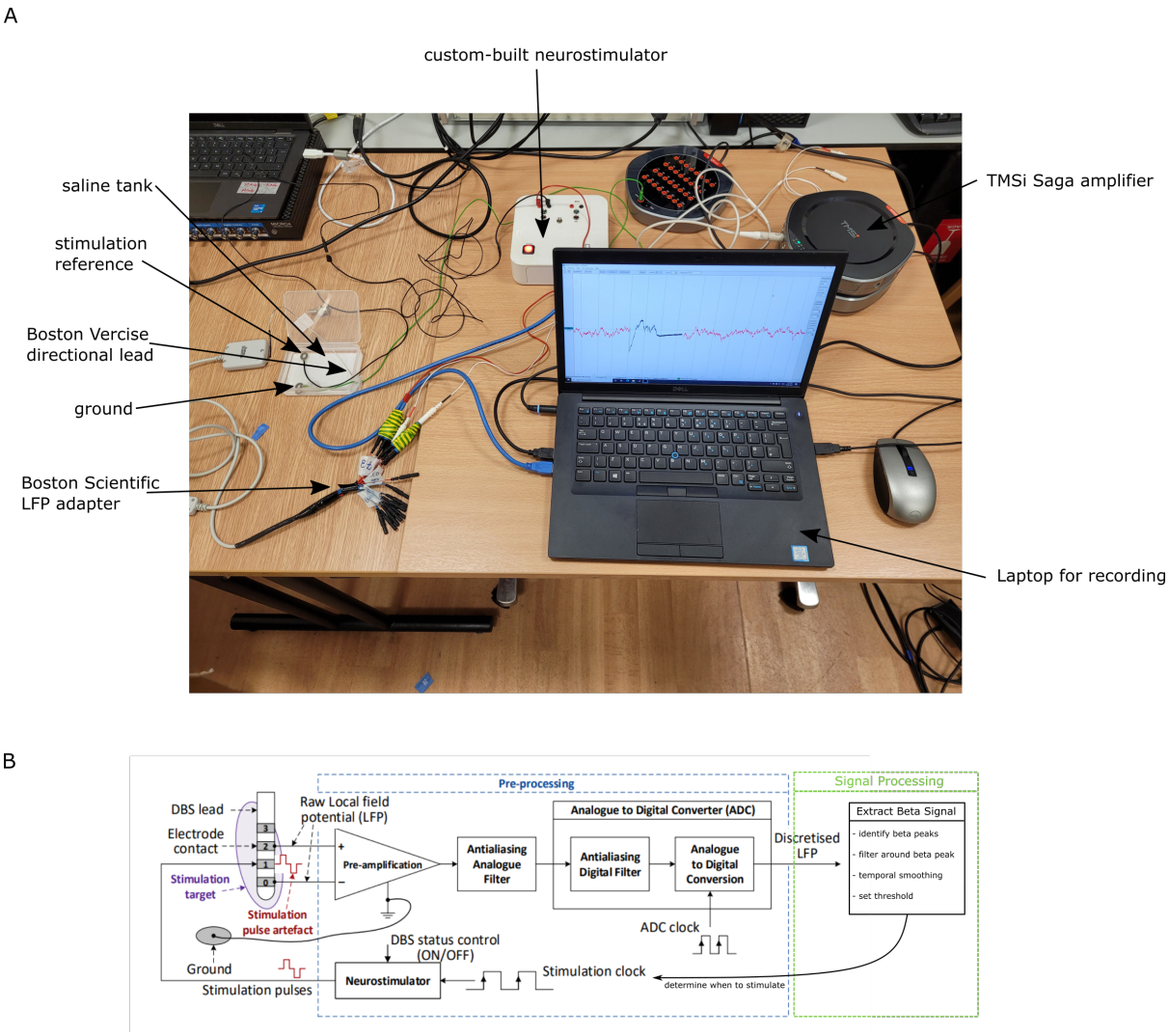


Figure 2.1. Recording Setup. A. The externalised deep brain stimulation electrode (here Boston Vercise directional) is connected to the TMSi Saga amplifier via a custom-built LFP adapter. In this test setup recordings are obtained from a saline tank. The custom-built neurostimulator is steered by custom-written scripts from the laptop and stimulation is referenced against the black electrode in the saline tank. **B.** Circuit schematic of the recording. LFPs are recorded in a bipolar configuration from contacts adjacent to the stimulated contact. LFPs are recorded after pre-amplification, anti-aliasing filtering and analogue to digital conversion (ADC). Based on the discretised LFP OFF dopaminergic medication, a beta peak is identified, the LFP is filtered around the beta peak frequency and smoothed as described in Little et al., 2013. A threshold is chosen such that stimulation is active around 50% of the time. Whenever the threshold is exceeded, the neurostimulator applies narrow biphasic pulses of 60 µs duration and 20 µs phase gap between the positive and negative deflection. (Schematic modified with permission from Debarros et al., 2020.)

We also provided a signal flow diagram for a beta-based adaptive DBS algorithm similar to that used in Little et al., 2013 (**Figure 2.1B**). We will revisit this signal flow chart throughout this thesis and outline how other feedback signals might be complementary to beta activity.

Three different stimulators were used in this thesis: the neuroBi stimulator (received from the Bionics Institute, Melbourne, Australia), the ISIS Neurostimulator (a commercial device by inomed, Germany) and a custom-built neurostimulator. The neuroBi, a highly configurable external neurostimulator, was used to deliver charge-balanced, constant-current biphasic pulses with widely adjustable parameters to output electrodes (Slater et al., 2015). This device adheres to design principles of safe electronic stimulation. Constant-current was applied so changes in impedance at the electrode-tissue interface are intrinsically compensated allowing predetermined amounts of charge to be delivered (Peckham and Knutson, 2005). Post-stimulation electrode shorting and output coupling capacitors served to maintain charge recovery (Donaldson and Donaldson, 1986) and charge limits to prevent damaging stimulation being delivered (Merrill et al., 2005). The neuroBi is PC-controlled via USB to configure device settings (pulse width: 60 μs; symmetric biphasic pulses, negative phase first).

We used the CE-marked ISIS neurostimulator to apply stimulation bursts and continuous stimulation while one pulse per second was skipped. The ISIS neurostimulator is a constant current stimulator with up to 12 output channels which allows high-current stimulation using monophasic, biphasic and alternating waveforms. Stimulation currents can range from 0.01 mA to 250 mA. The ISIS neurostimulator was controlled via inomed's proprietary software.

Our custom-built stimulator was also PC-controlled via USB and allowed us to apply stimulation frequencies up to 500 Hz, stimulation currents from 0.1 mA to 4.5 mA (in increments of 0.01 mA), stimulation pulse width from 20 μs to 500 μs and phase gap widths from 20 μs to 300 μs. This stimulator allowed us to stimulate maximum two channels in three

different modes: continuous, adaptive and burst stimulation. In all three modes, stimulation intensities could be ramped up and down at the start and end of stimulation over a variable period (e.g. 250 ms). When adaptive stimulation was used, it relied on the amplitude of a beta-filtered LFP signal and was switched on and off once a pre-defined threshold was exceeded or undercut (He et al., 2022; Little et al., 2013; Velisar et al., 2019).

Test stimulations were used to identify the contact and stimulation settings with best clinical improvement and least side-effects. Stimulation currents were incrementally increased until a clear clinical benefit or stimulation-related side-effects appeared. A self-adhesive electrode attached to the participant's shoulder served as a reference for stimulation. Recording from two equally-spaced ring contacts adjacent to the monopolar stimulation contact allows to recover the underlying physiological signal despite these potentials being orders of magnitude below stimulation voltages.

2.3. Pre-processing

Markers for stimulation or movement onset were created in Spike2. After the DC component was removed all further data processing was performed in MATLAB (v.2019b, The MathWorks Inc., Natick, Massachusetts) with custom routines. Offline filtering was performed using low-level fieldtrip functions such as *ft_preproc_lowpassfilter* and *ft_preproc_highpassfilter* (Oostenveld et al., 2011). Trials contaminated by movement artefacts were discarded following visual inspection or where possible partly analysed.

2.4. General data analysis

2.4.1. Time-frequency decomposition

Time-frequency analysis was performed on continuous time-series data which was subsequently cut into epochs, baseline-normalised, averaged across trials and subjected to statistical testing. The short-time fast fourier transform (FFT), wavelet convolution and filter-Hilbert methods were applied for time-frequency decomposition. All three methods are formally equivalent and interchangeable although results depend on the precise parameters chosen to resolve time-frequency trade-off (Bruns, 2004; Le Van Quyen et al., 2001). The short-time FFT relies on the discrete time fourier transform (FT) to represent a time-series in the frequency domain by computing the dot product between the time-series signal and sine waves of different frequencies (kernels) (Cohen and Grafman, 2014). Sine waves have three features: frequency, power (square of amplitude) and phase. Hence, results of the FT are a three-dimensional representation of the time-series. An improvement to the FT is the fast fourier transform (FFT) which is more efficient and faster without loss of information. The FT has two major downsides: it assumes data are stationary meaning the statistics of the data (mean, variance and frequency structure) do not change over time and the FT does not show how dynamics change over time. To perform temporally localised frequency decomposition other methods such as short-time FFT, wavelet convolution and filter-Hilbert need to be used. These methods assume that data are stationary within relatively brief periods of time.

The short-time FFT uses FFT to extract the frequency structure of brief segments of data rather than the entire time series (Makeig, 1993; Welch, 1967). To avoid edge artefacts, the data at the beginning and end of each brief time segment needs to be attenuated using tapers (Hann, Hamming, Gaussian, Kaiser, cosine, Blackman). The downside to this is that tapers attenuate valid LFP signal which can be mitigated using temporally overlapping segments. The Hann taper is advantageous since it tapers data fully to zero at the start and end of the time segment.

Two crucial parameters need to be set for the short-time FFT: time segment length and overlap. This hints at the trade-off between temporal and frequency precision since shorter segments provide better temporal resolution at the expense of frequency precision and vice versa. The choice of time segment length relates to the lowest frequency to analyse. Segments should be long enough to capture at least one full cycle of the lowest frequency and preferably more to increase signal-to-noise-ratio. However, long segments fail to capture transient high-frequency activity which is why the time segment length can be changed as a function of frequency with longer segments for lower frequencies and shorter segments for higher frequencies. The overlap of consecutive time segments is crucial for three reasons: it improves temporal precision, mitigates signal loss due to tapering and smoothes time-frequency plots. While power from the short-time FFT can be interpreted the same way as power values from wavelet convolution and filter-Hilbert, phase values from short-time FFT are different. In filter-Hilbert and wavelet convolution the phase-angle-time series is an estimate of the instantaneous phase at each time point whereas the phase from the short-time FFT represents the phase of the sine wave at each frequency (y-axis intercept of sine wave at zero).

In the wavelet transform, the time-series signal is convolved with complex Morlet wavelets which themselves are the result of a convolution between sine waves and a Gaussian kernel (Cohen and Grafman, 2014). The result of these dot products at any one time point is a complex number which can be plotted in polar space using Euler's formula (complex number conceptualised as an arrow starting at the origin of a cartesian coordinate system pointing toward the complex point). The projection of this point onto the real axis gives the bandpass-filtered signal. The length of the vector corresponds to the amplitude and the angle of the vector with respect to the positive real axis corresponds to the phase angle estimate. Parameters to set for wavelet convolution are the frequency range of interest (e.g. linearly or logarithmically spaced) and kernel width (number of cycles). The kernel width affects the results of time-

frequency decomposition. A larger number of cycles gives better frequency precision at the cost of worse temporal precision and vice versa (Heisenberg uncertainty principle). If the kernel width changes as a function of frequency, temporal precision at lower frequencies and frequency precision at higher frequencies can be increased.

In the filter-Hilbert method, time-series data is band-pass filtered for a frequency range of interest otherwise lower frequencies will contribute more to the time-frequency transformation than higher frequencies (power-law scaling) before applying the Hilbert transform (Cohen and Grafman, 2014). The Hilbert transform is an alternative approach to derive a complex signal of a real-valued signal. The real part contains the original data and the imaginary part contains the Hilbert transform. The Hilbert transform is a version of the original data phase-shifted by 90° in the frequency-domain (rotation of the positive-frequency Fourier coefficients anticlockwise by 90°, similar to converting cosine into sine). Filter-Hilbert allows more control over the frequency characteristics of the filter (e.g. filter bandwidth, filter order) than wavelet convolution but is computationally slower.

2.4.2. Recording artefacts

During passive LFP recordings electrical artefacts may occur. Those can be due to mains interference at 50 Hz and may be ameliorated by using common mode rejection on amplifiers, limiting mains powered devices in the vicinity, constraining wire lengths, using bipolar montages or a large area reference pad for stimulation. An efficient way to mitigate mains interference is a narrow band notch filter at 50 Hz. Further, electrical artefacts may appear due to wire movements which is why participants are instructed to move as little as possible and by excluding low frequency components of the LFP from analysis (< 4 Hz) which tend to be contaminated by movement.

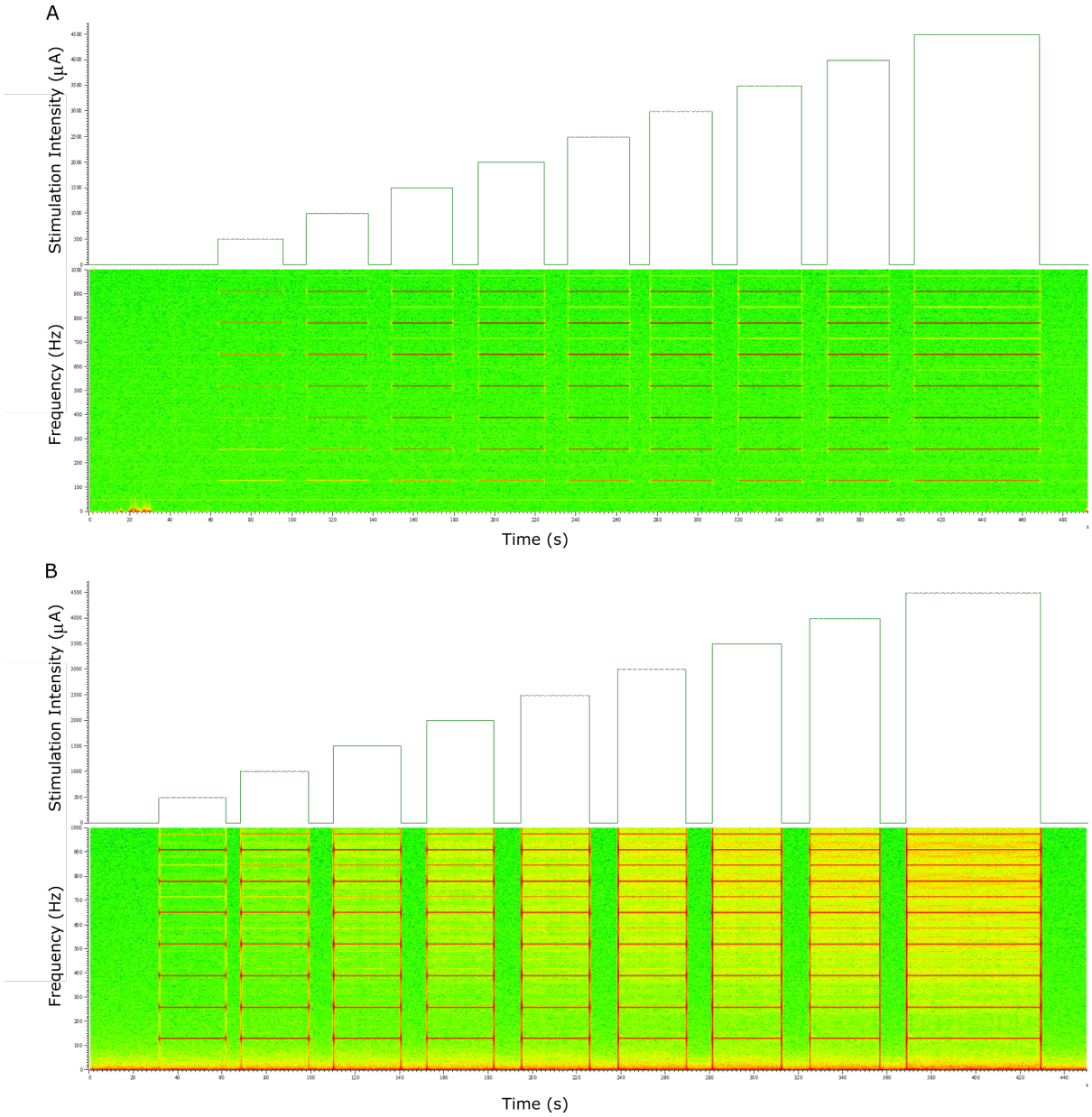


Figure 2.2. Saline Tank Recordings. Test recordings as shown in **Figure 2.1.** were conducted in saline solution to verify the presence of artefacts at harmonics of the stimulation frequency (here 130 Hz) using a Medtronic SenSight lead (A) and a directional Boston Scientific Vercise lead (B). Directional contacts were hardware fused to form a ring contact and recorded in bipolar configuration from contact levels adjacent to the stimulated ring. Signal was sampled at 4096 Hz using the TMSi Saga amplifier. Stimulation was applied via our custom-built neurostimulator (experimental setup as for our clinical recordings). Note the different signal to noise ratio between both leads. As stimulation intensity was increased from 0.5 mA to 4.5 mA (in steps of 0.5 mA) artefacts at half-harmonics (e.g. 5.5 x stimulation frequency) increased. With rising stimulation intensity, such half-harmonics appeared at lower frequencies. Note that in Boston directional leads we also observed harmonics at a quarter of the stimulation frequency. Note that recordings in saline do have a different impedance than patient recordings and different electrode-tissue interactions. Based on this, we cannot discount artefacts at half-harmonics of the stimulation frequency.

Stimulation-induced artefacts include spike artefacts during DBS which in the spectrogram appeared to span over a broad frequency range. Those spikes were inconsistent across patients, could be improved by repositioning of cables or the reference pad and most likely represent some breakthrough of the stimulation into the filtered LFP and/or amplifier saturation. Furthermore, stimulation-induced artefacts were seen in bipolar recordings at onset and offset of stimulation. Those artefacts at onset and offset were symmetrically inverted in the temporal domain, also present in saline and when deconstructed contained a broad frequency range in the spectrogram with decreasing amplitudes as frequency increases. Onset- and offset-artefacts were present with single pulses, trains and ramped stimulation but not during sustained bursts and hence likely related to rapid changes in stimulation state (Afshar et al., 2012). Their consistency, inverted shape at onset and offset and reproducibility point to a genuine effect at the tissue-electrode interface and likely present a capacitance effect related to charging and discharging of capacitors at onset and offset respectively. The offset-artefacts may self-trigger stimulation in a closed-loop paradigm which is why a refractory period following stimulation was introduced (Little et al., 2013). During stimulation, several harmonically and subharmonically related artefacts were visible. Those artefacts were not only observed at positive integer multiples of the fundamental frequency (stimulation frequency) but also in steps of a quarter of the stimulation frequency between two harmonics (three artefacts at quarter-, half- and three-quarter-distance between two harmonics (**Figure 2.2** and Debarros et al., 2020). In addition, it is possible that electrodes from different manufacturers have a different signal to noise ratio and may therefore affect the recorded LFPs. This is supported by our direct comparison of a Medtronic SenSight lead and a Boston Vercise directional lead in a saline tank (**Figure 2.2.**).

2.5. Statistical analysis

Statistical analysis was performed in Matlab using the statistics toolbox. Both parametric (two-sample t-test) and non-parametric tests (two-sided Wilcoxon rank sum test) were performed depending on the structure of the underlying data. Normality was assessed using the Lilliefors test. In case of non-normality data were transformed (e.g. logarithmic transformation) or non-parametric testing was conducted. Differences were considered statistically significant if $p < 0.05$. Pairwise comparisons were performed using paired-sample t-test or two-sided Wilcoxon signed rank test if normality assumptions were violated. The False Discovery Rate was computed using the Benjamini-Hochberg procedure (Benjamini, Y. Hochberg, 1995) to correct for multiple comparisons. Correlations with power data were computed as Spearman's rank correlation coefficient if not stated otherwise since power data are non-normally distributed (1/f profile) and contain outliers (Cohen and Grafman, 2014). Linear mixed-effects models (LMEMs) were used to analyse hierarchical data. LMEMs are an extension of linear regressions models that take into account both variation explained by the independent variables of interest (fixed effects) and variation that is not explained by the independent variables of interest (random effects). If not stated otherwise participants were treated as the random effect and stimulation blocks or power of a certain frequency band in the time series of individual patients as fixed effects. The normal distribution of each variable was visually inspected using quantile-quantile plots and histograms of distribution. LMEMs apply methods of maximum likelihood estimation (Etz, 2018), handle missing data and unbalanced designs well and may even be used on low sample sizes.

3. Project 1: Local field potential activity dynamics in response to deep brain stimulation of the subthalamic nucleus in Parkinson's disease

3.1. Introduction 63
3.2. Materials and methods 64
3.2.1. Patients and surgery 64
3.2.2. Stimulation and data recording 66
3.2.3. Lead localization determination 67
3.2.4. Experimental Protocol 68
3.2.5. Terminology 69
3.2.6. Signal processing: DBS evoked response 70
3.2.6.1. ERNA during stimulation 71
3.2.6.2. ERNA after stimulation 72
3.2.6.3. Signal processing: spontaneous neural activity 73
3.2.6.3.1. Lower frequency band (1-95 Hz) 73
3.2.6.3.2. High Frequency Oscillations (HFO, 200-400Hz) 73
3.2.7. Statistics 73
3.3. Results 74
3.3.1. ERNA during stimulation 74
3.3.2. ERNA after stimulation 79
3.3.3. Stimulation related dynamics in beta oscillations 81
3.3.4. Non-frequency selectivity of DBS induced power suppression 83
3.3.5. Dynamics in high frequency oscillations (HFO) 85
3.3.6. Clinical correlations 86
3.4. Discussion 87
3.4.1. Origin of the ERNA 88
3.4.2. Dynamics of the ERNA during and after DBS 89
3.4.3. Dynamics of background activities in response to DBS 91
3.4.4. Implications and applications of evoked and induced responses to DBS 92
3.4.5. Limitations of the study 94
3.4.6. Conclusions 94
3.5. Summarised Findings 95

In this project, we describe the ERNA in the frequency domain and contrast its temporal dynamics to those of beta and gamma power suppression during DBS. This project was published in Wiest et al., 2020.

3.1. Introduction

Deep brain stimulation (DBS) has proven a successful treatment for advanced Parkinson's Disease (PD) since it was pioneered by Alim-Louis Benabid in 1987 (Lozano et al., 2019; Okun, 2012). Since then the paradigm has remained relatively unchanged and comprises continuous high-frequency stimulation delivered at a fixed frequency (usually 130 Hz) to either the subthalamic nucleus (STN) or the internal globus pallidus (GPi). Despite its success, the mechanisms of action of DBS remain largely unexplained (Muthuraman et al., 2018). This is important as DBS can elicit stimulation-related side effects that include speech impairment, neuropsychiatric symptoms and paradoxical worsening of motor functions (Chiung Chu Chen et al., 2006a; Okun, 2012; Parsons et al., 2006). An understanding of the mechanisms of action of DBS could enable development of DBS strategies that are more specific, causing fewer side-effects, and even more effective, should it prove possible to directly counter the key malfunctions in neural circuits. In particular, there has been much recent interest in the possibility of controlling DBS using feedback from electrophysiological signals (Bouthour et al., 2019; Little and Brown, 2020; Lozano et al., 2019).

In order to clarify the mechanisms of action of DBS and seek suitable feedback signals it makes sense to examine the effects of DBS on neural circuits at the point of stimulation. Thus far two major direct consequences of stimulation have been identified in the STN; the suppression of beta-band activity in the local field potential (LFP) and the stimulation evoked resonant neural activity (ERNA; Sinclair et al., 2018). The former has been suggested as a potential mechanism underlying effective DBS, based on the growing evidence that Parkinson's disease is associated

with exaggerated synchronization of basal ganglia neurons in the beta frequency band (13-35 Hz; Brown, 2003; Eusebio et al., 2011; Kühn et al., 2008; Quinn et al., 2015). The ERNA has been more recently reported, and can be described as a robust, decaying, large-amplitude and high-frequency oscillation following DBS pulses (Sinclair et al., 2018a, 2019b). It has been confirmed to be of neural origin and is modulated by changes in DBS parameters, although its relationship to DBS mechanisms has barely been explored (Sinclair et al., 2019a).

The ERNA and beta activity are quite different, not least in their amplitudes, and yet both have been suggested as possible feedback signals to be used in adaptive DBS given evidence that they may correlate with motor impairment (Kühn et al., 2006; Kühn et al., 2009; Little et al., 2013; Sinclair et al., 2018). Here, we aim to investigate the responses of these two activities to high-frequency stimulation of the STN with special reference to the temporal dynamics of their responses. Our findings suggest that the different responses of the two activities may provide a window into different mechanisms underlying the effects of DBS of the STN whilst also constraining their use as feedback parameters in adaptive DBS.

3.2. Materials and methods

3.2.1. Patients and surgery

Fourteen patients with PD (two females) undergoing bilateral STN-DBS surgery participated in the study. Their mean age at the time of the recording was 58 ± 1.7 years (mean ± SEM) with average disease duration of 11.2 ± 1.1 years. Patients were recruited at St. George's University Hospital NHS Foundation Trust, London (UK) and at the University Medical Center of the Johannes Gutenberg University, Mainz (DE) and they all gave their written informed consent to participate in the experiment approved by the local ethics committees (St. George's University Hospital, IRAS: 46576; Mainz University Hospital: 837.208.17(11042)). The clinical details of the patients are reported in **Table 3.1** along with details of the surgical

interventions and recordings (**Table 3.2**). UPDRS Part III scores were determined pre-operatively.

The implanted leads were the Medtronic 3389 (Medtronic Inc, Neurological Division, USA) with four 0.5 mm spaced contacts of 1.5 mm length with platinum-iridium cylindrical surfaces, or the directional leads from Boston Scientific (model DB-2202, Boston Scientific, USA) or St. Jude Medical (model 6170, St. Jude Medical, now Abbott, USA), both having three segmented contacts on the middle levels. DBS implantation was guided either by magnetic resonance imaging alone (St. George's University Hospital) or with additional intra-operative micro-recordings and intra-operative stimulation (University Medical Center, Mainz).

Sub.	Gender (m/f)	Age (yr)	Disease Duration (yr)	Pre-OP UPDRS-III OFF	Pre-OP UPDRS-III ON	Pre-dominant symptoms
1	m	61	16	50	30	gait freezing, motor fluctuations
2	m	48	17	71	37	rigidity, tremor, gait freezing
3	m	54	7	38	24	tremor
4	m	56	16	51	19	rigidity, bradykinesia
5	m	65	5	34	16	gait freezing, motor fluctuations
6	m	51	5	27	13	bradykinesia, rigidity, motor fluctuations
7	f	63	11	40	17	gait freezing, motor fluctuations
8	m	64	13	52	21	gait freezing, motor fluctuations
9	m	61	10	31	19	akinetic-rigid, tremor
10	m	61	11	16	7	akinetic-rigid with fluctuations
11	m	53	7	23	12	tremor
12	m	61	9	33	12	right arm tremor, bradykinesia
13	m	48	8	45	34	tremor, bradykinesia
14	f	67	13	18	15	akinetic-rigid, tremor

Table 3.1. Patients clinical details. Pre-op: Preoperative. UPDRS-III: Part III motor score of the Unified Parkinson's Disease Rating Scale. The last three cases had no evidence of an ERNA (see **Table 3.2**).

3.2.2. Stimulation and data recording

Recordings were made between 2 and 5 days postoperatively (**Table 3.2**), while electrode leads were still externalised and before implantation of the subcutaneous pulse generator. All patients performed the experiments after overnight withdrawal of antiparkinsonian medication. For the patients implanted with directional leads, the directional contacts of levels 1 and 2 were joined together to form one 'ring contact' so that each lead afforded four monopolar ring contacts. The four contacts were then numbered from E0 to E3 with contact 0 being the most ventral and

contact 3 being the most dorsal (see **Figure 3.1A**). Stimulation was only tested at the two middle contacts (E1 and E2) to allow bipolar LFP recordings from the two adjacent contacts (see end of this paragraph and **Figure 3.1A**). A self-adhesive electrode (Pals, Nidd Valley Medical, Bordon, UK) attached to the back of the participants' shoulders served as reference for the stimulation, which was delivered using a highly configurable neurostimulator (Slater et al., 2015). Stimuli comprised symmetric constant-current biphasic pulses (60 μs per phase, negative phase first). For each of the two contacts, stimulation was started at 0.5 mA and slowly increased by 0.5 mA increments every 3 to 4 minutes until a clear clinical benefit in rigidity and/or bradykinesia was observed or side effects such as paresthesia became apparent. The stimulation contact and current associated with the most clinically effective stimulation without side effects was then selected and maintained for the entire experiment (**Table 3.2**). This procedure was performed on the side contralateral to the most affected upper limb in 12 subjects and bilaterally in 2 subjects. A stimulation frequency of 130 Hz was used throughout.

Signals were amplified and sampled at 2048 Hz using a TMSi Porti and its respective software (TMS International, Netherlands). STN LFPs were recorded bipolarly from the two contacts either side of the contact used for stimulation, for common reference removal (Schiff, 2005). The ground electrode was placed on the forearm.

3.2.3. Lead localization determination

Assessment of contact localisation was made through co-registration of immediate post-operative CT with pre-operative MRI by an experienced neurosurgeon (E.A.P) or neurologist (S.G.) specialising in deep brain stimulation. Assessment was blinded to the electrophysiological data and made using Renishaw Neuroinspire v6 software in London and Lead-DBS (v2.0, Horn et al., 2019) in Mainz. These assessments are summarised in **Table 3.2**.

Sub.	DBS lead	Site	Time Recording (d)	STN tested	Location Stim. Contact	Stim. Amp. (mA)	Cond.	no. of blocks in cond. 1	ERNA	LFP Power analysis
1	Boston	St. George's London	3	L	STN (SP)	2	1,2	4	D,A	Incl.
2	Boston	St. George's London	4	R	STN (SP)	2	1	4	D	Mvt art.
3	Boston	St. George's London	5	R	STN (SP)	3.5	1	4	D,A	Incl.
4	Medt	St. George's London	4	L	STN (SP)	4	1	4	D,A	Incl.
5	Boston	St. George's London	4 and 5	L	MBSTN (SP)	3	1,2	3	D,A	Incl.
			4	R	MBSTN (SP)	2.5	1,2	3	D,A	Incl.
6	Boston	St. George's London	4	R	MBSTN (SP)	4	1	4	D	Mvt art.
7	Boston	St. George's London	4	L	STN (SP)	2	1,2	3*	D,A	Incl.
8	Boston	St. George's London	4	R	STN (SP)	2	1,2	3*	D,A	Incl.
9	Medt	University Medical Center, Mainz	3	L	STN (SP)	4	1	4	D,A	Incl.
10	St. Jude	University Medical Center, Mainz	2	R	STN (SP)	3.5	1	4	D,A	Incl.
11	Boston	St. George's London	4	R	STN (SP)	2	1,2	4	D,A	Incl.
			5	L	STN (SP)	3	1,2	4	D,A	Incl.
12	Boston	St. George's London	4	L	MBSTN (SP)	4	1	4	none	Beta red.
13	Boston	St. George's London	5	L	MBSTN (SP)	3	1	4	none	No beta change
14	Medt	University Medical Center, Mainz	3	L	Post lat to STN(SP)	1.5	1	4	none	Beta red.

Table 3.2. Patients surgical and recordings details. Medt: Medtronic. L: Left, R: Right. STN(SP): Superior posterior part of sub-thalamic nucleus. MBSTN(SP): Medial border of the superior posterior part of the sub-thalamic nucleus. Post lat to STN (SP): Posterio-lateral to the superior posterior part of the sub-thalamic nucleus. D: ERNA during stimulation, A: ERNA after stimulation. Incl: STN included in the power analysis of local field potentials (LFP, beta and low gamma power). Mvt art: STN excluded from LFP power analysis because of movement artefacts. Beta red: beta reduced. *only two blocks of which were consecutive (patients excluded from linear mixed-effects models).

3.2.4. Experimental Protocol

During the experiment, patients were seated comfortably in an armchair. The experimental protocol is summarised in **Figure 3.1B** and consisted of two conditions preceded by 2 minutes of rest recordings without stimulation (baseline). In the first condition, continuous 130 Hz DBS

was applied for 181.2 ± 7.3 seconds (mean ± SEM) in up to four consecutive blocks separated by resting periods of on average 117.1 ± 10.8 seconds. These are termed long duration stimulation blocks. In the second condition, stimulation blocks were shortened to on average 14.2 ± 2.3 seconds with rest periods of 105.1 ± 16 seconds. This second condition was performed to study how the ERNA's characteristics are modulated by the duration of the preceding stimulation and both conditions were separated by a resting period. In addition, the long duration stimulation condition was long enough for clinical benefit to develop (Levin et al., 2009; Lopiano et al., 2003). The rest period duration did not differ between the two conditions ($t_{(18)}$= 0.55, p = 0.59). Note that due to patient fatigue and time constraints only a subset of patients performed the short duration condition (n = 7 STN from 5 patients).

3.2.5. Terminology

The ERNA has previously only been described in the temporal domain, with the same term being used to describe evoked responses during and at the termination of stimulation (Sinclair et al., 2018, 2019b). Here we also use the term ERNA to describe a feature in time-frequency plots that upon steady-state has a similar frequency to the repeating waves of the ERNA on cessation of stimulation. Time and spectral domain representations also shared similar dynamics following the onset of stimulation. Hence we use the term ERNA to denote all three phenomena; the high frequency evoked response in time series during stimulation, the high frequency response in time series evoked by the last stimulus in a block of stimulation and the high frequency spectral response during stimulation.

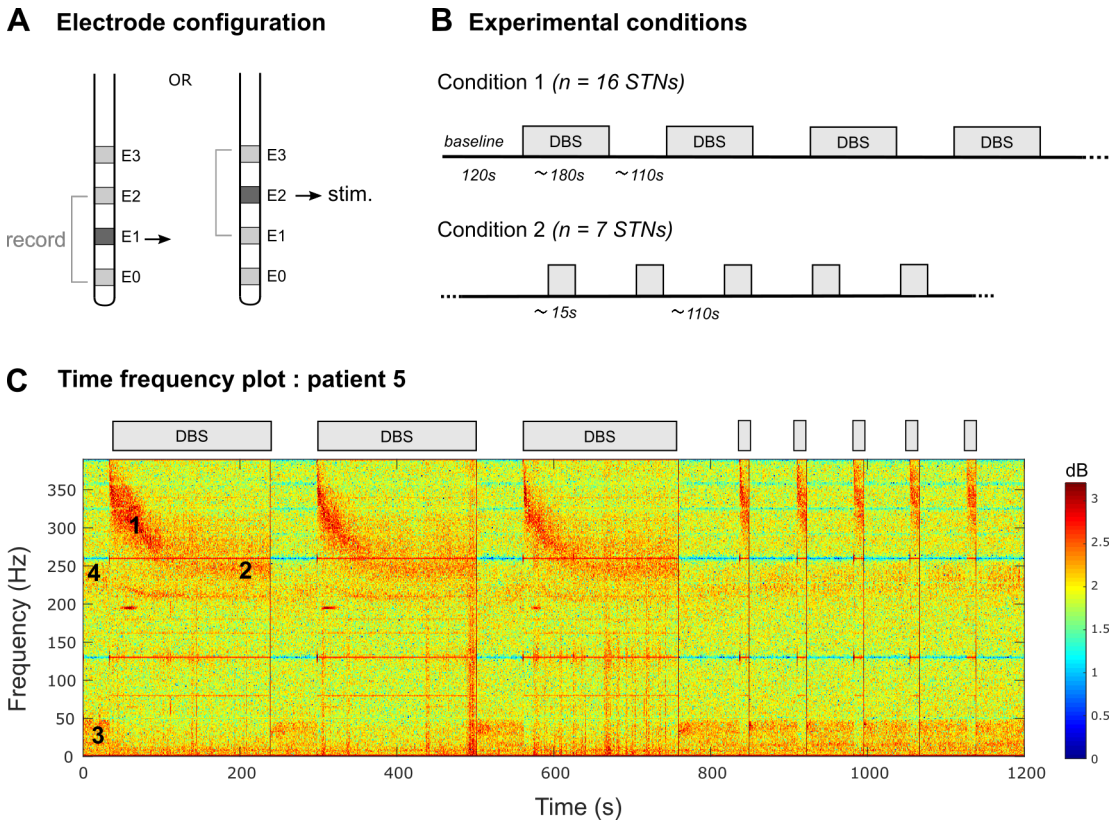


Figure 3.1. Stimulation settings and experimental conditions. A. Schematic of the electrode configuration. Stimulation was applied to one of the two middle electrode contacts (E1 or E2) and the LFPs recorded bipolarly from the two adjacent contacts (e.g.: E1-E3). **B.** Experimental protocol. The first condition started with a 2-minute baseline recording followed by continuous stimulation at 130 Hz in blocks of 181.2 ± 7.3 (mean ± SEM) seconds interleaved by about 117.1 ± 0.8 seconds of rest. In the second condition, stimulation was shortened to 14.2 ± 2.3 seconds and separated by about 105.1 ±16 seconds. Rest period duration did not differ between the two conditions ($t_{(18)}$= 0.55, p = 0.59) **C.** Spectral features over time in the two experimental conditions for patient 5. During stimulation, an ERNA appears between 300 Hz and 350 Hz (label 1) and its power attenuates while dropping in frequency until it reaches a steady state centred around 260 Hz (label 2). Stimulation blocks are denoted by the grey rectangles at the top of the trace. In addition, during stimulation there is a prompt suppression of beta and low gamma power (label 3) and a modulation of the HFO frequency (label 4) present before stimulation. Note that line noise artefacts are visible throughout the recordings at 50 Hz and its harmonics, along with the stimulation artefact at 130 Hz and its harmonics, despite being reduced by notch filters. Movement artefacts, affecting mostly lower frequencies, are particularly visible in the third stimulation block.

3.2.6. Signal processing: DBS evoked response

Signal processing was performed using custom-written scripts in MATLAB (version 2019a, Mathworks, Massachusetts, USA).

3.2.6.1. ERNA during stimulation

Here, we determine ERNA characteristics in the frequency domain, based on the premise that the ERNA is not sufficiently tuned as to be wholly obscured by the stimulation artefact in frequency spectra. These analyses were performed only during long stimulation blocks (condition 1). Continuous LFP signals were de-trended and stimulation artefacts were removed by applying second-order IIR notch filters (Q factors = 30) at the stimulation frequency and its harmonics. Spectral amplitudes were estimated between 1-512 Hz using the short-time Fourier transform with a window length of 1 second, 25 % of overlap and a Hamming window as implemented in MATLAB's *spectrogram* function (see **Figure 3.1C** for data from one STN). Each long stimulation block (condition 1) was then divided into consecutive non-overlapping 10-second epochs, in which power spectral densities (PSD) were estimated and smoothed using a Gaussian kernel with 50 sampling points full-width. The largest peak of the PSD between 200 and 400 Hz was used to define the ERNA frequency and amplitude in each 10-second epoch (see **Figure 3.2Aii**). Based on the changes observed along the consecutive 10-second epochs we then separately defined for each long duration stimulation block two steady states corresponding to the stabilisation of the ERNA frequency (**Figure 3.2Aiii**) and amplitude (**Figure 3.2Aiv**), respectively. The onset of the steady state was defined based on the derivative of the time profiles and corresponded to the centre of the first epoch at which the derivative was encompassed in a band of ± 5 Hz/s (or μV/s for amplitude) centred around zero. This method allowed a robust and objective threshold estimation while limiting the number of arbitrary selected parameters.

The spectral analysis of the ERNA during continuous stimulation was supported by its analysis in the time domain. To this end, the peaks of the stimulation artefacts were identified and removed from the de-trended LFP signals (removing 1.5 ms after each artefact to avoid any contamination of the inter-trial interval by residual stimulus artefact). Note that 1.5 ms was

selected as sufficient to remove stimulus artefact based on visual inspection. Then, the first ERNA peak was identified in the inter-artefact intervals (~ 7.7 ms long) of the stimulation block as the highest peak within the interval, and tracked throughout all consecutive intervals to measure its amplitude and latency (time between artefact peak and first peak of the ERNA).

3.2.6.2. ERNA after stimulation

After cessation of stimulation the ERNA was assessed over a longer time window which exposed its extended morphology characterized by a series of 2-8 regularly spaced, but diminishing waves (Sinclair et al., 2018a, 2019b). The ERNA after stimulation was analysed as follows. First, data were high-pass filtered at 80 Hz with a two-pass Butterworth IIR filter (Oostenveld et al., 2011) and 50 ms data epochs were aligned to the last reproducible stimulus artefact in a given block of stimulation. ERNA duration was defined as the time between the last artefact peak and the last detected ERNA peak within the 50-millisecond epoch. Thereafter, the first 1.5 ms of each epoch was deleted to avoid further contamination by residual stimulus artefact (see **Figure 3.4A**). Second, peaks and troughs in the ERNA response were found using the MATLAB *findpeaks* function, with the following criteria; MinPeakWidth = 0.5 ms, MinPeakProminence = 10 μV (Sinclair et al., 2019b). ERNA responses were not further analysed, and considered absent, if there were fewer than two peaks and two troughs. Finally, ERNA initial frequency was calculated as the inverse of the time difference between the first and second peak and the initial amplitude was calculated as the difference between the first peak and the subsequent trough (Sinclair et al., 2019b). To evaluate the ERNA frequency change after cessation of the stimulation, its frequency was also calculated as the inverse of the time between the subsequent peaks.

3.2.6.3. Signal processing: spontaneous neural activity

3.2.6.3.1. Lower frequency band (1-95 Hz)

LFP signals were band-pass filtered between 1-95 Hz and spectra were estimated using the short-time Fourier transform with a higher temporal resolution than for the previous analysis (window length of 125 ms, 50 % of overlap) and a Hamming window filter. All spectral power changes were defined in relation to a 10-second baseline epoch recorded prior to the first stimulation block of every subject which was free from any motion artefact. The modulation of resting, spontaneous beta (13-34 Hz) and low gamma (35-45 Hz) power by DBS was studied in two 30-second windows aligned to the first and last artefact in long duration stimulation blocks (from -10 to +20 seconds where zero seconds is the onset and offset of stimulation, respectively). For both frequency bands, the time of power recurrence was defined after the cessation of stimulation as an increase in power that reached or surpassed the 95 % confidence limits of baseline activity for at least 250 ms. For clinical correlations baseline beta power was normalised to the percentage of total power of 5 to 45 Hz.

3.2.6.3.2. High Frequency Oscillations (HFO, 200-400Hz)

Spontaneous activity in the high frequency range (200-400 Hz) was studied in the absence of stimulation, as it can overlap with the frequency range of the evolving ERNA. Power spectral densities were estimated using MATLAB's *spectrogram* function (same parameters as for the ERNA during DBS) in 20-second windows during the baseline and at the start or end of the resting periods (see **Figure 3.7A**). In each window, the HFO frequency peak was defined as the largest peak between 200 and 400 Hz.

3.2.7. Statistics

The statistical analyses were conducted using custom-written scripts in MATLAB (MathWorks). Normality of the data was controlled before any statistical test (Lilliefors test)

and nonparametric statistics were applied when necessary (as reported in Results). Comparison of group data (ERNA characteristics and averaged power changes) across stimulation blocks were performed with linear mixed-effects models and the normal distribution of each variable was visually inspected with quantile-quantile plots and histograms of distribution. All models were estimated by the method of maximum likelihood and included random intercept for subjects, to allow different intercepts for each subject capturing individual differences. The time courses of power changes were tested against zero with one-sample t-tests in sliding windows of 50 ms with a time shift between successive windows of 12.5 ms. The False Discovery Rate was computed using the Benjamini-Hochberg procedure (Benjamini and Hochberg, 1995) to correct for multiple comparisons along the time axis. Since power data are not normally distributed and contain outliers, we computed the Spearman correlation between suppression of activity in the beta band, time to reach ERNA steady state and symptom severity.

3.3. Results

3.3.1. ERNA during stimulation

We began by inspecting time-frequency plots of STN activity during stimulation. A typical example from a representative patient is illustrated in **Figure 3.1C** and shows, in the spectral domain, an activity sliding down in frequency over time before overlapping with the narrower band artefact at 260 Hz related to the first harmonic of the stimulation. This pattern was observed in 13/16 tested STNs. Here we term this activity ERNA based on its similarities to the ERNA previously described in the time-domain (see **Figure 3.3** and Sinclair et al., 2019b, 2018). Note that the absence of ERNA in three STNs is unlikely to be due to a weaker stimulation amplitude (see **Table 3.2** and **Figure 3.S1**). Rather it may be related to targeting in

so far as their stimulating contacts were localized to the medial border of the superior part of the STN or lay outside and posterio-lateral to this part of the STN (see **Table 3.2**).

In order to study the frequency dynamics of the ERNA in more detail we divided each stimulation block into consecutive 10-second windows and plotted the peak frequency observed between 200-400 Hz over time (see **Figure 3.2A**). We then extracted three parameters for each stimulation block: the initial and steady state frequencies, and the time at which the steady state was reached (see Methods). We first asked whether the three parameters were consistent over time, i.e. across stimulation blocks. To this end we only considered those patients with at least three consecutive long duration stimulation blocks (n=11 STNs, including seven with four blocks). The results of linear mixed-effects modelling revealed that both the initial and steady state frequencies were stable over long duration stimulation blocks (b = -0.45, $t_{(38)}$ = -0.37, p = 0.72 and b = 0.49, $t_{(38)}$ = 1.27, p = 0.21, respectively, **Figure 3.2B**). Moreover, the delay to reach the steady state was also similar in consecutive blocks (b = -2.48, $t_{(38)}$ = -1.86, p = 0.07). Thus, on average across all STNs and stimulation blocks, the ERNA started at a frequency of 352.4 ± 4.9 Hz (mean ± SEM) at the onset of stimulation and progressively decreased in frequency over time to stabilise after 71.4 ± 2.6 seconds at a frequency of 263.2 ± 2.1 Hz.

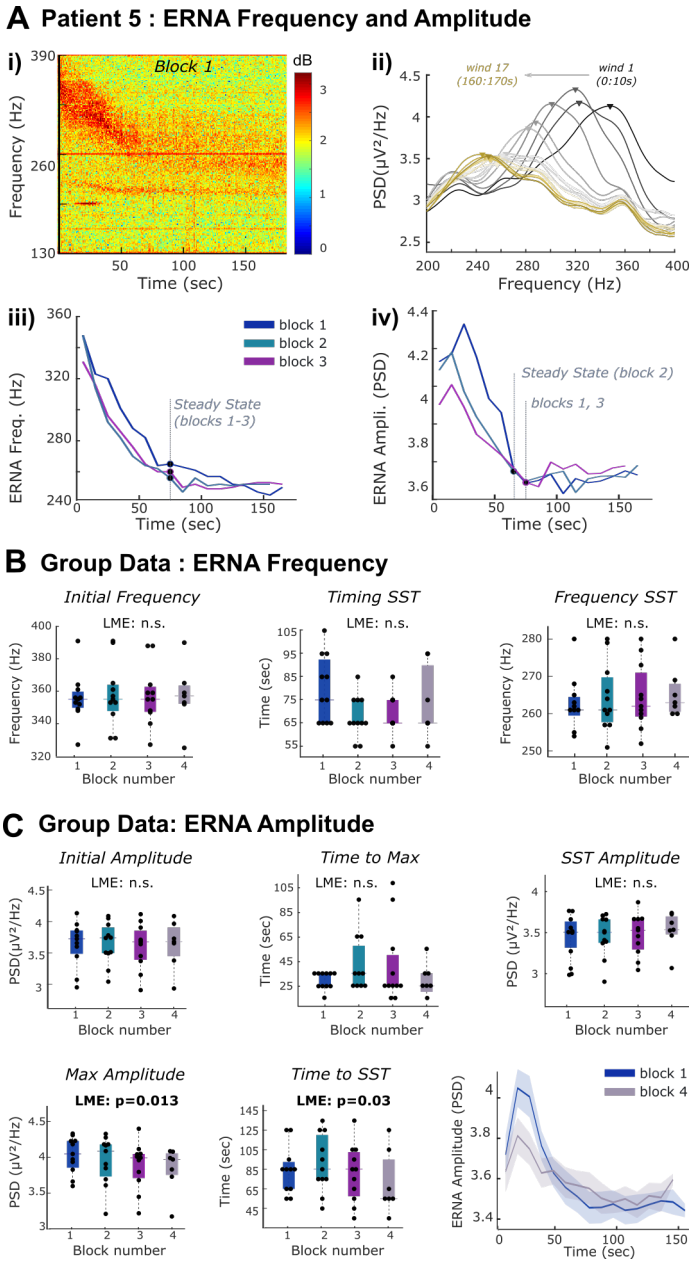


Figure 3.2. ERNA during long stimulation blocks (condition 1) characterised in the spectral domain. A. ERNA in Patient 5. ERNA representation in a time-frequency plot (i) and power spectral density (PSD) in serial 10-second windows (wind; n=17) (ii). Successive windows transition from black to light grey and then to brown, showing the progression to steady state. The arrow heads denote the frequency of the peak measured in each window. The amplitude and frequency of this peak was measured to give the results in (iii) and (iv). The change in the ERNA frequency (iii) and amplitude (iv) over time are plotted for the three blocks of stimulation separately. The time at which steady state (SST) is reached corresponds to the first point at which the derivate remains within a ± 5 Hz/s band around zero and is indicated by dots for each block (see dashed grey line)**. B.** Frequency characteristics of the ERNA at the group level and across stimulation blocks. Black dots represent individual STNs. Linear mixed-effects models (LME) reveal no significant modulation between blocks (see text). Initial frequency and initial amplitude refer to the value of the first 10-second bin. **C.** Amplitude characteristics of the ERNA at the group level and across stimulation blocks. Linear mixed-effects models reveal a significant modulation of the maximal amplitude ($b = -0.06$, $t_{(38)} = -3.56$, $p = 0.013$)

and the time to reach the steady state (b = -6.27, $t_{(38)}$ = -2.21, p = 0.03) over blocks. *Bottom right;* Averaged amplitude of the ERNA for block 1 and block 4 (mean ± SEM).

In addition to the dynamics in frequency, we also explored the dynamics in the ERNA amplitude, following the same procedure. As shown in **Figure 3.2Aiv and 3.2C**, the results revealed a different pattern. The amplitude of the evoked response first briefly increased and then decreased to stabilize around a steady state at the end of the stimulation block (after on average 81.7 ± 6.2 seconds). For each STN and each stimulation block, we extracted five parameters describing this amplitude dynamic; the initial, maximal and steady state amplitude, and the times at which the maximal and steady state amplitudes were reached. The linear mixed-effects modelling revealed a significant reduction of the maximal amplitude and a shortening of the delay to reach the steady state in consecutive blocks (b = -0.06, $t_{(38)}$ = -3.56, p = 0.013 and b = -6.27, $t_{(38)}$ = -2.21, p = 0.03, respectively). The results are confirmed when only the STNs with four consecutive blocks were included in the model (maximal amplitude: b = -0.06, $t_{(26)}$ = -2.68, p = 0.013 and steady state: b = -7.1, $t_{(26)}$ = -2.1, p = 0.047). This control was performed to confirm that the previously reported statistical effects were not related to the unbalanced design and the absence of block 4 in some of the STNs. This modulation can be easily seen in **Figure 3.2C** bottom right where the amplitude time course of the first and last stimulation block are overlaid. The three remaining parameters were however stable in consecutive blocks; the time at which the maximal amplitude was reached (b = 0.21, $t_{(38)}$ = 0.07, p = 0.94) as well as the initial and steady state amplitudes (b = -0.004, $t_{(38)}$ = -0.26, p = 0.8 and b = 0.01, $t_{(38)}$ = 1, p = 0.32, respectively). Finally, the frequency and amplitude steady states were reached after a similar delay (paired t-tests, $t_{(12)}$= -1.01, p = 0.3 for the first block, $t_{(12)}$ = 0.17, p = 0.87 for the last block).

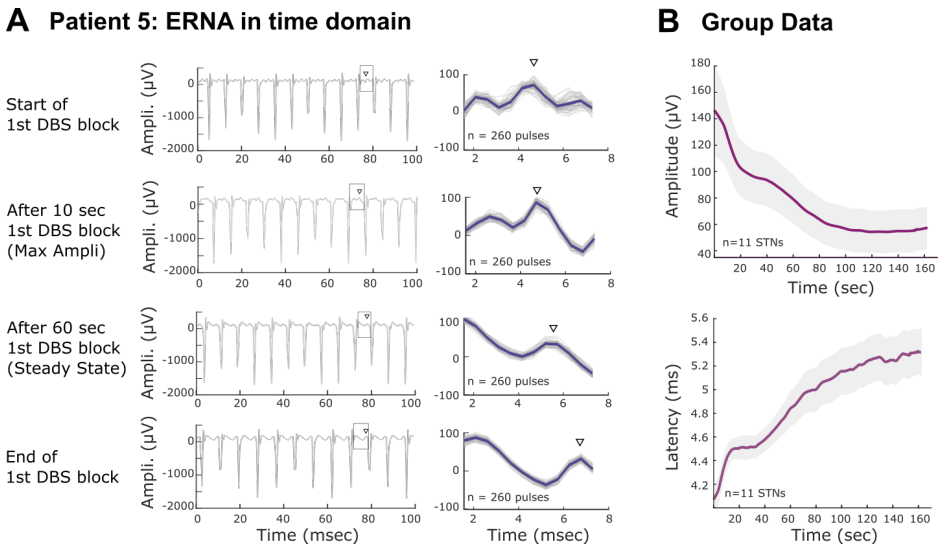


Figure 3.3. ERNA during long stimulation blocks (condition 1) in the temporal domain. A. *Left;* LFP traces at the start, when largest amplitude is reached, the middle (after 60 s) and the end of the first long duration stimulation block of patient 5, revealing the presence of a changing evoked response between stimulation artefacts. *Right:* Superimposition of 260 pulses (grey) and their average (blue). To demonstrate the changing nature of the evoked activity over time we selected the maximal discrete peak between the stimulus artefacts in the first interval, tracked this peak throughout the stimulation block (indicated with a black arrowhead) and measured the amplitude and latency of this evoked potential. **B.** Change in the averaged amplitude and latency of the selected peak over time at the group level (mean ± SEM).

Importantly, the above results were confirmed by studying the ERNA during stimulation in the temporal domain (**Figure 3.3A**). During continuous DBS the evoked response can be observed between each pair of consecutive stimulation artefacts, although it may also be present during the stimulus artefact but obscured by the latter (see **Figure 3.4C**). In order to demonstrate the changing nature of the evoked activity over time we selected the maximal discrete peak between the stimulus artefacts. This increased in latency and decreased in amplitude with stimulation duration (**Figure 3.3B**), is in line with the change in frequency and amplitude observed in the spectral domain (**Figure 3.S2**). Note that the latency of the selected peak may not exactly correspond to the frequency of the ERNA measured in the spectral domain, as in the latter case the analysis gives the dominant frequency of the whole evoked response, and may include portions of the evoked activity that overlap with the stimulation artefact (see

Figure 3.4C). The time-domain analysis also confirmed the absence of an ERNA during stimulation in the three patients mentioned previously (patients 12-14, **Table 3.2**, **Figure 3.S1**).

3.3.2. ERNA after stimulation

As mentioned above, time domain analyses of the ERNA during stimulation may be hindered by subsequent stimulation artefacts. Accordingly, we also examined any activity that persisted after stimulation was abruptly discontinued. As can be seen in **Figure 3.4A**, a series of high frequency waves followed cessation of stimulation and progressively diminished in amplitude, similar to the ERNA previously described in the literature (Sinclair et al., 2018a). Across all hemispheres, this resonant activity was composed of a series of 2 to 10 waves (4.9 ± 0.4 on average, see Methods for criteria) lasting for 24 ± 2 ms on average after the cessation of the stimulation. The initial frequency of the ERNA , measured as the inverse of the delay between the first two peaks, was similar to the steady state of the ERNA during stimulation (initial frequency: 271.3 ± 11.7 Hz and ERNA steady state: 263.2 ± 2.1 Hz, paired t-test, $t_{(10)} = 0.82$, $p = 0.43$). Note that two STNs with an evoked potential during stimulation did not meet our criteria for an ERNA response at offset of stimulation, although both had an evoked response during stimulation (patients 2 and 7). Moreover, this analysis confirmed the absence of an ERNA following cessation of stimulation in patients 12 to 14 (**Table 3.2**, **Figure 3.S1**).

In order to study the modulation of the ERNA by preceding stimulation we examined the data from 7 hemispheres (5 patients) in which a second experimental condition was performed. In this paradigm DBS was applied for a shorter period of time (14.1 ± 2 seconds). The comparison of the resonant activity after short versus long DBS blocks revealed a more marked ERNA after short stimulation blocks which lasted longer (29.4 ± 2 ms vs 21.7 ± 1 ms, paired t-tests: $t_{(6)} = 3.3$, $p = 0.024$) with more waves observed (7.3 ± 0.6 vs 4.4 ± 0.2, paired t-test: $t_{(6)} = 4.06$, $p = 0.007$). In addition, the initial frequency and amplitude of the ERNA were significantly

higher after short stimulations ($t_{(6)} = 5.2$, $p = 0.002$ and $t_{(6)} = 2.48$, $p = 0.047$, **Figure 3.4B**). This change in ERNA character following short and long duration stimulation periods is in line with the shift to a lower steady state frequency during long duration stimulation evident in the ERNA in the spectral domain (**Figure 3.2A**).

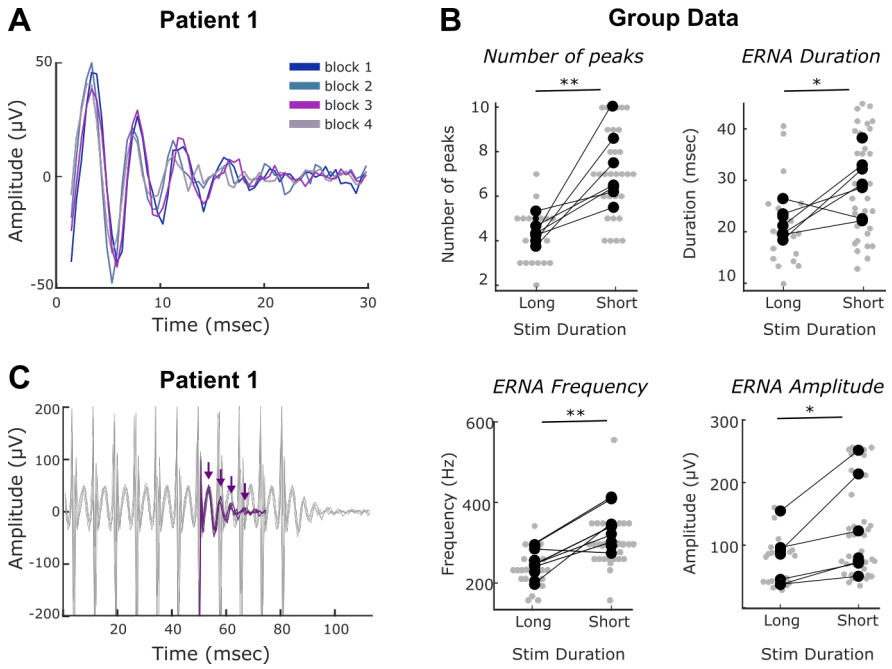


Figure 3.4. ERNA after DBS. A. The ERNA is characterised by a series of high frequency waves following cessation of stimulation (time 0). These waves progressively diminish in amplitude and frequency. Note that the first 1.5 ms (starting from the peak of the stimulation artefact) have been cut to avoid any contamination by the stimulation artefact. The ERNA observed after the four long blocks of stimulation are superimposed. **B.** The ERNA is more marked after short than long stimulation blocks. Grey dots; all individual ERNA for all blocks and STN. Black dots: averaged values for each STN. Gray dots are the results of individual stimulation blocks. Paired t-tests, * $p<0.05$, ** $p<0.01$. **C.** ERNA after DBS superimposed on the ERNA observed during DBS.

With the exception of patients 2 and 7, the ERNA following cessation of stimulation consisted of several waves lasting longer than the inter-stimulus interval (ISI) during DBS at 130 Hz. This raises the possibility that the steady state response during stimulation reflected the temporal summation of overlapping evoked responses, where each lasts longer than the ISI (see **Figure 3.4C**).

3.3.3. Stimulation related dynamics in beta oscillations

The time–frequency plots showed a decrease in beta oscillatory activity during continuous stimulation at 130 Hz, and a delayed return of beta activity upon cessation of stimulation (labelled with "3" in **Figure 3.1C**). The suppression during and the delayed return of beta activity are consistent with previous findings (Kühn et al., 2008; Eusebio et al., 2011; Quinn et al., 2015; Whitmer et al., 2012), but the precise time-course of beta suppression once stimulation has begun has not been previously quantified. For each stimulation block, time-evolving power changes were computed in the beta frequency band (13-34 Hz) in two 30-second windows aligned to the first or last stimulation artefact (**Figure 3.5A**). To allow the comparison with the previous ERNA analysis, only the STNs showing an ERNA during stimulation were considered in the following analysis (**Table 3.2**, patients 1 to 11, n=13). However, due to the contamination of the lower frequencies by involuntary movements unequal numbers of STNs were analyzed in consecutive stimulation blocks (see **Figure 3.5A** and **Figure 3.6C**). The averaged time courses revealed a rapid and sustained suppression of beta power during DBS followed by a slower return to baseline level when DBS was switched off. The first significant reduction of beta power ($p<0.05$ after FDR correction) was observed within the first 500 ms of stimulation (including a 200 ms period in which stimulation amplitude was ramped up) in all the blocks, whereas the baseline level was on average reached 8.9 ± 2.7 seconds after cessation of stimulation.

To quantify the dynamics of the stimulation-induced changes in the beta activity and compare them across consecutive blocks we averaged the beta percentage change in shorter epochs of 10 seconds within the two previously defined time windows (**Figure 3.5B**). Linear mixed-effects modelling indicated that the initial beta suppression was similar across the four consecutive blocks ($b = 1.9$, $t_{(30)} = 1.1$, $p = 0.31$). There was a trend for beta suppression to

reduce after long and repeated stimulation but this did not reach significance (b = 2.9, $t_{(28)}$ = -2.1, p = 0.054). During the washout epoch, the linear mixed-effects modelling was not significant across blocks (b = -3.66, $t_{(27)}$ = -1.23, p = 0.23).

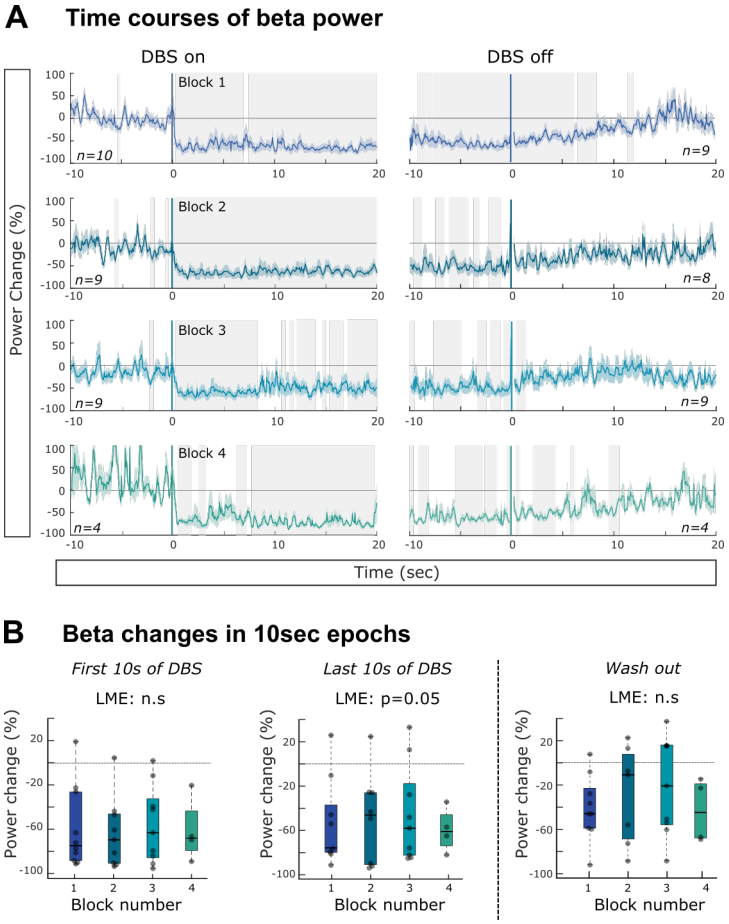


Figure 3.5. Modulation of beta power induced by DBS. A. Averaged time course of % beta power change relative to baseline (rest, without stimulation) aligned to the first (left) and last (right) stimulation artefact for four consecutive stimulation blocks. Mean ± SEM of %change from baseline power is shown. Note that, because we skipped data where movement occurred, the number of STN (given by n) included differs between windows. The periods during which the beta power was significantly different to zero are indicated by the grey shading (one sample t-test, p<0.05 after FDR correction). **B.** Comparison of averaged beta power changes in the first and last 10sec of DBS between the four consecutive blocks. Linear mixed-effects models (LME) revealed a trend for the last 10sec of DBS to differ (b = 2.9, $t_{(28)}$ = -2.1, p = 0.054).

In the three STNs showing no ERNA, either during or after stimulation blocks (see **Table 3.2** and **Figure 3.S1**), the averaged beta power was reduced during stimulation in two of them

(subject 12: averaged beta reduction of 20.1 ± 5.5 % across the 3 blocks; subject 14: 26.7 ± 0.2 %). In subject 13, there was no significant change in beta in the three stimulation blocks (averaged beta increase of 5.6 ± 4.7 % across the 3 blocks).

3.3.4. Non-frequency selectivity of DBS induced power suppression

The frequency selectivity of DBS power suppression was tested by quantifying the averaged power suppression across all blocks in three other frequency bands; alpha/theta (4-12 Hz), low gamma (35-45 Hz) and high gamma (70-90 Hz). Note that to avoid line noise, windows were selected excluding the 50 and 100 Hz bands. In addition to the beta power suppression ($t_{(11)}$ = 4.75, $p<0.001$), there was a significant decrease in low gamma power during stimulation ($t_{(11)}$ = 3.86, p = 0.003, **Figure 3.6A**). Based on these results we decided to explore the temporal evolution of power changes in this frequency band with the same procedure as for the beta band. When signals were aligned to the start of the stimulation, we observed an abrupt reduction in low gamma power, starting after 125 to 375ms across the four stimulation blocks and maintained throughout the entire stimulation (**Figure 3.6C**). The averaged initial power suppression was similar between the four stimulation blocks (b = 2.8, $t_{(30)}$ = 1.1, p = 0.27), as was the averaged power suppression in the last 10 seconds of stimulation (b = 0.8, $t_{(28)}$ = 0.73, p = 0.47, **Figure 3.6B**). Thus, when DBS was switched on the low gamma power was rapidly suppressed, as previously observed for beta power. The two frequency bands however showed different patterns when DBS was switched off. As illustrated in **Figure 3.6D**, after cessation of the stimulation, low gamma power returned faster to its baseline level, showing a slight overshoot (3.8 ± 0.9 seconds across all blocks and sides), than beta power (8.9 ± 2.7 seconds, Wilcoxon signed-rank test; Z = 33, p = 0.039).

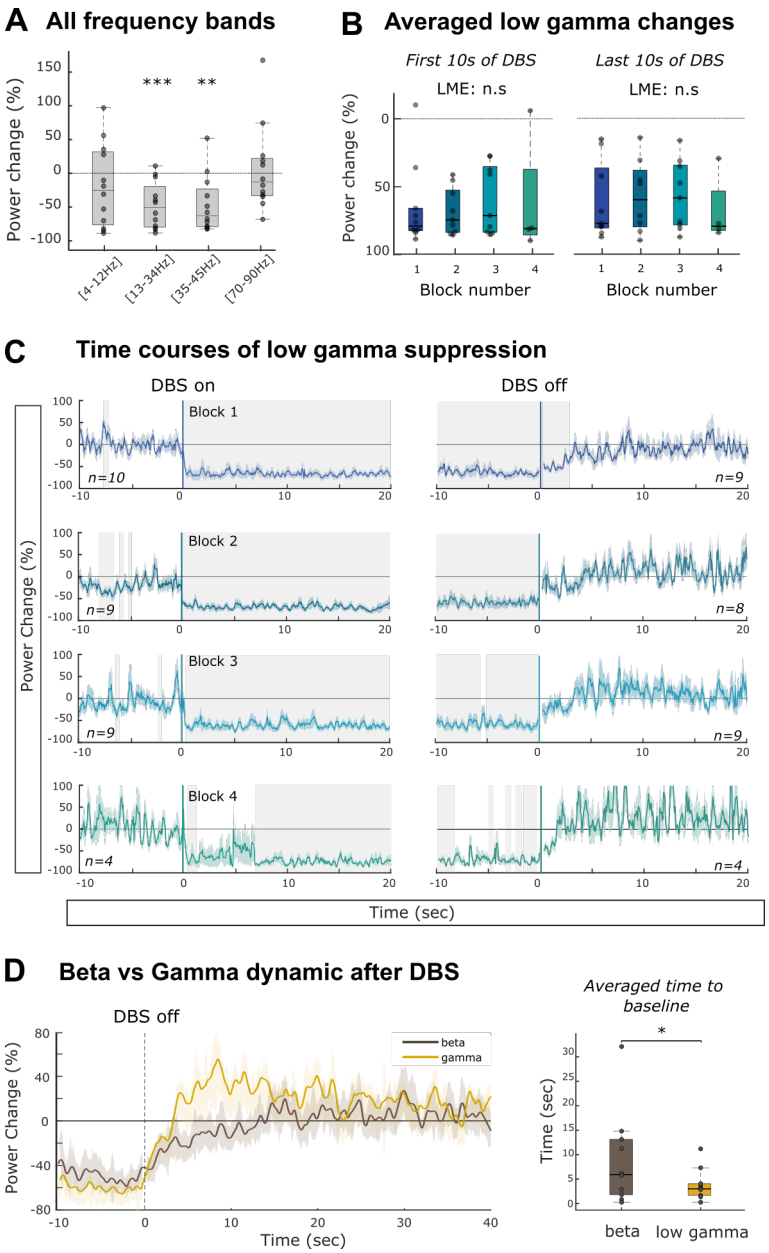


Figure 3.6. DBS modulation of LFP in other frequency bands. A. Averaged power changes in the four frequency bands. One sample t-test, ** $p<0.01$, *** $p<0.001$. **B.** Averaged low gamma power changes in the first and last 10sec of DBS. Both are similar across the four stimulation blocks (linear mixed-effects models, LME, $b = 3.0$, $t_{(33)} = 1.3$, $p = 0.21$ and $b = 0.2$, $t_{(23)} = 0.14$, $p = 0.89$). **C.** Averaged time course of low gamma power aligned to the first (left) and last (right) stimulation artefact for four consecutive stimulation blocks. Note that, because we skipped data where movement occurred, the number of STNs (given by n) included differs between windows. The periods during which the low gamma power was significantly different to zero are indicated by grey shading (one sample t-test, $p<0.05$ after FDR correction). **D.** Comparison of power recurrence after cessation of DBS. *Left:* averaged group dynamics of spectral signals. *Right:* Power recurrence to baseline across spectral components. Wilcoxon signed rank test, * $p<0.05$.

3.3.5. Dynamics in high frequency oscillations (HFO)

The ERNA elicited by stimulation occurs in the same frequency range as HFO (200-400 Hz). As suggested by the time frequency plot of patient 5, the HFO activity seemed to decrease in frequency during DBS (**Figure 3.1C**, label 4). To test the modulation of this high frequency activity we identified the HFO frequency peak in the absence of stimulation (to avoid contamination by the ERNA, see methods) in five 20-second time windows; one during the baseline, two immediately following long duration blocks of DBS, and two at the end of the resting periods between such blocks (**Figure 3.7A**). Note that only the first two DBS blocks were considered to keep enough data points across all the tested STNs (n=13 STNs) as 2 patients performed only two long duration stimulation blocks. A clear HFO peak was found in the baseline period in six STNs (five patients), with a peak frequency of 242.5 ± 2.8 Hz, significantly less than the initial ($t_{(5)} = -30.8$, $p<0.001$) or steady state frequency of the ERNA ($t_{(5)} = -5.26$, $p = 0.033$). The peak frequencies of these HFO were significantly modulated across the five different time windows ($b = -5.1$, $t_{(26)} = -2.82$, $p = 0.01$, **Figure 3.7B**). After the first stimulation block, the HFO frequency was found to be significantly decreased compared to baseline (OFF1: $t_{(5)} = 4.85$, $p = 0.005$), before increasing again and reaching a frequency close to baseline in the last 20 seconds of the resting period without stimulation ($t_{(5)} = 1.8$, $p = 0.13$). This pattern was also observed after the second stimulation block with an initial reduction of the HFO frequency compared to the baseline ($t_{(5)} = 4.89$, $p = 0.008$) or the end of the previous rest period ($t_{(5)} = 3.67$, $p = 0.02$). Again, over the following rest period the HFO peaks increased in frequency ($t_{(5)} = -5.6$, $p = 0.005$) without, however, reaching the frequency observed during the baseline ($t_{(5)} = 3.44$, $p = 0.026$). Note that some authors describe two HFO peaks (Özkurt et al., 2011), one centred around 250 Hz and another at higher frequencies, with the latter peak preferentially occurring after treatment with levodopa. We did not detect a peak at higher frequencies when not stimulating, as our patients were recorded off medication.

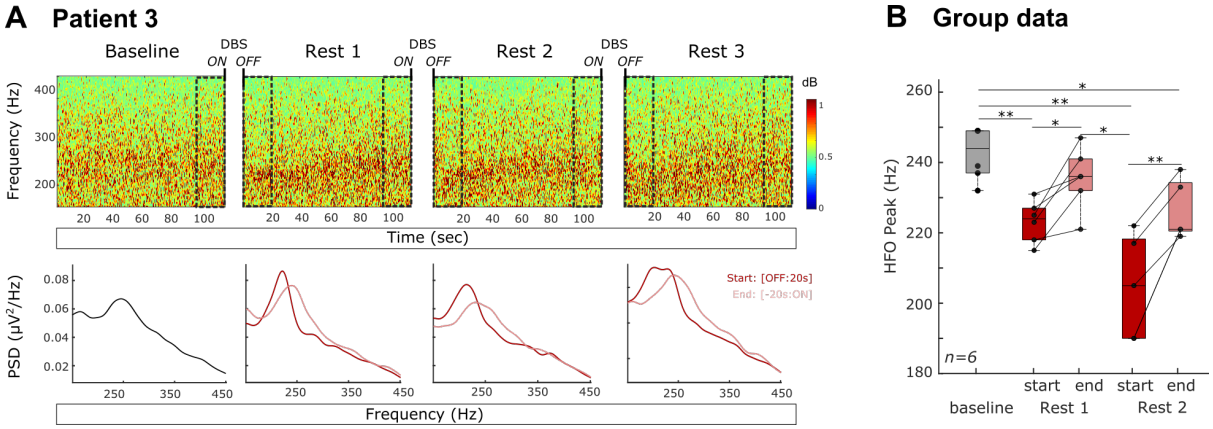


Figure 3.7. Modulation of HFO by DBS. A. Time frequency plots of the baseline and the 3 resting periods between long duration stimulation blocks in the HFO frequency range for one patient. Power spectral densities were computed in 20 sec windows as indicated by the dashed rectangles and either followed cessation of stimulation (OFF: 20s) or preceded stimulation (-20s: ON). **B.** HFO peaks are significantly different between the baseline and the two first resting periods (b = -5.1, $t_{(26)}$ = -2.82, p=0.01). Following paired t-test with FDR correction, *, p<0.05, ** p<0.01.

3.3.6. Clinical correlations

As previously reported (Neumann et al., 2016a), we confirmed the correlation between normalised baseline beta power and the contralateral UPDRS motor hemibody score OFF medication assessed pre-operatively (r = 0.67, p = 0.024; see **Figure 3.8**). In addition, there was a trend towards a significant correlation between baseline beta power and the UPDRS difference between OFF-ON medication (r = 0.58, p = 0.06). In a further exploratory analysis we correlated the different ERNA parameters with the pre-operative contralateral motor UPDRS scores. This revealed a significant positive correlation between the time taken for the ERNA amplitude to reach steady state and both the UPDRS score OFF medication (r = 0.58, p = 0.037) and the difference between UPDRS OFF and ON (r = 0.62, p = 0.024; see **Figure 3.8**). For both the beta power and the ERNA parameters, no significant correlation was observed with the ipsilateral motor UPDRS scores.

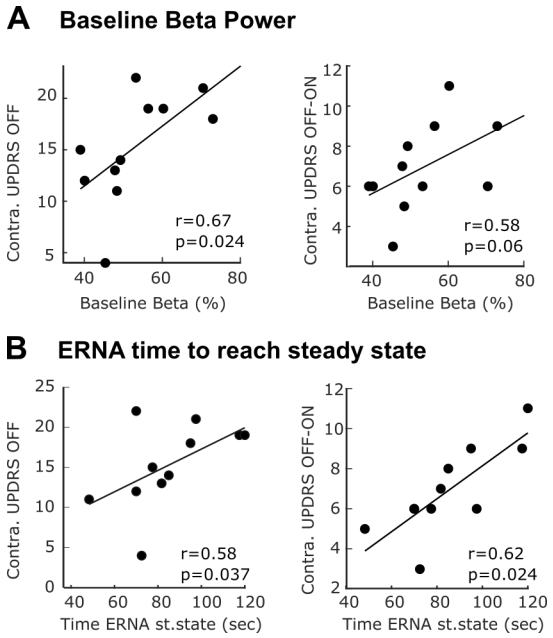


Figure 3.8. Clinical correlations. A. Correlation between normalised baseline beta power and both the contralateral UPDRS Part III motor hemibody score OFF and the difference between OFF and ON medication state. Spearman correlation. Black dots; individual STN. **B.** Similar correlation with the time to reach the ERNA steady state amplitude. Diff: difference between UPDRS OFF and ON medication state.

3.4. Discussion

Here we analyse and contrast the evoked and induced changes in STN activity in response to DBS of this target. The evoked response or ERNA recorded during high frequency stimulation is known to initially increase in amplitude at the start and then to decrease in both frequency and amplitude over the course of a 60-90 s block of stimulation (Sinclair et al., 2019b). Here we describe these dynamics in greater detail, demonstrating that steady state frequency and amplitude are reached after a minute or so of stimulation, and show a previously unreported further diminution of maximal ERNA amplitude when long duration blocks of stimulation are repeated. When stimulation ceases, or more generally when stimulation frequency is low enough, the ERNA is exposed as a series of waves of diminishing amplitude (Sinclair et al., 2018a, 2019b). Here we show that these waves last longer after cessation of short periods of stimulation than after longer periods of stimulation. In contrast, DBS rapidly suppresses beta

and low gamma band activity in the STN LFP and steady-state levels are thereafter relatively maintained during stimulation. In addition, the frequency of HFO in the STN is below that of the ERNA, and is further reduced during DBS.

3.4.1. Origin of the ERNA

The ERNA consists of high amplitude and brief waves of local activity time-locked to and evoked by stimulation pulses. One possibility raised by the evoked nature of the ERNA is that it is due to axonal stimulation of inputs to the STN and is an analogue of the fibre volleys measured *in vitro*, or compound action potentials measured *in vivo*, or, related to this, it represents the post-synaptic response to synchronised fibre volleys. Compound action potentials in the STN due to orthodromic axonal stimulation of afferents have onset latencies of a millisecond or so (Gmel et al., 2015), and would have been obscured by the stimulation artefact and relatively low sampling rate in our study. However, longer latency compound action potentials may also be recorded in the STN and may reflect recurrent discharge due to antidromic stimulation of the cerebral cortex through the hyperdirect pathway (Gmel et al., 2015; Johnson et al., 2020; Miocinovic et al., 2018a; Walker et al., 2012), or possibly of recurrent discharge due to stimulation of more local targets like the globus pallidus (Ramirez-Zamora et al., 2020). In support of an origin of the ERNA related to synchronised fibre volleys or the subsequent post-synaptic response to them, both are reported to diminish in amplitude and increase in latency during prolonged high frequency stimulation, due to the effects of progressive axonal and synaptic failure (Rosenbaum et al., 2014; Steiner et al., 2019). Short-term synaptic depression during high frequency stimulation is mediated by decreased presynaptic calcium influx, desensitisation and saturation of postsynaptic receptors and fewer release-competent vesicles (Schneggenburger et al., 2002). While the readily releasable vesicle pool and recycling pool in the presynapse are exhausted within milliseconds to seconds, the reserve vesicle pool is released during unphysiological high-frequency stimulation with slower

release kinetics and can last for tens of seconds to minutes. One possibility therefore is that the initial increase in ERNA amplitude relates to the short-lived increase in synaptic release or post-synaptic potentiation during high frequency stimulation, and the progressive relative exhaustion of the reserve vesicle pool thereafter accounts for the drift to steady-state of the ERNA at lower amplitude and frequency (Denker and Rizzoli, 2010; Rizzoli and Betz, 2005a). This hypothesis is supported by the observation that the progressive diminution of ERNA frequency and amplitude is absent when stimulation is applied at only 20 Hz (Sinclair et al., 2019b), as diminution of the reserve vesicle pool only occurs with high frequency stimulation (Rizzoli and Betz, 2005a).

The above, however, does not explain the repetitive nature of the ERNA unless it is assumed that the response to stimulation of the hyperdirect or indirect pathways is repetitive. Another possible mechanism for the ERNA is that it reflects an exaggeration of the network responsible for spontaneously occurring HFO at rest (Sinclair et al., 2019b). However, the HFO in our series had a lower initial frequency than the ERNA, was driven to an even lower frequency, distinct from that of the ERNA, during long duration stimulation and was only present in less than half of cases demonstrating the ERNA. In contrast, though, Sinclair et al (2019b) reported that the median HFO peak frequency immediately post-DBS shared the same frequency as the ERNA during clinical stimulation.

3.4.2. Dynamics of the ERNA during and after DBS

A particular focus of the current study were the frequency and amplitude dynamics of the ERNA. The cessation of stimulation reveals that the ERNA consists of a series of oscillations at a similar frequency to the steady state oscillation during stimulation, but of diminishing amplitude. Such ‘ringing’ is suggestive of an underdamped resonance, although it is possible that each wave is an independent evoked component. During continued stimulation, after a

brief amplitude increase, there is a progressive drop in both the ERNA frequency and amplitude until a steady state is reached. Assuming resonance, the drop in frequency and amplitude would be consistent with the increasing damping of a driven oscillation that reaches and holds peak damping during the steady state recording. These two damping processes seen during and at the end of stimulation may be one-and-the-same. Thus, if stimulation is ended early, before steady state amplitude and frequency are reached, then the cessation of stimulation is followed by a ringing with a higher initial amplitude and greater number of wave cycles, consistent with reduced damping.

Two subjects did not show ringing upon termination of stimulation, although, like others, they demonstrated an evoked activity during stimulation. In these two cases we suggest that the damping process was more marked leading to critical damping of the oscillations so that these were not seen as repetitive on cessation of stimulation. More importantly, with respect to some of the potential clinical applications to be discussed later, these two cases raise the possibility that a multiphasic ERNA may not be consistently seen during chronic DBS.

Although a damped resonance might describe the neural network behaviour it does not define the underlying mechanisms. We suggest that damping might be due to the effects of relative axonal failure and synaptic depression discussed above (Rosenbaum et al., 2014; Steiner et al., 2019). Even so the nature of the resonance that is damped is unclear. The correlation between the time for the ERNA to reach steady-state and the severity of contralateral motor impairment off medication might suggest that resonance is stronger when the Parkinsonian state is worse. The correlation between the time for the ERNA to reach steady state and the degree of improvement possible with levodopa might further suggest that resonance is exaggerated by dopaminergic under activity. A key question is whether the time taken to establish damping of the evoked response may be related to the time taken for the development of clinical DBS

effects. This would necessitate frequent probing of motor function over the first minute or two after stimulation onset; data that is not available in the literature.

3.4.3. Dynamics of background activities in response to DBS

Beta band oscillations in the STN LFP occur spontaneously, without the need for extrinsic stimulation (Peter Brown et al., 2001). Their amplitude is one to two orders of magnitude less than that of the ERNA suggesting that, although post-synaptic in origin, they represent either a far less tightly synchronised activity in time, a sparser synchronisation in space, or both. This synchronisation is coupled to cortical activity at the same frequency, but lags this by about 20 ms, and is diminished by voluntary movement (Oswal et al., 2013). Beta amplitude in the STN correlates with pre-operative assessments of motor impairment (Neumann et al., 2016a), as confirmed here. Gamma band oscillations in the STN LFP are also recorded at rest, but are of even smaller amplitude, tending to be increased as a broad band activity during voluntary movement. This increase during movement has led to speculation that they are somehow involved in the coding of movement (Oswal et al., 2013).

The dynamics of the response to the continuous 130 Hz stimulation of the STN differed between the ERNA and beta-low gamma activity. The ERNA, or its damping, evolved slowly as stimulation was maintained or repeated, whereas beta and gamma oscillations responded rapidly. These contrasting dynamics argue for differences in underlying mechanisms, with the rapid suppression and recovery of the beta and low gamma activity suggesting that this might be due to the more direct desynchronising effects of high-frequency stimulation. These may reflect chaotic desynchronisation (Wilson et al., 2011), or the driving of afferents to STN at high frequency, which supplants or over-rides pathological inputs at lower frequency (Birdno and Grill, 2008; Hashimoto et al., 2003; Moran et al., 2011). Both are physical phenomena that may be able to establish themselves and desynchronise population activity over relatively few

stimulation cycles. The recovery of beta activity following cessation of stimulation was, however, slower, as previously reported (Bronte-Stewart et al., 2009; Andrea A Kühn et al., 2008), and might reflect the time taken for synchronisation to be re-established at the network level. The time course of beta recovery was similar to that reported for the acute return of bradykinesia and rigidity (Bronte-Stewart et al., 2009; Kühn et al., 2009; Levin et al., 2009), but there are additional slower recovery dynamics likely in rigidity, tremor, axial impairment and postural instability (Koop et al., 2006; Shivitz et al., 2006; Temperli et al., 2003; Vaillancourt et al., 2006). Whether the decrement in maximal ERNA amplitude following repeated long duration blocks of high frequency stimulation relates to some of these slower symptom modulations seen with DBS requires further investigation.

3.4.4. Implications and applications of evoked and induced responses to DBS

The differing dynamics between the ERNA and beta activity have implications with regard to their use as feedback signals in adaptive DBS. Specifically, the rapid response of beta activity to the onset and offset of stimulation means that it can be used to target beta bursts in the STN (Little et al., 2013, 2016b, 2016a; Tinkhauser et al., 2017a; Velisar et al., 2019). These are increasingly reported to play a key role in the mechanism of bradykinesia and rigidity in PD (Deffains et al., 2018; Tinkhauser et al., 2020, 2017a, 2017b; Torrecillos et al., 2018). The ERNA does not provide direct feedback relevant to beta bursts and undergoes relatively slow changes with respect to the duration of stimulation. The ERNA could potentially better subserve more slowly responsive control algorithms (Arlotti et al., 2018; Rosa et al., 2017a). Both the ERNA and beta activity may be of additional value in localising the dorsal ‘motor’ region of the STN during surgery (Sinclair et al., 2018a; Thevathasan et al., 2020; Zaidel et al., 2009), although it is possible that the former may be particularly well suited to this as, in one case it remained despite general anaesthesia (Sinclair et al., 2018a). In addition, both activities

may facilitate prediction of the optimal contact for stimulation following surgery (Chiung Chu Chen et al., 2006d; Ince et al., 2010; Sinclair et al., 2018a; Thevathasan et al., 2020; Tinkhauser et al., 2018; Yoshida et al., 2010).

The suppression of low gamma activity by DBS is interesting as this activity is thought to help encode voluntary movements. Accordingly its suppression by DBS may point to the non-specificity of this intervention and help explain some of the motoric deterioration that may complicate DBS. This is most clearly seen in isolated cranial dystonia patients, when high frequency stimulation of the pallidum can cause paradoxical motor deficits (Berman et al., 2009; Blahak et al., 2011; Huebl et al., 2015; Wolf et al., 2016). However, stimulation of the STN may also cause motor deficits. For example, this may be the case in verbal fluency, which is impaired by DBS (Parsons et al., 2006), and has been specifically linked to increased subthalamic gamma activity (Anzak et al., 2011). It may also help explain the modest impairments in limb motor function in PD patients who otherwise perform well when not stimulated, i.e. those subjects who have relatively good background motor performance at the time of testing (Chiung Chu Chen et al., 2006a). The latter may also contribute to the impairment of swimming ability during STN DBS that has been recently highlighted (Waldvogel et al., 2020). Finally, the possibility should be acknowledged that the DBS induced suppression of LFP activity spread to even higher frequency bands than the low gamma range, but was masked by a coincidental rise in the noise floor of the amplifier during stimulation.

These considerations are important as they argue that patients may potentially never be able to achieve their optimal performance during conventional continuous DBS, which might be relatively indiscriminate in its effects on spontaneous oscillatory activity, and affect both pathological and physiological oscillations. Such observations help motivate the development of adaptive DBS approaches which partially spare residual physiological processing in the subthalamic nucleus by reducing the duration or intensity of stimulation (Arlotti et al., 2018;

Little et al., 2013), or by delivering phase-dependent stimulation according to neural feedback (Cagnan et al., 2017; Holt et al., 2019).

3.4.5. Limitations of the study

Our results may have been confounded by the post-operative stun effect, which is known to lower beta activity (Chiung Chu Chen et al., 2006d). In addition, we did not simultaneously evaluate clinical state during our recordings, which would be necessary to directly relate the dynamics of ERNA characteristics and of beta suppression to the dynamics of the clinical effects of DBS. This again would require a bigger cohort or the opportunity to record in chronically implanted patients to avoid confounding DBS related LFP changes with movement-related effects imposed by clinical testing. Moreover, the symmetric biphasic pulse used in the present study is not standard in clinical practice and our sampling rate of 2048 Hz might have been too low to precisely describe and follow the dynamics of the ERNA in the time domain. Finally, only 14 patients participated in our study and some of our contrasts involved small subsets of patients (see **Figure 3.5A** and **Figure 3.6C**), so that these results need to be confirmed in a larger series.

3.4.6. Conclusions

We have characterised the temporal dynamics of different responses to DBS in the STN LFP, and speculated on the phenomena that may underlie these changes. In particular, the relatively slow development of damping evident in the ERNA after stimulation onset raises the possibility of an underlying progressive axonal and synaptic failure. Conversely, the very rapid onset of beta suppression following DBS onset may reflect more direct desynchronising effects of high-frequency stimulation. Notwithstanding the underlying mechanisms, the different temporal

dynamics exhibited by evoked and induced activities in response to stimulation may impact on their use as feedback signals in adaptive DBS.

3.5. Summarised Findings

- ERNA frequency and amplitude reach a steady state after ~70 s stimulation
- Beta activity is suppressed within 0.5 s by stimulation and then remains stable
- Different response dynamics provide different insights into stimulation effects
- Different response dynamics may impact how signals may be used in adaptive DBS

4. Project 2: Evoked Resonant Neural Activity in subthalamic local field potentials reflects basal ganglia network dynamics

4.1. Introduction 97
4.2. Methods 98
4.2.1. Consent, regulatory approval, patient selection and clinical details 98
4.2.2. Surgery and lead localisation assessment 100
4.2.3. Stimulation and data recording 100
4.2.4. Experimental paradigm 101
4.2.5. Signal processing 103
4.2.5.1. Signal processing: Time series-based ERNA analysis 104
4.2.5.2. Signal processing: Fast Fourier transform (FFT)-based ERNA analysis 105
4.2.5.3. Signal processing: Beta power analysis 106
4.2.6. Statistics 106
4.3. Results 107
4.3.1. Time series and FFT-based ERNA dynamics follow similar slow dynamics during stimulation 107
4.3.2. ERNA has slow dynamics after cessation of stimulation 108
4.3.3. ERNA has fast dynamics on a sub-second timescale 109
4.3.4. ERNA dynamics are modulated by different DBS frequencies 111
4.3.5. ERNA dynamics are modulated with increasing DBS intensity 113
4.3.6. ERNA dynamics are modulated by levodopa 114
4.3.7. ERNA parameters differ between continuous and adaptive DBS 116
4.4. Discussion 117
4.4.1. Time series and FFT-based ERNA reflect the same activity 118
4.4.2. Mechanisms underlying the fast and slow ERNA dynamics 119
4.4.3. The ERNA as a marker to predict the best DBS frequency and lowest effective intensity 121
4.4.4. The ERNA is modulated in PD and may become a useful marker in aDBS 122
4.4.5. cDBS and aDBS may lead to differences in the synaptic status of the cortico-subthalamic-GPe circuit 124
4.4.6. Conclusion 124
4.5. Summarised Findings 125
4.6. Summary of Key Contributions 125

This is a follow-up project on chapter 3 where we probe the ERNA under different DBS settings and speculate on its underlying mechanism. This project was published in (Wiest et al., 2023a).

4.1. Introduction

Deep brain stimulation (DBS) to the subthalamic nuclei (STN) is an effective treatment option for advanced Parkinson's disease (PD) and yet its underlying mechanisms are still a matter in dispute (Chiken and Nambu, 2016). To help unravel the intricacies of DBS, we take the approach of studying DBS-induced changes in the STN. Beta power suppression is the clearest and most robust spectral change during STN-DBS, which was linked with therapeutic effects of stimulation (Andrea A. Kühn et al., 2008; Whitmer et al., 2012). Another prominent feature of STN-DBS is evoked resonant neural activity (ERNA). The ERNA was initially reported in the time domain as a high-amplitude, high-frequency oscillation with underdamped characteristics (Sinclair et al., 2018a). In the spectrogram, the ERNA presents as a high-frequency oscillation, which decreases in frequency over the first minute of stimulation to the STN (Wiest et al., 2020). However, the link between ERNA in time and frequency domain has recently been contested (Ozturk et al., 2021). In a first step, we seek to compare the two ERNA analysis approaches to show that ERNA quantified in time and frequency domain reflect the same activity.

The ERNA has recently been suggested as a marker for intraoperative lead placement even during general anaesthesia and postoperative contact selection (Sinclair et al., 2018a; Xu et al., 2022), but it is yet unclear what the underlying mechanism is and to what extent it is modulated by dopaminergic medication or other DBS settings. It was previously shown that pallidal and STN neurons fire rhythmically and time-locked to DBS pulses (Bar-Gad et al., 2004; Hashimoto et al., 2003), which led to the information jam theory of DBS (a pathological rhythm is drowned by a physiological rhythm) and may have been a first hint at the mechanism underlying the ERNA. More recently, a computational model suggested that the ERNA may be initiated through direct activation of cortico-subthalamic fibres and subsequently sustained by reciprocal connections between the external globus pallidus (GPe) and STN (Schmidt et al.,

2020). Therefore, the ERNA may indicate the connectivity and circuit dynamics of the STN-GPe network. Here, we want to scrutinise the effects of dopaminergic medication, different stimulation frequencies, intensities and stimulation modes (continuous vs. adaptive DBS) on the ERNA. We hypothesise that these manipulations change the circuit dynamics of the cortico-subthalamic-GPe-network and therefore would lead to different ERNA dynamics.

4.2. Methods

4.2.1. Consent, regulatory approval, patient selection and clinical details

This protocol was approved by the Health Research Authority UK and the National Research Ethics Service local Research Ethics Committee (IRAS: 46576). Patients with PD were recruited for LFP recording at St. George's University Hospital NHS Foundation Trust, London, King's College Hospital NHS Foundation Trust, London, and University Medical Center Mainz. Written informed consent was obtained in line with the Declaration of the Principles of Helsinki. 27 patients with idiopathic PD undergoing bilateral STN-DBS surgery were included in the study. Patients were selected by an interdisciplinary team of movement disorder neurologists, neuropsychologists, functional neurosurgeons and DBS nurses if they met the UK Parkinson's Disease Society Brain Bank Diagnostic Criteria for diagnosis of PD (Hughes et al., 1992). The average age at the time of recording was 60.42 ± 1.22 years (mean ± SEM) with average disease duration of 10.85 ± 0.98 years. 9 patients were recorded bilaterally, resulting in a total of 36 STNs included in the study. During the recordings, an experienced neurologist was present to screen for unwanted side effects of stimulation. Clinical details are summarised in **Table 4.1**. Baseline motor function in the ON and OFF medication state were assessed pre-operatively in 25 patients and on the day of the recording in 2 patients using part III of the Unified Parkinson's Disease Rating Scale motor subscale (UPDRS-III).

Patient #	Gender (m/f)	Age (yr)	Disease Duration (yr)	UPDRS-III OFF meds (pre-OP)	UPDRS-III ON meds (pre-OP)	Predominant Symptoms	Time of Recording (days post-OP)	DBS system	STN tested (L/R)	DBS Intensity (mA)	Meds state	Skipped pulse paradigm	aDBS (paradigm 3) (L/R)	Site
1	m	54	6	51	35	tremor, bradykinesia	5	Boston Cartesia HX	L+R	L: 4 R: 3	ON	yes	no	SG
2	m	58	11	41	16	tremor, bradykinesia	5	Boston dir	L+R	L: 2.5 R: 2	ON	yes	no	SG
3	m	60	6	31	4	motor fluctuations, dyskinesia	5	Boston Cartesia X	L+R	L: 3 R: 2	ON	yes	R	SG
4	f	64	10	29	6	bradykinesia, motor fluctuations	5	Medtronic SenSight	L+R	L: 1.5 R: 1.5	ON	yes	R	SG
5	m	63	20	51	27	tremor, motor fluctuations	4	Boston Cartesia X	L+R	L: 2.5 R: 2.5	ON	yes	L+R	SG
6	f	64	7	29	8	bradykinesia, motor fluctuations	4	Medtronic SenSight	L+R	L: 2.5 R: 2	ON	yes	no	SG
7	f	67	6	60	17	tremor, bradykinesia	4	Medtronic SenSight	R	3	ON	yes	no	K
8	m	71	8	67	12.5	tremor, FOG	3	Medtronic model 3389	L	3.5	ON	yes	no	K
9	f	64	15	26	13	gait disturbance, bradykinesia, motor fluctuations	5	Medtronic SenSight	L	2	ON	yes	L	SG
10	f	66	6	16	6	tremor, bradykinesia, rigidity	5	Medtronic SenSight	R	2	ON	yes	R	SG
11	m	60	15	47	13	tremor	4	Medtronic SenSight	L	3.5	ON	yes	L	K
12	m	63	13	46	13	motor fluctuations, dyskinesia, unpredictable OFF periods	6	Medtronic model 3389	L	3	ON	no	L	K
13	f		22	48	5.5	dyskinesia, motor fluctuations	4	Abbott dir	L	3.5	ON	no	no	K
14	m	67	6	61	26	tremor	6	Medtronic SenSight	L+R	L: 3.5 R: 3.5	ON	no	L	K
15	m	65	5	34	16	FOG, motor fluctuations	4 and 5	Boston dir	L+R	L: 3 R: 2.5	ON+OFF	no	no	SG
16	m	64	13	52	21	FOG, motor fluctuations	4	Boston dir	R	2	ON+OFF	no	no	SG
17	m	53	7	23	12	tremor, bradykinesia	4 and 5	Boston dir	L+R	L: 3 R: 2	ON+OFF	no	no	SG
18	m	51	5	27	13	bradykinesia, rigidity, motor fluctuations	4	Boston dir	R	4	OFF	no	no	SG
19	m	60	15	50	30	FOG, motor fluctuations	3	Boston dir	L	2	OFF	no	no	SG
20	f	63	11	40	17	FOG, motor fluctuations	4	Boston dir	L	2	OFF	no	no	SG
21	m	47	16	71	37	rigidity, FOG, tremor	4	Boston dir	R	2	OFF	no	no	SG
22	m	53	7	38	25	tremor	5	Boston dir	R	3.5	OFF	no	no	SG
23	m	55	16	51	19	rigidity, bradykinesia	4	Medtronic model 3389	L	4	OFF	no	no	SG
24	m	69	20	37	18.5	motor fluctuations, camptocormia	n.a.	Medtronic model 3389	L	n.a.	OFF	no	no	K
25	m	61	10	24	12	akinetic-rigic with tremor	3	Medtronic model 3389	L	4	OFF	no	no	M
26	m	61	11	16	7	akinetic-rigid with motor fluctuations	2	Abbott dir	L	3.5	OFF	no	no	M
27	f	48	6	73.5	30	rigidity, dyskinesia	3	Abbott dir	R	n.a.	OFF	no	R	K

Table 4.1. Clinical and recording details. UPDRS: Unified Parkinson's Disease Rating Scale, FOG: freezing of gait, dir: directional, L: left, R: right, aDBS: adaptive deep brain stimulation, SG: St. George's Hospital, K: King's College Hospital, M: University Medical Centre Mainz, STN: subthalamic nucleus.

4.2.2. Surgery and lead localisation assessment

The surgical target was STN. DBS systems from 3 manufacturers were used (see **Table 4.1**): Medtronic Inc. Neurological Division, USA (either a quadripolar non-directional lead (model 3389) or octopolar directional lead with 1-3-3-1 configuration (SenSight^{TM})), Boston Scientific, USA (either an octopolar directional lead with 1-3-3-1 configuration (Vercise^{TM} model DB-2202) or new experimental leads with 16 contacts and either 3-3-3-3-1-1-1-1 or 3-3-3-3-3-3-1 configuration (Cartesia^{TM} X/HX)) and Abbott Inc., USA (octopolar directional leads with 1-3-3-1 configuration (Infinity^{TM} model 6172ANS)). Directional contacts were fused to form a ring contact (**Figure 4.1Aiii**). Electrodes were implanted under general anaesthesia using frame-based stereotaxy, MRI guidance and CT-fusion verification (St. George's) or during awake surgery with additional intra-operative stimulation testing (King's). The implanted leads were connected to temporary lead extensions and externalised through the left temporal or frontal scalp. Assessment of contact localisation was blinded to the electrophysiological data, by co-registration of immediate post-operative CT with pre-operative MRI using the open-source LEAD-DBS toolbox (Horn et al., 2019). Lead placement for an example patient is shown in **Figure 4.1Ai**.

4.2.3. Stimulation and data recording

Recordings were made between 2 and 6 days postoperatively (**Table 4.1**), while electrode leads were still externalised and before implantation of the subcutaneous pulse generator. Patients performed the experiments either ON dopaminergic medication and/or after overnight withdrawal as indicated in **Table 4.1**. Monopolar high-frequency stimulation was only tested at the 2 middle contacts (the 2 lowest bipolar montages in STN if Cartesia X/HX was implanted) to allow bipolar LFP recordings from the two adjacent contacts (**Figure 4.1Aiv**). A self-adhesive electrode (Pals, Nidd Valley Medical Cordon, UK) attached to the patients' back served as a reference for stimulation, which was delivered using a highly-configurable custom-

built neurostimulator. Stimuli comprised symmetric, constant-current, biphasic pulses (60 μs per phase, negative phase first). Stimulation was applied at different intensity and frequency, according to a protocol described below. LFPs were amplified and sampled at 4096 Hz using a CE-marked multi-channel amplifier (TMSi Saga, TMSi International, Netherlands) or at 2048 Hz using a TMSi Porti (TMSi International, Netherlands) and custom-written software developed using the C programming language (**Figure 4.1Aii**). The ground electrode was placed on the forearm.

4.2.4. Experimental paradigm

During the experiments, patients were comfortably seated in an armchair. We tested 3 different paradigms. Paradigm 1 was designed to test the effect of increasing stimulation intensity on the ERNA. 11 participants (15 hemispheres, Patients 1-11 see **Table 4.1**) were recorded in paradigm 1, where each of the 2 middle contacts was stimulated with increasing intensity from 0.5 mA in steps of 0.5 mA until either 4.5 mA or side effect threshold was reached (**Figure 4.1B**). Data from 2 hemispheres was excluded since no ERNA was detectable. DBS was applied continuously at 130 Hz in consecutive blocks that lasted on average 34.16 ± 1.37 s for each intensity level and were separated by resting periods of 31.96 ± 2.06 s. After paradigm 1, LFP spectrograms and waveforms were visually inspected to select the contact and current that elicited the clearest ERNA for paradigm 2 (**Figure 4.1B**, DBS intensity listed in **Table 4.1**). The same participants were recorded in paradigm 2, which helped to test the effect of stimulation frequency on the ERNA. In paradigm 2, we applied seven continuous DBS blocks at different frequencies (70, 100, 130, 150 and 180 Hz) according to the order and times indicated in **Figure 4.1C**. Both paradigms 1 and 2 were repeated using "skipped pulse DBS", where one pulse per second was skipped to increase the inter-pulse interval (IPI) and to study the ERNA in the time domain. After blocks of 'skipped' DBS, we applied ~ 20 bursts

(consisting of 10 pulses at the frequency of the previous DBS block) spaced 1 s apart to study the post-DBS ERNA (**Figure 4.2Ai**). A third paradigm was tested in 9 participants (10 hemispheres, see **Table 4.1**), where we applied blocks of continuous (243.02 ± 29.29 s) and beta-triggered adaptive DBS (aDBS, 341.51 ± 53.99 s) as described before (Little et al., 2013). aDBS was applied such that the LFP was filtered around a pre-defined beta peak at rest ± 3 Hz, rectified and smoothed (over 400 ms) in real-time. Stimulation was triggered when the amplitude of beta band activity processed as described exceeded a certain threshold with a 250 ms ramp at the start and end of each burst (**Figure 4.8A**). The threshold was defined for each hemisphere at rest such that DBS was ON for ~ 50% of the time. Paradigm 1 and 2 were recorded ON medication (see **Table 4.1**); paradigm 3 was recorded OFF medication. Data recorded for previous studies with patients OFF levodopa (patients 15 to 23 and 25 to 26) are included to investigate the effect of medication (Wiest et al., 2021, 2020). If not indicated differently, a stimulation frequency of 130 Hz was used. Data from patients 1-17 (ON meds) and patients 15-26 (OFF meds) were included for the ON/OFF medication comparison in **Figure 4.7**.

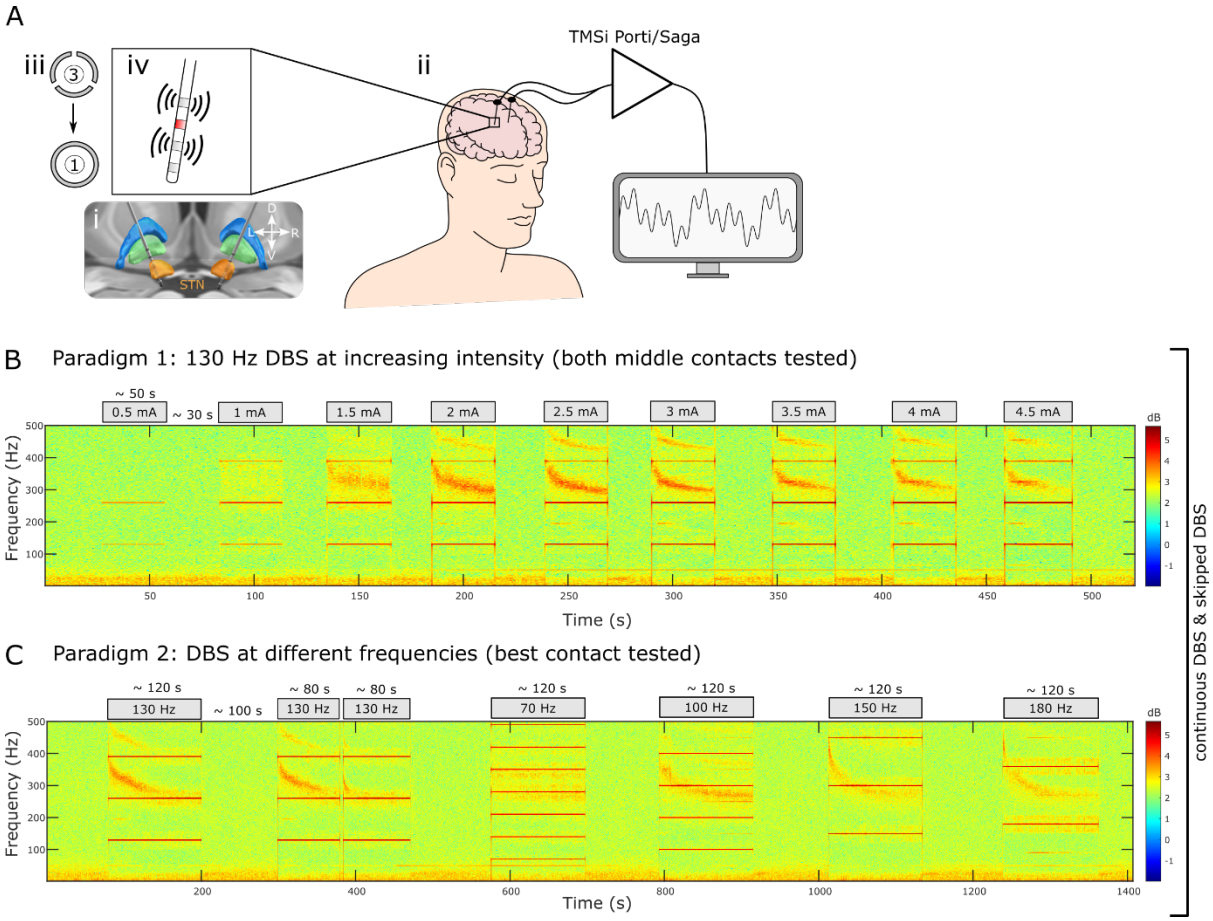


Figure 4.1. Recording setup and experimental paradigm. A. Bilateral electrodes were implanted in the subthalamic nucleus (STN) (i) and externalised (ii). Directional contacts were fused to form a ring contact (iii) and stimulation was applied to either of the two middle contact levels (red), which allowed recording from the adjacent contact levels in a bipolar montage (iv). **B.** Spectrogram of the bipolar channel that surrounds the stimulation contact (Paradigm1, shown for one example hemisphere: Patient 6 left). DBS intensity was increased in steps of 0.5 mA. **C.** The contact level and current that elicited the largest ERNA amplitudes without side effects in paradigm 1 were chosen to test the effect of different stimulation frequencies on the ERNA in paradigm 2. Both paradigms (B+C) were tested with continuous DBS and skipped DBS (1 pulse was skipped every second during DBS and after DBS blocks the ERNA was probed with bursts of 10 pulses spaced 1 second apart, see Methods).

4.2.5. Signal processing

All data analysis was performed using custom-written scripts in MATLAB (version 2020b, Mathworks, Massachusetts, USA). Continuous LFP signals were high-pass filtered at 1 Hz and notch-filtered at 50 Hz (second-order IIR notch filter). The ERNA was extracted from the time series waveform and the spectrogram.

4.2.5.1. Signal processing: Time series-based ERNA analysis

When stimulation is applied at 130 Hz, the IPI of ~ 7.7 ms only allows to study the latency and amplitude of the first ERNA peak. To do this, we removed a period of 1.2 ms after the positive deflection of the previous DBS pulse, as this was contaminated by artefact. Afterwards, we linearly detrended the signal during the IPI, applied a second-order low pass filter at 500 Hz and upsampled the IPI using a spline interpolation by factor 10. We defined the ERNA latency as the time between the previous DBS pulse (positive deflection of the artefact) and the first ERNA peak. The ERNA amplitude was defined as the absolute height of the first ERNA peak (as ERNA latencies increased towards the end of DBS blocks, the trough disappeared in some recordings, hence, we chose the absolute height of the peak to define the amplitude, **Figure 4.2Av**).

To test if the ERNA during stimulation was actually oscillatory, we skipped one DBS pulse per second during stimulation, which creates a larger window (~ 15.4 ms when DBS at 130 Hz) to study more than just the first ERNA peak (**Figure 4.2Aii**). Here, we processed LFPs during the IPI as described above and defined the ERNA frequency based on the distance between the first and second ERNA peak and the amplitude as the distance between the first ERNA peak and the next trough (**Figure 4.2Aiv**). The ERNA after bursts following the DBS blocks was analysed in a similar way (**Figure 4.2Aiii**).

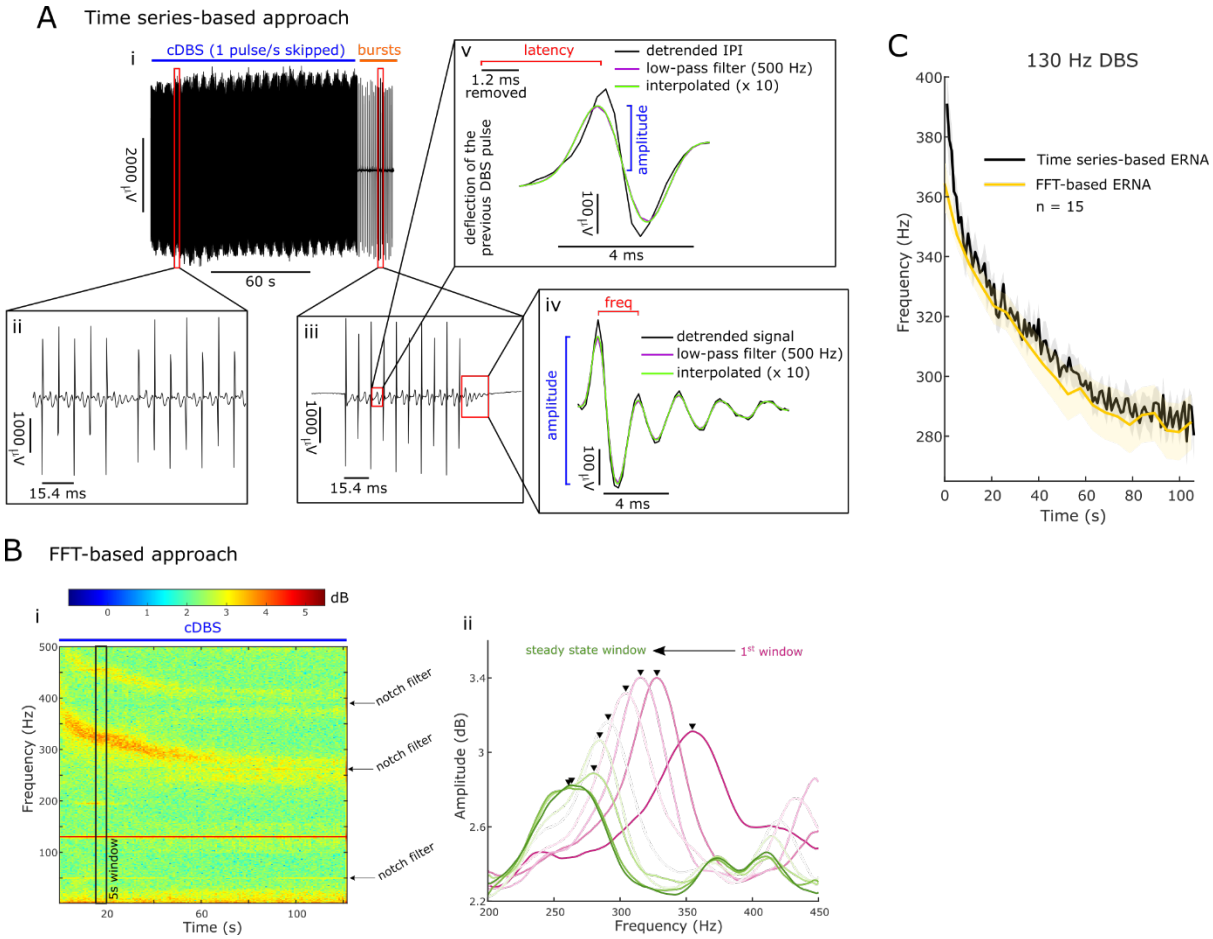


Figure 4.2. Time series and FFT-based ERNA represent the same activity. A. Skipping 1 DBS pulse per second (i) created an inter-pulse interval (IPI) that is twice as long (ii; 15.4 ms when DBS at 130 Hz). After DBS blocks, the ERNA was probed with 1 burst per second (each burst consisted of 10 pulses) for ~ 20 s (iii). This allowed us to extract ERNA frequencies and amplitudes based on the time series (iv) during and after a DBS block. In addition, we also extracted ERNA amplitudes and latencies after every pulse (v). **B.** Based on the spectrogram (short-time FFT; i), we calculated the average PSD for consecutive non-overlapping 5 s windows and tracked the ERNA as the largest peak between 200 and 450 Hz over time (ii). **C.** ERNA frequency dynamics calculated based on the time series and FFT-based approach (mean ± SEM) were not significantly different (permutation test for consecutive time points), which suggests they represent the same underlying phenomenon.

4.2.5.2. Signal processing: Fast Fourier transform (FFT)-based ERNA analysis

To compare this study with previously reported results, we also used an FFT-based approach to quantify the ERNA during continuous DBS. To this end, spectral amplitudes were estimated between 1 and 500 Hz using the short-time FFT with a window length of 1 s, 25% overlap of consecutive windows and a Hamming window as implemented in MATLAB's *spectrogram* function yielding a frequency resolution of 1 Hz (**Figure 4.2Bi**). We calculated power spectral

densities (PSD) of consecutive non-overlapping 5-s windows and tracked the largest peak between 200 and 450 Hz (as the ERNA peak) over time (**Figure 4.2Bii**). To avoid tracking harmonics of stimulation, we applied additional notch filters at 260 and 390 Hz. A similar method to quantify ERNAs in an FFT-dependent manner was used before (Wiest et al., 2020). ERNA frequency steady states were defined as in Wiest et al., 2020.

4.2.5.3. Signal processing: Beta power analysis

Power change during DBS in **Figure 4.5D** was quantified relative to a 30 s baseline period before respective DBS blocks and the following formula:

$$\%\ power\ change = \frac{DBS\ power - baseline\ power}{baseline\ power} * 100$$

for average beta (13-35 Hz) power. Thus, negative change corresponds to power suppression with stimulation and vice versa.

Beta power (13-35 Hz) recovery after DBS blocks (**Figure 4.3B**) was calculated based on the 1-s windows between consecutive bursts. For better temporal precision, we changed parameters of short-time FFT and used 500-ms windows with 50% overlap.

4.2.6. Statistics

Statistical analyses were conducted using custom-written scripts in MATLAB. To take repeated measures per hemisphere into account (hierarchical data), linear mixed-effect models were used to assess the effect of increasing DBS frequency and intensity on ERNA amplitudes and latencies. The ERNA features were set as dependent variable, the different frequency and intensity levels as fixed effects and the recorded hemispheres as repeated measures. The normal distribution of each variable and the residual were visually inspected with quantile-quantile

plots and histograms of distribution. All models were estimated by the method of maximum likelihood and included random intercept for each hemisphere to capture individual differences. Changes of ERNA features between cDBS and aDBS were analysed in a similar way (**Figure 4.8C**). To identify clusters of significant differences between time series and FFT-based ERNA or ERNA ON and OFF medication, we used non-parametric permutation tests with 1000 permutations (**Figure 4.2C** and **Figure 4.7A**). To perform paired comparisons between different medication conditions, we used a paired samples permutation *t*-test with multiple comparison correction (50,000 permutations each; **Figure 4.7C**) as implemented in Groppe, 2022. When correlations were reported, we calculated Spearman's rank coefficients because the non-baseline-transformed power data are non-normally distributed and contain outliers. Multiple statistical tests were performed in this study under FDR control at 5% using the adaptive linear step-up procedure, a modification of the original Benjamini and Hochberg procedure (see Duchet et al., 2021). This ensures that the expectation of the number of false positives over the total number of positives is less than 5% when many statistical tests are performed. All data are shown as mean ± standard error of the mean (SEM) unless mentioned otherwise.

4.3. Results

4.3.1. Time series and FFT-based ERNA dynamics follow similar slow dynamics during stimulation

A recent study suggested that high-frequency activity in the spectrogram during high-frequency DBS and evoked compound activity in the time domain were independent (Ozturk et al., 2021). Here, we directly compared the two activities in the same data set.

First, we defined ERNA frequencies based on the LFP waveform after every skipped pulse and found that their dynamics ON medication and their time to reach a steady state 75.25 ± 1.14 s are similar to the FFT-based ERNA frequency dynamics OFF medication described before

(**Figure 4.2C,** Wiest et al., 2020). ERNA frequency dynamics quantified based on the times series and FFT (n = 15 hemispheres each) did not differ significantly (paired permutation *t*-test, p > .05, **Figure 4.2C**). To corroborate the link between the ERNA calculated based on time series and FFT, we found a strong positive correlation between time series and FFT-based ERNA frequencies (Spearman; $\rho = .98$, $p < .001$) and amplitudes (Spearman; $\rho = .93$, $p < .001$). In addition to ERNA frequencies, we also quantified ERNA amplitudes over time (**Figure 4.3Aii**). ERNA amplitudes briefly increased after stimulation start before gradually decreasing to a steady state. ERNA amplitude dynamics, here shown for time series-based ERNA, are similar to what was previously shown in FFT-based ERNA (Wiest et al., 2020). In the rest of the manuscript (except **Figure 4.7A**) we focused on time series-based ERNA.

4.3.2. ERNA has slow dynamics after cessation of stimulation

To study if and how fast ERNA parameters return from steady state to baseline after DBS, which may reflect the recovery of the underlying network, repetitive DBS bursts (consisting of 10 pulses) were applied to probe the ERNA every second for ~ 20 s after continuous DBS was stopped. To reach steady state, continuous DBS was applied for 131.80 ± 5.80 s. As observed in **Figure 4.3A**, ERNA frequencies and amplitudes tended to progressively return to their starting values, following a similar time course (Spearman, $\rho = .86$, $p < .001$). The recovery of ERNA frequencies and amplitudes (and by inference the recovery of the underlying circuit) followed a similar time scale as beta power recovery (**Figure 4.3B**), as confirmed by significant positive correlations between beta power and ERNA frequencies ($\rho = .96$, $p < .001$) and ERNA amplitudes ($\rho = .89$, $p < .001$). Altogether, this suggests that these activities may reflect a related underlying process.

To confirm the slowness of ERNA dynamics, we paused continuous DBS for 5 s and hypothesised that this would be insufficient for complete recovery of ERNA parameters to baseline (**Figure 4.3C**). As predicted by **Figure 4.3A**, after pausing DBS for 5 s, both ERNA

frequencies and amplitudes only partially returned to their starting values (86.75 ± 1.58% and 87.00 ± 5.53% of the starting values for frequencies and amplitudes, respectively).

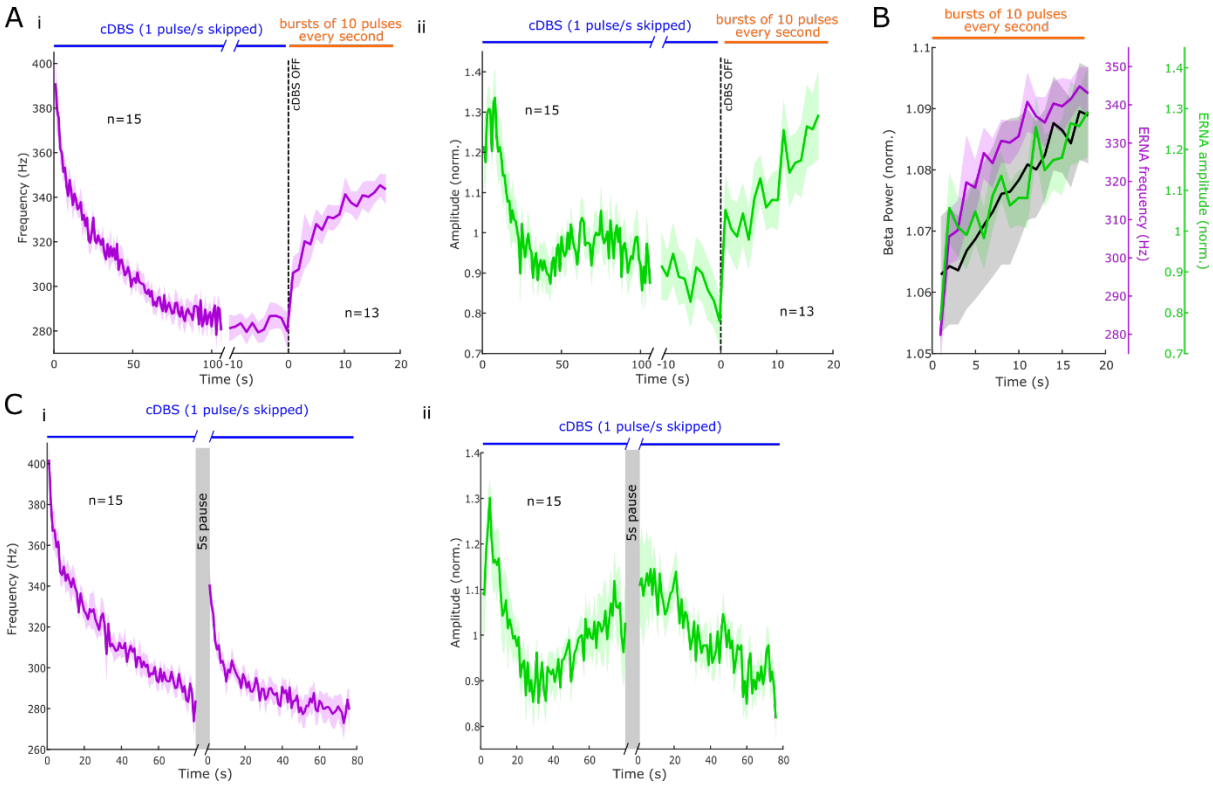


Figure 4.3. ERNA dynamics are relatively slow. A. Time series-based ERNA frequencies (i) and amplitudes (ii) during DBS initially decrease before reaching a steady state (mean ± SEM). When continuous DBS is turned off, ERNA steady state is not maintained, however, ERNA parameters need several seconds to return to baseline. **B.** The recovery of ERNA parameters and beta power after DBS happens at a similar rate. **C.** When pausing DBS for 5 s, ERNA frequencies (i) and amplitudes (ii) partially return to baseline values.

4.3.3. ERNA has fast dynamics on a sub-second timescale

Analysing the ERNA in the time domain and quantifying its parameters after every DBS pulse allowed us to investigate its dynamics on a more refined time scale. In doing so, we found that in addition to the slow frequency and amplitude dynamics described above (**Figure 4.3**), the ERNA is modulated on a much faster scale. ERNA latencies and amplitudes change within the first 10 pulses (**Figure 4.4Ai**) and ERNA latencies decrease between the first and the 10th pulse (paired permutation *t*-test, $p < .001$, **Figure 4.4Aii**).

The fast ERNA dynamics are also reflected in the changes after just a single pulse is skipped (**Figure 4.4B**). When aligned to the skipped pulse during DBS, ERNA latencies increased on

average by 9.18 ± 0.92% compared to the previous DBS pulse (paired permutation *t*-test, t = -9.35, p < .001, **Figure 4.4C+E**) while ERNA amplitudes decreased by 23.32 ± 3.97% (t = 5.78, p < .001, **Figure 4.4D+E**). After about 30 pulses (~ 230 ms) this modulation wore off and ERNA frequencies and amplitudes returned to similar levels as observed before pulses were skipped (**Figure 4.4C+D**, for one example hemisphere). These fast dynamics, observed at the sub-second timescale, happened in addition to the slow ERNA dynamics over tens of seconds to a minute (**Figure 4.3**).

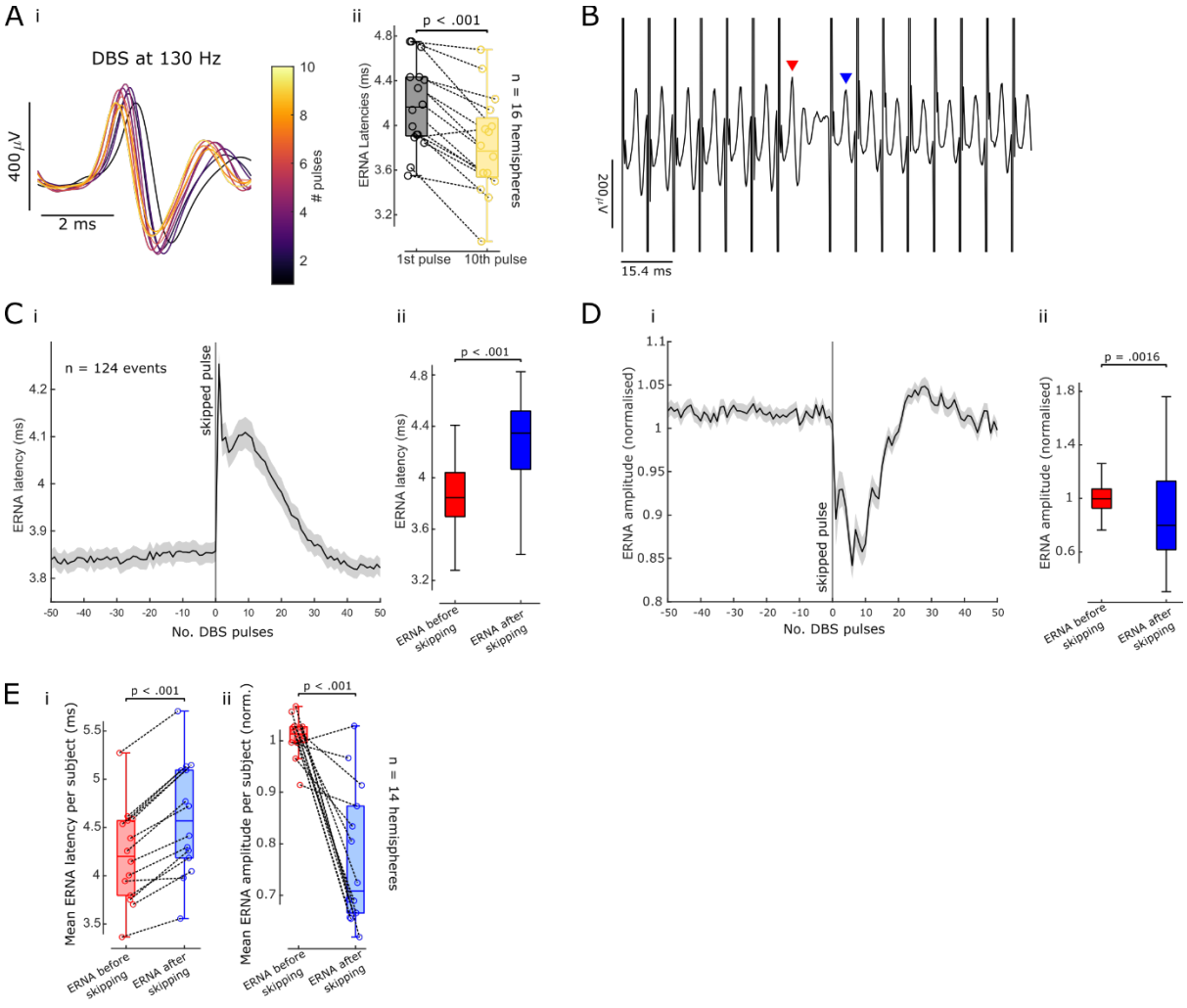


Figure 4.4. Fast ERNA dynamics. A. ERNA latencies and amplitudes change over the first 10 pulses (i, data from one example hemisphere shown). ERNA latencies decrease between the first and 10th pulse (ii, paired-sample permutation *t*-test, p < .001). **B.** Skipping a single pulse affects ERNA parameters after the subsequent pulses (example time series shown, red and blue arrowheads denote the ERNA events that were analysed in C-E). **C.** ERNA latencies were aligned to the skipped pulse (mean ± SEM) over 124 events in one example hemisphere (i). ERNA latencies increase after skipping a single pulse in this subject (ii). **D.** ERNA amplitudes were aligned to the skipped pulse as in C (i). ERNA amplitudes decrease after skipping a DBS pulse (ii). **E.** When skipping one DBS pulse, average ERNA latencies

increase (i, paired-sample permutation *t*-test, $p < .001$, n = 14 hemispheres), while average ERNA amplitudes decrease (ii, $p < .001$).

4.3.4. ERNA dynamics are modulated by different DBS frequencies

The above analyses focused on DBS at 130 Hz. To assess the impact of different DBS frequencies on slow and fast ERNA dynamics, we additionally applied stimulation at 70, 100, 150 and 180 Hz and analysed the ERNA in the time domain. First, we studied the slow ERNA dynamics over 2-min blocks of continuous DBS (**Figure 4.5A**). While ERNA frequencies were not significantly different at the start of the stimulation block across the 5 tested DBS frequencies, they diverged after ~ 20 s and stayed different until the end of the stimulation block. DBS at higher frequencies (150 and 180 Hz) led to lower ERNA frequency steady states compared to DBS at lower frequencies. ERNA amplitude dynamics at different DBS frequencies were more heterogeneous with most prominent modulation at 180 Hz.

Second, we investigated the effect of different DBS frequencies on the fast ERNA dynamics during the first 10 pulses (**Figure 4.5B**). The ERNA latency difference between the first and 10^{th} pulse increased from 70 to 180 Hz (**Figure 4.5Ciii**; LME: estimated effect of frequency = $9.69*10^{-5}$, $t = 5.11$, $p < .001$), whereas the ERNA amplitude difference between the same pulses did not differ across DBS frequencies (**Figure 4.5Civ**; LME: estimate = 4.75, $t = 0.77$, $p = .44$ from 70 to 130 Hz and estimate = -8.65, $t = -1.50$, $p = .14$ from 130 to 180 Hz). The mean latency of the ERNA peak after the first 10 pulses gradually decreased with rising DBS frequency (**Figure 4.5Ci**; LME: estimate = $-5.65*10^{-5}$, $t = -4.27$, $p < .001$), and the mean amplitude of the first 10 ERNA peaks increased from 70 to 130 Hz (**Figure 4.5Cii**; LME: estimate = 15.21, $t = 2.33$, $p = .024$) and decreased from 130 to 180 Hz (LME: estimate = -13.19, $t = -3.35$, $p = .0016$).

To put the frequency-dependent effect of fast ERNA dynamics into context, we analysed the effect of increasing DBS frequencies on beta (13-35 Hz) power suppression (**Figure 4.5D**). To this end, we calculated beta power change during a given DBS block relative to a 30 s baseline

period before respective DBS blocks and found that beta power suppression became more prominent as DBS frequencies were increased from 70 to 180 Hz (LME: estimate = -1.38, t = -5.24, p < .001). Beta power suppression with increasing stimulation frequency followed a similar pattern as average ERNA latencies of the first 10 pulses (**Figure 4.5Ci**), but there was no correlation between the two (Spearman, ρ = .06, p = .58).

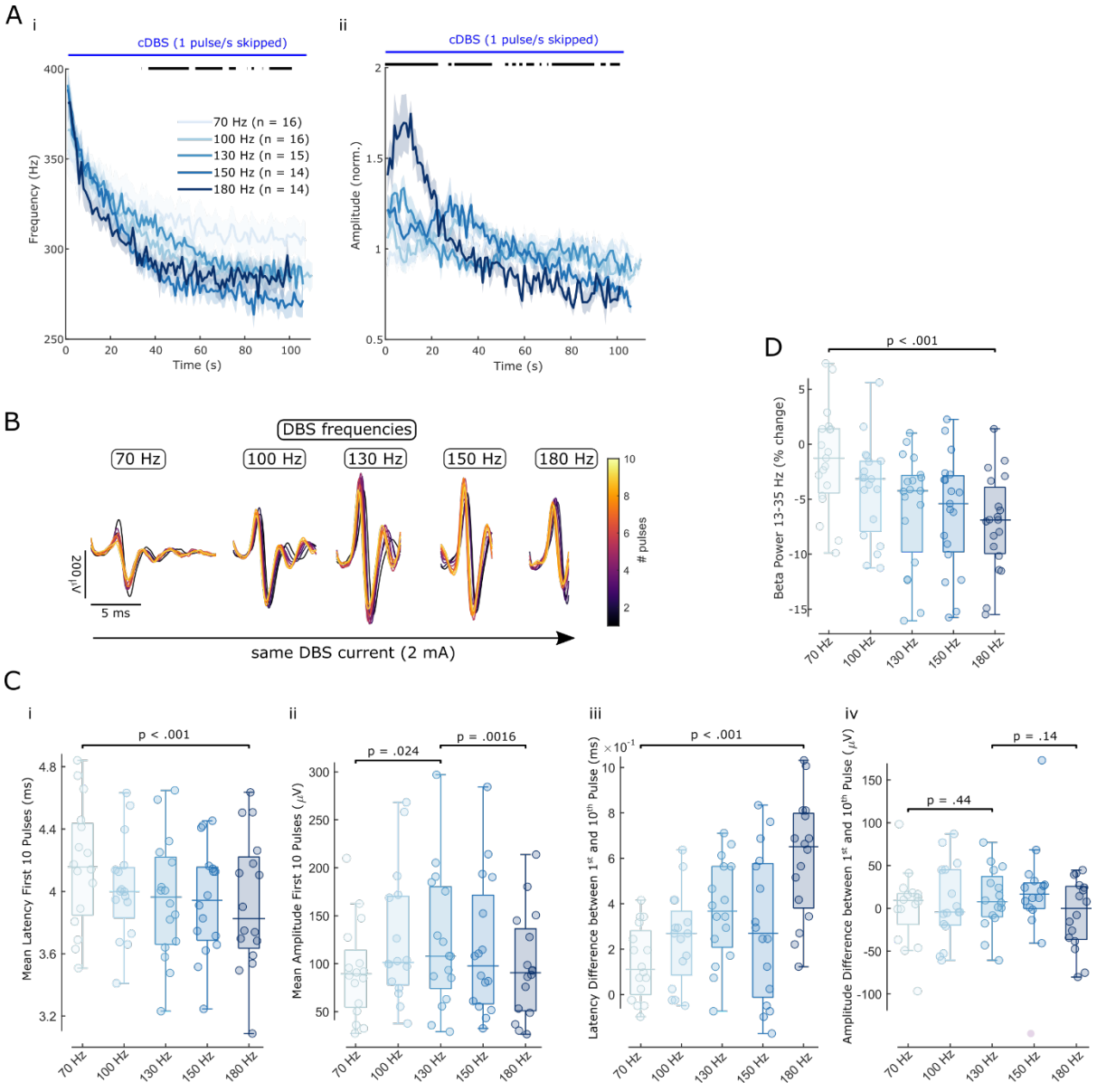


Figure 4.5. ERNA dynamics are modulated by different DBS frequencies. A. The slow dynamics of time series-based ERNA frequencies (i) and amplitudes (ii) are differently affected by increasing DBS frequencies over the first 100 s of stimulation. Bars above the plots denote significant clusters of a one-way ANOVA after multiple comparison correction. **B.** ERNA after the first 10 pulses of DBS blocks of increasing DBS frequency (shown for one example subject at 2 mA). **C.** Fast ERNA latency (i+iii) and amplitude (ii+iv) dynamics (of the first 10 pulses) are differently affected by increasing DBS frequencies. **D.** Beta power suppression during DBS relative to a 30 s baseline before the respective

blocks becomes stronger with increasing DBS frequencies. C and D show p-values of linear mixed-effect models.

4.3.5. ERNA dynamics are modulated with increasing DBS intensity

Next, we studied the effect of different DBS intensities separately for slow and fast ERNA dynamics by applying 30 s blocks of cDBS at increasing intensity. While ERNA frequencies are not significantly different between the 8 intensity levels throughout the first 30 s, there is a trend that higher intensity elicits a steeper ERNA frequency drop resulting in lower values after ~ 5 s of DBS. ERNA amplitudes tend to differ between 2-7 s after DBS was switched on with larger amplitudes when higher intensity was used (**Figure 4.6A**). This tendency disappeared with prolonged stimulation (> 15 s).

Fast ERNA dynamics were equally affected by changing the DBS intensity (**Figure 4.6B**). Mean ERNA latencies of the first 10 ERNA events decreased (LME: estimate = $-2.69*10^{-5}$, t = -2.42, p = .018) and mean ERNA amplitudes increased (LME: estimate = 23.12, t = 4.71, p < .001) when DBS intensity was increased from 1 to 4.5 mA (**Figure 4.6C**). The ERNA latency difference between the first and 10^{th} pulse was not affected by increasing DBS intensity (LME: estimate = $3.74*10^{-5}$, t = 1.37, p = .18), but the ERNA amplitude change across the first 10 pulses increased (**Figure 4.6C**; LME: estimate = 8.19, t = 2.00, p = .049).

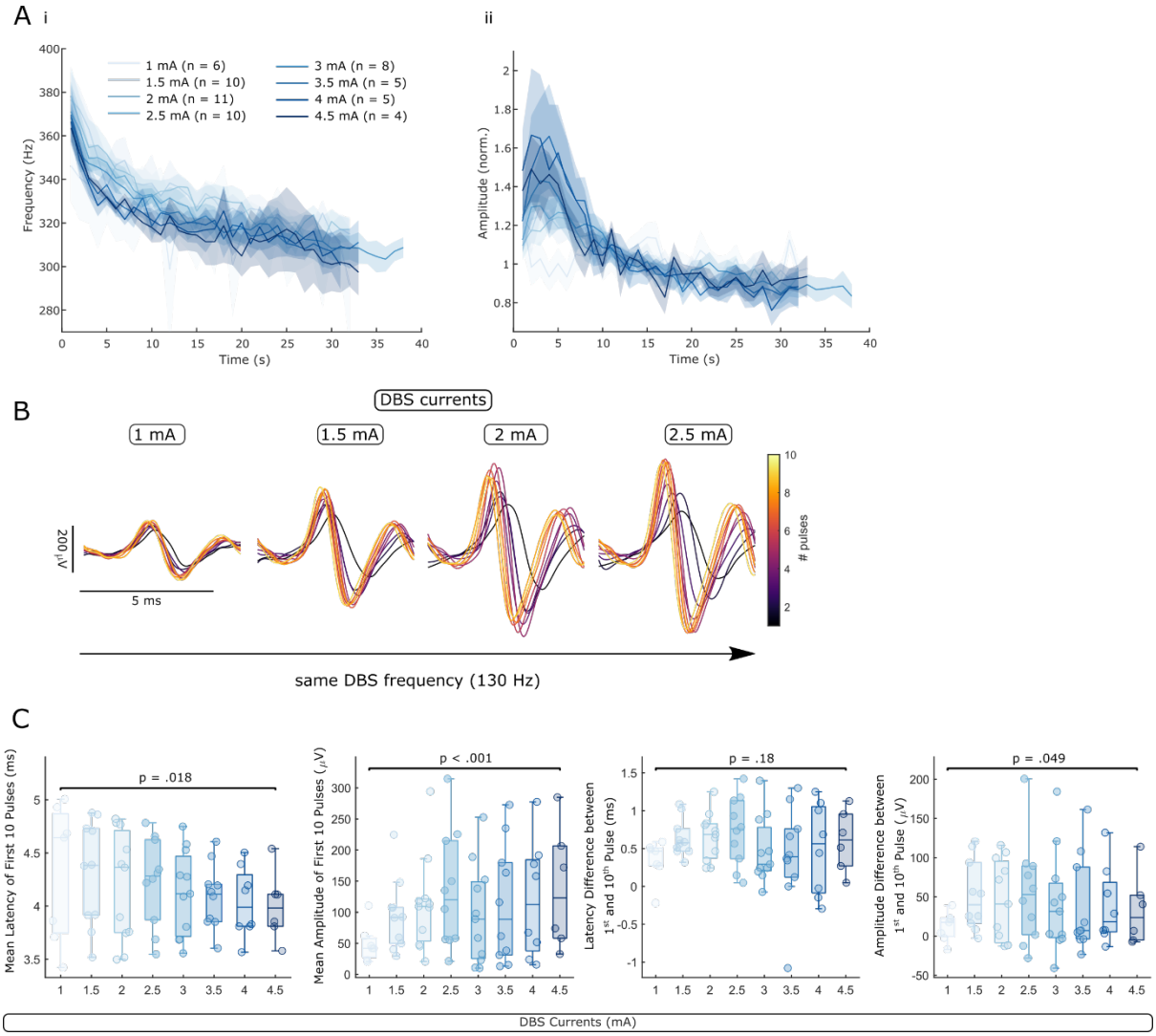


Figure 4.6. ERNA dynamics are modulated by different DBS intensity. A. The slow dynamics of time series-based ERNA frequencies (i) and amplitudes (ii) are differently affected by increasing DBS intensity over the first ~ 30 s of stimulation. After multiple comparison correction, no significant cluster of a one-way ANOVA survived. **B.** Fast ERNA dynamics are also modulated by increasing DBS intensity (ERNA after the first 10 pulses is shown for one example hemisphere). **C.** Mean ERNA latencies decrease and mean ERNA amplitudes increase with rising DBS intensity (in both cases the mean of the first 10 pulses). The ERNA amplitude difference between the first and 10th pulse increases with rising DBS currents. C shows p-values of linear mixed-effect models..

4.3.6. ERNA dynamics are modulated by levodopa

Previously, ERNA parameters were linked with beta power and by inference parkinsonian symptoms (Schmidt et al., 2020; Sinclair et al., 2019b; Wiest et al., 2020). Thus, we hypothesised that ERNA dynamics would differ with dopaminergic medication. We first studied the slow FFT-based ERNA dynamics ON and OFF levodopa during 130 Hz DBS. ERNA frequencies started at similar levels with and without levodopa, but ON medication they

tended to reach steady state faster and at a higher frequency compared to the OFF medication state, yielding a significant difference after ~ 60 s (cluster-based permutation test, p = .013, **Figure 4.7Ai**). FFT-based ERNA amplitudes did not differ between both medication states (**Figure 4.7Aii**). DBS intensities and the resting time before respective DBS blocks did not differ between both groups (**Figure 4.7B**).

Furthermore, we tested if fast time series-based ERNA amplitude and latency dynamics over the first 10 ERNA events would differ between ON and OFF levodopa (**Figure 4.7C**). Mean ERNA amplitudes of the first 10 pulses were larger ON medication (paired samples permutation *t*-test, t = 3.87, p < .001, n = 14 hemispheres) and mean ERNA latencies were lower ON medication (paired samples permutation *t*-test, t = -3.14, p = .011). To highlight fast changes within the first 10 pulses, we calculated the maximum amplitude and latency difference. The maximal ERNA amplitude difference within the first 10 pulses was larger ON medication (t = 2.38, p = 0.035), while the largest latency difference did not differ between both conditions (t = 0.41, p = .71).

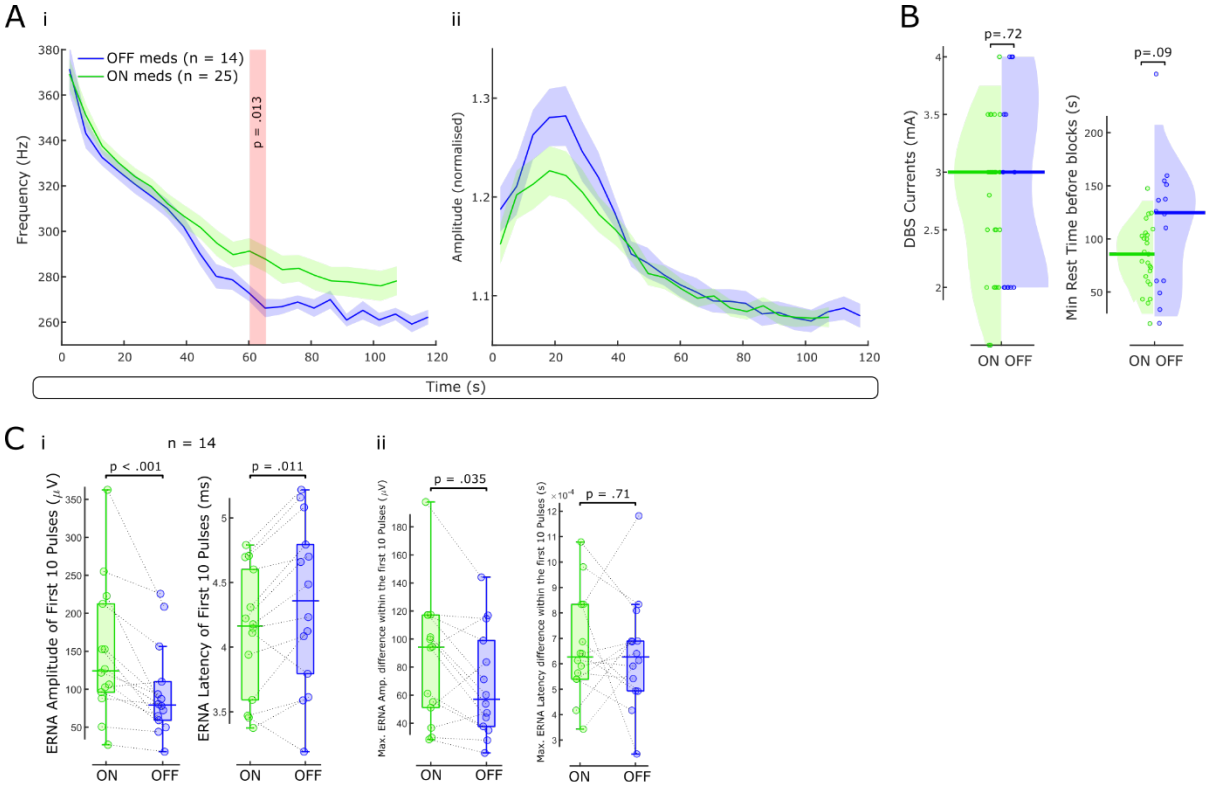


Figure 4.7. ERNA dynamics are modulated by levodopa. A. We first examined medication effects on the slow ERNA dynamics. FFT-based ERNA frequencies (i) and amplitudes (ii) are shown ON (n = 25 hemispheres) and OFF (n = 14) levodopa. **B.** DBS intensity and the rest time before DBS blocks did not differ between the ON and OFF levodopa groups. **C.** Mean ERNA amplitudes of the first 10 pulses of a DBS block (fast ERNA dynamics) are larger ON than OFF levodopa (paired samples permutation *t*-test, $p < .001$, n = 14 hemispheres). Mean ERNA latencies after the first 10 pulses are higher OFF medication ($p < .011$). The largest ERNA amplitude difference within the first 10 pulses is higher ON medication ($p = .035$); maximal ERNA latency differences across the first 10 pulses do not differ between both conditions.

4.3.7. ERNA parameters differ between continuous and adaptive DBS

Continuous and beta burst-triggered adaptive DBS were shown to be at least equally effective in the past (Little and Brown, 2020). Here, we sought to compare ERNA dynamics between cDBS and aDBS. Within the same subjects, we stimulated continuously at 130 Hz and applied blocks of aDBS (**Figure 4.8A**). aDBS was applied when the band-pass filtered (around the beta peak at rest ± 3 Hz), rectified and smoothed (over 400 ms) LFP exceeded a threshold with a ramping period of 250 ms at the start and end of each burst. Thresholds were set such that DBS was ON ~ 50% of the time at rest. Subsequently, we extracted ERNA latencies and amplitudes after every DBS pulse of cDBS and aDBS (each burst separately, see **Figure 4.2Av**).

When mean ERNA latencies of all stimulation bursts in one aDBS block were plotted in sequence, we did not observe the same dynamics as during cDBS (**Figure 4.8B**, one representative hemisphere shown), due to the discontinuous, bursting nature of the stimulation. During aDBS, each stimulation burst lasted on average for 0.83 ± 0.007 s (bursts < 500 ms were excluded from analysis due to the ramping periods) and stimulation was switched ON for 48.86 ± 4.48% of the time. We then compared average ERNA amplitudes and latencies of the first and last 10 pulses of cDBS blocks with average ERNA parameters of the first and last burst of an aDBS block. While ERNA latencies increased during cDBS from start to end (LME: estimate = 1.08, t = 5.44, $p < .001$, n = 10 hemispheres), ERNA latencies during blocks of aDBS only showed a slight increase (LME: estimate = 0.16, t = 3.01, $p = .006$; **Figure 4.8Ci**). ERNA amplitudes of cDBS decreased from start to end (LME: estimate = -71.78, t = -4.02, p

< .001), while ERNA amplitudes of aDBS were unaffected (LME: estimate = -6.81, t = -0.88, p = .39; **Figure 4.8Cii**). The resting time before blocks of aDBS and cDBS (LME: estimate = 132.04, t = 1.49, p = .15) and duration of aDBS and cDBS blocks did not differ (LME: estimate = 98.49, t = 1.45, p = 0.16).

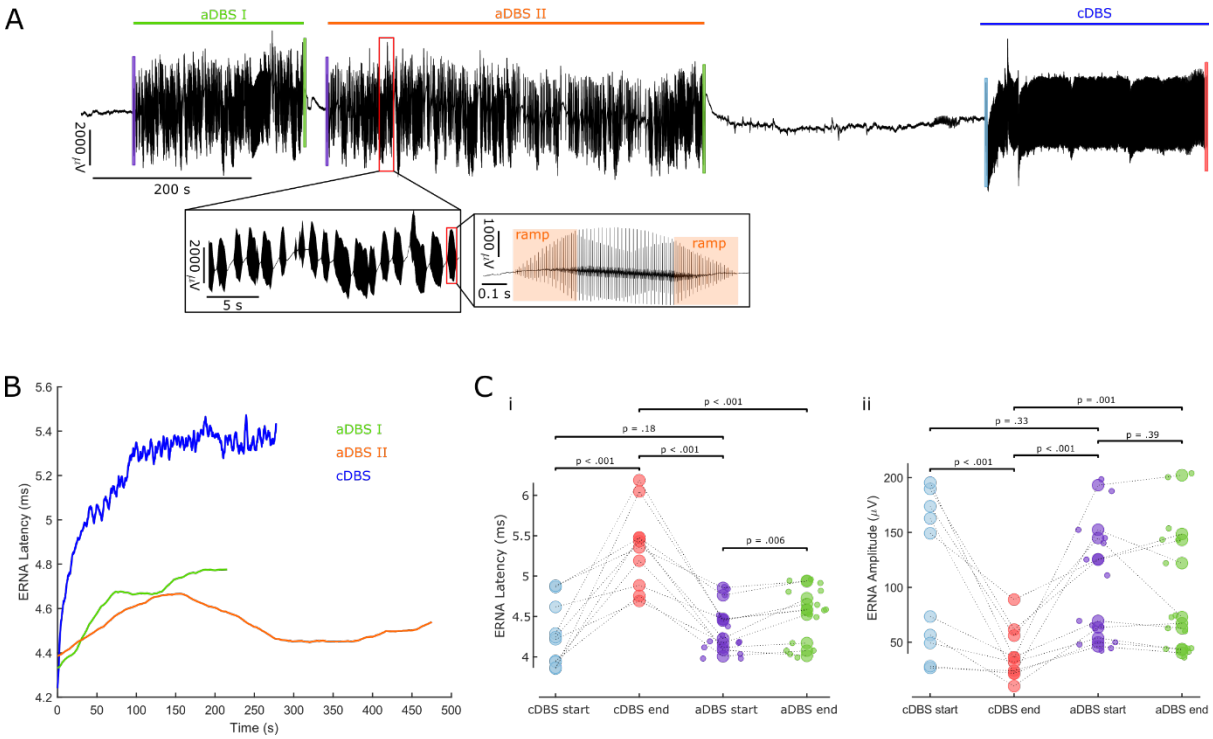


Figure 4.8. ERNA parameters differ between continuous and adaptive DBS. A. We recorded blocks of continuous DBS (130 Hz, blue) and beta burst-triggered adaptive DBS (DBS was switched on when beta activity exceeded a pre-defined threshold; green and orange) in the same subjects. The insets show a zoomed in view on DBS bursts. Note the 250 ms ramp on and off period. **B.** During cDBS, ERNA latencies and amplitudes were extracted after every DBS pulse (see Figure 2Av). During blocks of aDBS, only bursts > 0.5s were analysed and ERNA parameters were extracted after every pulse. We show ERNA latency dynamics during cDBS and aDBS (average values per burst) blocks in one representative hemisphere. **C.** ERNA latencies (i; p < .001) and amplitudes (ii; p < .001) during cDBS change from start (average of the first 10 pulses) to end (average of the last 10 pulses). Modulation with sustained aDBS is less pronounced (i; p = .006) or not present at all (ii; p = .39). (n = 10 hemispheres, small dots denote multiple aDBS blocks per hemisphere)

4.4. Discussion

In this study, we present three main findings. First, we show that the time series and FFT-based approaches are two separate ways of investigating the same activity, the ERNA. Second, we distinguish fast and slow ERNA dynamics and show how they are differently affected by DBS

frequency, intensity and levodopa, which allows for speculations on the mechanisms underlying the ERNA. Third, we show that ERNA parameters differ between sustained aDBS and cDBS, which may point towards different states of the STN-GPe loop in both conditions.

4.4.1. Time series and FFT-based ERNA reflect the same activity

Previously, FFT-base ERNA (referred to as stimulation-induced high frequency oscillations (HFO)) and time series-based ERNA (referred to as evoked compound activity) were considered independent (Ozturk et al., 2021). This is contentious as by definition every activity in the time domain must have a representation in the frequency domain and vice versa. If the time series-based ERNA was not the time domain representation of FFT-based ERNA, we would expect to see another activity in the time frequency map that better mirrors the ERNA waveform. We show in this study that both time series and FFT-based ERNA frequencies have very similar time courses during the first 100 s of stimulation, which suggests they are caused by the same underlying process (**Figure 4.2C**). In addition, we found a strong positive correlation between time series and FFT-based ERNA amplitudes (see section 3.1), which was reported before (Ozturk et al., 2021). This tight correlation would be expected if FFT-based ERNA was identical with the time series-based ERNA.

Ozturk et al. attempted to separate evoked compound activity from HFOs by removing an average template in the time domain. They subsequently performed wavelet transformation and showed that residual signal still contained HFO (Ozturk et al., 2021). However, their residual still shows persistent stimulation artefact, which suggests the denoising is not completely effective. In this study, we show that ERNA dynamics change over time and contain complex dynamics, which explains why removing a constant template will not completely remove the ERNA. Furthermore, Ozturk et al. argue that 20 Hz DBS elicits ERNA in the time domain but not in the frequency domain and therefore both activities must be independent. We argue that 20 Hz stimulation does not elicit a clear ERNA in the frequency domain because the ERNA

does not summate over consecutive DBS pulses, as it is too brief (ERNA at low frequency is damped earlier), inter-pulse intervals are too long and its amplitudes are lower. In addition, DBS at 130 Hz yields 130 separate ERNA events per second, which will result in higher amplitudes at ERNA frequency if a 1-s window is used for FFT. In comparison, 20 Hz DBS only yields 20 ERNA events per window and therefore a lower amplitude signal. Here, we show that stimulation at lower frequencies (e.g. 70 Hz) leads to a slower frequency decrease compared to higher DBS frequencies (**Figure 4.5A**). We hypothesise that the ERNA induced by stimulation at 20 Hz may not decrease in frequency at all over the first 22 s of stimulation and, hence, will not yield the stereotypical ERNA frequency drop in the spectrogram.

4.4.2. Mechanisms underlying the fast and slow ERNA dynamics

Previously, we reported the slow ERNA dynamics that reach a steady state after the first minute of cDBS (Wiest et al., 2020); dynamics that could be explained by synaptic failure (Denker and Rizzoli, 2010). Nevertheless, it was unclear whether ERNA steady state, and by inference the status of the neural network underlying the ERNA, was maintained after DBS is terminated and if so how long it would last. In this work, we corroborate the slow ERNA dynamics during DBS by analysing the ERNA in a time series-based approach and we demonstrate that ERNA frequency and amplitude steady states are not maintained once DBS is turned off. However, it takes several seconds for both parameters to reach starting values (**Figure 4.3A**). Such slow dynamics in the recovery period may be reconcilable with the time required to replenish presynaptic vesicle pools (Rizzoli and Betz, 2005b). In addition, the partial recovery of ERNA parameters during a 5-s DBS pause speaks in favour of synaptic failure as underlying these slow dynamics (**Figure 4.3C**). The different slow ERNA frequency and amplitude dynamics at different DBS frequencies and intensities could also be explained by the synaptic failure hypothesis (**Figure 4.5A+4.6A**). The higher the stimulation frequency or current, the more pulses and energy are delivered, the steeper and faster is the ERNA frequency decrease.

Accordingly, ERNA amplitude modulation was more pronounced at higher DBS frequencies and intensities.

Synaptic depletion could explain most of the above slow ERNA dynamics, but how exactly would that be the case? Recently, a computational model suggested the ERNA may be initiated by direct activation of cortico-subthalamic fibres and subsequently sustained by reciprocal STN-GPe connections (Schmidt et al., 2020). STN neurons and afferent and efferent axons in the STN may well be able to follow high-frequency stimulation for a prolonged period of time, however, synapses would most likely be depleted after a few seconds to minutes, resulting in functional disconnection of the STN from the basal ganglia network (Bergman, 2021). In that case, the ERNA could reflect STN intrinsic properties, however, the existence of functional intranuclear connectivity in STN is contentious (Steiner et al., 2019). We can further speculate on the origin of the ERNA. Direct activation of prototypic GPe terminals may lead to orthodromic activation of STN, which is likely obscured by the artefact in our recordings, and antidromic activation of GPe. GPe may then inhibit STN, yielding an ERNA deflection after ~ 4 ms, and inhibit itself. This auto-inhibition paired with its intrinsic pacemaker capabilities may produce the stereotypical ringing of the ERNA recorded in STN, which decreases in amplitude as GPe neurons become less synchronised. The ringing and time-locked firing pattern of pallidal neurons was described before (Bar-Gad et al., 2004).

In addition to the slow ERNA dynamics, we report fast dynamics at the start of stimulation (**Figure 4.4A**) and after pulses are skipped (**Figure 4.4B-E**). These fast ERNA dynamics are particularly interesting as they are modulated by levodopa (**Figure 4.7C**), and tend to be sensitive to changes in DBS frequency and intensity. We speculate that glutamate may have a modulatory effect on the ERNA. Fast glutamatergic hyperdirect pathway neurons were shown to be depressed after just a few pulses of high-frequency stimulation of the STN (Steiner et al., 2019). Medication-related differences over the first 10 pulses of stimulation could be explained

by the levodopa effect on glutamatergic firing of these neurons. Given that fast ERNA dynamics are also sensitive to changes in DBS frequency and intensity suggests that these stimulation parameters may modulate glutamatergic, hyperdirect pathway inputs in STN. In contrast, slower GABAergic neurons were shown to be able to follow high-frequency DBS at moderate levels of depression (Steiner et al., 2019). The slow ERNA dynamics over the first minute of DBS may either be explained by synaptic failure of the glutamatergic STN-GPe synapse, which may have slower kinetics than the cortico-subthalamic synapses, or progressive synaptic depletion of GPe neurons.

4.4.3. The ERNA as a marker to predict the best DBS frequency and lowest effective intensity

Previous studies suggested ERNA amplitudes as a marker for DBS contact selection (Sinclair et al., 2018a; Xu et al., 2022). Here, we observed that average ERNA amplitudes of the first 10 pulses change as a function of DBS frequency (**Figure 4.5Cii**), and are also modulated by dopaminergic medication (**Figure 4.7C**). In particular, average ERNA amplitudes of the first 10 pulses were larger ON medication compared to OFF medication and similarly, they were larger at 130 Hz, which most often yields the best clinical outcome. This suggests that ERNA amplitudes may be useful to predict the most effective frequency. These findings are consistent with previous studies showing that ERNA amplitudes increased from 5 to 130 Hz (Schmidt et al., 2020) and decreased from 130 to 180 Hz (Ozturk et al., 2021). This observation may be caused by resonance and positive interference between the ERNA and the next DBS pulse. It is possible that if the next DBS pulse is delivered during a sensitive phase of the ERNA oscillation, the next ERNA event is enhanced, while stimulation during a different phase (± 180°) might have the opposite effect (Ozturk et al., 2021). Inter-pulse intervals of 130 Hz DBS are ~ 7.7 ms long, which potentially corresponds to the sensitive period and may lead to augmented ERNA amplitudes. In the future, this will have to be tested with more granular

frequency steps. However, this theory is complicated by the fast and slow ERNA dynamics presented in this study. The latency, and therefore the phase of the ERNA, change substantially throughout DBS blocks with continuous DBS (**Figure 4.3**). Would that mean that the best DBS frequency would have to be dynamically adjusted over the first minute of stimulation until the ERNA reaches a steady state?

Previously, beta and gamma power were shown to be suppressed by high-frequency DBS and were suggested as markers for placement and contact selection (Shah et al., 2022; Wiest et al., 2020). Here, we found increasing beta power suppression, a reduction of ERNA latencies and an increasing latency difference between the first and 10th pulse while increasing DBS frequencies from 70 to 180 Hz (**Figure 4.5**). In contrast, ERNA amplitudes were not linearly modulated by rising DBS frequencies but revealed highest values at the frequency that empirically has best clinical effect. This may hint towards ERNA amplitudes as a better marker for DBS frequency selection than ERNA latencies and power suppression in the beta band.

Similar to DBS frequencies, ERNA parameters were modulated by changing DBS intensities. ERNA amplitudes increase with rising DBS intensity (**Figure 4.6A+B**), but in some hemispheres higher intensities were needed than in others to induce the same ERNA amplitudes. This likely relates to differences in placement and could be used to estimate the minimal effective DBS current. In future studies, this will have to be benchmarked against the DBS intensity used at the clinically most effective directional contact.

4.4.4. The ERNA is modulated in PD and may become a useful marker in aDBS

In the past, several attempts were undertaken to link ERNA features with parkinsonian symptoms. The time for ERNA amplitudes to reach steady state was linked with contralateral UPDRS scores (Wiest et al., 2020) and stimulation to the contact with highest ERNA amplitudes resulted in best UPDRS improvement (Sinclair et al., 2018a). Given the strong link between beta activity and bradykinesia and rigidity (Kuhn et al., 2006), other groups linked

ERNA features with beta power and by inference with parkinsonian symptoms. Beta power has been positively correlated with ERNA parameters after paired pulses (Awad et al., 2021), ERNA frequencies (Sinclair et al., 2019b) and ERNA amplitudes over the first 10 s of DBS (Schmidt et al., 2020). Here, we expand on this and report levodopa-induced changes of fast ERNA dynamics (**Figure 4.7C**). Mean ERNA amplitudes of the first 10 pulses are higher ON medication, while mean ERNA latencies are lower ON medication, in keeping with increased frequencies. This change may be due to plastic changes in the dopamine-deficient brain (Alberquilla et al., 2020; Smith et al., 2009), which affects reciprocal STN-GPe connections. If the ERNA was a reflection of the STN intrinsic properties, ERNA changes with medication might reflect changes of the STN intrinsic properties due to STN dopaminergic receptors (Galvan et al., 2014). Alternatively, it is possible that the reduced overall functional cortico-striatal connectivity in the dopamine-deficient state leads to reduced resonance and lower ERNA amplitudes (Baggio et al., 2015; Vancea et al., 2019). In addition, we found a significant difference between ERNA frequencies ON and OFF medication after ~ 1 min, which might hint at different times to reach steady state and potentially a steady state at higher frequencies ON medication (**Figure 4.7Ai**). Furthermore, we found a link between ERNA parameters and beta power after DBS is switched off (**Figure 4.3B**), which is promising given the well-established link between beta activity and bradykinesia and rigidity (Kuhn et al., 2006). This may indicate that ERNA and beta power in the dopamine-deficient brain are modulated by the same underlying process.

These results together suggest that the fast ERNA dynamics, mostly ERNA amplitudes, could act as a biomarker for parkinsonian symptoms and may be useful in aDBS paradigms. In this context, it may be possible to calculate ERNA parameters of aDBS bursts in real-time and extract information about medication states or fast motor fluctuations and in turn adapt the threshold to trigger aDBS.

4.4.5. cDBS and aDBS may lead to differences in the synaptic status of the cortico-subthalamic-GPe circuit

aDBS was shown to be more effective than sham stimulation or no stimulation and at least as effective as cDBS with fewer side effects (Little et al., 2013; Little and Brown, 2020). While the exact mechanism underlying aDBS is unclear, it is believed to specifically target long beta bursts, which are linked with bradykinetic movements (Tinkhauser et al., 2017b; Torrecillos et al., 2018). Here, we show that ERNA parameters are differently modulated during cDBS and aDBS (**Figure 4.8C**). While both ERNA amplitudes and latencies drift towards a steady state in cDBS, we did not observe that drift in aDBS due to the discontinuous burst stimulation during aDBS. If the slow ERNA dynamics during cDBS are caused by synaptic failure, it is conceivable that synapses have ample time to replenish between aDBS bursts and therefore never deplete completely and never reach a steady state. While aDBS was at least as effective as cDBS in previous studies (Little and Brown, 2020), we hypothesise that different network states could cause clinical improvement in both instances. More studies will be needed to explore if the difference in the synaptic status during aDBS compared with cDBS, as revealed by the ERNA, could explain why aDBS can help reduce side effects and preserve physiological function of the cortico-subthalamic-GPe circuit.

4.4.6. Conclusion

This study provides evidence that time series and FFT-based ERNA describe the same activity. We further describe the fast and slow ERNA dynamics during and after DBS blocks, how these are modulated by different DBS frequencies, intensities and medication states and speculate on how these dynamics may be caused by synaptic failure. We report different ERNA dynamics during cDBS and aDBS, which together with the marked difference of the fast ERNA dynamics ON levodopa, might create a basis for the ERNA as a complimentary feedback marker in aDBS that signals changes in medication or motor fluctuations in real-time. We speculate on the

origin of the ERNA and our results are in keeping with the ERNA in STN LFPs reflecting rhythmic inhibitory input from GPe.

4.5. Summarised Findings

- Waveform and spectrogram-based ERNA very likely represent the same activity
- The ERNA has a fast and slow component which are modulated by different DBS frequencies and intensities and medication states
- ERNA dynamics differ between adaptive and continuous stimulation
- The described ERNA dynamics may be caused by synaptic depletion and are in keeping with the ERNA being generated between GPe and STN

4.6. Summary of Key Contributions

The ERNA could act as a complementary feedback signal to beta activity, where beta activity is the main feedback marker and helps curtailing long beta bursts. Average ERNA amplitudes (after ramps are removed) can then be calculated for every stimulation burst and help identify when PD patients slide into an OFF state. To gauge estimates of ERNA amplitudes ON and OFF medication, a calibration in both states is necessary. For calibration purposes, 10 bursts of 400 ms duration could be applied both ON and OFF dopaminergic medication and the average ERNA amplitudes of all 10 bursts could serve as a baseline. If during therapeutic aDBS ERNA amplitudes consistently sink below a certain value (e.g. 110 % of the average ERNA amplitude in the OFF state calibration), stimulation intensity or the beta threshold could be adjusted (**Figure 4.9**). The main caveat of this approach is that ERNA amplitudes primarily differed between medication states at the start of stimulation. We demonstrated that ERNA amplitudes during beta burst-triggered aDBS do not reach a steady state and it is therefore possible that differences with medication are preserved. We did not observe ERNA parameter

differences with medication during sustained stimulation, which challenges their usefulness as a complementary marker in this state. A further caveat is that beta activity and ERNA change inversely during sleep. Beta activity was shown to decrease overnight (van Rheede et al., 2022), which may serve as an argument to switch DBS off completely at night. Inversely, in preliminary recordings ERNA amplitudes appeared to decrease as the patient dozed off, which would suggest higher stimulation intensities at night. This conundrum will have to be resolved in future studies. We reviewed further details of the ERNA as a putative feedback signal for aDBS in **Table 4.2**. Note that in addition to aDBS, the ERNA may also serve as a marker for lead placement, contact, frequency, intensity and pulse width selection.

	ERNA
Sensitive and specific to the pathological state	ERNA separates medication states but unclear correlation with UPDRS scores. ERNA amplitudes decrease during sleep.
Reliable over time	Yes, over 30 + min in an acute setting. Robust against movement artefacts.
Localise to stimulation sweet spot	Yes, focal to dorsolateral STN.
Calculable with low computational requirements	Yes, only peak detection and simple arithmetics required.
Provide rapid feedback	ERNA parameters could be calculated for every burst of a beta burst-triggered aDBS algorithm.

Table 4.2. ERNA as a feedback marker for aDBS.

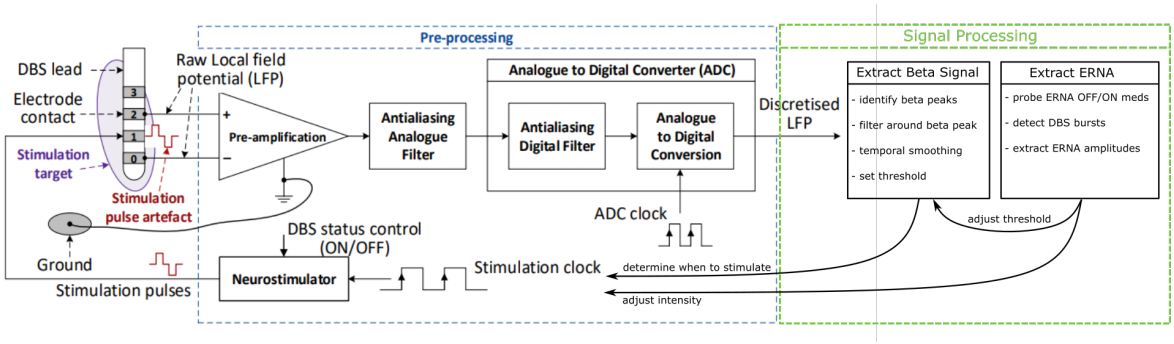


Figure 4.9. ERNA as a feedback marker for aDBS.

5. Project 3: Subthalamic deep brain stimulation induces finely-tuned gamma oscillations in the absence of levodopa

5.1. Introduction 129
5.2. Materials and methods 131
5.2.1. Consent, regulatory approvals and patient selection 131
5.2.2. Clinical characterisation 131
5.2.3. Surgery and lead localisation determination 132
5.2.4. Stimulation and data recording 133
5.2.5. Experimental design 134
5.2.6. Signal processing: pre-processing 135
5.2.6.1. Signal processing: FTG detection 135
5.2.6.2. Signal processing: FTG amplitude and frequency evolution during DBS 136
5.2.6.3. Signal processing: FTG duration, amplitude and frequency evolution after DBS 137
5.2.6.4. Signal processing: LFP-EEG coherence analysis 138
5.2.7. Statistics 139
5.3. Results 140
5.3.1. FTG can be induced by DBS off medication 140
5.3.2. FTG dynamics during DBS 142
5.3.3. FTG dynamics after DBS 145
5.3.4. FTG frequency does not change with different DBS frequencies off medication 145
5.3.5. LFP-EEG coherence at FTG frequencies 148
5.4. Discussion 149
5.4.1. Was FTG induced or entrained by DBS? 150
5.4.2. Why is the FTG an inconsistent finding across patients? 152
5.4.3. Study Limitations 154
5.4.4. Conclusions 154
5.5. Summarised Findings 154

This projects builds on previous work where the FTG was described on medication in the dyskinetic state and entrained at half stimulation frequency (Swann et al., 2016). Our results challenge the FTG as a faithful marker of dyskinesias and suggest that FTG does not have to be entrained to DBS. This project was published in Wiest et al., 2021.

5.1. Introduction

A finely-tuned gamma (FTG), occupying a narrow frequency band within the 60 and 90 Hz range, has been reported in the subthalamic nucleus, globus pallidus, thalamus and cortex in patients with various neurological disorders (Alegre et al., 2005; Alonso-Frech et al., 2006; Androulidakis et al., 2007a; P Brown et al., 2001a; Foffani et al., 2005; Fogelson et al., 2006; Kempf et al., 2009; Litvak et al., 2012; Miocinovic et al., 2018b; Swann et al., 2016). The FTG appears as a network oscillation in so far as it is coherent between sites in the cortico-basal ganglia-thalamic loop (P Brown et al., 2001a; Fogelson et al., 2006; Kempf et al., 2009; Litvak et al., 2012). In unexaggerated form it may be a primarily physiologic phenomenon related to arousal and voluntary movement, and its sharpness distinguishes it from canonical broadband gamma reactivity in the cortico-basal ganglia system (Jenkinson et al., 2013; Litvak et al., 2012). In patients with Parkinson's disease (PD), FTG appears following medication with levodopa and is further increased during voluntary movements (Brown et al., 2001; Alonso-Frech et al., 2006; Androulidakis et al., 2007), observations that have led it to be considered a prokinetic rhythm (Androulidakis et al., 2007a; Brown, 2003; Cassidy et al., 2002; Litvak et al., 2012). Hence, the extent of amplification of FTG during voluntary movement correlates positively with movement velocity in PD (Lofredi et al., 2018), although a broader gamma increase has also been linked to successful stopping of movements (Fischer et al., 2017). Moreover, when excessively exaggerated, FTG in the basal ganglia thalamo-cortical loop may contribute to involuntary movements, such as levodopa-induced dyskinesias in PD (Swann et al., 2016), or dystonic posturing in isolated dystonia (Miocinovic et al., 2018b). The link to levodopa-induced dyskinesias has also been noted in animal models of Parkinsonism (Güttler et al., 2020).

The generally prokinetic effect of FTG has led to speculation that it may mediate some of the effects of deep brain stimulation (DBS). Thus stimulating the subthalamic nucleus (STN) with

individually detected FTG-frequencies can produce similar clinical benefit as stimulating with frequencies above 100 Hz (E W Tsang et al., 2012). Indeed, cortical FTG may shift in frequency to half that of DBS during stimulation of the STN, signalling possible entrainment by stimulation when dyskinesias appear on medication (Swann et al., 2016). However, what happens to FTG during DBS when off medication or when dyskinesias are absent? Is it still affected by DBS, and if so in what way? Technical issues mean that, hitherto, it has been easiest to record LFP activity in the STN immediately after DBS to this target, and one study has reported that 60-90 Hz activity in the STN is not temporarily increased following STN-DBS performed off medication (Foffani et al., 2006). However, this study averaged gamma activity over patients with PD and as FTG is sharply tuned and inconsistent between patients, modulation may have been missed (Foffani et al., 2005). Another study managed to record FTG during DBS using high-density EEG and demonstrated a correlation between the power at FTG frequencies in both cortical regions and STN, which was derived using a beamformer algorithm, and local power at the stimulation frequency (Muthuraman et al., 2020). This occurred without a shift in the frequency of the presumed FTG activity, although the two stimulation frequencies used had subharmonics that were already close to the frequency of FTG. Moreover, this study reported co-modulation and did not directly demonstrate endogenous FTG. Here we explore whether STN-DBS off medication has an effect on local FTG activity allowing for the fact that this activity may only be recorded in a subset of patients ("high gamma" activity in López-Azcárate et al., 2010). We address two major questions; is FTG in the STN promoted by DBS, appearing *de-novo* with stimulation, and if so is the new activity entrained by DBS?

5.2. Materials and methods

5.2.1. Consent, regulatory approvals and patient selection

This protocol was approved by the Health Research Authority UK and the National Research Ethics Service local Research Ethics Committee (IRAS: 46576). Patients were recruited at St. George's University Hospital NHS Foundation Trust, London. Written informed consent was obtained in line with the Declaration of the Principles of Helsinki. Fourteen patients with PD (1 female) undergoing bilateral STN-DBS surgery were included in the study. Their average age at the time of recording was 57.2 ± 1.6 years (mean ± SEM) with average disease duration of 10.1 ± 1.2 years. Three patients were recorded bilaterally, giving a total of 17 STNs included in the study. Clinical details are summarised in **Table 5.1**. Data from patients 1 to 9 and patients 11 and 12 were previously published (Wiest et al., 2020).

5.2.2. Clinical characterisation

Study participants were evaluated by an interdisciplinary team of movement disorder neurologists and functional neurosurgeons and met the UK Parkinson's Disease Society Brain Bank Diagnostic Criteria for diagnosis of PD (Hughes et al., 1992). Baseline motor function in the on and off medication state was characterised pre-operatively using part III of the Unified Parkinson Disease Rating Scale motor subscale (UPDRS III). Patients were evaluated by a neuropsychologist to exclude significant cognitive impairment or untreated affective disorders. During the recordings, an experienced neurologist was present to screen for dyskinesia.

Patient	Gender (m/f)	Age (yr)	Disease Duration (yr)	Pre-OP UPDRS-III OFF	Pre-OP UPDRS-III ON	Pre-dominant symptoms	DBS lead	Time Recording (d)	STN tested (L/R)	Location Stim. Contact	Stim. Amp. (mA)	FTG present OFF meds ON DBS	LID contralat. to tested STN pre-OP (RDRS)	DID contralat. to tested STN post-OP
1	m	48	17	71	37	tigidity, gait freezing (FOG), tremor	Boston	4	R	STN (SP)	2	yes	yes (6)	no
2	m	54	7	38	24	tremor	Boston	5	R	STN (SP)	3.5	yes	no (0)	yes
3	m	51	5	27	13	bradykinesia, rigidity, motor fluctuations	Boston	4	R	STN/cZI	4	yes	no (0)	yes
4	m	64	13	52	21	FOG, motor fluctuations	Boston	4	R	STN (SP)	2	yes	no (0)	no
5	m	53	7	23	12	tremor	Boston	4	R	STN (SP)	2	no	no (0)	no
								5	L	STN (SP)	3	yes	no (0)	no
6	m	61	16	50	30	FOG, motor fluctuations	Boston	3	L	STN (SP)	2	no	no (0)	no
7	m	56	16	51	19	rigidity, bradykinesia	Medt	4	L	STN (SP)	4	no	no (0)	no
8	m	65	5	34	16	FOG, motor fluctuations	Boston	4 + 5	L	STN/cZI	3	no	yes (2)	no
								4	R	STN/cZI	2.5	no	yes (3)	yes
9	f	63	11	40	17	FOG, motor fluctuations	Boston	4	L	STN (SP)	2	no	yes (2)	no
10	m	65	15	77	27	akinetic-rigid, tremor	Boston	5	L	STN (SP)	1.8	no	yes (1)	no
11	m	61	9	33	12	rigth arm tremor, bradykinesia	Boston	4	L	STN/cZI	4	no	no (0)	no
12	m	48	8	45	34	tremor, bradykinesia	Boston	5	L	STN/cZI	3	no	no (0)	no
13	m	59	6	48	14	akinetic-rigid	Medt	5	R	STN (SP)	n.a.	no	yes (1)	no
14	m	53	7	18	1	motor fluctuations, dyskinesia	Boston	4	L	STN/cZI	4	no	no (0)	no
								4	R	STN/cZI	2.5	no	yes (1)	no

Table 5.1. Patients clinical and recording details. Pre-OP: pre-operative; Post-OP: post-operative; UPDRS-III: Unified Parkinson Disease Rating Scale (subunit III); FTG: finely-tuned gamma; Boston: Boston Scientific; Medt: Medtronic; STN (SP): superior-posterior part of the subthalamic nucleus; FOG: freezing of gait; STN/cZI: subthalamic nucleus/caudal Zona incerta; LID: levodopa-induced dyskinesia; RDRS: Rush Dyskinesia Rating Scale; DID: DBS-induced dyskinesia; n.a.: not applicable.

5.2.3. Surgery and lead localisation determination

The surgical target was STN. Two models of DBS leads were used; either a quadripolar subthalamic lead (model 3389, Medtronic Inc., Neurological Division, USA) with four 0.5 mm spaced contacts of 1.5 mm length with platinum-iridium cylindrical surfaces or a directional subthalamic lead (model DB-2202, Boston Scientific, USA) with three segmented contacts on each of the middle two levels. These middle two levels sat above and below a concentric electrode contact. Electrodes were implanted using frame-based stereotaxy and MRI guidance. The subthalamic leads were connected to temporary extension leads and these externalised over the left temporal bone. Assessment of contact localisation was made through co-registration of immediate post-operative CT with pre-operative MRI by two experienced neurosurgeons (E.A.P and A.M.) specialising in DBS. Assessment was blinded to the electrophysiological data and made using Renishaw Neuroinspire v6 software. Localisation specifics are summarised in **Table 5.1**.

Patient	number of long DBS blocks	DBS Freq. (Hz)	FTG during DBS (at 130 Hz)	FTG duration during DBS (% of block) (mean & range)	FTG Freq. during DBS (Hz) (mean & range)	FTG after DBS (at 130 Hz)	FTG duration after DBS (sec) (mean & range)	FTG Freq. after DBS (Hz) (5-sec window) (mean & range)	notes	EEG channel of greatest coherence
1	4	130	yes	69.8 [35.1 - 84.9]	74.3 [74 - 75]	yes	14.3 [9.0 - 18.8]	74 [73 - 75]		during R DBS: C3
2	3	130	no	n.a.	n.a.	yes	16.3 [14.3 - 20.3]	77 [77 - 77]		after (5 sec) R DBS: C3
3	9	4 x 130 3 x 180 2 x 70	yes	59.2 [54.2 - 66.7]	79.3 [78 - 81]	yes	38.5 [26.3 - 57.1]	82 [82 - 82]	70 Hz: no FTG 130 and 180 Hz: FTG during and after DBS	during R 130 Hz: FCz after R 130 Hz: C4 during R 180 Hz: CP4 after R 180 Hz: Fz
4	5 (long) 12 (short)	long: 3 x 130, 1 x 190, 1 x 180 short: 4 x 70, 4 x 130, 4 x 190	no	n.a.	n.a.	yes	16.5 [7.5 - 25.6]	81.5 [81 - 82]	70 Hz: no FTG 130 Hz: FTG after DBS 190 Hz: FTG during and after DBS	after R 130 Hz: CP4 during R 180+190 Hz: CP3 after R 190 Hz: CP4
5	4 (long) 5 (short)	130	yes	14.3 [5.8 - 23.1]	78.5 [78 - 80]	no	n.a.	n.a.		during L blocks: Fz

Table 5.2. Details of the finely-tuned gamma. Electroencephalogram (EEG) contacts are labelled according to the extended 10-20 EEG system at Fz, FCz, Cz, Oz, C3, C4, CP3 and CP4. FTG duration, amplitude and frequency were extracted using a cluster based approach (see Methods). Freq.: frequency; R: right; L: left; n.a.: not applicable.

5.2.4. Stimulation and data recording

Recordings were made between 3 and 5 days postoperatively (**Table 5.1**), while electrode leads were still externalised and before implantation of the subcutaneous pulse generator. All patients performed the experiments after overnight withdrawal of antiparkinsonian medication (**Table 5.1**). In patients with directional leads, the three directional contacts of level 1 and 2 were joined to form two 'ring contacts' so that each lead afforded four monopolar ring contacts. The four contacts were numbered E0 to E3 with contact E0 being the most ventral and contact E3 being the most dorsal (see **Figure 5.1A**). Stimulation was only tested at the two middle contacts (E1 and E2) to allow bipolar LFP recordings from the two adjacent contacts. A self-adhesive electrode (Pals, Nidd Valley Medical Cordon, UK) attached to the patients' back served as a reference for stimulation, which was delivered using a highly configurable neurostimulator (Slater et al., 2015). Stimuli comprised symmetric constant-current biphasic pulses (60 μs per phase, negative phase first). In each of the two middle contacts, stimulation was started at 0.5 mA and slowly increased in steps of 0.5 mA every 3 to 4 minutes until first a clear benefit in rigidity and/or bradykinesia was observed and second side effects such as paraesthesia became apparent. The stimulation contact and current associated with the most clinically effective

stimulation without side effects was selected and maintained throughout the entire experiment (DBS currents listed in **Table 5.1**). This procedure was performed on the side contralateral to the most affected upper limb in 11 subjects and bilaterally in 3 subjects (**Table 5.1**). If not indicated differently in the results, a stimulation frequency of 130 Hz was used. STN-LFPs were recorded in bipolar mode from the two contacts on either side of the stimulation contact, for common reference removal (see **Figure 5.1A**). Limited concomitant EEG electrodes were placed at Fz, FCz, Cz, Oz, C3, C4, CP3 and CP4 according to the extended 10-20 EEG system and allowing at least a 3 cm distance from all incisions. EEG time series were recorded with a common average reference (that did not include LFP channels). All signals were amplified and sampled at 2048 Hz using a TMSi Porti (TMS International, Netherlands) and custom-written software developed using the C programming language. The ground electrode was placed on the forearm.

5.2.5. Experimental design

During the experiments, patients were comfortably seated in an armchair. Note that recordings were performed using different experimental protocols (some already published, see Wiest et al., 2020). Only a few patients were tested at different stimulation frequencies (patients 3, 4, 8 and 9) and durations (patients 4, 5, 6 and 9). However, all recordings started with two minutes of rest recording without stimulation (baseline) followed by blocks of continuous 130 Hz DBS. Stimulation blocks lasted for 163.1 ± 11.1 seconds (mean ± SEM) in up to four consecutive blocks separated by resting periods of on average 110.2 ± 9.9 seconds. Additional blocks with different DBS frequencies were tested in two of the five subjects showing the FTG (see **Table 5.2**). In patient 3, two blocks at 70 Hz DBS (150.5 ± 1.4 seconds) were recorded followed by two blocks at 180 Hz (153.5 ± 4.0 seconds), with resting periods of on average 118.9 ± 2.7 seconds between them. In patient 4, one DBS block at 180 Hz for 24.0 seconds and another

block at 190 Hz for 24.1 seconds separated by a series of short DBS bursts at the same frequency (25 bursts of on average 115.2 pulses at 180 Hz and 15 bursts of on average 143.5 pulses at 190 Hz; **Figure 5.5B**) were recorded. Also in patient 4, four short duration DBS blocks (13.1 ± 0.2 seconds) were recorded at 70 Hz, 130 Hz and 190 Hz each (see **Table 5.2**), each separated by resting periods of on average 149.0 ± 3.9 seconds.

5.2.6. Signal processing: pre-processing

All data analysis was performed using custom-written scripts in MATLAB (version 2019a, Mathworks, Massachusetts, USA). Continuous LFP signals were linearly de-trended to remove low-frequency drifts using MATLAB's *detrend* function and DBS artefacts were removed by applying second-order IIR notch filters (Q-factor = 200; see **Figure 5.1B**). These artefacts include line noise at 50 Hz (all records), a peak at the subharmonic frequency of 65 Hz during stimulation at 130 Hz in 11/17 STNs (and all 5 patients displaying FTG), and a narrowband signal that appeared at 80 Hz in 8/17 STNs (**Figure 5.1C**; only patients 1 and 2 displaying FTG). The narrowband character of these signals and the fact that they were not delayed in onset and did not outlast the DBS blocks or change in frequency over time differentiated them from the FTG. Spectral amplitudes were estimated between 65 and 90 Hz using the short-time Fast Fourier transform with a window length of 1 second, 25% overlap of consecutive windows and a Hamming window as implemented in MATLAB's *spectrogram* function yielding a frequency resolution of 1 Hz.

5.2.6.1. Signal processing: FTG detection

We restricted our search for the FTG to the frequency range from 65 to 90 Hz (Kempf et al., 2009; Swann et al., 2016) to avoid DBS subharmonics (only DBS stimulation frequencies of 70, 130, 180 and 190 Hz were used across patients). The presence of FTG was assessed in each

STN and stimulation block by visual inspection of both the time-frequency spectrograms and power spectral densities (PSD). To this end, PSDs were computed in three time windows. First, a baseline PSD was computed in a 50-second window before each DBS block (-52 sec to -2 sec; to avoid contamination from artefacts when DBS was switched on). Second, PSDs were computed during stimulation and finally, post-DBS PSDs were computed in a 5-second window after DBS was switched off. This window length was selected based on visual inspection of the time-frequency maps to include short lasting FTGs persisting after DBS. The PSD from all four epochs was flattened using a fourth order polynomial (*detrend* function) to correct for the 1/f pattern (Pritchard, 1992) and z-scored (Swann et al., 2016). The presence of FTG was determined by the presence of a peak between 65 and 90 Hz that was over two standard deviations above the average of the respective time window using MATLAB's *findpeaks* function (MinPeakHeight: 2) and confirmed by visual inspection of the time-frequency maps. This approach was effective even in 10-sec windows if the FTG is present and allows to track the FTG peak during and after DBS.

5.2.6.2. Signal processing: FTG amplitude and frequency evolution during DBS

In subjects that showed an FTG in the PSD and time-frequency plot during DBS (see **Table 5.2**), the amplitude and frequency profiles of the FTG were further characterised. To this end, we first defined a more constrained region of interest (ROI) in the time-frequency domain. The frequency-axis of the ROI was determined based on the largest PSD peak during the whole DBS block (signal flattened and z-scored as described above) ± 5 Hz. The time-axis equalled the block duration. Further, power estimates within the ROI were binarised. All power estimates that were equal to or above the 70th percentile of all power estimates in the ROI were given the value 1 and all remaining power estimates the value 0. Clusters of connected pixels of value 1 were identified using MATLAB's *bwconncomp* function (8-connected mode; pixels

are connected if their edges or corners touch). Note that each estimate corresponds to 1 Hz x 0.75 seconds (ROI size: 11 Hz x DBS duration in bins of 0.75 seconds), except in patient 5 where the ROI was changed to 14 Hz x DBS duration*0.25 since the FTG feature was only present in the first quarter of the block and it was further spread along the frequency axis (average ROI size 1666.5 ± 234.1 power estimates). Clusters consisting of less than 15 individual power estimates were removed from the cluster map to exclude possible random fluctuations. All clusters that survived this selection were considered as components of the FTG (see **Figure 5.3A**). Frequencies and amplitudes of the FTG were determined for each time bin (0.75 seconds, based on settings of the frequency decomposition) for the power estimate with the highest activity within the cluster. To quantify FTG features during and after DBS (**Figure 5.3 and 5.4**), average FTG frequency and amplitude profiles per subject (mean of all blocks) were z-scored as in:

$$FTG_Z = \frac{FTG_S - mean(FTG_S)}{std(FTG_S)}$$

where FTG_S represents the average FTG feature per subject (mean of all blocks) and FTG_Z the z-scored FTG feature.

5.2.6.3. Signal processing: FTG duration, amplitude and frequency evolution after DBS

In subjects that showed an FTG after DBS in the PSD and time-frequency plot, we used a similar method to the above to precisely define the frequency and amplitude profiles of the FTG activity. Differences from the procedure above were as follows. The frequency-axis of the ROI was based on the post-DBS PSD peak and the time-axis was set to 30 seconds (60 seconds in subject 3) based on visual inspection (average ROI size: 641.7 ± 67.2 power estimates). Only the largest cluster was kept to define FTG duration, amplitude and frequency.

FTG duration was defined as the length of the FTG cluster following cessation of DBS (see **Figure 5.4A**).

5.2.6.4. Signal processing: LFP-EEG coherence analysis

In all subjects with significant FTG peaks in the power spectrum we computed coherence between the STN-LFP and EEG. EEG signals were linearly de-trended and data from consecutive DBS blocks were concatenated within subjects. Coherence analysis was performed on unfiltered data. Magnitude-squared coherence was computed using the short-time Fast Fourier Transform with window length 0.5 s and 0% overlap as in:

$$C_{xy}(f) = \frac{|P_{xy}(f)|^2}{P_{xx}(f) * P_{yy}(f)}$$

where $P_{xx}(f)$ and $P_{yy}(f)$ correspond to the power spectral densities and $P_{xy}(f)$ to the cross power spectral density. Significance levels of coherence were assessed using an upper 95% confidence limit based on the assumption of independence; for details see (Halliday et al., 1995). The EEG channel with greatest coherence per subject is shown in **Table 5.2** and **Figure 5.7**. To compute coherence after DBS blocks, 5-second windows after the last stimulation artefact were concatenated within subjects. EEG-LFP coherence was considered to be present when it exceeded the upper 95% confidence limit at the same frequency as the corresponding FTG in the STN-LFP.

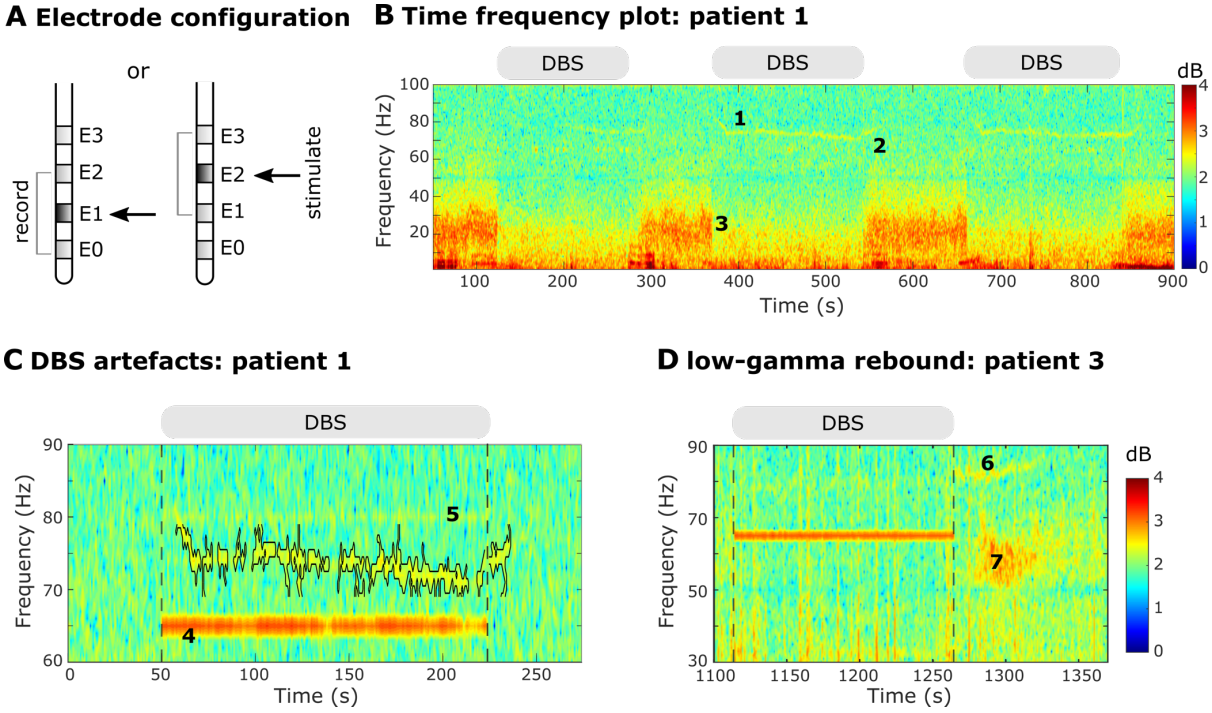


Figure 5.1. Stimulation settings and experimental paradigm. A. Schematic illustration of the electrode configuration. DBS was applied to one of the two middle contacts (E1 or E2) and LFPs were recorded bipolarly from the two adjacent contacts (E0 and E2 or E1 and E3). Bipolar contacts were recorded directly and not recovered off-line. **B.** Time-frequency spectrogram of first three DBS blocks in patient 1. During stimulation the finely-tuned gamma (FTG) arises (label 1) and then outlasts DBS (label 2) when it increases in frequency. In addition, beta suppression is evident during DBS (label 3). DBS blocks at 130 Hz are denoted by the grey bars at the top of the trace. Note that line noise artefacts were present throughout the recording at 50 Hz along with the DBS subharmonic at 65 Hz but are reduced by second-order IIR notch filters. **C.** DBS-induced narrowband artefacts at a subharmonic DBS frequency (65 Hz; label 4) or due to an aliasing phenomenon (80 Hz; label 5). Time-frequency spectrum shown for block 2 of patient 1with DBS at 130 Hz and before applying IIR notch filters (see Methods). The grey bar and vertical lines denote DBS onset and offset. The FTG feature is contoured (see Methods). Note that DBS-induced artefacts do not change in frequency throughout stimulation and cease immediately after DBS is stopped. **D.** Representative time-frequency spectrogram from patient 3 block 2. Apart from the FTG after DBS (label 6) we observe a low-gamma rebound (label 7) which appears after DBS is stopped with a slight delay, spans from 50-70 Hz and lasts for several seconds.

5.2.7. Statistics

Statistical analyses were conducted using custom-written scripts in MATLAB. Comparisons of the FTG features (duration, frequency and amplitude) between the start and end of the stimulation blocks were performed using linear mixed-effects models on individual data. The FTG features were set as dependent variables (raw features) and the first and last 5-second time windows as fixed effects. A similar approach was used to compare the FTG features across

consecutive blocks. The normal distribution of each variable and the residuals were visually inspected with quantile-quantile plots and histograms of distribution. All models were estimated by the method of maximum likelihood and included random intercept for subjects to allow different intercepts for each subject, thereby capturing individual differences. Linear mixed-effects models allow for missing data and comparisons of small sample sizes (Muth et al., 2016).

5.3. Results

5.3.1. FTG can be induced by DBS off medication

Five of 14 patients (35.7%) revealed FTG activity either during or after DBS following overnight withdrawal of antiparkinsonian medication (see **Table 5.1** and significant peaks in PSD of **Figure 5.2**). The FTG arose *de-novo* as it was not discernible during a 50-second baseline period prior to DBS start (**Figure 5.2**). During continuous stimulation at 130 Hz, FTG was observed in the spectrogram of 3 patients (cases 1, 3 and 5) with at least a few seconds delay from stimulation onset (**Figure 5.2A, C and E**). Case 4 displayed an FTG during stimulation at 180 and 190 Hz, and will be considered separately, later.

After DBS, FTG was observed in four patients and changed in pattern. In two patients the FTG outlasted DBS (patient 1 and 3; **Figure 5.2A+C**), whereas in the other two it only started after DBS ceased (patient 2 and 4; see **Figure 5.2B+D**). In 4 of 5 patients that displayed any FTG we observed an additional broad low-gamma rebound after stimulation was stopped (**Figure 5.1D**), as seen in an earlier study (Wiest et al., 2020). This activity spanned from 40-70 Hz. Its broadband character and lower frequency range helped to differentiate it from the FTG.

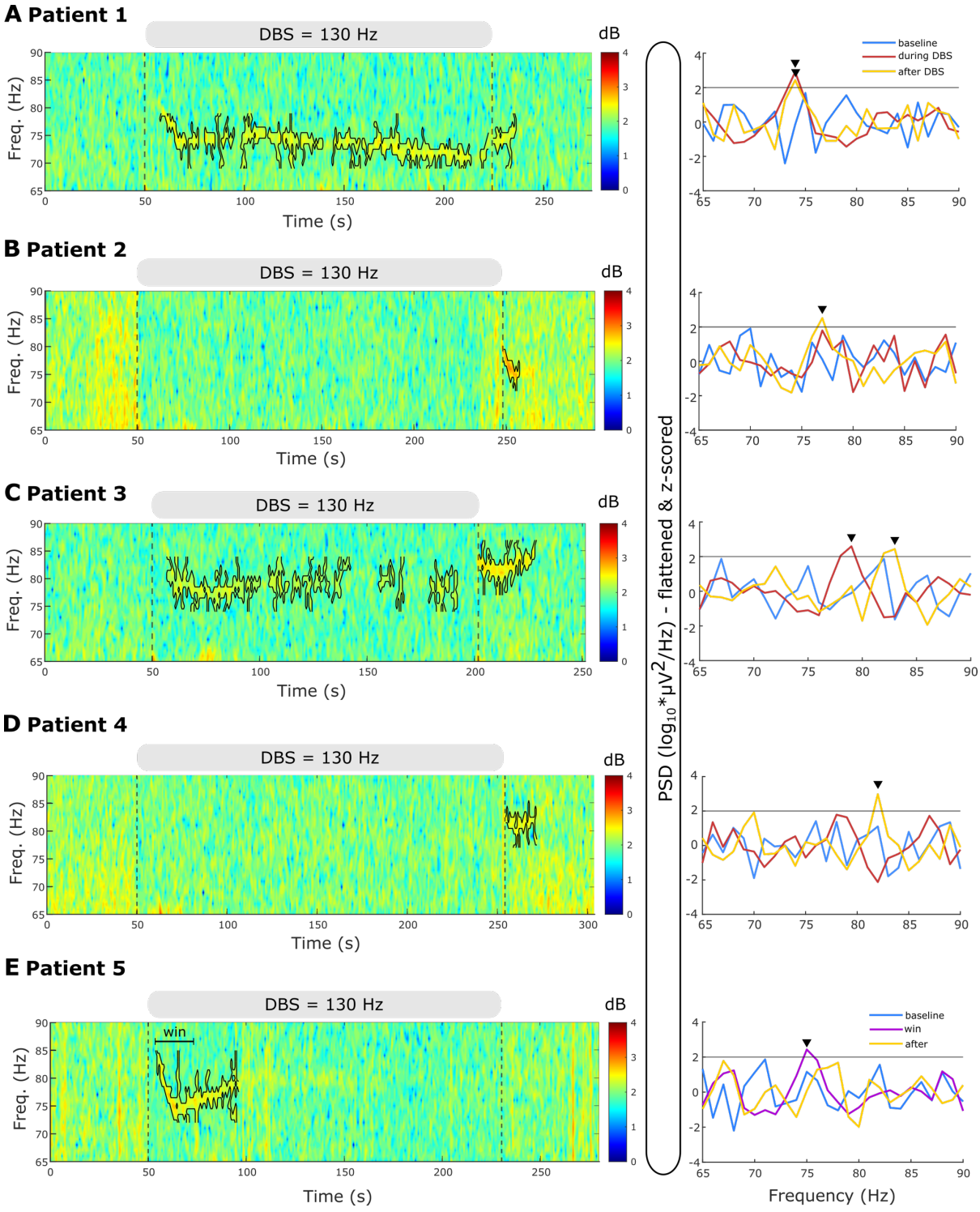


Figure 5.2. 130 Hz DBS induces finely-tuned gamma (FTG) oscillations in the absence of levodopa and dyskinesia. A-E. *Left*: time-frequency spectrograms of representative DBS blocks. The grey bar on top of the trace and the vertical dashed lines denote DBS onset and offset. The FTG feature is surrounded by a contour in each case (based on a 70th percentile threshold of a ROI, see definition in methods section and **Figure 5.3A**). *Right:* Power spectral densities (PSD) during a 50-second baseline period before DBS onset, during the DBS block and during a 5-second window after DBS cessation, with the exception of case 5 (E) in whom the spectrum of a narrower region of interest (win; 20 seconds long) is presented. The grey horizontal line denotes the FTG threshold at 2 standard deviations above

average baseline. Peaks above the threshold are considered significant (black arrowheads). This analysis was confirmed by visual inspection.

No dyskinesias were reported during or after stimulation in the subjects with FTG (Unified Dyskinesia Rating Scale Part III = 0, (Goetz et al., 2008)), suggesting that FTG can be observed in PD patients OFF medication without dyskinesia.

5.3.2. FTG dynamics during DBS

FTG dynamics were further explored during stimulation in patients 1, 3 and 5. As can be observed in **Figure 5.2**, during 130 Hz DBS, the FTG varied between patients. However, in all three the FTG began only after a few seconds of stimulation and demonstrated an initial drop in frequency during the first 20s of stimulation (**Figure 5.2A, C and E**). To better describe the modulation of the FTG in time, we first identified the FTG in the spectral domain using a cluster-based approach (see Methods and **Figure 5.3A**). Subsequently, we extracted duration, frequency and amplitude over time from the identified cluster. On average, the FTG lasted for 77.6 ± 13.5 seconds (47.8 ± 8.2 % of the time during DBS; all blocks of patients 1, 3 and 5 included) with a high inter- and intra-subject variability (see **Table 5.2**). The averaged FTG frequency profile suggests a decrease with stimulation duration (**Figure 5.3C**) which was significant when comparing the average frequency of the first and last 5 seconds of the FTG in all blocks of all 3 patients (LME: $b = -2.6$, $t = -5.2$, $p < 0.001$; **Figure 5.3D**). In contrast, there was no significant difference between the initial and final FTG amplitude (LME: $b = -0.02$, $t = -0.7$, $p = 0.47$; **Figure 5.3G**).

To differentiate the FTG from a broadband gamma increase during DBS, we computed relative changes of power estimates with respect to a 50-second baseline period before DBS onset. Power estimate changes of patients 1, 3 and 5 were averaged across 4 DBS blocks each. The

FTG feature showed a greater power increase than adjacent frequencies in the gamma band (**Figure 5.S1**). Hence, FTG induction is selective and not accompanied by a broadband DBS-induced gamma event-related synchronisation (ERS).

All three patients showing FTG during DBS performed four consecutive blocks at 130 Hz, allowing us to assess FTG dynamics across consecutive DBS blocks. Linear mixed-effects models revealed a significant reduction of the average FTG frequency across DBS blocks (LME: $b = -0.72$, $t = -4.7$, $p < 0.001$; **Figure 5.3E**), but no change in average FTG amplitude (LME: $b = 0.01$, $t = 0.6$, $p = 0.56$; **Figure 5.3H**) or FTG duration during DBS across blocks (LME: $b = 5.89$, $t = 1.85$, $p = 0.09$; **Figure 5.3B**).

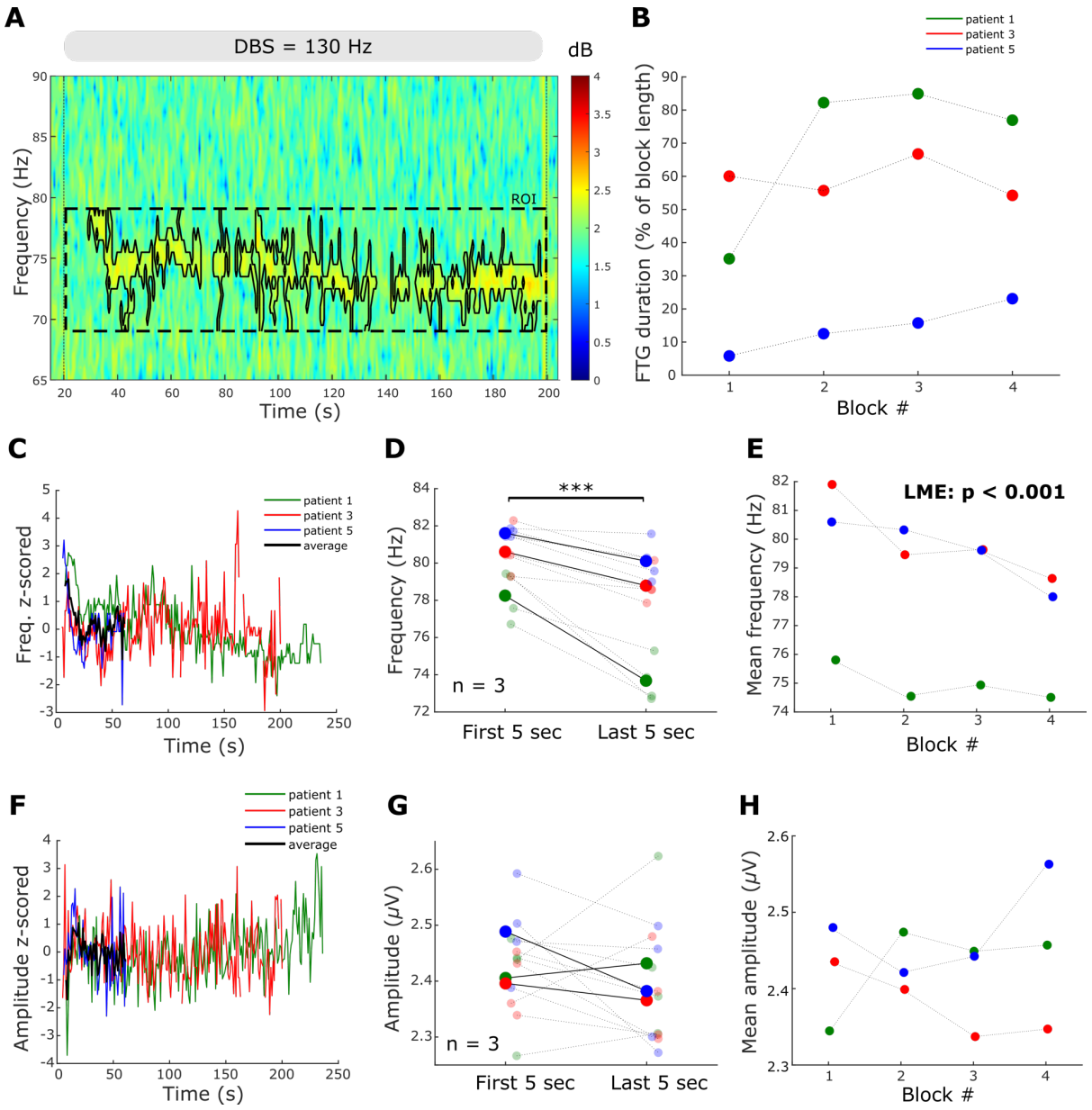


Figure 5.3. FTG dynamics during DBS blocks. A. Time-frequency spectrogram of a representative DBS block from patient 1. The grey bar and vertical dotted lines denote DBS onset and offset. The black contour surrounds power estimates above the 70th percentile of the ROI (see Methods). **B.** FTG durations during DBS in percentage of the total length of the stimulation block (linear mixed-effects model (LME): b = 5.89, t = 1.85, p = 0.09). **C.** FTG frequency during DBS over time averaged across blocks for each patient (data z-scored to frequencies during DBS; n = 3). Note the different FTG durations during DBS. Group average in black only given when data from all 3 patients was available. **D.** FTG frequency decreases between the first and last 5 seconds of a DBS block (LME: b = -2.6, t = -5.2, p < 0.001). Big dots denote averages of patients, small dots denote single blocks. Patients colour coded as in B. **E.** Mean FTG frequencies decreased across consecutive DBS blocks (LME: b = -0.72, t = -4.7, p < 0.001). **F.** FTG amplitude during DBS over time (data z-scored to amplitudes during DBS; n = 3). **G.** FTG amplitude in the first and final 5 seconds of a DBS block (LME: b = -0.02, t = -0.7, p = 0.47). Big dots denote averages of patients, small dots denote single blocks. **H.** Average FTG amplitude does not change across consecutive DBS blocks (LME: b = 0.01, t = 0.6, p = 0.56)

5.3.3. FTG dynamics after DBS

After discontinuation of 130 Hz DBS, the FTG lasted on average 23.2 ± 4.1 seconds (**Figure 5.4C** and **Table 5.2**). There was no significant difference in frequency between the first and last 5 seconds (LME: b = 0.82, t = 1.6, p = 0.12; **Figure 5.4D**). However, post-DBS FTG frequencies appeared to be very variable across patients. While patients 3 and 4 displayed an almost U-shaped frequency curve, FTG frequencies tended to increase in patient 1 and decrease in patient 2. In contrast, the FTG amplitude after DBS decreased (**Figure 5.4F**), with a significant difference when comparing amplitudes between the first and last 5 seconds (LME: b = -0.15, t = -5.2, $p < 0.001$; **Figure 5.4G**). Across consecutive blocks, no trends or significant differences were observed in FTG duration (LME: b = -5.26, t = -1.59, p = 0.15; **Figure 5.4B**), maximal FTG amplitude (LME: b = -0.03, t = -0.76, p = 0.46; **Figure 5.4H**) and average FTG frequency (LME: b = -0.01, t = -0.04, p = 0.97; **Figure 5.4E**). Note that only the first 3 DBS blocks were included as it was the minimum number of repetitions performed across the 4 patients showing post-DBS FTG. These results suggest that the FTG appears to be consistent after multiple DBS blocks in individual patients.

5.3.4. FTG frequency does not change with different DBS frequencies off medication

In two patients that displayed FTG during or after 130 Hz DBS, we tested if different DBS frequencies elicited changes in FTG peak frequency, suggestive of entrainment. In patient 3, DBS was tested at 70 Hz and 180 Hz, as well as the standard 130 Hz. Stimulation at 70 Hz did not induce an FTG, however, we cannot preclude the presence of an FTG feature underneath the stimulation artefact or its subharmonics. Stimulation at 180 Hz led to an FTG at about 80 Hz, similar to the FTG elicited by DBS at 130 Hz (compare **Figure 5.5A** with **Figure 5.2C**). In contrast to the artefact at 80 Hz (**Figure 5.1C**), this 80 Hz-signal started with a delay after DBS onset and outlasted stimulation. Moreover, it showed dynamic changes and was hence

considered as an FTG feature. In patient 4, DBS was delivered at 180 Hz and at 190 Hz separated by short stimulation bursts consisting of repetitive periods on and off DBS at these frequencies (**Figure 5.5B**). While DBS at 130 Hz only elicited an FTG after DBS in this patient (**Figure 5.2D**), DBS at 180 Hz and 190 Hz induced a significant FTG peak during stimulation which outlasted DBS. FTG frequency was at about 80 Hz for all three DBS frequencies (compare **Figure 5.5B** and **Figure 5.2D**). While the patients and block numbers are too small to make definitive inferences, two trends are apparent: Firstly, FTG frequencies remained reasonably constant during and after DBS at different driving frequencies (**Figure 5.5C+D**) and, secondly, FTG amplitudes during DBS seemed to increase with DBS frequency (**Figure 5.5E**) while FTG amplitude after DBS was similar at 130, 180 and 190 Hz stimulation (**Figure 5.5F**). The latter is underpinned by the results observed in short blocks of DBS (four blocks per DBS frequency of on average 13.1 ± 0.2 seconds) at 70 Hz, 130 Hz and 190 Hz in patient 4. While DBS at 70 Hz and 130 Hz did not induce an FTG meeting our criteria either during or after DBS, 190 Hz stimulation triggered an FTG during short blocks (**Figure 5.6A**). In patient 5, the FTG was evident in short blocks of on average 22.4 ± 1.2 seconds even at 130 Hz (**Figure 5.6B**) with a similar profile as in long blocks but cut short by DBS termination.

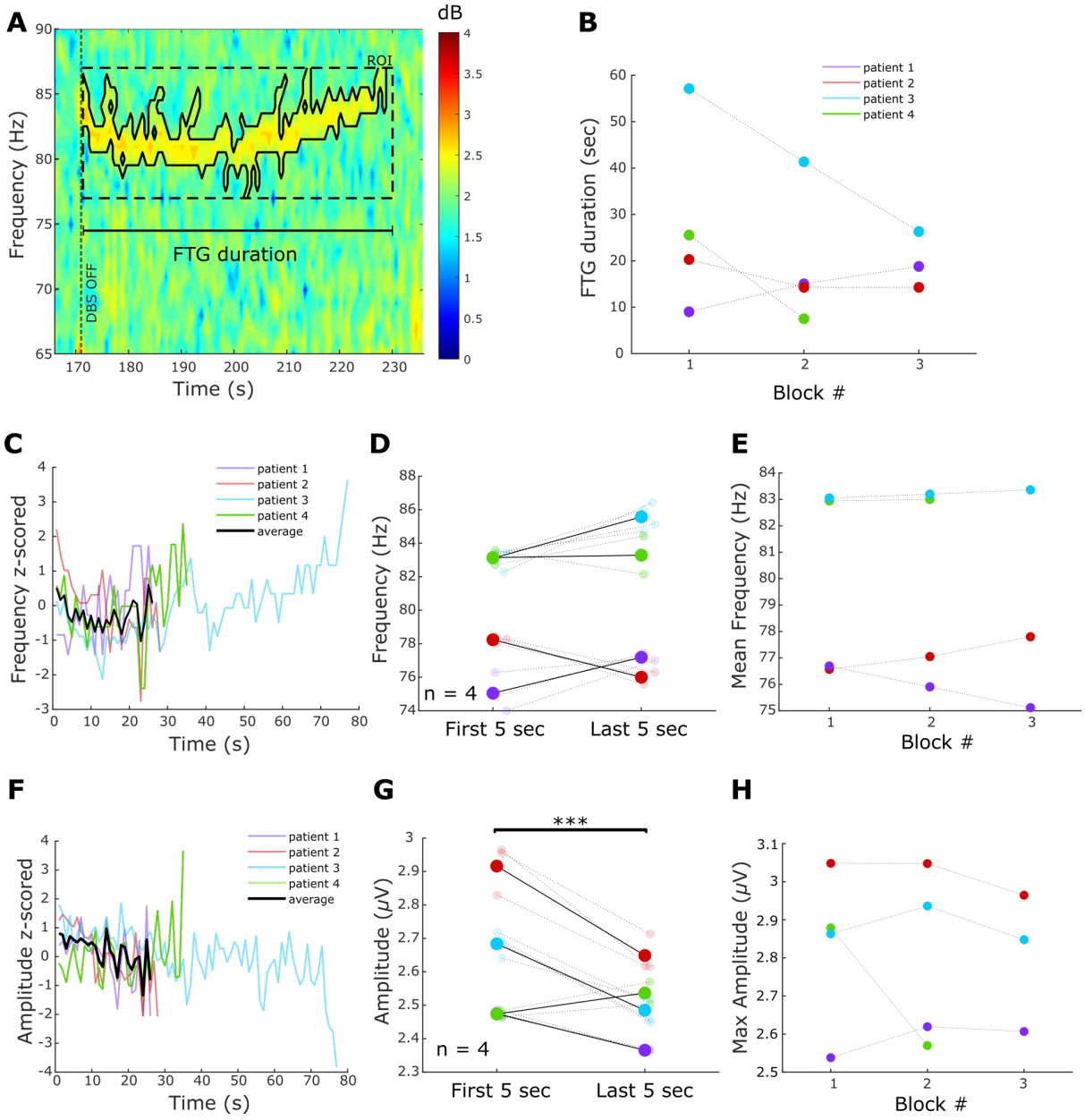


Figure 5.4. FTG dynamics after DBS blocks A. Representative time-frequency spectrogram of FTG after DBS termination in patient 3. Vertical dashed line denotes the DBS offset and the scale shows FTG duration. The black contour surrounds power estimates above the 70th percentile of the ROI (see Methods). **B.** FTG duration across blocks. Linear mixed-effects models do not show a significant change (LME: b = -5.26, t = -1.59, p = 0.15; only first 3 blocks included). **C.** FTG frequency after DBS over time averaged across blocks for each patient (data z-scored to FTG frequencies after DBS; n = 4). Note the different FTG durations after DBS. Group average in black only given when data from all 4 patients was available. **D.** FTG frequencies after DBS do not differ between the first and last 5 seconds (LME: b = 0.82, t = 1.6, p = 0.12). Patients are colour coded as in C. **E.** Average FTG frequencies across blocks (LME: b = -0.01, t = -0.04, p = 0.94; only first 3 blocks included). **F.** FTG amplitude after DBS over time averaged across blocks for each patient (data z-scored to FTG amplitudes after DBS; n = 4). **G.** FTG amplitude decreases between the first and last 5 seconds of the post-DBS FTG (LME, b = -0.15, t = -5.2, p < 0.001). **H.** Maximal FTG amplitudes do not change across consecutive DBS blocks (LME: b = -0.03, t = -0.76, p = 0.46; only first 3 blocks included).

5.3.5. LFP-EEG coherence at FTG frequencies

Since the FTG has previously been detected in cortical recordings we studied LFP-EEG coherence. We found significant LFP-EEG coherence at FTG frequencies in all the patients exhibiting FTG in their STN-LFP (**Figure 5.7** and **Table 5.2**). Based on patients 3 and 4, coherence tended to be greater at higher DBS frequencies (**Figure 5.7C+D**) similar to the increased FTG amplitude during blocks of increased DBS frequencies.

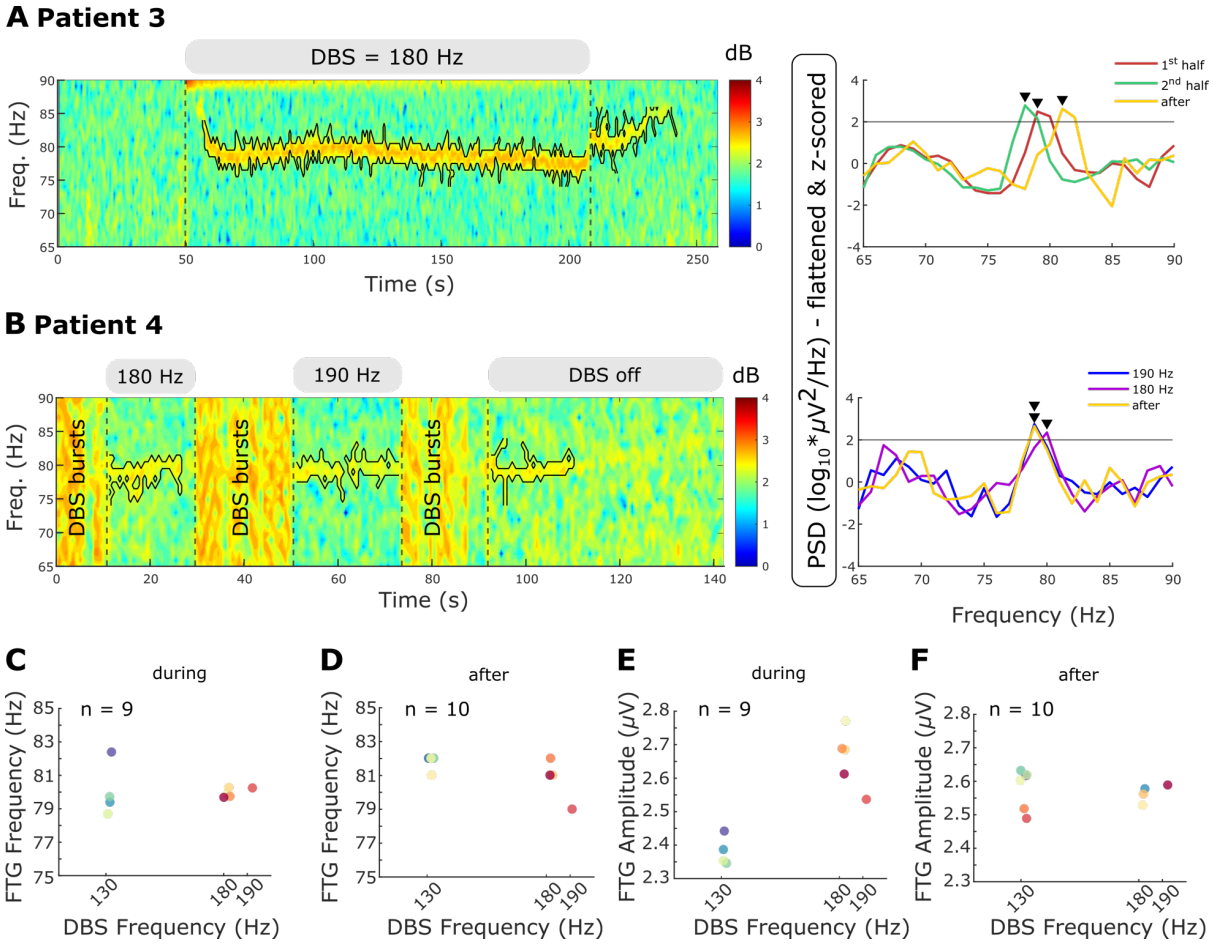


Figure 5.5. Different DBS frequencies do not change FTG frequency A. *Left:* Time-frequency spectrogram of representative DBS block. Grey bars above the spectrogram and the vertical dashed lines denote DBS onset and offset. Different DBS frequencies are shown in the grey bars. The black contour surrounds the FTG feature within the ROI (see Methods). PSD shown for the first and second half during DBS and the 5-second reference period after DBS cessation. Grey horizontal line denote the FTG threshold at two standard deviations above average of the respective reference periods. Black arrowheads denote significant PSD peaks. **B.** *Left:* Time-frequency spectrogram of DBS at 180 and 190 Hz. Both DBS blocks are separated by DBS bursts (label: DBS bursts) consisting of repetitive periods on and off DBS of variable length. *Right:* PSD shown for periods during DBS at 180 and 190 Hz and a 5-second reference after DBS ceased. Horizontal line, contours and arrowheads as in A. **C+D.** FTG frequencies during (C) and after (D) long DBS blocks plotted over DBS frequencies at 130 Hz, 180 Hz and 190 Hz (all blocks from patients 3 and 4). Despite varying DBS frequencies, the FTG stays at a

similar frequency. **E+F.** FTG amplitudes during (E) and after (F) long DBS blocks plotted over DBS frequencies at 130 Hz, 180 Hz and 190 Hz (all blocks from patients 3 and 4). During DBS, FTG amplitudes tend to be increased at higher driving frequencies.

5.4. Discussion

In this study, we show that STN-DBS induces FTG in the STN-LFP of about a third of patients after overnight withdrawal of antiparkinsonian medication. As previously reported, we also found significant coherence at FTG frequencies between the STN-LFP and EEG. However, unlike the FTG described in PD patients on dopaminergic medication, we recorded FTG while dyskinesias were absent. Furthermore, there was no evidence to suggest a shifting of the FTG frequency in the STN according to stimulation frequency off medication, and FTG could be maintained for ~ 20 seconds after DBS. These observations suggest that off medication the FTG was not entrained by DBS, although we did find that FTG frequencies subtly, but significantly, declined within and across consecutive DBS blocks.

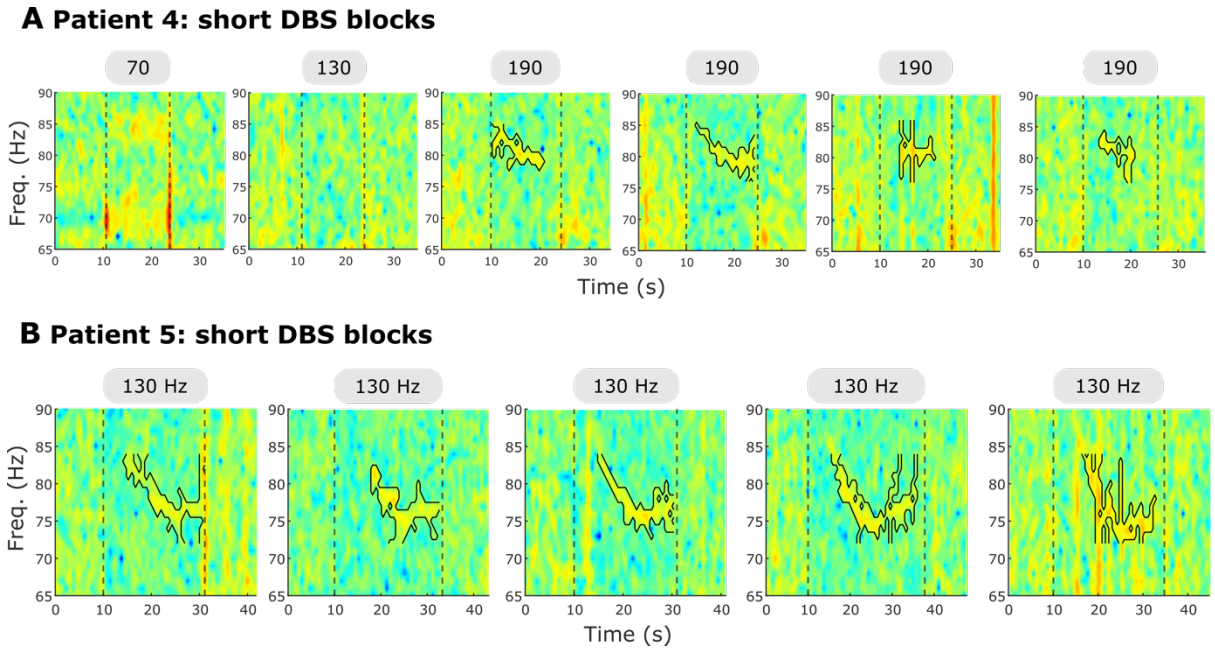


Figure 5.6. FTG in short DBS blocks. A. In patient 4, short DBS blocks of on average 13.1 ± 0.2 seconds (separated by resting periods of 149.0 ± 3.9 seconds) were tested at different DBS frequencies. The grey bars and vertical lines denote DBS onset and offset. DBS frequencies are shown in the boxes. Every frequency was tested four times (only one block shown for 70 and 130 Hz). Note the notch filter at 70 Hz when stimulation was at 70 Hz. Colour bar as in **Figure 5.6A**. The FTG feature is surrounded by a contour where present. **B.** In patient 5, short DBS blocks of on average 22.4 ± 1.2 seconds

(separated by resting periods of 177.2 ± 18.6 seconds) were tested at 130 Hz. The grey bars and vertical lines denote DBS onset and offset. Colour bar as in **Figure 5.6A**. The FTG feature is surrounded by a contour.

5.4.1. Was FTG induced or entrained by DBS?

Swann et al. (2016 and 2018) previously demonstrated that the FTG recorded at the cortical level in PD patients on medication may be entrained by high frequency stimulation of the STN when patients experience dyskinesia. This entrainment was manifest as a shift in the frequency of the FTG peak to that of the subharmonic of the stimulation frequency. Another study reported a correlation between power at FTG frequencies in STN and cortex and local power at the stimulation frequency (Muthuraman et al., 2020). However, this study could not establish entrainment through a shifting of FTG frequency to match subharmonics of the stimulation frequency, and did not directly demonstrate endogenous FTG at the stimulation sites during stimulation in the off medication state. In the current study, also off medication, we were able to record *de-novo* FTG, and demonstrate that it outlasted stimulation by on average 20s, or even appeared for the first time during this period. These relatively sustained stimulation after-effects in addition to the stability of FTG frequencies independent of the DBS frequency argue against simple entrainment of the FTG by DBS.

The lack of evidence of shifts in FTG frequency (or in LFP-EEG coherence) with different stimulation frequencies would also be against direct entrainment of FTG. Here, however, some caution is required. We recorded both a stereotyped frequency FTG in the power spectra density during stimulation, and signal at stimulation subharmonics. Totally discounting a physiological contribution to those subharmonics is difficult, although their narrow, fixed frequency and their duration precisely matching the duration of stimulation might point more to stimulus artefact. Also of note, the LFP-EEG coherence during DBS only disclosed a peak

at the same frequency as the FTG in corresponding power spectra of the LFP and not at half the stimulation frequency in patients 1, 4 and 5 (**Figure 5.7**).

In summary, the evidence argues against entrainment of the FTG by DBS off medication and is more in favour of the inducing of FTG as stimulation reconfigures networks to support this oscillation, perhaps paralleling how levodopa reconfigures networks to induce FTG (Jenkinson et al., 2013). Interestingly, the duration over which FTG outlasted stimulation is similar to the time beta oscillations take to return to pre-stimulation levels (Wiest et al., 2020), and corresponds to the delayed recovery of bradykinesia after cessation of DBS (Kühn et al., 2009).

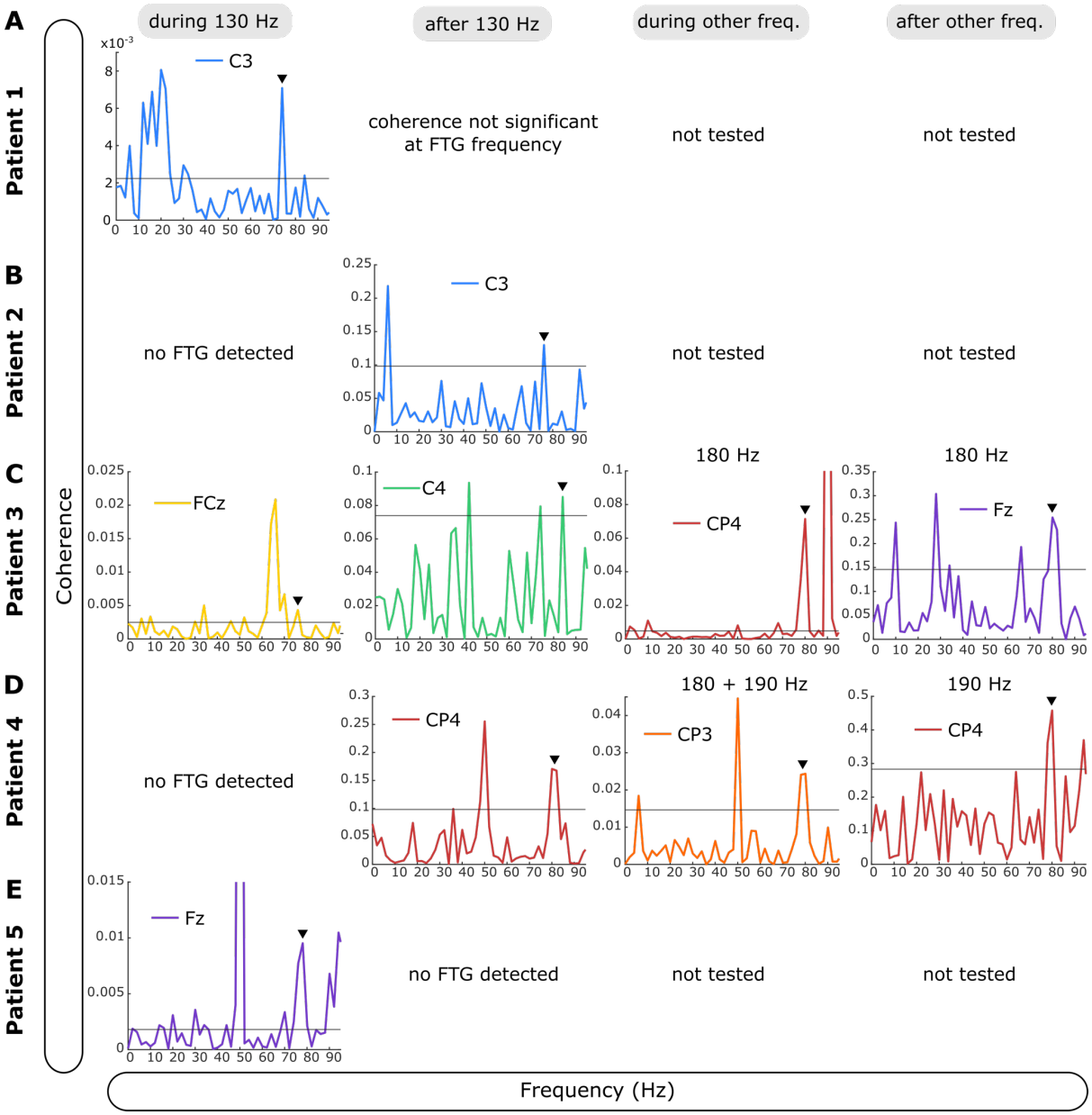


Figure 5.7. LFP-EEG coherence at FTG frequencies. A.-E. EEG channel with greatest coherence is shown for all FTG subjects. For during blocks analysis, time series were concatenated within subjects. For after block analysis, signals in a 5-second time window following cessation of DBS were concatenated within subjects. In patient 4 and 5 short and long DBS blocks were concatenated together. If not 130 Hz, DBS frequencies are shown on top of the plots. EEG channels are colour coded. Black horizontal line denotes the significance level (see Methods). Black arrowheads indicate the corresponding frequency of the FTG peak in the STN-LFP power spectrum. Coherence at FTG frequency was significant in all subjects shown. Note that artefactual coherence is variously seen at 50 Hz (line noise), 65 Hz (subharmonic of 130 Hz DBS) and 90 Hz (subharmonic of 180 Hz DBS).

Why might STN-DBS entrain FTG when patients are dyskinetic on medication in the case of the study by Swann et al (2016), but not when not dyskinetic off medication, as here? The former study sampled FTG from sensorimotor cortex, but this is unlikely to be responsible for the difference given that STN and cortical activities are coherent at FTG frequencies as reported previously (Brown et al., 2001; Cassidy et al., 2002; Litvak et al., 2012; Williams et al., 2002) and confirmed here. Perhaps more likely the difference arises from the effects of dopaminergic therapy. When this medication is withdrawn overnight, spontaneous FTG in the STN is absent or diminished (Jenkinson et al., 2013), and when induced by stimulation FTG does not shift in frequency according to the frequency of stimulation. On dopaminergic medication FTG is exaggerated and sharply tuned (in those recordings displaying such activity), suggesting an under-damped oscillation that is more likely to be subject to resonance-related phenomena like amplitude enhancement and entrainment by driving frequencies, or subharmonics thereof, that are relatively closely related in frequency. In summary, although off medication DBS may induce, but not entrain, FTG, the situation may be different on medication.

5.4.2. Why is the FTG an inconsistent finding across patients?

Only about a third of patients had an FTG induced by stimulation. One explanation might be that the FTG was obscured by a broadband power suppression during DBS in many patients. However, this is unlikely given that power suppression is only significant in the beta and low-

gamma range (Wiest et al., 2020). Another explanation might be that patients without FTG were under-stimulated. However, stimulation amplitudes ranged from 1.8 - 4 mA in both FTG and non-FTG subjects (**Table 5.1**). Instead, it is possible that the factors determining the presence or absence of FTG during or immediately after stimulation might be similar to those determining the presence or absence of FTG in patients on medication, where a similar proportion of patients display FTG (López-Azcárate et al., 2010b). While the FTG can be detected in a widely distributed network, including thalamus, internal segment of the globus pallidus, STN and cortex, within these sites it may be highly focal. In the STN, in particular, FTG arises within the dorsolateral STN and adjacent Zona incerta (Lofredi et al., 2018; Trottenberg et al., 2006), raising the possibility that minor differences in electrode placement may account for the presence or absence of FTG within our, and other, cohorts. These differences, if they exist, were too small to be picked up by the imaging co-registration techniques in our limited sample (see **Table 5.1**). It could also be that the processes supporting gamma synchrony are susceptible to the stun effect of surgery, but chronic recordings in the same patients will be necessary to establish this. Finally, there might be phenotypic differences that determine the presence of FTG. Of these, the propensity for dyskinesias has received the most interest (Alonso-Frech et al., 2006; Fogelson et al., 2005; Swann et al., 2016). The induced FTG lasted 10s of seconds following the cessation of stimulation which mirrors the time necessary for DBS-induced dyskinesias to subside. However, we studied patients in the off medication state, without dyskinesias. The FTG therefore does not seem to be exclusively linked to dyskinesias (see **Table 5.1**) as it has also been shown in invasive recordings from patients suffering from dystonia and myoclonus epilepsy at rest (Kempf et al., 2009). At best therefore, the FTG induced by stimulation in the off medication state may be a trait marker of the propensity for dyskinesias, even if on medication it may be more directly involved in the generation of these involuntary movements (Swann et al., 2016; Swann et al., 2018).

5.4.3. Study Limitations

Our study has a relatively low sample size of 14 patients (17 STNs), with only a minority of these showing an induced FTG. Although we used linear mixed-effects models which allow for comparisons of small sample sizes (Muth et al., 2016), we acknowledge that our results should be interpreted carefully and require corroboration in a larger sample. In addition, recordings shortly after DBS surgery may be confounded by transient symptom alleviation and circuit disruption due to electrode implantation (Chiung Chu Chen et al., 2006b; Mann et al., 2009).

5.4.4. Conclusions

We report FTG oscillations that arise *de-novo* during or immediately after STN-DBS in the off-medication state, which can be seen in the STN-LFP and in the coherence between this and EEG. The response to different stimulation frequencies and the prolonged stimulation after-effects suggest that in the off medication state the FTG is induced rather than entrained, providing evidence of a stimulation-related reconfiguration of basal ganglia circuits to support gamma oscillations. The presence of slow changes in FTG frequency within and across consecutive DBS blocks suggests that such circuit reconfiguration may itself subtly evolve over time.

5.5. Summarised Findings

- DBS induces *de-novo* finely-tuned gamma (FTG) oscillations in the subthalamic LFP
- Induced FTG appears off levodopa and without dyskinesias
- FTG frequencies change within and across consecutive stimulation periods
- STN-LFP and cortical activities are coherent at FTG frequencies

6. Project 4: Finely-tuned gamma oscillations: Spectral characteristics and links to dyskinesia

6.1. Introduction 156
6.2. Comparison of different gamma oscillations 158
6.2.1. Levodopa-induced finely-tuned gamma oscillations 159
6.2.2. Stimulation-induced finely-tuned gamma oscillations 160
6.2.3. Movement-related broadband gamma synchronisation 161
6.2.4. Differences in spectral and temporal characteristics between FTG and movement-related gamma synchronization 162
6.3. Functional role of FTG 164
6.3.1. FTG is modulated by movement 164
6.3.2. FTG varies with wakefulness, sleep stages, arousal and startle reactions 165
6.3.3. FTG accompanies dyskinesias 165
6.3.3.1. Human studies supporting the link between FTG and levodopa-induced dyskinesia 165
6.3.3.2. Human studies challenging the link between FTG and levodopa-induced dyskinesia 166
6.3.3.3. Evidence from animal studies supporting the link between cortical FTG and dyskinesia 167
6.3.3.4. Animal studies challenging the link between cortical FTG and dyskinesia 168
6.3.4. Controversies emanating from cortical and subcortical FTG 169
6.4. Implications for deep brain stimulation 170
6.4.1. A marker for stimulating the correct circuit 170
6.4.2. A feedback signal for aDBS 171
6.4.2.1. Advantages and promises of cortical FTG as a biomarker for levodopa-induced dyskinesia 171
6.4.2.2. Practical concerns of cortical FTG as a biomarker for levodopa-induced dyskinesia 172
6.4.2.3. Subcortical FTG may lack the specificity and consistency required for a biomarker for levodopa-induced dyskinesia 173
6.5. Conclusions 174
6.6. Summarised Findings 175
6.7. Summary of Key Contributions 175

Here, we provide an in depth comparison of levodopa-induced FTG, DBS-induced FTG and movement-related gamma synchronisation. We further elaborate on a potential clinical use of the FTG. This work was published in (C Wiest et al., 2022).

6.1. Introduction

Gamma rhythms generally refer to neural activities recorded within the 30-100 Hz frequency range (or higher) and are ubiquitous within the human motor system. The first link between voluntary movement and gamma rhythms was made by Hans Piper in the beginning of the 20th century, who demonstrated that EMGs recorded during strong voluntary contractions showed rhythmic activity at around 40 Hz (Piper rhythm) (Piper, 1907). Later, it was shown that this muscle rhythm was driven by comparable oscillatory activities in the contralateral motor cortex (Brown et al., 1998). Ever since, interest in the role of gamma oscillations in motor control soared leading to the observation that the gamma range comprises several heterogeneous activities, which are easily conflated in the scientific literature. Two main activities seem to crystallise.

First, finely-tuned gamma (FTG) oscillations comprise a narrowband activity with peak frequencies between 60-90 Hz and can be extracted from local field potentials (LFP) recorded from cortical and subcortical areas. FTG is primarily an induced activity in patients with Parkinson's disease (PD), either by dopaminergic medication or deep brain stimulation (DBS). Recently, FTG measured invasively over the motor cortex has been proposed as a promising biomarker for dyskinesia in adaptive stimulation algorithms (Swann et al., 2016).

Second, movement execution elicits a rapid increase of broad gamma activity that can be recorded from both cortical and subcortical motor regions contralateral to movement. This gamma event-related synchronisation (gamma ERS) is typically described as a prokinetic rhythm that promotes movement and encodes vigour of motor output (Androulidakis et al., 2007b; Anzak et al., 2012). However, broad gamma ERS was also observed when movements were successfully stopped (Fischer et al., 2017; Ray et al., 2012) and it changes with different levels of alertness (Brücke et al., 2013), which suggests a more versatile role.

Adaptive deep brain stimulation (aDBS) aims to automatically adjust stimulation parameters in response to real-time detection of temporal changes in the patient's neurophysiological or clinical state. It has been suggested as an improvement to conventional continuous DBS of the subthalamic nucleus (STN) for PD given its potential to decrease side-effects while maintaining clinical efficacy (Arlotti et al., 2018; Little et al., 2013; Little and Brown, 2020; Swann et al., 2016; Velisar et al., 2019). In aDBS, the clinical state inferred from brain signals, peripheral biomarkers, or a combination of both determines when and how much to stimulate. Ideally, a prospective marker comprises as many of the following requirements as possible: signals need to be sensitive and specific to the pathological state, tightly time-locked to symptoms, reliable over time and localise to the respective target nucleus (Steiner et al., 2019); they must be calculable with low computational requirements, feasible for implantable devices and provide rapid feedback. Markers with a causal link to pathological symptoms allow DBS to be specifically patterned to maximally disrupt causal circuit dynamics (Little et al., 2016b). However, secondary activities with good correlation to clinical state may still prove to be helpful as feedback.

In this review, we put emphasis on the FTG and discuss its functional role and potential use for aDBS in the future. At first, we describe spectral and temporal characteristics of levodopa and DBS-induced FTG, and compare them with those of movement-related gamma synchronisation. We use our data to reproduce findings that support the narrative. Afterwards, we review literature on the potential functional role of FTG, such as its modulation with voluntary movement and changes in alertness and states of wakefulness. We conclude this section with the link between FTG and dyskinesias. The third part focuses on the potential use of the FTG in aDBS; either as a marker for stimulating the most effective circuit or as a biomarker to track dyskinesias.

6.2. Comparison of different gamma oscillations

FTG comprises oscillations in a narrow frequency band between 60-90 Hz. However, the scientific literature so far has not provided a clear distinction between FTG and movement-related gamma ERS with the two often considered equivalent and at times used interchangeably (Cheyne et al., 2008; Fischer, 2021; Jenkinson et al., 2013; Lofredi et al., 2018). Here, we first review the literature on these different gamma oscillations, compare their temporal and spectral characteristics and discuss how different analysis methods may lead to conflation.

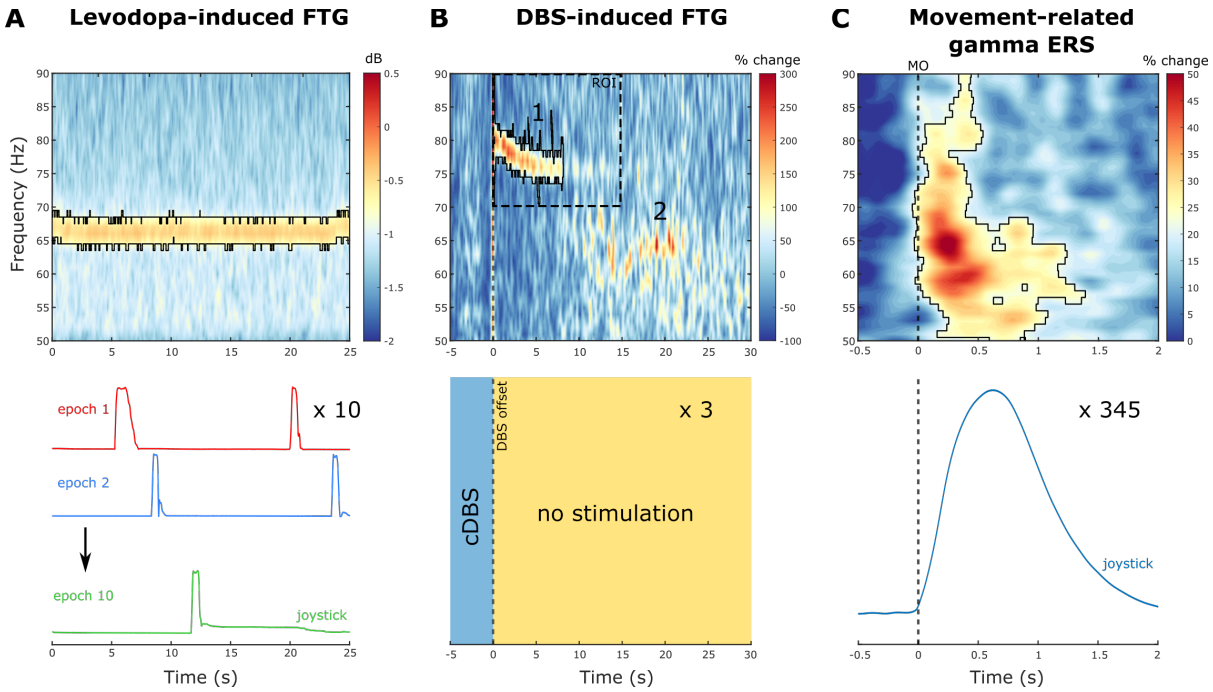


Figure 6.1. Comparison of different gamma rhythms. A. Time-frequency spectrogram of levodopa-induced FTG at rest. The spectrogram of a 250 s recording during a joystick task on dopaminergic medication was divided into 10 segments of 25 s, which were averaged to cancel out movement effects. *Bottom*: Examples of the unaligned joystick movements of 3 epochs. **B.** Time-frequency spectrogram of activity changes in the gamma range after deep brain stimulation was switched off (at 0 s). Three consecutive blocks (3 minutes each) of continuous STN-stimulation were applied in this patient (with sufficient resting in between). Spectrograms were aligned to DBS offset, baseline normalised to a 60-second window before each stimulation block and averaged. A post-DBS induced FTG is observed (label 1) along with a broader post-DBS gamma rebound at a lower frequency band (label 2). *Bottom:* Schematic of when stimulation was switched off. **C.** Time-frequency spectrogram of broadband movement-related gamma activity off dopaminergic medication. 345 joystick movements from one patient were aligned to movement onset (at 0 s), baseline normalised using a 2-second windows (-2.5 to -0.5 s) and averaged. *Bottom:* Average of all 345 joystick movements aligned to movement onset (MO). Data in A-C was recorded from 3 different patients with Parkinson's disease with different bipolar configurations. The same time-frequency decomposition was performed using complex Morlet wavelet transform (50 cycles) for A-C (see Methods). The black contour contains all power estimates

above the 70th/90th percentile (see Methods for details). The region of interest (ROI) to compute the contour is shown in B. In A and C the ROI corresponds to the shown axes. Note the different time axes and colour bars.

6.2.1. Levodopa-induced finely-tuned gamma oscillations

FTG in motor cortex and basal ganglia can be induced by dopaminergic medication – primarily levodopa – in PD patients (**Table 6.S1**) or hemiparkinsonian rats after 6-OHDA (6-Hydroxydopamine) lesion (**Table 6.S2**). Levodopa-induced FTG occurs minutes to hours after levodopa intake in about 23% of PD patients (López-Azcárate et al., 2010a) and comprises a narrowband activity with slightly varying peak frequencies across subjects between 60-90 Hz (**Table 6.S3**). It is present at rest (**Figure 6.1A**) or during the execution of a motor task, where it appears either continuously (**Figure 6.2**) or sporadically (Jenkinson et al., 2013, see section 3.1). Levodopa-induced FTG has been recorded from a widely distributed network including STN (Cassidy et al., 2002), GPi (Brown et al., 2001; Williams et al., 2002), Zona incerta (Pogosyan et al., 2006; Trottenberg et al., 2006), thalamus (Kempf et al., 2009), striatum (Halje et al., 2012) and motor cortex (Swann et al., 2018, 2016; Williams et al., 2002). Significant coherence at FTG frequencies has been reported across the cortico-basal ganglia-thalamic loop (Brown et al., 2001; Cassidy et al., 2002; Lalo et al., 2008). Despite its ubiquity, within every nucleus it is highly focal (Pogosyan et al., 2006; Trottenberg et al., 2006). Apart from PD, thalamic FTG has been detected in a variety of neurological disorders including ET, dystonia and myoclonic epilepsy, where it was not related to dopaminergic medication (Kempf et al., 2009).

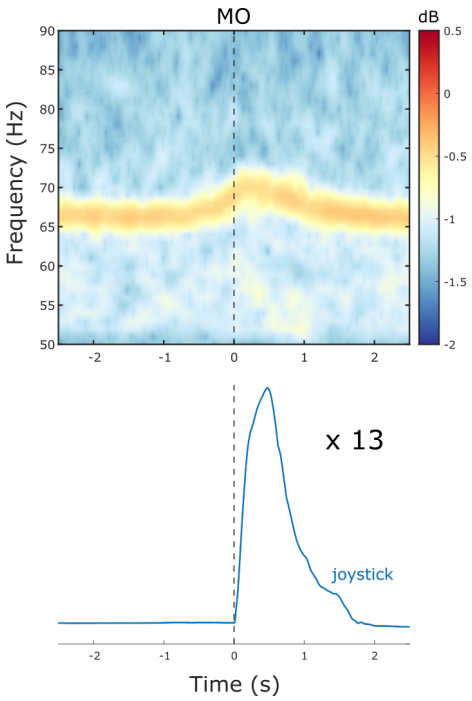


Figure 6.2. Levodopa-induced finely-tuned gamma (FTG) oscillations are modulated by movement. A patient with Parkinson's disease performed a joystick task while contralateral local field potentials were recorded from an externalised electrode in the subthalamic nucleus. Time-frequency spectrogram on dopaminergic medication is shown. All 13 joystick movements were aligned to movement onset (MO) and averaged. Note the FTG frequency increase just before MO which lasts for about 1 s. Bottom: Average of all joystick movements aligned to MO.

6.2.2. Stimulation-induced finely-tuned gamma oscillations

Recently, FTG activity was reported in patients with PD in the absence of dopaminergic medication; either during or after continuous high-frequency stimulation of the STN at 130 Hz (**Table 6.S4** and **Figure 6.1B**). More specifically, we reported DBS-induced FTG in about a third of patients starting with a slight delay of a few seconds after stimulation was switched on and slightly decreasing in frequency over time (Wiest et al., 2021). In 4 out of 5 patients, FTG was observed for several seconds after stimulation was switched off; either outlasting continuous DBS or starting de-novo after stimulation offset. Similar to levodopa-induced FTG, DBS-induced FTG is sharply tuned and occupies a narrow frequency band between 60-90 Hz (**Figure 6.1B**), with peak frequencies slightly varying across subjects (**Table 6.S3**). The occurrence of such a finely-tuned oscillatory activity concomitantly with DBS raises the question of entrainment. In a previous study on levodopa-induced FTG, Swann and colleagues

described that cortical FTG peak frequencies shifted from ~80 Hz to a subharmonic of stimulation when 130 Hz STN-DBS was switched on (Swann et al., 2016). This argues in favour of entrainment of cortical FTG to DBS. However, DBS-induced FTG off medication in STN and STN-cortical coherence were not locked at a subharmonic of the stimulation frequency (Muthuraman et al., 2020; Wiest et al., 2021) and the authors showed relatively sustained stimulation after-effects arguing against simple entrainment.

6.2.3. Movement-related broadband gamma synchronisation

Following the first observations of Hans Piper, numerous human studies confirmed movement-related changes in the gamma band (**Table 6.S5**) and extended the frequency range from 30-100 Hz (**Figure 6.1C**) and sometimes even beyond up to 400 Hz (Anzak et al., 2012). Broadband gamma synchrony at movement onset has been recorded in the contralateral motor cortex (Cheyne and Ferrari, 2013), STN, GPi and thalamus (Brücke et al., 2012; Litvak et al., 2012; Lofredi et al., 2018; Tan et al., 2013) and increases on levodopa (Androulidakis et al., 2007b). Moreover, gamma ERS peaks at movement onset and declines throughout the duration of sustained movements (Anzak et al., 2012; Lofredi et al., 2018; Muthukumaraswamy, 2010). Although most studies on basal ganglia electrophysiology were performed in PD, movement-related gamma synchronisation has been evidenced in healthy humans in motor cortex (Cheyne et al., 2008; Muthukumaraswamy, 2010) and patients with dystonia in the GPi (Brücke et al., 2008; Eric W Tsang et al., 2012) or essential tremor (ET) in the thalamus (Brücke et al., 2013). Broadband movement-related gamma synchronisation appeared to correlate with gripping force, size and velocity of voluntary movements and motor effort (Anzak et al., 2012; Brücke et al., 2012; Joundi et al., 2013; Lofredi et al., 2018; Tan et al., 2013). Brücke and colleagues found that baseline broadband gamma power recorded from thalamus before a Go cue correlated with reaction times in a Go-noGo task (Brücke et al., 2013). Thus, broadband gamma ERS may promote movement and encode vigour of motor output. The prokinetic nature of

broad gamma ERS is underlined by studies in which movement preparation and passive limb displacements without active movements are accompanied by firing rate changes but not gamma synchronisation (Cassidy et al., 2002; Liu et al., 2008; Muthukumaraswamy, 2010) suggesting their involvement in movement initiation. A recent review suggested that small temporal shifts of cortical activity may unleash broadband gamma synchronisation in the basal ganglia and trigger movement initiation (Fischer, 2021) and broadband corticospinal gamma coherence may aid to optimally couple remote regions (Schoffelen et al., 2005). Interestingly, gamma ERS also occurred in successfully inhibited stop-trials without any obvious movements arguing for a more versatile role and suggesting that broadband gamma may relate to facilitation of dynamic processing instead of solely being prokinetic (Fischer et al., 2017; Ray et al., 2012). In line with this, broad gamma ERS has also been linked to arousal during sleep and alertness during cognitive tasks in epileptic patients (Gross and Gotman, 1999).

Given the relatively large frequency range of movement-related gamma synchronisation, it is also possible that it is divided into multiple subunits. Crone and colleagues report two different gamma bands during movements – low gamma ERS from 35-50 Hz and high gamma ERS from 75-100 Hz – with distinct temporal and spatial characteristics (Crone et al., 1998). Low gamma oscillations often began after movement onset and were sustained throughout while high gamma ERS started during, or slightly before, movements and was short-lived, ending before completion of the movement response. This hints at different neurophysiological mechanisms.

6.2.4. Differences in spectral and temporal characteristics between FTG and movement-related gamma synchronization

Conflation and confusion of FTG and movement-related gamma in the literature may be partly due to different methods and parameter settings used for time-frequency decomposition, in which there is always a trade-off between frequency precision and temporal precision. When

studying movement-related changes, methods and parameter settings with higher temporal resolution tend to be used to capture fast changes over time, which may lead to extension of synchrony along the frequency axis. When movement-related broad gamma ERS was reported in previous literature, normalised power spectra relative to a pre-cue baseline were presented and results were averaged across subjects and trials. Thus, the broad frequency band with activity increase shown in the averaged power spectra may be due to cross-subject variance. Inversely, when studying activities at rest, methods and settings with higher frequency precision are often used, as in most cases for FTG analysis. In addition, when FTG was reported, data from individual subjects were presented partly due to the paucity of the data. To get an overview of the variance in methods used for spectral decomposition see **Tables 6.S1, 6.S2, 6.S4 and 6.S5**.

Here, we used the same method with the same parameters for time-frequency decomposition and re-analysed previously published data to compare spectral and temporal characteristics of FTG and movement-related gamma ERS. As shown in **Figure 6.1**, broadband gamma ERS spans an eponymous larger frequency range and on average has a lower peak frequency compared to both levodopa-induced and DBS-induced FTG. The peak frequency, frequency bandwidth, average duration and peak amplitude of movement-related gamma ERS, levodopa-induced FTG and DBS-induced FTG are presented in **Table 6.S3**. Movement-related gamma ERS is transient and vanishes after milliseconds to a few seconds whereas DBS-induced FTG may outlast stimulation for several seconds to more than a minute and levodopa-induced FTG may be present over many minutes to hours. Also, the relative amplitude increase of broad gamma ERS is less pronounced than that of DBS-induced FTG (**Table 6.S3**).

6.3. Functional role of FTG

Given the paucity of studies on DBS-induced FTG, this section mostly relates to levodopa-induced FTG.

6.3.1. FTG is modulated by movement

Levodopa-induced FTG in STN of PD patients is observable at rest, and its amplitude and frequency slightly increase with voluntary movements when compared to baseline (Alegre et al., 2005). This modulation is transient and subsides within 1-2 s. Similarly, FTG modulation with voluntary movements was observed in thalamic LFPs in patients with PD on levodopa and other pathologies (Kempf et al., 2009), indicating that movement-related modulation of the FTG in the basal ganglia and thalamus may reflect healthy motor function. Movement-related synchronisation in these two studies is sharper than broadband gamma ERS (**Table 6.S5**) and unlikely due to differences in time-frequency decomposition. We reproduced their findings in a PD patient that displayed levodopa-induced FTG in the STN at rest while performing a joystick task (**Figure 6.2**). This suggests that levodopa-induced FTG is directly modulated by movement and likely not overlaid by broadband gamma ERS. In support of this, Lofredi and colleagues suggest that FTG may scale with motor output and broadband gamma may reflect local spiking in STN (Lofredi et al., 2018). On the other hand, a single observation in one PD patient revealed that levodopa-induced FTG may sporadically appear and disappear over time without time-locking to movements (Jenkinson et al., 2013).

Note, however, that cortical FTG seems to be relatively unaffected by voluntary movement when described at the single trial level (de Hemptinne et al., 2019; Miocinovic et al., 2018; Swann et al., 2016). Of note, simultaneous recordings of cortical and subcortical FTG so far are sparse. Whether both are equally modulated by movement would be best addressed in a controlled within subject movement task, which may be complicated by concomitant dyskinesias.

6.3.2. FTG varies with wakefulness, sleep stages, arousal and startle reactions

The connection between levodopa-induced FTG and wakefulness was suggested following the observation that in one PD patient STN-FTG disappeared, as he became drowsy (Brown et al., 2001). The authors suggest this ~70 Hz signal to be a carrier rhythm for motor commands while the patient is awake. In another study, Kempf and colleagues showed modulation of thalamic FTG throughout the sleep-wake cycle (Kempf et al., 2009). While FTG was manifest during waking, it was suppressed during slow-wave sleep and re-emerged during REM phases. Of note, FTG was not exclusively linked to periods of rapid eye movement and hence underlying motor processing. It should, however, be acknowledged that arousal, drowsiness and sleep stages are linked with other spectral changes in addition to FTG (Cantero et al., 2002; Santamaria and Chiappa, 1987).

Kempf and colleagues also report an increase of FTG amplitude and/or frequency in response to unexpected acoustic stimuli. Of note, startle-related FTG changes outlasted associated motor activation.

6.3.3. FTG accompanies dyskinesias

Following treatment with levodopa, PD patients may develop abnormal involuntary movements, referred as levodopa-induced dyskinesias (LID). First, we will discuss human studies in support of and against a link between FTG and dyskinesias before moving to animal studies that support and challenge this connection.

6.3.3.1. Human studies supporting the link between FTG and levodopa-induced dyskinesia

Table 6.S1 shows studies in which LFP recordings in the STN or over the motor cortex of PD patients displayed levodopa-induced FTG during episodes of dyskinesia, suggesting that the

two might be related (Alonso-Frech et al., 2006; Fogelson et al., 2005; Swann et al., 2018, 2016). Swann and colleagues recorded FTG over the primary motor cortex (M1) and in STN with coherence between these two sites during periods of dyskinesia in two patients using chronically implanted pulse generators (Swann et al., 2016). All four measures (M1-FTG power, STN-FTG power, phase coherence and magnitude-squared coherence) in this study distinguished the dyskinetic from the non-dyskinetic state. Furthermore, the authors reported frequency shifts of levodopa-induced FTG as DBS frequency changes, suggesting entrainment of FTG at half the stimulation frequency. Swann and colleagues also report constant phase coupling between cortical and STN-FTG during dyskinesia regardless of whether DBS was switched on or off, suggesting that this phase relationship is unlikely explained by a subharmonic of stimulation. However, other studies up to date could not replicate FTG entrainment at a subharmonic frequency when patients were off medication (Muthuraman et al., 2020; Wiest et al., 2021). It is possible that activities in subcortical areas are less susceptible to entrainment and frequency shifting especially in the dopamine-deficient state. Alternatively, entrainment may also be dependent on stimulation currents.

6.3.3.2. Human studies challenging the link between FTG and levodopa-induced dyskinesia

A clear link between the presence of STN-FTG and LID in humans may be difficult to prove. Stimulation-induced FTG was recorded in the STN-LFP of PD patients when they were off dopaminergic medication while no dyskinesias were present and the FTG was not locked at a subharmonic of stimulation as reported for cortical FTG (Wiest et al., 2021). Even if subtle dyskinesias may have not been detected in this study, in 2 out of 5 subjects FTG only started after DBS offset and was absent during DBS when dyskinesias are supposed to be strongest. This paradox argues against a fixed temporal relationship between dyskinesias and DBS-induced FTG recorded in STN. Furthermore, the authors observed a broader post-DBS gamma

rebound that comes in about 15 seconds after DBS offset (Wiest et al., 2021 and **Figure 6.1B**). While its frequency and broad character are more similar to movement-related gamma ERS, this activity appears movement-independent. Given the gap of several seconds from stimulation, this activity is unlikely to reflect the weaning of DBS-induced dyskinesias; it may rather represent a rebound following low-gamma desynchronization during DBS (Wiest et al., 2021, 2020). A different study used indirect measures to estimate subcortical electrophysiology and reports cross-frequency-coupling between FTG power and power at stimulation frequency off dopaminergic medication, without dyskinesias and not locked at a subharmonic of stimulation (Muthuraman et al., 2020). In addition, an earlier study found a more prominent change of low frequency activity (4-10 Hz) mirroring LID (Alonso-Frech et al., 2006). Fogelson and colleagues reported that over 70% of patients with STN macroelectrodes showing a negative correlation between levodopa-induced FTG and low-frequency power were dyskinetic in the contralateral limb during recording (Fogelson et al., 2005). However, this study hinted at insufficient specificity and sensitivity since some patients displayed negative correlations without dyskinesias and others had dyskinesias without negative correlations.

6.3.3.3. Evidence from animal studies supporting the link between cortical FTG and dyskinesia

Several rodent studies (summarised in **Table 6.S2**) support the link between FTG and dyskinesias. Halje and colleagues recorded FTG over the primary motor cortex during LID in hemiparkinsonian rats (Halje et al., 2012). Both cortical FTG and dyskinesias were reversed with a dopamine antagonist. Interestingly, this study found more prominent FTG in motor cortex than in striatum suggesting that loss of cortical dopaminergic innervation may be a key predisposing factor for LID, which makes cortex prone to network resonance at FTG frequency. However, it is still unclear if there exists a causal relationship between LID and cortical FTG or if it is epiphenomenal. The same study found a sigmoidal relationship between

FTG power and dyskinesia severity and suggested that FTG frequencies may depend on the time of recording relative to levodopa intake (Halje et al., 2012). Dupre and colleagues demonstrated similar reversibility of cortical FTG and dyskinesia. Dyskinesias along with an 80 Hz oscillatory signal in the motor cortex could be induced by levodopa, D_1 and D_2 receptor agonists, reversed by a serotonin agonist and brought back using a serotonin antagonist (Brys et al., 2018; Dupre et al., 2016). This study casts doubt on the prevailing view of striatal hypersensitivity to dopamine and D_1R-mediated signalling in the dopamine-denervated striatum as a source for LID (Cenci and Konradi, 2010; Espay et al., 2018). Delaville and colleagues confirmed the link between FTG and LID and report coherence between motor cortex and STN or mPFC at FTG frequencies (Delaville et al., 2015). More recently, Güttler and colleagues proposed cortical gamma burst duration and amplitude as a correlative marker for LID (Güttler et al., 2020). Interestingly, FTG detected in the motor cortex in all four animal studies showed an initial frequency drop; a dynamic which was also observed at a different time scale in DBS-induced FTG in PD patients in STN (Wiest et al., 2021) but not in cortical human recordings (Swann et al., 2018).

6.3.3.4. Animal studies challenging the link between cortical FTG and dyskinesia

Although Dupre and colleagues report a positive relationship between dyskinesia and cortical FTG occurrence, they also provide compelling arguments against a direct relationship between the two (Dupre et al., 2016). First, in this study only forelimb AIMs (abnormal involuntary movements) were positively and constantly correlated with FTG. Orolingual AIMs only on the first day and axial AIMs never showed a positive correlation between the two. Second, while a serotonin agonist similarly improved LID and dopamine-agonist-induced dyskinesia, the FTG in motor cortex was diminished by varying degrees in both cases. Third, muscimol injection to the ventromedial thalamus before or after levodopa injection eliminates cortical

FTG without modifying dyskinesia scores (Dupre et al., 2016). This supports the subcortical genesis of FTG and dissociation between cortical FTG and dyskinesia. Fourth, a recent study in 6-OHDA lesioned rats linked high-dose levodopa priming with an FTG ~80 Hz and LID; however, low-dose priming resulted in LID without FTG, indicating ~80 Hz FTG is not an exclusive marker for LID (Ye et al., 2021). Instead, the authors found striatal broadband gamma and corticostriatal theta to high-gamma cross-frequency coupling (CFC) were enhanced in LID and sub-anaesthetic ketamine effectively reduced LID and theta to high-gamma CFC.

6.3.4. Controversies emanating from cortical and subcortical FTG

The literature discussed above points towards different relationships of cortical and subcortical FTG with dyskinesia, with more evidence supporting a positive relationship between cortical FTG and dyskinesia. It is unclear, however, if FTG is of cortical or subcortical origin. While neuronal spiking tends to be phase-locked to exaggerated beta oscillations (Kühn et al., 2005; Levy et al., 2002; Weinberger et al., 2006), phase locking of cortical spikes is negatively correlated with high gamma LFP (Dupre et al., 2016). This argues against earlier views of cortical subcircuits generating recurrent rhythms via interactions of pyramidal neurons and interneurons (Börgers et al., 2005; Lee and Jones, 2013). It rather supports the hypothesis that cortical FTG is driven by subcortical input such as thalamus (Jenkinson et al., 2013). Moreover, gamma coupling between STN and cortex is driven by STN (Litvak et al., 2012; Sharott et al., 2018) which affords a more executive role to the basal ganglia. However, Halje and colleagues report stronger FTG in cortex than in striatum suggesting a cortical origin.

Despite the abundance of literature on STN-cortex coherence in the gamma range (Brown et al., 2001; Cassidy et al., 2002; Lalo et al., 2008; Wiest et al., 2021), cortical and subcortical FTG differ with respect to sensitivity and specificity to dyskinesias, entrainment at half

stimulation frequency and modulation by voluntary movements. Given this functional disparity, it is possible that both activities are unrelated.

6.4. Implications for deep brain stimulation

6.4.1. A marker for stimulating the correct circuit

In previous studies, FTG was shown to be focal to the dorsolateral STN and adjacent caudal Zona incerta in intraoperative recordings (Pogosyan et al., 2006; Trottenberg et al., 2006). A recent study recorded levodopa-induced FTG along the trajectory during lead implantation and found that FTG power was stronger superior of the STN than within STN (Ozturk et al., 2020). FTG was detected up to 10 mm above the dorsal STN border, an area likely within thalamus. Of note, the patient presented generalised choreiform dyskinesias during the recording. This is interesting since a common approach to improve stimulation-induced dyskinesias is to switch to more dorsal contacts that are likely placed within Zona incerta (Picillo et al., 2016). The antidyskinetic effect of this is believed to be mediated through stimulation of pallidofugal fibres resembling combined stimulation of ventral GPi and STN (Herzog et al., 2007).

It has been shown that cortical FTG can be unleashed by pallidotomy and its emergence was suggested to be mechanistically related to improvement in bradykinesia (de Hemptinne et al., 2019). DBS-induced FTG in the STN that starts a couple of seconds after DBS onset and outlasts stimulation by several seconds, as we reported in a previous study, may similarly reflect clinical improvement (Wiest et al., 2021). Recently, Muthuraman and colleagues reported CFC between FTG and DBS frequency in cortical (motor cortex, supplementary motor area, premotor cortex) and subcortical areas (STN and cerebellum) (Muthuraman et al., 2020). CFC negatively correlated with clinical impairment, and was only present when DBS was delivered to STN at clinically effective stimulation frequencies. Therefore, FTG or coherence at this frequency may serve as an indicator for good clinical response and as a marker of

interference with the right neural circuit. The fact that FTG can be recorded from multiple nuclei within the basal ganglia loop and cortex is in support of this. Critically, the link between FTG and dyskinesia points in the same direction. While DBS-induced dyskinesias represent a bothersome side effect, they are also an indicator of stimulating the sweet spot when stimulation currents are sufficiently increased and the contact eliciting dyskinesia is generally the most effective in relieving PD symptoms (Picillo et al., 2016).

6.4.2. A feedback signal for aDBS

Although there is good reason to believe in a link between cortical FTG and dyskinesias based on preclinical and clinical studies, several points are unclear. Next, we will discuss advantages and disadvantages of cortical FTG as a biomarker and finish with a few challenges to its use in aDBS.

6.4.2.1. Advantages and promises of cortical FTG as a biomarker for levodopa-induced dyskinesia

The specificity and sensitivity of separating periods with and without dyskinesia by means of cortical FTG is promising (Swann et al., 2016) and a couple of practical considerations speak in favour of cortical FTG as a control signal. First, while stimulating, STN-LFP has to be recorded in bipolar mode from contacts either side of stimulation in order to reduce stimulation artefacts, which limits the flexibility in selecting recording and stimulation contacts. In contrast, cortical sensing is less limited by the choice of available contacts for stimulation in the target structure. Second, STN-LFP is a low amplitude signal – gamma oscillations even lower than beta, which is still affected by stimulation artefacts delivered to adjacent contacts. Nevertheless, several studies have managed to extract meaningful information using externalised electrodes (Deffains et al., 2018; Little et al., 2013; Tinkhauser et al., 2017; Wiest et al., 2020 and more). However, whether signals in the gamma frequency band in the STN can

be reliably detected in real-time from an implantable device in the presence of stimulation artefacts is still unclear. Third, even though DBS-induced FTG was recorded from STN in some cases, this activity is coherent with cortical activities at FTG frequencies as we showed in a previous study (Wiest et al., 2021) and ECoG electrodes placed over the motor cortex may have picked this activity up as well. Fourth, a recent study used wireless, multichannel streaming of LFPs during normal daily activities and found better decoding with multisite sensing (Gilron et al., 2021). They used STN-M1 coherence in the beta and gamma range to distinguish mobile from immobile states and found that multisite sensing can be particularly useful for individuals with milder motor fluctuations. Another study in PD patients undergoing DBS implantation concluded that contralateral sensorimotor ECoG recordings outperformed contralateral STN-LFPs for grip force decoding when different machine learning methods are used, with gradient boosted trees (XGBOOST framework) showing the highest performance (Merk et al., 2021).

6.4.2.2. Practical concerns of cortical FTG as a biomarker for levodopa-induced dyskinesia

Cortical FTG has been trialled in two patients as a feedback signal to track dyskinetic states in a proof of principle study, however, this short-term study of aDBS could not show therapeutic superiority over cDBS (Swann et al., 2018).

A couple of practical concerns need to be considered when using cortical FTG as feedback signals for aDBS in long-term studies. First, chronic ECoG recordings require the insertion of subdural leads. Although these have not been linked with increased risks of infection (Sisterson et al., 2021), their insertion in addition to DBS electrodes creates a small additional risk of haemorrhage and disability. Second, currently existing FTG-based DBS algorithms would not modulate stimulation outside of periods with dyskinesia. Coupling the algorithm with an additional feedback loop to index bradykinesia or tremor might further improve symptom

control. Third, signal to noise ratio for gamma band activities may still be low even if ECoG recordings were less affected by stimulation artefacts. In an earlier study using cortical sensing, data recorded from 3 out of 5 patients had to be excluded in part because the FTG did not rise over the amplifier signal to noise ratio when using the Medtronic Activa PC+S device (Swann et al., 2016). Despite a relatively high sampling rate for chronically implanted pulse generators with sensing capability which would require manufacturer approval to unlock more technical features, stimulation can still sometimes produce narrowband artefacts, due to aliasing, which need to be distinguished from physiological signal. Last but not least, the dyskinesia-related FTG may need to be differentiated from voluntary movement-related gamma ERS, based on the spectral characteristics or temporal dynamics, as we discussed.

6.4.2.3. Subcortical FTG may lack the specificity and consistency required for a biomarker for levodopa-induced dyskinesia

FTG in subcortical areas, no matter if levodopa or stimulation-induced, is not consistently observed in every tested patient. The sparseness of FTG in many recordings argues for selective utility. In addition, levodopa and DBS-induced FTG appear to be unstable over time which makes them less reliable biomarkers (Jenkinson et al., 2013; Wiest et al., 2021). Given its modulation with different functional states (e.g. alertness), across other neurological conditions (dystonia, ET, myoclonic epilepsy) and other therapeutic interventions (e.g. post pallidotomy where it was suggested to represent clinical improvement), FTG in the basal ganglia or thalamic LFP has low specificity to levodopa or DBS-induced dyskinesias. In addition, FTG activity (46-70 Hz) has also been recorded in the basal ganglia of healthy alert rats at rest and further emphasised by movement and dopaminergic stimulation (Brown et al., 2002), suggesting that FTG in the basal ganglia may represent the physiological nature of the recorded structure. If DBS-induced FTG in the STN turns out to be unspecific to dyskinesias, this activity may have to be separated from dyskinesia-related FTG to prevent DBS from being switched off.

Nevertheless, it is possible that very mild dyskinesias were missed in the studies reporting DBS-induced FTG in STN or STN-motor cortex coherence at FTG frequency (Muthuraman et al., 2020; Wiest et al., 2021). In that case, the time between FTG and dyskinesia onset and the link of FTG with symptom severity are crucial. If DBS-induced FTG in the STN appears only a few seconds to minutes before severe dyskinetic symptoms, it may indicate DBS currents close to side effect threshold and may be useful to adjust currents before dyskinesias become manifest. Alternatively, if the time between DBS-induced FTG in the STN and dyskinesia appearance is variable and in the range of minutes, decreasing stimulation currents based on this FTG activity may lead to suboptimal stimulation adjustment. Similarly, if DBS-induced FTG in the STN also reflects mild dyskinesias, this might strengthen their pathophysiological correlation but lessen their utility as a biomarker to modulate stimulation.

6.5. Conclusions

We contrasted levodopa and DBS-induced FTG from broad movement-related gamma changes and appeal for more careful separation of the two in the future. We further reviewed the functional role of FTG, its link to dyskinesias and eventually its role as a biomarker for aDBS: be it as a marker for stimulating the right circuit or as a marker to track dyskinesias. Although preclinical and early clinical studies are reason to be optimistic about cortical FTG as a potential biomarker for dyskinesia, the utility of subcortical FTG recorded from STN is more questionable since it is not consistently measured in all patients and evidence supporting its link to dyskinesias is scarce. A large clinical study will be needed to quantify the sensitivity and specificity of both cortical and subcortical FTG to track the dyskinetic state and their robustness across patients, which may be facilitated by the advent of implantable pulse generators that allow for chronic data streaming during daily activities.

6.6. Summarised Findings

- Finely-tuned gamma (FTG) can be induced by deep brain stimulation (DBS) or levodopa
- DBS and levodopa-induced FTG are functionally distinct from movement-related gamma
- Levodopa-induced FTG is modulated by movement and varies with wakefulness and sleep
- Cortical FTG and dyskinesia can co-occur but their direct link is still unclear
- Subcortical FTG lacks specificity and sensitivity required for a biomarker in aDBS

6.7. Summary of Key Contributions

Subcortical FTG, cortical FTG or coherence between the two may play a role in adaptive DBS in the future. If future studies will find a robust link between any of the three FTG measures and dyskinesia, the FTG could serve as a feedback marker complementary to beta activity. In this approach, beta activity will still be the main feedback signal and determine when to stimulate outside of dyskinetic periods (**Figure 6.3**). When patients become dyskinetic – as evinced by the FTG feature – stimulation intensity could be adjusted or DBS could be paused. Our results and literature review suggest that subcortical FTG is an unlikely candidate since it is insensitive and unspecific to dyskinesia. However, it is possible that cortical FTG and M1-STN coherence at FTG frequencies are more faithful markers (Gilron et al., 2021; Swann et al., 2016). Still, cortical FTG has two main limitations. First, it is unclear what percentage of PD patients will display FTG during dyskinesia and if it will be robust over time. In our subcortical recordings, DBS and levodopa-induced FTG were detected in about one third of the cohort. However, this ratio can be different for cortical FTG. Second, cortical FTG was shown to be entrained at half stimulation frequency (Swann et al., 2016). We show in our saline

tank recordings (**Figure 2.2**) that half-harmonics of the stimulation frequency can be induced by the experimental setup. Given the different impedances and electrode-tissue interactions between a saline tank and the brain, it is possible that such half-harmonics will also overlap with an entrained signal at half stimulation frequency. Further details on subcortical and cortical FTG as putative feedback markers for aDBS are summarised in **Table 6.1**.

	Subcortical FTG	**Cortical FTG**
Sensitive and specific to the pathological state	No, FTG can also be induced by DBS when patients are not dyskinetic and vice versa.	Possibly more closely linked with dyskinesias.
Reliable over time	No, FTG comes and goes and is modulated by movement. Only present in ~ 1/3 of patients.	Yes, over many hours to days.
Localise to stimulation sweet spot	Yes, focal to dorsolateral STN and ZI.	Yes, over M1.
Calculable with low computational requirements	Yes, devices like Percept can track spectral peaks over time.	Same as subcortical FTG.
Provide rapid feedback	Yes, but FTG would have to be combined with another marker as DBS would be continuously on outside of dyskinetic periods.	Same as subcortical FTG.

Table 6.1. FTG as a feedback marker for aDBS.

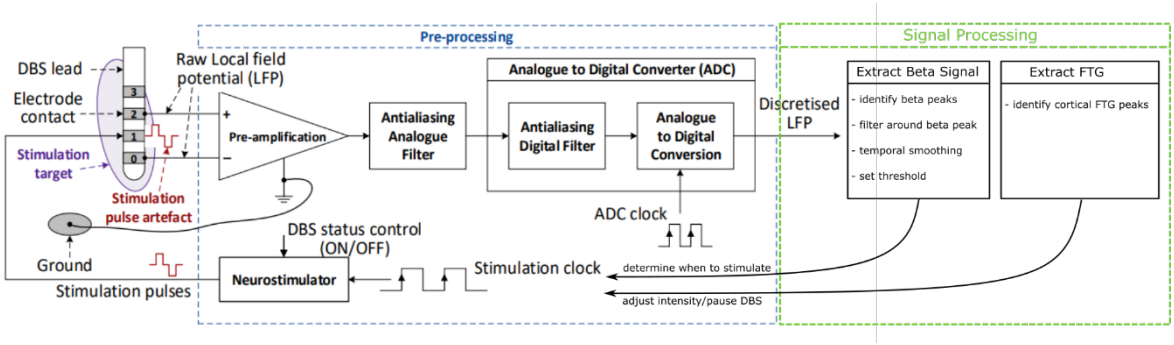


Figure 6.3. FTG as a feedback marker for aDBS.

7. Project 5: The aperiodic exponent of subthalamic field potentials reflects excitation/inhibition balance in Parkinsonism: a cross-species study *in vivo*

7.1. Introduction 178
7.2. Methods 180
7.2.1. Rodent data 180
7.2.1.1. 6-Hydroxydopamine lesion of dopaminergic neurons 180
7.2.1.2. Electrophysiological recordings 181
7.2.1.3. Signal processing 182
7.2.1.3.1. Extraction of single unit activity 182
7.2.1.3.2. Re-referencing 182
7.2.1.3.3. Spectral decomposition 183
7.2.1.3.4. FoooF parameterisation 183
7.2.2. Human data 184
7.2.2.1. Patients and surgery 184
7.2.2.2. Data recording and lead localisation determination 185
7.2.2.3. Signal processing 186
7.2.3. Statistics 187
7.2.4. Sample-size estimation, replicates and group allocation 187
7.3. Results 188
7.3.1. Establishing the validity of STN-LFP aperiodic exponents as a marker of E/I balance 188
7.3.2. Aperiodic exponents from 40 to 90 Hz separate levodopa medication states in PD patients 190
7.3.3. Aperiodic exponents of STN-LFPs from 10 to 50 Hz distinguish periods ON and OFF DBS 193
7.4. Discussion 195
7.4.1. The aperiodic exponent as a marker of E/I balance 195
7.4.2. Can the aperiodic exponent be useful as a feedback signal in adaptive DBS? 197
7.4.3. Limitations 198
7.4.4. Conclusions 199
7.5. Summarised Findings 200
7.6. Summary of Key Contributions 200

In this chapter, we provide evidence for the aperiodic exponent of STN-LFPs to reflect changes in E/I and for a potential modulation under therapeutic conditions in PD. This project was published in (Wiest et al., 2023b).

7.1. Introduction

Power spectral densities (PSD) of neural time series, such as electroencephalography (EEG), electrocorticography (ECoG) or local field potentials (LFP), tend to follow a 1/f power law distribution, where f is frequency, meaning that power is greatest at low frequencies and diminishes rapidly as frequencies increase (He et al., 2010). In this study, we will refer to the slope of the PSD as aperiodic exponent. For decades, the aperiodic exponent has been deemed unimportant and was often removed from analyses to emphasise brain oscillations (He, 2014). Only recently did the aperiodic exponent gain more attention and was attributed a physiological meaning. Aperiodic exponents in LFP, EEG and ECoG recordings vary by age (He et al., 2019; Schaworonkow and Voytek, 2021; Voytek et al., 2015), cortical depth (Halgren et al., 2021), psychiatric disorders (Adelhöfer et al., 2021; Molina et al., 2020; Robertson et al., 2019; Veerakumar et al., 2019) and Parkinson's disease (PD) (Mostile et al., 2019). They track sensory stimuli (Waschke et al., 2021) and change with movement (Belova et al., 2021). Moreover, the aperiodic exponent was suggested to reflect neuronal spiking (Manning et al., 2009; Ray and Maunsell, 2011), synaptic currents (Baranauskas et al., 2012; Buzsáki et al., 2012) and excitation-inhibition (E/I) balance, which describes the delicate balance of inhibitory and excitatory synaptic inputs to neurons (Chini et al., 2022; Gao et al., 2017; Trakoshis et al., 2020). The latter is supported by multiple studies showing that aperiodic exponents in non-invasive EEG and invasive LFP measurements were modulated by sleep and anaesthesia, with lower exponents, corresponding to slower decay of power with increasing frequencies, during the conscious state, which is linked with increased excitation. Inversely, higher aperiodic exponents, corresponding to faster decay of power with increasing frequencies, were observed

during the unconscious state (NREM sleep, anaesthesia), which is linked with more inhibition (Colombo et al., 2019; Huang et al., 2020; Lendner et al., 2020; Miskovic et al., 2019; Niethard et al., 2016; Waschke et al., 2021). In addition, Gao and colleagues found that theta cycle-modulated E/I changes in the rat hippocampus are reflected in the per-cycle PSD exponent of hippocampal LFPs calculated at different theta phases (peaks or troughs) confirming the E/I hypothesis for LFPs (Gao et al., 2017).

In our study, we seek to test whether the aperiodic exponent of LFPs recorded in the subthalamic nucleus (STN) tracks changes in E/I balance. To this end, we take advantage of the well-characterised rhythmic changes in neuronal firing patterns within the basal ganglia during slow-wave activity (SWA, see **Figure 7.1A**) induced in dopamine-depleted rats by general anaesthesia. STN and external globus pallidus (GPe) neurons are rhythmically active in time with cortical SWA in rats rendered Parkinsonian by lesion of midbrain dopamine neurons with 6-Hydroxydopamine (6-OHDA) (**Figure 7.1A**). STN neurons are predominantly active during the active phase of cortical slow (~1 Hz) oscillations (Magill et al., 2001; Mallet et al., 2008a). Inversely, STN neurons reduce their firing around the inactive phase, when GPe-Ti ("type-inactive") neurons tend to fire most. GPe-Ti neurons largely correspond to prototypic GPe neurons that are GABAergic and project to and inhibit STN (Abdi et al., 2015a; Mallet et al., 2012b); the GPe is considered the primary source of inhibitory inputs to the STN (Smith et al., 1998). Based on single-unit activity, we extracted separate periods with high levels of STN excitation or inhibition, and applied the FoooF algorithm to parameterise PSDs of LFPs during both states (Donoghue et al., 2020). Aperiodic exponents of STN- LFPs were consistently modulated with expected differences of the E/I ratio of STN in these states.

In a second step, we tested whether similar findings can be obtained in human STN-LFP recordings from awake patients with PD. In PD, STN shows exaggerated and synchronised

oscillatory activity in the beta range (Bergman et al., 1994; P Brown et al., 2001b; Levy et al., 2000). Dopaminergic medication and deep brain stimulation (DBS) desynchronise STN in the beta range (Eusebio et al., 2011b; Andrea A. Kühn et al., 2008; Kuhn et al., 2006; Whitmer et al., 2012) and reduce STN single-unit activity (Filali et al., 2004). Here, we compare aperiodic exponents of the STN-LFP ON and OFF dopaminergic medication and ON and OFF DBS. We show that aperiodic exponents of the STN-LFP were increased with both therapies and these results from PD patients are also consistent with the E/I hypothesis.

7.2. Methods

7.2.1. Rodent data

Experiments were performed on adult male Sprague Dawley rats (Charles River), and were conducted in accordance with the Animals (Scientific Procedures) Act, 1986 (UK) and the provisions of the Society for Neuroscience Policies on the Use of Animals in Neuroscience Research. Animal data that was analysed in this paper has been generated under the project licence numbers 30/2131 and 30/2629. All details on the 6-OHDA lesion and electrophysiological recordings were published before (Mallet et al., 2008a).

7.2.1.1. 6-Hydroxydopamine lesion of dopaminergic neurons

Unilateral 6-OHDA lesion was performed as described in (Magill et al., 2001; Mallet et al., 2008a). 25 min before injection, animals received desipramine i.p. to minimise uptake of 6-OHDA by noradrenergic neurons. 6-OHDA was dissolved in NaCl to a concentration of 4 mg/ml of which 3 µl were injected medial to the substantia nigra pars compacta to target the medial forebrain bundle, which results in widespread loss of midbrain dopaminergic neurons. The extent of the dopamine lesion was assessed 14-15 d after injection by apomorphine challenge. Lesions were considered successful if animals made > 80 contraversive rotations in 20 min. Electrophysiological recordings were performed ipsilateral to 6-OHDA lesion 21-45 d

after surgery when pathophysiological changes in the basal ganglia have likely reached their maxima.

7.2.1.2. Electrophysiological recordings

Data was recorded as described in Mallet et al., 2008a from eight 6-OHDA-lesioned rats. Here, we summarise key steps of the experimental procedure and data acquisition. Anaesthesia was induced with isoflurane and maintained with urethane, ketamine and xylazine throughout the recording (Magill et al., 2006). Animals were placed in a stereotaxic frame where their body temperature was maintained at 37°C. ECoG, electrocardiograms (ECG) and respiration rate were monitored to ensure animal well-being. ECoG was recorded via a 1 mm steel screw juxtaposed to the dura mater above the frontal cortex and referenced against another screw in the skull above the ipsilateral cerebellum (**Figure 7.S1A**). Raw ECoG traces were bandpass filtered (0.3-1500 Hz) and amplified (2000x) before acquisition. Extracellular recordings of unit activity and LFPs in the globus pallidus (GP) and STN were simultaneously made using silicon probes with high-impedance microelectrodes (**Figure 7.S1A**). Each probe had 1 or 2 vertical arrays (500 µm apart) with 16 recording contacts along the arrays with 100 µm spacing. Monopolar probe signals were referenced against a screw above the contralateral cerebellum. Probes were advanced into the brain under stereotaxic control and extracellular signals were lowpass filtered (6000 Hz). ECoG and probe signals were each sampled at 17.9 kHz using a Power 1401 Analog-Digital converter. Recording locations were verified after experiments using histological procedures. STN was identified by comparison of recorded unit activity with the known characteristics of STN neurons in urethane anaesthesia (Magill et al., 2001).

The ECoG measurements were used to assess if the rodent was in SWA state, which accompanies deep anaesthesia and is similar to activity observed during natural sleep (Steriade, 2000). We analysed a total of 28 extracellular LFP channels within STN during SWA (3.5 ±

0.18 channels per animal (mean ± SEM)). STN single unit activity was isolated from 20 of these channels (2.5 ± 0.07 per animal).

7.2.1.3. Signal processing

7.2.1.3.1. Extraction of single unit activity

Data analysis was performed using custom-written scripts in MATLAB (R2020b). Periods of robust SWA were selected according to previously described characteristics of these brain states (Magill et al., 2006, 2001). Analyses were performed on 97.61 ± 2.17 s of data during SWA in 6-OHDA-lesioned animals. After offline bandpass filtering (500-6000 Hz) of the probe signals, single unit activity was isolated with standard spike sorting procedures including template matching, principal component analysis and supervised clustering (Spike2) as described in Mallet et al., 2008a. Isolation of single units was verified by the presence of a distinct refractory period. Only neurons in which < 1% of interspike intervals were < 2 ms were analysed in this study. For further analysis, single unit activity was converted such that each spike was represented by a single digital event. To analyse aperiodic exponents of STN-LFPs, raw signals were lowpass filtered at 300 Hz (3^{rd} order Butterworth filter Oostenveld et al., 2011). A similar procedure to analyse LFPs from silicon probe electrodes was described before (Mallet et al., 2008b).

7.2.1.3.2. Re-referencing

LFPs were downsampled to 2048 Hz. Target channels within STN were re-referenced by subtracting the mean signal across the 6 neighbouring channels to reduce volume conduction (**Figure 7.S1C**). We computed wavelet magnitude squared coherence between the target LFP channel in STN and ECoG to control for volume conduction and opted for the above re-referencing approach with coherence < 0.1 for all frequencies > 10 Hz (**Figure 7.S1C**).

7.2.1.3.3. Spectral decomposition

Spectral parameters were evaluated using continuous complex Morlet wavelet convolution. The entire 100-s time series was decomposed from 1-100 Hz with a frequency resolution of 1 Hz (frequencies increased linearly) before epoching to reduce the edge effect on each epoch. Morlet wavelets of 50 cycles were used which did not change as a function of frequency. We counted the spike events per consecutive non-overlapping 250 ms epoch for all unit activity channels (**Figure 7.S1B**). The epoch duration was chosen such that it captures the rhythmic dynamics during SWA. For every unit channel, we defined epochs with a spike rate > 75^{th} percentile as "high spiking" and all epochs with a spike rate < 25^{th} percentile as "low spiking" (**Figure 7.S1B**). We computed the mean PSD for every 250-ms epoch and normalised it by dividing through the mean power from 1 to 100 Hz (**Figure 7.S1D**).

7.2.1.3.4. FoooF parameterisation

For every LFP channel within STN, we computed the mean PSD of all high and all low spiking epochs separately. To isolate the aperiodic component from these spectra, we used the open-source FoooF algorithm (version 1.0.0) (Donoghue et al., 2020). Settings for the algorithm were set as: peak width limits: 2-12; max number of peaks: *infinite*; minimum peak height: 0; peak threshold: 2; and aperiodic mode: *fixed*. Power spectra were parameterised across the frequency range 30 to 100 Hz. The lower bound was selected to avoid the impact of low frequency oscillations, the upper bound was selected to avoid the impact of spectral plateaus (Gerster et al., 2022). Moreover, PSDs were linear across this frequency range in log-log space assuming a single 1/f like characteristic and did not contain overlapping periodic components (**Figure 7.S1E+F**). Hence, higher aperiodic exponents indicate steeper power reduction with increasing frequencies in the PSD and vice versa as shown in **Figure 7.S1F**. We evaluated the goodness of fit (R^2) for all data used in this study (**Figure 7.S4**). Using the '*knee*' mode for parameterisation did not improve aperiodic fitting (**Figure 7.S5**). To compare power across

different spiking states, we computed the mean power between 30-100 Hz of the average PSD of all high or low spiking epochs.

7.2.2. Human data

This protocol was approved by the Health Research Authority UK, the National Research Ethics Service local Research Ethics Committee (IRAS: 46576) and the local ethics committee at the University of Mainz (837.208.17(11042)). Patients were recruited at St. George's University Hospital NHS Foundation Trust, London, King's College Hospital NHS Foundation Trust, London, and the University Medical Center Mainz. Written informed consent, and consent to publish, was obtained before surgery in line with the Declaration of the Principles of Helsinki. We analysed data from 24 patients from these 3 centres. Data from 17 patients were previously published (Wiest et al., 2021, 2020).

7.2.2.1. Patients and surgery

Study participants were evaluated by an interdisciplinary team of movement disorder neurologists and functional neurosurgeons and met the UK Parkinson's Disorder Society Brain Bank Diagnostic Criteria for diagnosis of PD. Baseline motor function in the ON and OFF medication state was assessed pre-operatively using the part III of the Unified Parkinson's disease rating scale motor subscale (UPDRS-III). When UPDRS part III scores were reported in **Figure 7.2**, we used the contralateral appendicular categories (bradykinesia and rigidity scores only). The surgical target was STN. Five models of DBS leads were used: quadripolar (model 3389) or directional (SenSight^{TM}) leads from Medtronic Inc., Neurological Division, USA, directional (Vercise^{TM} model DB-2202) or non-directional (model DB-2201) leads from Boston Scientific, USA, and directional leads (Infinity^{TM} model 6172ANS) from Abbott Inc., USA. DBS implantation was guided either by magnetic resonance imaging alone (St. George's University Hospital) or with additional intra-operative microelectrode recordings and

stimulation (King's College Hospital and University Medical Center Mainz). The subthalamic leads were connected to temporary extension leads and these were externalised. Assessment of contact localisation was made through co-registration of immediate post-operative CT with pre-operative MRI by an experienced neurosurgeon or neurologist specialising in deep brain stimulation. Assessment was blinded to the electrophysiological data and made using Lead-DBS (Horn et al., 2019).

7.2.2.2. Data recording and lead localisation determination

Recordings were made between 3 and 6 days postoperatively, while lead extensions were still externalised and before implantation of the subcutaneous pulse generator. In total, 24 patients (37 hemispheres) were recorded for this study; 17 patients (30 hemispheres) were recorded on and off dopaminergic medication and 17 patients (26 hemispheres) on and off stimulation. In patients with directional leads, the 3 directional contacts were joined to form a ring contact (**Figure 7.2Ai**). All LFPs were amplified and sampled at either 2048 Hz using a TMSi Porti (TMS International, Netherlands) or at 4096 Hz using a TMSi Saga32 (TMS International, Netherlands). The ground electrode was placed on the non-dominant forearm. High-frequency stimulation at 130 Hz was only tested at the middle contacts to allow bipolar LFP recordings from the two surrounding contacts (**Figure 7.2Aii**). A self-adhesive electrode attached to the patient's back served as a reference for stimulation, which was delivered using a custom-built highly-configurable in-house neurostimulator. Stimuli comprised symmetric constant-current biphasic pulses (60 μs pulse width, negative phase first). The stimulation current was started at 0.5 mA and increased in increments of 0.5 mA until first a benefit in Parkinsonian motor symptoms was observed and second side-effect threshold was reached. The contact and current associated with the best clinical improvement were selected. If no stimulation was applied and multiple bipolar configurations were available, we selected the bipolar channel with the largest

beta peak at rest. If only one hemisphere was recorded per patient, it was the hemisphere contralateral to the most affected upper limb.

7.2.2.3. Signal processing

Analyses were performed on 60 s of data while patients were awake and at rest. LFP time series were highpass filtered at 1 Hz. Complex Morlet wavelet convolution was used for time-frequency decomposition with 50 wavelet cycles between 1-90 Hz as described in section 4.1.3.3. To exclude artefacts from mains interference at 50 Hz before isolating the aperiodic component, frequencies between 47-53 Hz were removed and the gap was linearly interpolated using the *fillmissing* function. To run the FoooF algorithm, the same settings were used as described in 4.1.3.4., and power spectra were parameterised across the frequency range 40 to 90 Hz. The lower bound was increased to avoid high-amplitude beta peaks crossing the fitting range (see **Figure 7.2B**). The upper bound was lowered to avoid the harmonic of mains interference. To isolate periodic beta activity, the PSD was parameterised using FoooF between 5-90 Hz (knee mode as such a wide frequency range is unlikely to only have a single aperiodic component), otherwise using the same settings, and the largest peak within the canonical beta range from 8-35 Hz was selected (**Figure 7.2B**). In the stimulation ON condition, stimulation artefacts led to a plateau at frequencies > 50 Hz in the spectra (**Figure 7.3A**). Therefore, aperiodic exponents were estimated between 10 to 50 Hz to evaluate the effect of DBS. A similar frequency range (5-45 Hz) was used in a previous study (Chini et al., 2022). Beta (13-35 Hz), low beta (13-20 Hz), high beta (21-35 Hz), gamma (35-90 Hz), low gamma (35-50 Hz) and high gamma (51-90 Hz) power were computed as the mean power of the normalised (divided by the mean power from 1 to 90 Hz), 50 Hz removed and 1/F-corrected PSD across the respective frequency range.

7.2.3. Statistics

Statistical analyses were performed using custom-written scripts in MATLAB (R2020b). To perform paired comparisons between the two medication or stimulation conditions, we used a paired samples permutation *t*-test with multiple comparison correction (50,000 permutations each) as implemented in (Groppe, 2022b). When correlations were reported, we calculated Spearman's rank coefficients because the non-baseline-transformed power data are non-normally distributed and contain outliers. When multiple channels within one animal were available, hierarchical comparisons of aperiodic exponents and power across different epochs was performed using linear mixed-effects models to take repeated measures from multiple electrodes for each animal into account. The exponent or power data was set as dependent variable and different STN spiking conditions (e.g. high STN spiking epochs, low STN spiking epochs) as fixed effects. The normal distribution of each variable and the residuals were visually inspected with quantile-quantile plots and histograms of distribution. All models were estimated by the method of maximum likelihood and included random intercept for subjects to allow different intercepts for each subject, thereby capturing individual differences. Multiple statistical tests were performed in this study under FDR control at 5% using the adaptive linear step-up procedure, a modification of the original Benjamini and Hochberg procedure (Duchet et al., 2021). This ensures that the expectation of the number of false positives over the total number of positives is less than 5% when many statistical tests are performed. When histograms of distribution are shown, the optimal number of histogram bins was determined using the Freedman-Diaconis rule (Freedman and Diaconis, 1981). All data are shown as mean ± standard error of the mean (SEM) unless mentioned otherwise.

7.2.4. Sample-size estimation, replicates and group allocation

Due to the explorative nature of this study, we did not perform prospective sample-size estimations but included all animal data with wideband recordings from STN that were

available to us (n = 8). Since 6-OHDA-lesion was performed unilateral, only one STN was recorded per animal. Similarly, we did not perform prospective sample-size calculations for human data, but included all STN recordings we had available (37 STNs from 24 patients). This approach was chosen as postoperative LFP recordings from DBS electrodes are rare research opportunities. Fortunately, due to the relatively high signal-to-noise ratio of LFP recordings, a small number of patients between 7-12 is considered sufficient to detect robust effects in LFP studies (Alegre et al., 2013; Brittain et al., 2012; Wessel et al., 2016).

In our study, each STN was treated as one independent sample. In doing so, we follow the definition that 'biological replicates are parallel measurements of biologically distinct samples that capture random biological variation' (Blainey et al., 2014). It should be recognised that the variations we observed in our sample can be caused by variability in the phenotype of PD, of the target location of the electrode, or in the temporary lesion effect of DBS surgery.

This was not a clinical study. We used a within-subject design to test the effects of DBS and dopaminergic medication. All available animal and human data recordings were included in the analysis (no attrition).

7.3. Results

7.3.1. Establishing the validity of STN-LFP aperiodic exponents as a marker of E/I balance

To validate the aperiodic exponent of STN activity as an estimate for E/I changes, we first took advantage of the distinct rhythmic changes in neuronal firing patterns within the basal ganglia during SWA in 6-OHDA-lesioned rats under anaesthesia. During SWA, STN neurons exhibit distinct periodic changes in firing rates, which are tightly linked with the phase of cortical slow (~ 1 Hz) oscillations that dominate SWA (**Figure 7.1A**) (Magill et al., 2001). These changes in STN firing rates have been defined, by us and others, in relation to their major excitatory and inhibitory inputs (Abdi et al., 2015a; Magill et al., 2001; Mallet et al., 2008a).

To contrast STN activity during opposing conditions of E/I balance, we first distinguished 250 ms epochs of "high" and "low" levels of spiking of STN single units during SWA (**Figure 7.S1B**). Because STN and GPe-Ti neurons fire in a near anti-phase relationship during cortical SWA (Mallet et al., 2008a), high and low spiking epochs of STN neurons tend to occur in time with, respectively, low and high levels of GPe-Ti spiking (**Figure 7.1B**). We assume that, during low and high levels of GPe-Ti spiking, STN neurons receive low and high levels of inhibitory input from the GPe, respectively. Previous studies have shown that during SWA, excitatory input from cortical projection neurons would be in-phase with the high spiking epochs of STN neurons, and thus, anti-phase to inhibitory inputs from GPe (Parr-Brownlie et al., 2007). First, we computed PSDs of STN-LFPs for the two states (high and low STN spiking epochs, **Figure 7.1C**) and extracted both aperiodic exponents and average power between 30 and 100 Hz. Aperiodic exponents were smaller in high compared to low STN spiking epochs, consistent with small exponents being generated in conditions of more excitation/less inhibition and vice versa (LME: estimate = 0.12, t = 3.92, $p < .001$; **Figure 7.1D**). The total power of activities between 30 and 100 Hz in STN-LFP was smaller during low STN spiking epochs compared to high STN spiking epochs (LME: estimate = -0.02, t = -2.34, p = .02; **Figure 7.1E**). Furthermore, the lack of correlations between power and aperiodic exponents suggests that both power and exponents from the same frequency range are dissociable and might contain different information (Spearman; $\rho = -.07$, p = .56 and $\rho = -.18$, p = .14 for high and low STN spiking epochs respectively). When pooling aperiodic exponents and power from high and low STN spiking epochs, we still did not observe a significant correlation ($\rho = -.15$, p = .07).

Overall, these results from 6-OHDA-lesioned rats suggest that the aperiodic exponent of STN-LFPs is altered according to different levels of STN spiking. The high and low spiking epochs of single STN neurons can in turn be ascribed with confidence to an E/I balance that is tipped

in favour of excitation and inhibition, respectively. As such, these results support the notion that STN-LFP aperiodic exponents may become valid markers of overall E/I balance in STN.

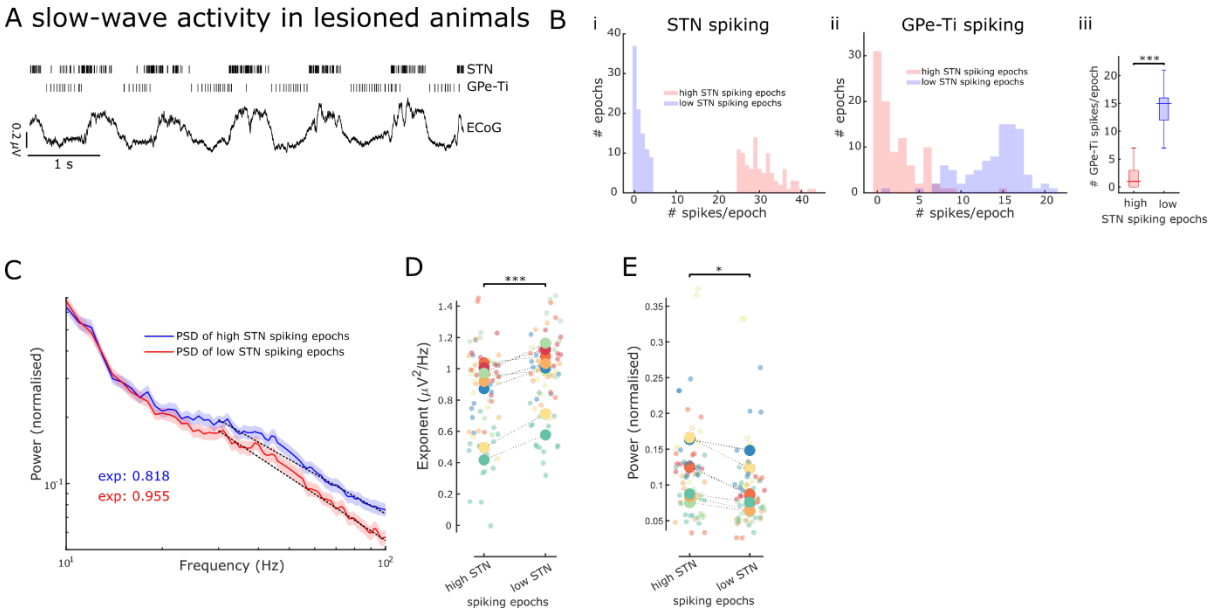


Figure 7.1. Aperiodic exponents and power of STN-LFPs between 30 and 100 Hz reflect STN excitation and inhibition in lesioned animals. A. Example traces of ECoG and single-unit spiking activity of STN and GPe-Ti neurons during slow-wave activity (SWA) in anaesthetised 6-OHDA-lesioned animals. Note the rhythmic spiking pattern of both neuron types, which either aligns with peaks or troughs of cortical slow (~1 Hz) oscillations. **B.** We identified 250 ms epochs of relatively high spiking (> 75th percentile) and epochs of low spiking (< 25th percentile) based on STN neuron activity during cortical SWA. The distribution of STN (i) and GPe-Ti (ii) spiking activity is shown for one example animal, which confirms that spiking rates are clearly differentiable for the two high and low STN spiking states. GPe-Ti neurons are most active when STN neurons are relatively inactive and vice versa (iii; ***p < .001, Wilcoxon rank sum test). **C.** Average PSDs of STN-LFPs in the two states identified above (mean ± SEM, n = 8 animals). The black dotted lines denote the aperiodic fits (exponent values (exp) are colour-coded) for the respective PSDs between 30 and 100 Hz. **D.** Aperiodic exponents are high during low STN spiking epochs corresponding to more GPe-Ti activity and, by inference, more inhibition of STN. Inversely, aperiodic exponents are low during high STN spiking epochs associated with less GPe-Ti activity and, by inference, disinhibition (LME: estimate = 0.12, t = 3.92, p < .001). **E.** Average power between 30 and100 Hz in the STN-LFPs is higher when STN neurons are highly active than when STN spiking is low (LME: estimate = -0.02, t = -2.34, p = .02). **D & E**: Large dots denote the mean per animal and are colour-coded. Small dots denote individual LFP channels. n = 8 animals, *p < .05, **p < .01, ***p < .001, LME.

7.3.2. Aperiodic exponents from 40 to 90 Hz separate levodopa medication states in PD patients

After corroborating the link between aperiodic exponents in STN-LFPs and changes in E/I balance in the STN in an animal model under anaesthesia, we sought to apply the same concept to clinical data from awake PD patients. According to the classical direct/indirect pathways

model of basal ganglia functional organisation, the parkinsonian STN is overactive (reduced inhibition), which is alleviated by dopaminergic stimulation (Albin et al., 1989; DeLong, 1990). Therefore, we hypothesised that aperiodic exponents of STN-LFPs are relatively low in the untreated Parkinsonian state, and would be increased with dopaminergic medication. To test this hypothesis, we estimated aperiodic exponents in STN-LFPs recorded from 30 hemispheres in 17 patients both ON and OFF levodopa (**Figure 7.2A+B**). Aperiodic exponents at 40-90 Hz successfully distinguished dopaminergic medication states (paired samples permutation *t*-test; t = -3.31, p = .0015, Cohen's *d*: 0.60) and were larger ON medication (in 66% of hemispheres), suggesting a faster drop of power with increasing frequencies and in keeping with more inhibition of STN (**Figure 7.2C**). The levodopa effect on aperiodic exponents was robust against different settings for FoooF parameterisation (**Figure 7.S2**). Note that for human data, the frequency range was adjusted to 40-90 Hz (the lower bound due to high-amplitude beta peaks crossing the fitting range and the upper bound due to the harmonic of mains interference; see section 7.2.2.3. for more details).

In addition, we quantified periodic beta power identified using the FoooF parameterisation (**Figure 7.2B**) and average power of six different frequency bands and compared them between conditions ON and OFF levodopa. Periodic beta power differed between the two medication states (paired samples permutation *t*-test, t = 2.08, p = .048), with higher power in the OFF medication state consistent with previous studies (Brown et al., 2001; Neumann et al., 2017) (**Figure 7.2C**). Of the six frequency ranges, only beta power distinguished medication states (**Figure 7.S3A**). However, neither average (Spearman; ρ = -.08, p = .67), low (Spearman; ρ = -.20, p = .28) nor high beta power (Spearman; ρ = .004, p = .99) correlated with aperiodic exponents (**Figure 7.S3B**). In 10 of 20 cases in which the aperiodic exponent was higher ON medication, there was either no clear beta peak in the OFF state or no clear beta reduction with levodopa. This underlines the benefit of multi-biomarker aDBS compared to an algorithm that

only relies on beta power as a feedback signal. In 8 of 10 hemispheres in which aperiodic exponents were not higher ON medication, exponents were either very similar and the difference between medication states was < 0.1 (4 cases) or beta power was not affected by levodopa either (4 cases).

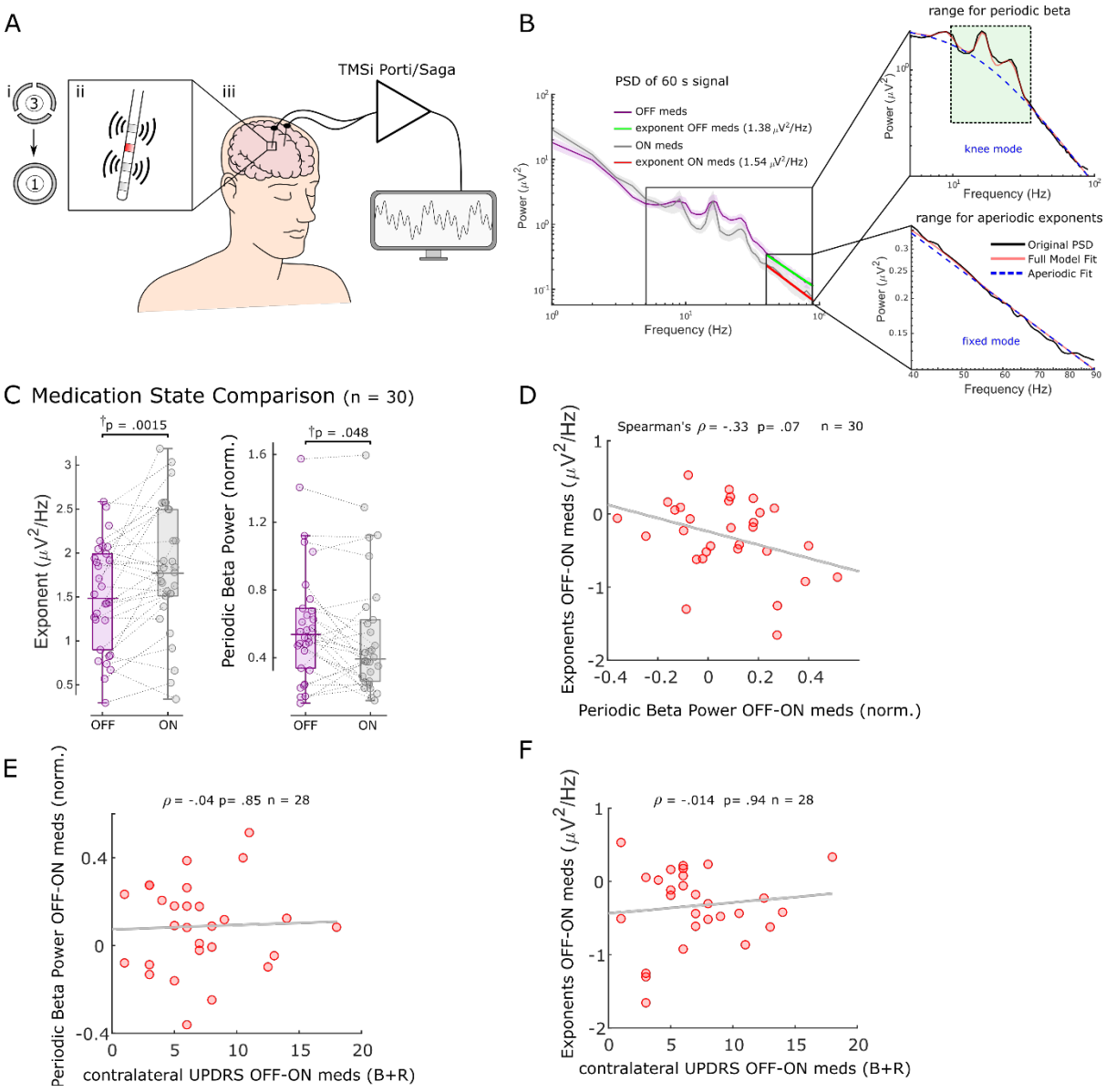


Figure 7.2. Aperiodic exponents between 40-90 Hz of STN-LFPs distinguish medication states in externalised recordings from Parkinson's patients. A. We analysed 60-s segments of bipolar STN-LFP recorded from Parkinson's patients at rest while leads were externalised (iii). Recordings were performed ON and OFF dopaminergic medication. Directional contacts were fused (i) and bipolar recordings were conducted from contacts adjacent to the stimulation contact (red; ii). **B.** Average PSD from 30 hemispheres (17 patients) ON and OFF medication of 60-s recordings using Morlet Wavelet transforms (mean ± SEM). Aperiodic exponents were computed between 40-90 Hz (fixed mode) to avoid high-amplitude beta peaks and harmonics of mains noise at 100 Hz and the PSD was relatively linear in log-log space within this range. To obtain periodic beta power, we fit the FoooF algorithm between 5-90 Hz (knee mode) and picked the power of the largest oscillatory component within the

beta range (13-35 Hz, green rectangle). **C.** Aperiodic exponents and periodic beta power differ between medication states (p = .0015 and p = .048). †p-values were computed using a paired samples permutation *t*-test with multiple comparison correction on 30 hemispheres recorded from 17 PD patients. **D.** Aperiodic exponent and periodic beta power changes with levodopa are not correlated (Spearman; ρ = -.33, p = .07, n = 30). **E & F.** Neither periodic beta power (E) nor the aperiodic exponent (F) changes with medication are correlated with contralateral appendicular bradykinesia and rigidity UPDRS part III sub-scores OFF-ON levodopa (Spearman: ρ = -.04, p = .85, n = 28 hemispheres for periodic beta; Spearman: ρ = -.014, p = .94, n = 28 hemispheres for aperiodic exponents).

Medication-induced changes of aperiodic exponents and periodic beta power displayed a trend for a negative correlation (Spearman; ρ = -.33, p = .07, n = 30; **Figure 7.2D**) indicating that they may contain similar information on levodopa-induced changes in the STN. This may also hint at a physiological meaning of aperiodic exponents. Furthermore, neither levodopa-induced changes of periodic beta power (Spearman; ρ = -.04, p = .85, n = 28; **Figure 7.2E**) nor aperiodic exponents (Spearman; ρ = -.014, p = .94, n = 28; **Figure 7.2F**) were correlated with contralateral appendicular bradykinesia and rigidity UPDRS part III sub-scores OFF-ON levodopa in this cohort.

These results suggest that aperiodic exponents of STN-LFPs may be a useful measure to distinguish and track medication states and might add complimentary information to a beta activity-based feedback algorithm.

7.3.3. Aperiodic exponents of STN-LFPs from 10 to 50 Hz distinguish periods ON and OFF DBS

High-frequency DBS was thought to induce functional inactivation of the neurons in the stimulated area (Aziz et al., 1991; Benabid et al., 1994; Bergman et al., 1990; Limousin et al., 1995). Furthermore, the inactivation hypothesis was corroborated when suppression of neuronal activity was recorded surrounding STN-DBS leads in patients, non-human primates and rodents (Filali et al., 2004; Meissner et al., 2005; Shi et al., 2006) in line with the classical rate model of movement disorders. Here, we compared aperiodic exponents at 10-50 Hz of STN-LFPs ON and OFF high-frequency DBS in 26 hemispheres from 17 PD patients.

Compared to previous analyses, we lowered the frequency range for parameterisation to avoid a spectral plateau starting > 50 Hz when stimulation was on (**Figure 7.3A**). We found increased aperiodic exponents ON DBS (paired samples permutation *t*-test; t = -6.27, p < .001, Cohen's *d*: 1.23, **Figure 7.3B**), a similar effect as levodopa, in keeping with the E/I hypothesis and of the notion that DBS supresses STN firing to some degree.

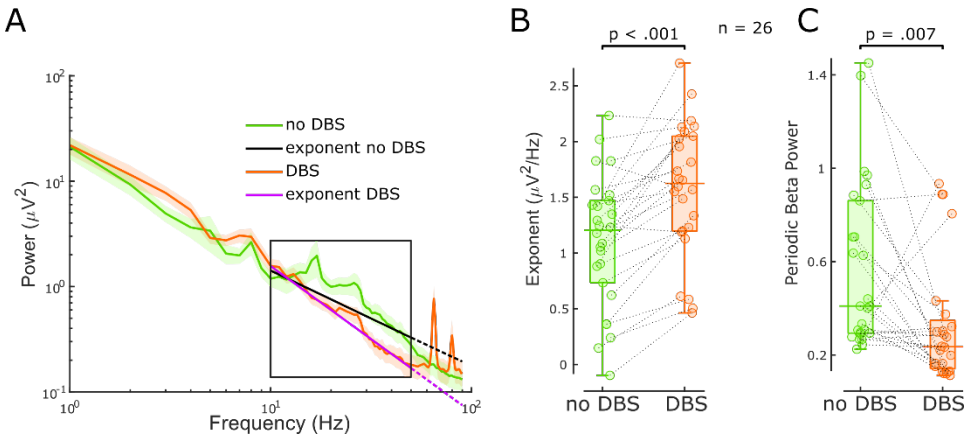


Figure 7.3. The aperiodic exponent between 10-50 Hz of STN-LFP distinguishes stimulation states in externalised recordings from PD patients. A. Average PSDs and linear fitting in the exponential scale of 60-s segments of bipolar STN-LFPs ON and OFF 130 Hz STN-DBS recorded from externalised electrodes in 26 hemispheres from 17 PD patients (mean ± SEM). PSDs during DBS (red) display a spectral plateau > 50 Hz, hence, exponents were isolated between 10 to 50 Hz (black rectangle). Linear fitting of the aperiodic exponents between 10-50 Hz for no DBS and DBS are shown in black and yellow, respectively. While the dotted extension of the black line is still a relatively good fit for the no DBS PSD, the yellow dotted line deviates from the DBS PSD due to the plateau at around 50 Hz. **B.** Aperiodic exponents differ between periods of no DBS and periods of 130 Hz STN-DBS. (Paired samples permutation *t*-test, n=26, p < .001) **C.** Periodic beta power was compared before and during 130 Hz STN-DBS. (Paired samples permutation *t*-test, n=26, p = .007)

When average power of six different frequency ranges and periodic beta power were compared immediately before and during 130 Hz STN-DBS, beta power (primarily high beta) and low gamma power were suppressed with DBS (**Figure 7.3C** and **Figure 7.S3C**) in accordance with our previous work (Wiest et al., 2020). The power increase of the high gamma band (51-90 Hz) was driven by artefacts of stimulation in that range (**Figure 7.3A**). Aperiodic exponent changes with DBS were not correlated with spectral changes of any frequency (**Figure 7.S3D**). Again, this implies that the aperiodic exponent is independent of spectral changes averaged

over pre-defined frequency ranges or periodic beta power and might provide additional information.

7.4. Discussion

In this study, we validated the aperiodic exponent of STN-LFPs as a marker of E/I balance using single unit activity from the basal ganglia in 6-OHDA-lesioned animals, under conditions of where the activity levels of neurons providing major excitatory and inhibitory inputs to STN neurons are well defined. Having validated the approach with single unit activities under these controlled conditions in rodents, we found that the aperiodic exponent of STN-LFPs recorded from awake PD patients distinguishes medication and stimulation states. Its sensitivity to levodopa and DBS underlines the notion that the aperiodic exponent of the STN-LFP may indicate pathological states of PD and can potentially serve as a feedback signal for adaptive DBS.

7.4.1. The aperiodic exponent as a marker of E/I balance

Our results support that the aperiodic exponent of STN-LFPs changes with excitatory and inhibitory inputs to STN in both a rodent PD model and patients with PD. STN dendrites are innervated by glutamatergic inputs from ipsilateral somatomotor and frontal cortical areas (Monakow et al., 1978), glutamatergic intralaminar thalamic nuclei (Kita et al., 2016) and GABAergic inputs from prototypic GPe neurons (Mallet et al., 2012b). In lesioned animals, on the active phase of the cortical slow oscillation (here referred to as high STN spiking epochs), STN neurons are expected to receive intense excitatory input from cortical and thalamic afferents and decreased inhibitory input from prototypic GPe neurons (Mallet et al., 2012b, 2008a), conditions that lead to vigorous STN spiking. In contrast, during the inactive phase of the cortical slow oscillation, inhibition from prototypic GPe neurons should be high and excitation from cortex and thalamus is relatively low, conditions that can completely prevent

STN spiking (Mallet et al., 2012b, 2008a). We found clear differences in the aperiodic exponents of STN-LFPs between these extreme states of local excitation and inhibition (**Figure 7.1**).

The majority of previous studies into the relationship between the aperiodic exponent and neuronal activity have been investigated in cortex (Waschke et al., 2021). However, the anatomy and physiology of STN differs significantly from cortex in that it is made up of relatively homogenous, glutamatergic projection neurons that fire action potentials autonomously and receive tonic inhibition from prototypic GPe neurons. Cortical circuits, in contrast, comprise a vast array of neuron types and activity of cortical projection neurons is predominantly input driven. Thus, our findings provide important validation that aperiodic exponents reflect changes in E/I balance at the synaptic (LFP) levels, specifically in STN. In addition, in contrast to these previous efforts examining the E/I hypothesis (Gao et al., 2017; Lendner et al., 2020; Waschke et al., 2021), we directly link aperiodic exponents to single neuron spiking and predefined parameters of the dynamic E/I balance that specifically relate to the majority of neurons in the recorded structure (**Figure 7.1**). This approach provided a platform for understanding changes in the aperiodic exponent in STN-LFP recordings from humans.

Building on these findings, our clinical results hold up against the E/I hypothesis as well (**Figure 7.2+7.3**). Aperiodic exponents of STN-LFPs recorded from awake PD patients are increased ON medication and ON DBS when STN local activity is believed to be decreased according to the classical direct/indirect pathways model (Albin et al., 1989; DeLong, 1990). The increased exponents ON dopaminergic medication in PD are consistent with a recent study that reported higher aperiodic exponents in dopamine-intact compared to lesioned animals (Kim et al., 2022). Furthermore, our results indicate that periodic beta power differs between the two dopaminergic medication states (**Figures 7.2C**), consistent with previous findings

(Kim et al., 2022; Kühn et al., 2006; Neumann et al., 2017; Ray et al., 2008). Finally, the missing correlation between medication-induced changes of aperiodic exponents and average beta power suggests that aperiodic exponents capture changes with medication that are not reflected by beta power alone and might be complimentary in an adaptive DBS algorithm (**Figure 7.S3**).

7.4.2. Can the aperiodic exponent be useful as a feedback signal in adaptive DBS?

Beta-band oscillations were identified as the most promising feedback signal for adaptive DBS considering their strong relationship with motor impairment in PD (Kuhn et al., 2006; Priori et al., 2004). However, the correlation between beta and contralateral appendicular bradykinesia and rigidity UPDRS scores was not significant in our cohort, and abnormal beta activity is not observed in all patients (Giannicola et al., 2010) nor is it correlated with tremor, freezing of gait or dyskinesia (Marceglia et al., 2021). It is therefore unlikely that a beta-only feedback model will address all PD symptoms. Several factors point towards the aperiodic exponent as a candidate feedback signal. First, it changes with medication and DBS (**Figure 7.2+7.3**), similar characteristics which brought beta oscillations into the spotlight and which may suggest a link to clinical improvement (Andrea A. Kühn et al., 2008; Kuhn et al., 2006). Second, we observed medication-related changes of the aperiodic exponent in hemispheres without clear beta peaks or medication-related beta changes. Third, we estimate the aperiodic exponent between 40 and 90 Hz, when studying the effect of levodopa, avoiding lower frequencies, which are particularly susceptible to movement-related artefacts (van Rheede et al., 2022).

However, there are some obstacles to its use as a feedback marker. First, we could not show a direct link between the aperiodic exponent and clinical symptoms, but in our data set UPDRS part III scores were not correlated with periodic beta power either (**Figure 7.2E+F**). To unequivocally assess clinical relevance of aperiodic exponents, motor tests with higher

discriminatory power than UPDRS motor sub-scores such as the BRAIN TEST may be useful (Giovannoni et al., 1999). Second, the aperiodic exponent would present a feedback signal with low temporal resolution. We averaged PSDs over 60 s to isolate exponents of STN-LFPs. Shortening this time window will introduce noise into the PSD and increase the error of aperiodic estimates. While these temporal dynamics prevent aperiodic exponents from targeting beta bursts, they may provide additional information about the E/I balance with slower temporal dynamics. Third, the frequency range is critical for isolating the aperiodic exponent and results may vary considerably depending on this. Moreover, for some PSDs with large oscillatory components and a spectral plateau at low frequencies, it may even be impossible to obtain an unequivocal linear fit (Gerster et al., 2022). Fourth, it is unclear if a miniaturised implantable device will have the computational power to parameterise PSDs in real-time and what effects this may have on battery longevity. If aperiodic exponents can be combined with other LFP parameters to improve optimal DBS settings, will depend on if they can add additional clinical information than beta power alone, which our results imply (**Figure 7.S3**).

7.4.3. Limitations

The chosen frequency band for linear fitting can affect FoooF parameterisation. In the past, many different fitting ranges were applied to extract the aperiodic exponent (reviewed in Gerster et al., 2022). Most of these frequency ranges comprise low frequency oscillations and start in the delta, theta, alpha or beta range. If prominent low frequency oscillations are present, this may lead to steepening of the spectrum and error-prone aperiodic fits (Gerster et al., 2022). In this study, when parameterising PSDs from rodent data recorded using high-impedance microelectrodes, we chose the frequency band from 30 to 100 Hz to avoid false-high exponents due to high power in the lower frequency bands. The lower fitting bound of 30 Hz was chosen to exclude overlap of the lower fitting bound with the rising or falling arm of alpha or beta

oscillations (**Figure 7.1D**). A similar frequency range has been recommended to estimate the E/I ratio before (from 30 to 70 Hz, if this range is uncorrupted by oscillatory peaks) (Gao et al., 2017; Trakoshis et al., 2020). To asses differences with medication in clinical data recorded using macro-electrodes, we narrowed the fitting range to 40 to 90 Hz to avoid overlap and false-high estimates due to peaks in the high beta range (**Figure 7.2B**), and to avoid the harmonic of mains interference. These results are robust as long as the selected frequency range covers 40-70 Hz (**Figure 7.S2**). For DBS data analysis, we adapted the fitting range to avoid a spectral plateau (**Figure 7.3A**) which would have resulted in false-low exponents had we used the same fitting range as for the previous analysis. We observed this prominent plateau at frequencies larger than 50 Hz when DBS was switched ON in addition to prominent peaks at half stimulation frequency and other harmonics (**Figure 7.3A**). However, we did observe reduced power in the high beta and low gamma frequency bands (21-50 Hz) with stimulation, suggesting that the signal to noise ratio is sufficient to detect physiological signals in this frequency band. Therefore, we have focused on the lower frequency bands (10-50 Hz) for quantifying aperiodic exponents ON and OFF stimulation. In addition, in our dataset we did not see a link between medication-induced changes of either the aperiodic exponent or periodic beta power and contralateral bradykinesia and rigidity scores OFF-ON levodopa (**Figure 7.2E+F**) and further studies will be required to investigate if and to what extent aperiodic exponents of STN-LFPs correlate with parkinsonian symptoms.

7.4.4. Conclusions

We showed that aperiodic exponents of STN-LFPs reflect STN excitation and inhibition as evinced by single neuron activity in states of extreme spiking differences in rodents. We further showed that aperiodic exponents of STN-LFP in PD patients are larger ON dopaminergic medication and ON DBS reflecting more inhibition of STN compared to the dopamine-depleted and OFF DBS states. Our results corroborate that the aperiodic exponent contains

information with respect to E/I balance and our clinical results give reason to believe the aperiodic component may be useful in a closed-loop feedback algorithm for PD.

7.5. Summarised Findings

- The aperiodic exponent of STN-LFPs separates states of high and low STN spiking during slow-wave sleep in rats.
- The aperiodic exponent of STN-LFPs may be an indicator of excitation/inhibition (E/I) balance.
- Aperiodic exponents are modulated by levodopa and subthalamic deep brain stimulation (DBS) in Parkinson's disease patients.
- Aperiodic exponents may be complementary to beta activity in adaptive DBS.

7.6. Summary of Key Contributions

The aperiodic exponent of the power spectrum may play a role in adaptive DBS in combination with beta activity (**Figure 7.4**). In this approach, beta activity – smoothed over a short (Little et al., 2013; Velisar et al., 2019) or long (Arlotti et al., 2018; Rosa et al., 2017a) time window – will serve as the main feedback signal. When PD patients slide into the OFF state, information extracted from the aperiodic exponent may then help to adjust stimulation intensity and/or the beta threshold. The main advantage of this complementary approach is that the aperiodic exponent may add information on medication states in those subjects where beta activity is not sensitive enough to do so. The two main disadvantages of this feedback marker are the required signal length for FoooF parameterisation and the heterogeneity of PSDs. First, in our study we averaged LFPs over 60 s. Calculating spectra over epochs that are comparable to those used in a fast beta burst-triggered aDBS algorithm, will lead to noisy spectra and error-prone parameterisations. However, medication changes occur on a slower scale and 1-minute epochs are likely to detect those. Second, LFP power spectra can be very heterogeneous and if a

pronounced spectral plateau or many oscillatory components are presents, fitting ranges need to be adjusted accordingly (and unequivocal fits may even be impossible). While we visually inspected all PSDs before parameterisation, in a real-time approach an unsupervised machine learning algorithm may decide if PSDs are appropriate for FoooF fitting and if the preferred frequency range is uncorrupted. Further details on the aperiodic exponent as a feedback signal for aDBS are summarised in **Table 7.1**.

	Aperiodic Exponents
Sensitive and specific to the pathological state	Yes, they track different medication states in PD and signal excitation/inhibition of STN.
Reliable over time	Unclear, PSDs with spectral plateaus or prominent oscillatory components may make unequivocal aperiodic fits challenging or even impossible.
Localise to stimulation sweet spot	No
Calculable with low computational requirements	Unclear. While spectral decomposition can be easily done, FoooF is fast but unclear if miniaturised devices will have the computational power to do this.
Provide rapid feedback	No, spectra will have to be averaged over ~ 60 s otherwise parameterisation will be error-prone.

Table 7.1. Aperiodic Exponents as a feedback marker for aDBS.

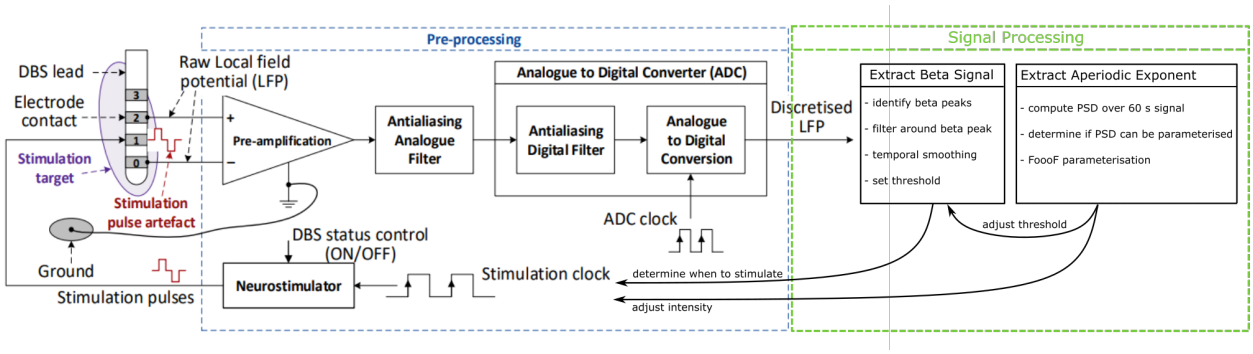


Figure 7.4. Aperiodic Exponents as a feedback marker for aDBS.

8. Project 6: Subthalamic stimulation-induced local field potential changes in dystonia

8.1. Introduction 203
8.2. Methods 204
8.2.1. Consent, regulatory approval, patient selection and clinical details 204
8.2.2. Surgery and lead localisation assessment 205
8.2.3. Stimulation and data recording 205
8.2.4. Experimental paradigm 206
8.2.5. Signal processing: Pre-processing and time frequency decomposition 206
8.2.6. Signal processing: ERNA analysis 207
8.2.7. Signal processing: Evoked Neural Activity (ENA) after single pulse stimulation 208
8.2.8. Signal processing: Beta power and aperiodic exponents 208
8.2.9. Signal processing: Finely-tuned gamma (FTG) analysis 209
8.2.10. Statistics 209
8.3. Results 209
8.3.1. Subthalamic and thalamic power spectral densities in dystonia 209
8.3.2. DBS induces a broad power suppression in the STN of dystonic patients 211
8.3.3. ERNA can be elicited by STN-DBS in dystonia 213
8.3.4. Single pulse stimulation induces ENA and its parameters change with distance from the STN 214
8.3.5. DBS induced FTG in the STN of dystonic patients when stimulation is switched off 217
8.4. Discussion 218
8.4.1. Spectral features of the dystonic STN and thalamus 218
8.4.2. DBS-induced power suppression, ERNA and DBS-induced FTG are not specific to PD 219
8.4.3. ERNA/ENA amplitudes and DBS-induced power suppression are largest within STN 221
8.4.4. Aperiodic exponents of STN-LFPs and DBS-induced FTG are modulated by increasing DBS intensity 222
8.4.5. Limitations 223
8.5. Summarised Findings 223

In this project we had the unique opportunity to record LFPs from thalamic and subthalamic areas in dystonic patients and report several STN-DBS induces spectral changes, which are not specific to PD. This project was published in (Christoph Wiest et al., 2022a).

8.1. Introduction

Dystonia is a movement disorder characterised by patterned torsional movements, abnormal postures and tremor (Albanese et al., 2013). The prominent role of the basal ganglia-sensorimotor network in the generation of dystonic symptoms (Neychev et al., 2011) has led to use of deep brain stimulation (DBS) of the internal globus pallidus (GPi) in the treatment of severe and disabling generalised and segmental dystonia (Volkmann et al., 2012). Theta oscillations in GPi have been associated with dystonic symptoms and suggested as a potential signal for adaptive stimulation in dystonia (Chiung Chu Chen et al., 2006c; Neumann et al., 2017a). While GPi remains the DBS target of choice, subthalamic nucleus (STN) stimulation has been reported to be effective in case series of people with isolated generalised dystonia (Kleiner-Fisman et al., 2007) and cervical dystonia (CD) (Ostrem et al., 2017, 2011; Schjerling et al., 2013). The rationale for using STN-DBS in dystonia comes from evidence that, besides its well-known effectiveness on bradykinesia, rigidity and tremor, this target is very effective against painful OFF-period dystonia in people with Parkinson's disease (PD) (Krack et al., 1999). Nevertheless, it is unclear if enhanced theta is also present in STN.

Subthalamic stimulation in PD is associated with several spectral changes in the STN local field potential (LFP) including beta power suppression (Kuhn et al., 2008), evoked resonant neural activity (ERNA) (Sinclair et al., 2018b; Wiest et al., 2020) and finely-tuned gamma (FTG) oscillations (Muthuraman et al., 2020; C Wiest et al., 2022). These spectral fingerprints have been linked with improvement of parkinsonian symptoms with DBS: beta suppression is linked with improvement of bradykinesia and rigidity (Kuhn et al., 2008; Kühn et al., 2009), and ERNA features are linked with beta activity (Schmidt et al., 2020; Sinclair et al., 2019b) and levodopa-induced high frequency oscillations (Ozturk et al., 2021). The link of these features to clinical symptom severity has driven the development of adaptive DBS for PD,

where, for example, beta power is used as a biomarker to modulate stimulation parameters in a closed-loop fashion. It is unknown if these same spectral features are present during STN stimulation of people with isolated dystonia, and if so how these relate to lead placement and clinical symptoms. Filling this knowledge gap would help understanding of the pathophysiology of isolated dystonia, the contribution of the STN to the generation of dystonic symptoms, as well as the development of invasive and non-invasive neuromodulation strategies.

As a first stage of this work, we took advantage of the unique opportunity to record subthalamic LFPs from people with isolated dystonia. We included seven patients with idiopathic isolated CD and recorded LFPs through an octopolar DBS lead spanning from STN to the ventrolateral thalamus. We asked two main questions. First, how are the power spectra recorded from STN in our patients different from those reported from GPi recordings in isolated dystonia and from STN recordings in PD? Second, are the stimulation-induced phenomena observed in PD also seen in people with dystonia and how do these relate to lead placement?

8.2. Methods

8.2.1. Consent, regulatory approval, patient selection and clinical details

This protocol was approved by the Health Research Authority UK and the National Research Ethics Service local Research Ethics Committee (IRAS: 46576). Seven patients with isolated idiopathic dystonia were recruited at St George's University Hospitals NHS Foundation Trust, London, and received STN-thalamic dual targeted DBS. Written informed consent was obtained in line with the Declaration of the Principles of Helsinki. Five patients were recorded bilaterally, resulting in a total of 12 STNs included in the study. Clinical details and the tested hemispheres are summarised in **Table 8.1**.

Patient #	Gender (m/f)	Age (yr)	Diagnosis	Disease Duration (yr)	TWSTRS/ JRS before DBS	TWSTRS/ JRS at recording	Predominant symptoms	Time of Recording (days post-OP)	Data in Figures 2-4 (L/R)	FTG present (L/R)	Single pulse paradigm (L/R)
1	f	64	Segmental dystonia: CD, UL	28	18	4	Tonic posturing of the head	4	L+R	no	no
2	f	49	CD	6	26	16	Tonic posturing of the head	4	L+R	L+R	no
3	f	68	Cranio-cervical dystonia	55	3/8	0/1	Blepharospasm	4	R	no	no
4	f	59	CD	5	23	23	Tonic posturing of the head	5	L+R	no	no
5	f	45	Segmental dystonia: CD, UL	25	22	12	Tonic posturing of the head	7	no	L	L
6	m	52	CD	8	24	21	Tonic posturing of the head	7	L+R	no	L+R
7	m	51	Segmental dystonia: CD, trunk	10	26	18	Tonic posturing of the head	7	L+R	no	L+R

Table 8.1. Clinical and recording details. CD: cervical dystonia; FTG: finely-tuned gamma; JRS: Jankovic rating scale; TWSTRS: Toronto Western Spasmodic Torticollis Rating Scale (range 0-35); UL: upper limb; L: left; R: right.

8.2.2. Surgery and lead localisation assessment

The surgical targets were the ventrolateral thalamus (nucleus ventralis intermedius, VIM, and nucleus ventralis oralis posterior, VOP), rostral Zona incerta (rZI) and STN (Hassler, 1959). The non-directional Vercise Standard Lead (model 2201, Boston Scientific Corporation, Marlborough, Massachusetts, USA) with 8 ring contacts (30 cm length, 1.3 mm diameter, 0.5 mm contact spacing, 1.5 mm contact length and 15.5 mm contact span) was implanted such that inferior contacts were placed in STN, superior contacts in ventrolateral thalamus and intervening contacts within or close to the rZI. Electrodes were implanted, externalised and lead trajectories reconstructed (**Figure 8.2B**) as described before (Wiest et al., 2020).

8.2.3. Stimulation and data recording

Recordings were made between 4 and 7 days postoperatively (**Table 8.1**), while electrode leads were externalised and patients were OFF all anti-dystonic medication. Monopolar high-frequency stimulation was tested at the 6 middle contacts (C2-C7 in **Figure 8.4A**) as described before (Wiest et al., 2020). LFPs and EMGs from the affected neck muscles were amplified and sampled at 4096 Hz using a TMSi Saga (TMSi International, Netherlands) and custom-written software developed using the C programming language (**Figure 8.1ii**).

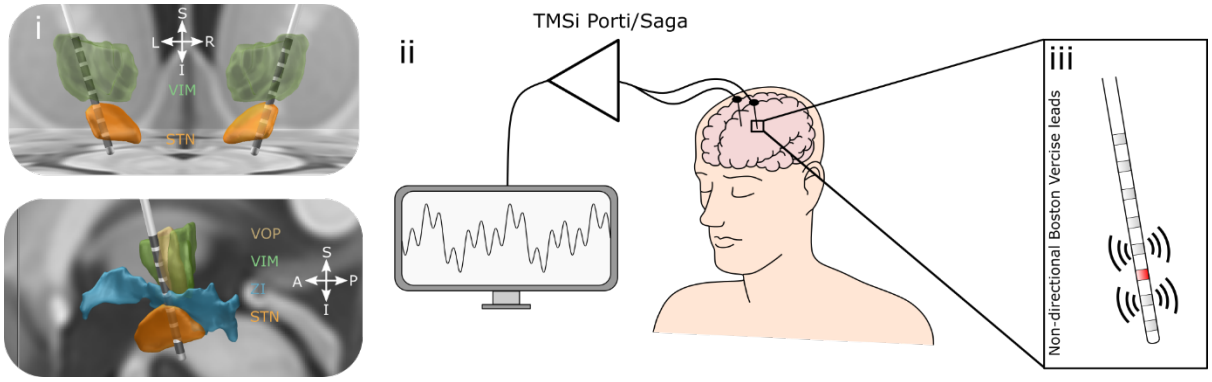


Figure 8.1. Recording Setup. Non-directional Boston Vercise leads were implanted such that inferior contacts were targeting the posterior subthalamic nucleus (STN), superior contacts targeting motor thalamus (VIM or VOP) and any of the middle contacts targeting rostral Zona incerta (ZI) (i; lead reconstruction shown for Patient 2). Leads were temporarily externalised and local field potentials (LFPs) were recorded 4-7 days after implantation using a CE-marked amplifier system (ii). The six middle contact levels were successively stimulated (red), which allowed bipolar LFP recordings from the two adjacent contact levels (iii). (S: superior, I: inferior, A: anterior, P: posterior, R: right, L: left)

8.2.4. Experimental paradigm

In patients 1-4 and 6-7 (11 hemispheres), continuous stimulation to each of the 6 middle contacts was applied with increasing DBS intensity (**Figure 8.4A**). For each tested contact, stimulation was delivered at 130 Hz and intensity was increased from 0.5 mA to 4.5 mA or until side effect threshold was reached in steps of 0.5 mA (**Figure 8.4A**). Each DBS block lasted for 46.92 ± 0.99 s (mean ± SEM) separated by resting periods of 27.50 ± 0.59 s. In addition, different stimulation frequencies (100, 130, 150 and 180 Hz for 2 min each) were tested in patient 2 using the contact and current that elicited the most prominent ERNA without side effects. In patients 5-7, single pulse stimulation was subsequently applied at 2 mA (Patient 5) or 4 mA (Patients 6 and 7) to all 8 contact levels (25 pulses to all contacts) and the remaining 7 contacts were recorded in unipolar mode. If not indicated differently, a stimulation frequency of 130 Hz was used.

8.2.5. Signal processing: Pre-processing and time frequency decomposition

All data analysis was performed using custom-written scripts in MATLAB (version 2020b, The MathWorks Inc., USA). Continuous LFP signals were high-pass filtered at 1 Hz and notch-

filtered at 50 Hz (second-order IIR notch filter). Spectral amplitudes were estimated between 1 and 500 Hz using the short-time Fast Fourier transform with a window length of 1 s, 25% overlap of consecutive windows and a Hamming window yielding a frequency resolution of 1 Hz.

8.2.6. Signal processing: ERNA analysis

The presence of the ERNA was assessed in two ways. In the power spectrum, it was defined as a high-amplitude and high-frequency activity which starts at about 350 Hz and decreases in frequency and amplitude with sustained stimulation (see the lowest panel in **Figure 8.4A** and Wiest et al., 2020). In the time series waveform, the ERNA was defined as a high-amplitude evoked response between two stimulation pulses (**Figure 8.4B**) which resonates as DBS is switched off or paused (Wiest et al., 2020).

To map ERNA amplitudes onto subcortical space, stimulation contact positions in MNI space (MNI 152 2009b NLIN ASYM) were extracted from the Lead-DBS pipeline. To calculate ERNA amplitudes, the inter-pulse interval was linearly detrended, low-pass filtered at 700 Hz and upsampled by factor 10 using a spline interpolation (**Figure 8.4B**). ERNA amplitudes following the first 10 pulses at 2 mA were averaged since this was the highest intensity that was tested across all hemispheres. Average ERNA amplitudes of the first 10 pulses were assigned to their respective stimulation contacts in MNI space and linearly interpolated in three-dimensional space (**Figure 8.4C**). Only contacts with a clear ERNA peak were included in the analysis, which resulted in a total of 21 contacts shown in **Figure 8.4C**. Contacts from the right STN were mirrored to the left and are presented in one combined image.

8.2.7. Signal processing: Evoked Neural Activity (ENA) after single pulse stimulation

In patients 5-7, we studied evoked neural activities (ENAs) after single pulse stimulation with an average inter-pulse interval of 3.97 ± 0.04 s. To quantify ENAs, LFPs were aligned to individual pulses and averaged. We extracted ENA amplitudes and latencies after every DBS pulse as shown in **Figure 8.4B**.

8.2.8. Signal processing: Beta power and aperiodic exponents

Power spectral densities (PSDs) from 1-95 Hz were calculated for LFPs recorded in bipolar montage and each DBS setting. We defined a 30 s epoch before the first DBS block as baseline. Power around the 50 Hz artefact of mains interference was removed (48-52 Hz) and the gap in the PSD was linearly interpolated. PSDs of both the baseline and all DBS blocks were normalised to the mean power between 1-95 Hz of the baseline PSD.

Power change during DBS in **Figure 8.3B** was quantified relative to a 30 s baseline period before respective DBS blocks at 2 mA and the following formula:

$$\%\ power\ change = \frac{DBS\ power - baseline\ power}{baseline\ power} * 100$$

for three frequency ranges: beta (13-35 Hz), low gamma (36-48 Hz) and high gamma (52-80 Hz).

Aperiodic exponents were isolated from the PSD using the open-source FoooF algorithm (version 1.0.0) (Donoghue et al., 2020). Settings for the algorithm were set as: peak width limits: 2-12; max number of peaks: *infinite*; minimum peak height: 0; peak threshold: 2; and aperiodic mode: *fixed*. Power spectra were parameterised across the frequency range 5 to 50 Hz. The lower bound was selected to avoid the impact of low frequency oscillations, the upper bound was selected to avoid the impact of spectral plateaus at high DBS intensity (Gerster et

al., 2022). The same FoooF settings were used to identify meaningful changes of the aperiodic exponent of STN-LFPs with dopaminergic medication and high-frequency stimulation (Christoph Wiest et al., 2022b).

8.2.9. Signal processing: Finely-tuned gamma (FTG) analysis

The post-DBS FTG was identified after each stimulation block at increasing intensity (see **Figure 8.6A**), analysed as described before (Wiest et al., 2021) and baseline-normalised to the mean amplitude of all power estimates between 1-95 Hz of a 30 s period before the first stimulation block.

8.2.10. Statistics

Statistical analyses were conducted using custom-written scripts in MATLAB. Linear mixed-effect models were used to assess the effect of stimulation contacts on ENA parameters and aperiodic exponents as described before (Wiest et al., 2020). To identify clusters of significant power suppression during DBS, we used non-parametric permutation tests with 1000 permutations. Only clusters with $p < .001$ are highlighted in **Figures 8.2 and 8.3A**.

8.3. Results

8.3.1. Subthalamic and thalamic power spectral densities in dystonia

Dual targeting of subthalamic and thalamic areas afforded the opportunity of concomitant LFP recordings from both regions. We recorded blocks of 37.88 ± 4.86 s at rest without any stimulation from 10 (thalamus) and 11 (STN) hemispheres and did not observe prominent peaks in the theta (4-8 Hz) or beta (13-35 Hz) range in the power spectra of both STN and thalamus (**Figure 8.2A**). Dystonic symptoms could still be detected based on clinical assessment despite the post-operative stun effect. However, there was no correlation between muscle activity and LFP power of any frequency range in either STN or thalamus. When

comparing power spectra recorded from within or close to STN (recorded from the C2 contact, **Figure 8.2B**) and thalamus (C6), amplitudes were larger in STN between 31-55 Hz and vice versa from 75-95 Hz (cluster-based permutation test, $p < .001$).

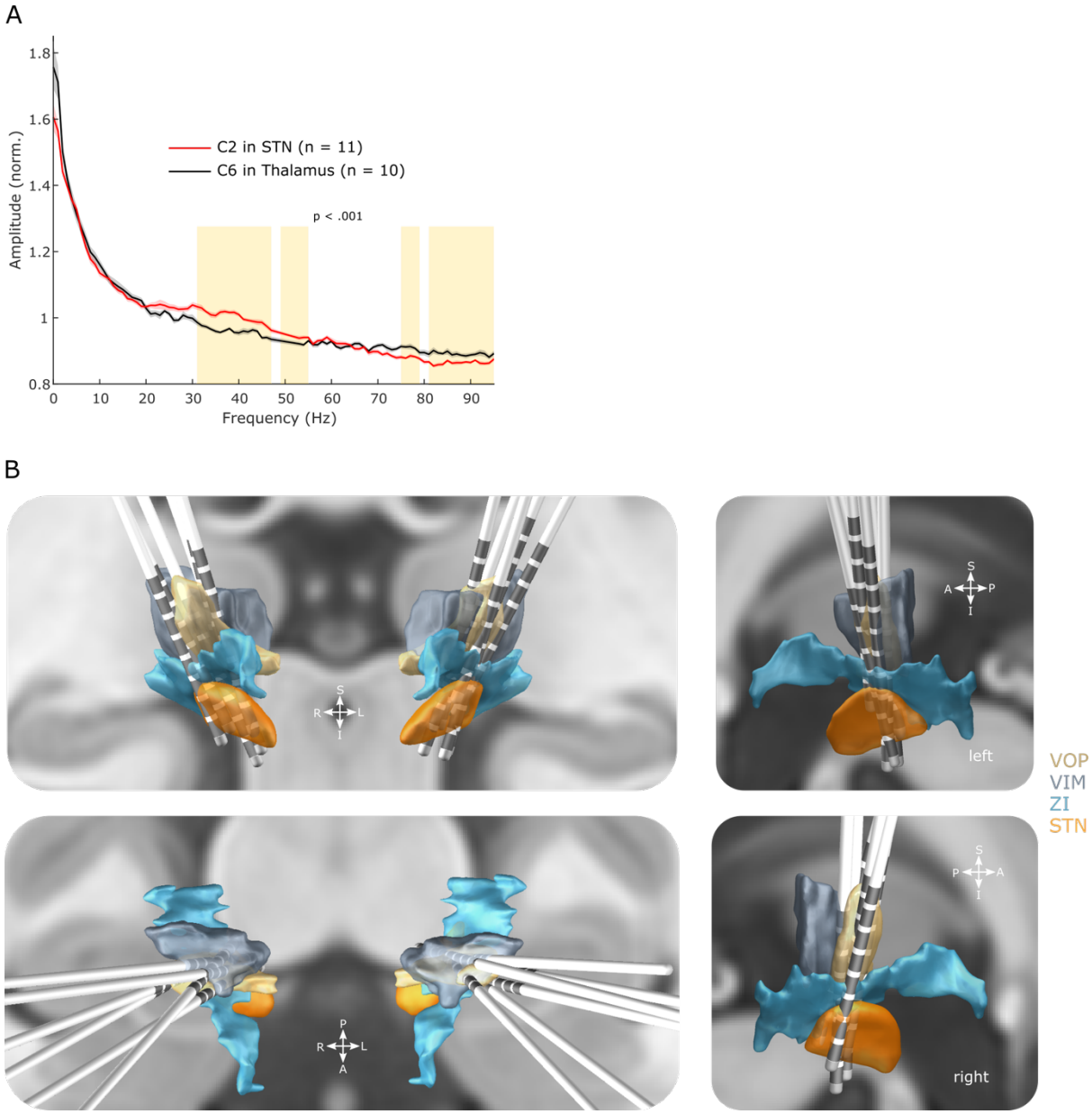


Figure 8.2. Subthalamic and thalamic power spectra in dystonia. A. Power spectral densities (PSD, mean ± SEM) are shown for LFP recordings from the C2 contact in STN (as judged by Lead-DBS, n = 11 hemispheres) and the C6 contact in ventrolateral thalamus (n = 10) without stimulation. Note the lack of a clear theta or beta peak in STN (red). Clusters that are significantly different (cluster-based permutation test, $p < .001$) between STN and thalamus are highlighted in amber. **B.** Lead reconstructions of all 12 electrodes used in this study. STN: subthalamic nucleus, ZI: Zona incerta, VIM: nucleus ventralis intermedius of the thalamus, VOP: nucleus ventralis oralis posterior of the thalamus.

8.3.2. DBS induces a broad power suppression in the STN of dystonic patients

Continuous 130 Hz STN-DBS (delivered to the C2 level) at 2 mA induced power suppression over a broad frequency range (25-80 Hz; $p < .001$; recorded from the adjacent contacts) whereas stimulation to any of the more superior contacts in rZI and thalamus did not lead to significant power changes (in adjacent contacts; **Figure 8.3A**). Power suppression of the beta, low gamma and high gamma range was strongest in the dorsolateral part of STN and decreased to all directions (62 contacts from 11 hemispheres included; **Figure 8.3B**). In keeping with this, power suppression in STN was more pronounced with increasing DBS intensity (**Figure 8.3C**) while increasing DBS currents in VIM/VOP thalamus did not affect the PSD (**Figure 8.3D**).

Recently, the aperiodic exponent (1/F slope of the PSD) was suggested as a marker for E/I balance (Gao et al., 2017; Waschke et al., 2021; Christoph Wiest et al., 2022b). We extracted the aperiodic exponent between 5 and 50 Hz to avoid a spectral plateau at ~ 50 Hz and found that aperiodic exponents in STN increase with rising DBS currents (LME: estimate = 0.006, $t = 8.15$, $p < .001$, $n = 11$ hemispheres), in keeping with the hypothesis that high-frequency stimulation inhibits STN (**Figure 8.3E**). This process appears to be non-linear and to flatten out with further increasing currents. In contrast, aperiodic exponents in VIM-LFPs were less affected by increasing intensity of VIM-DBS (LME: estimate = 0.002, $t = 2.30$, $p = .024$, $n = 10$; **Figure 8.3F**).

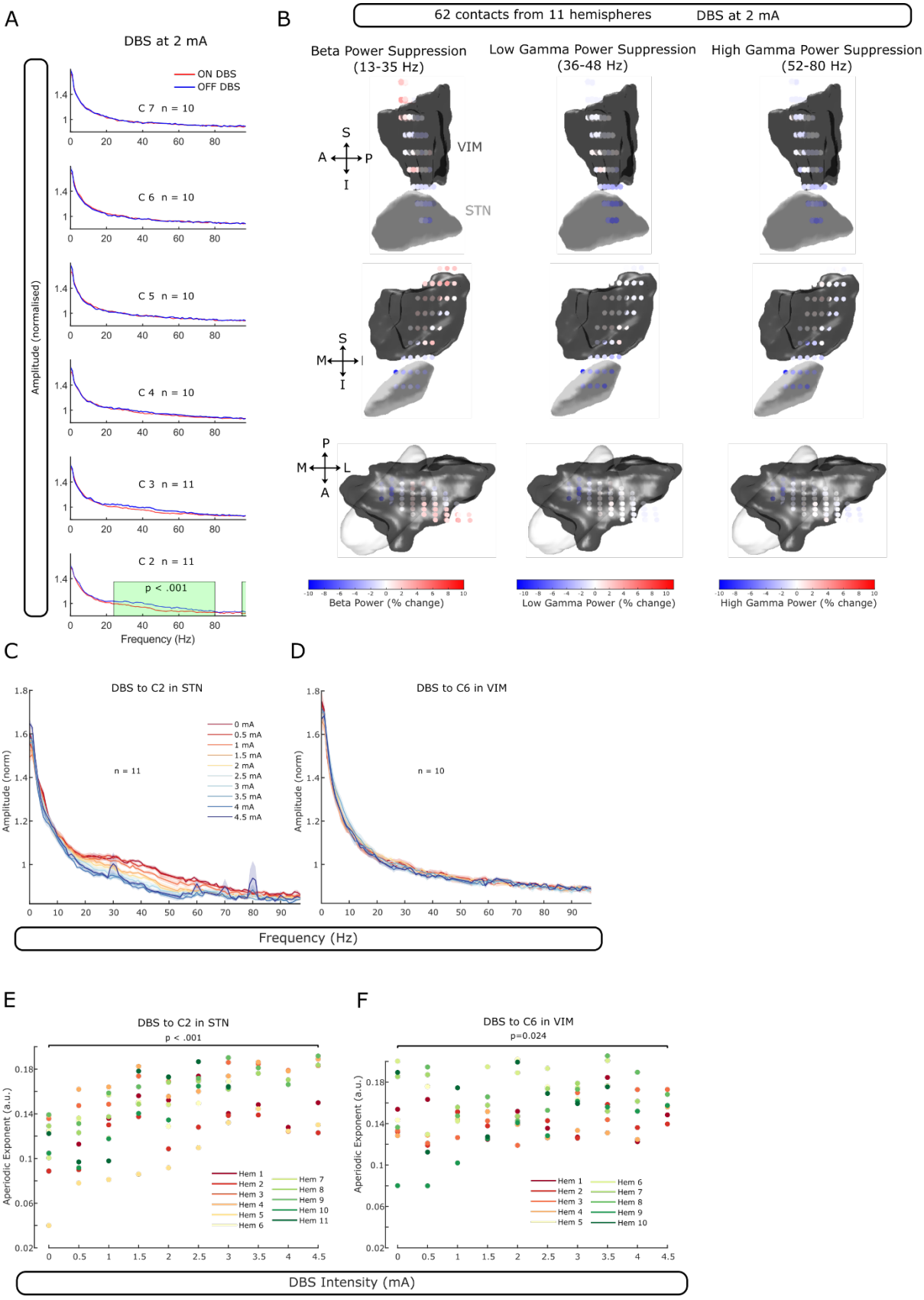


Figure 8.3. DBS-induced power suppression in STN-LFPs of dystonic patients. A. When stimulating contacts C2 to C7 at 2 mA and recording from the adjacent contact pair, average power (mean ± SEM) in the beta (24-35 Hz) and gamma (36-80 Hz) range was suppressed compared to baseline in the most inferior contact only (in STN). Significant clusters are highlighted in green (cluster-

based permutation test, $p < .001$). **B.** Beta (13-35 Hz), low gamma (36-48 Hz) and high gamma (51-80 Hz) power suppression is strongest in the dorsolateral part of STN (n = 62 contacts). **C.** Average power between ~ 20 and ~ 80 Hz is increasingly suppressed in STN with rising DBS intensity. Note the artefacts of stimulation at 4.5 mA manifesting as prominent peaks in different frequency bands (at about 30, 60, 70 and 80 Hz). **D.** No power suppression with increasing DBS intensity when VIM is stimulated. **E.** Aperiodic exponents of the power spectrum increase (1/F slope on a log-log scale becomes steeper) in STN-LFPs with increasing DBS intensity (LME: estimate = 0.006, t = 8.15, $p < .001$). **F.** Aperiodic exponents of VIM-LFPs only slightly increase with rising DBS intensity (LME: estimate = 0.002, t = 2.30, p = .024). (Hem: hemisphere)

8.3.3. ERNA can be elicited by STN-DBS in dystonia

When stimulation was delivered at 130 Hz to contacts within or close to the STN (C2), we observed ERNA recorded from neighbouring contacts progressively with increasing DBS intensity in 11 of 12 tested hemispheres (**Figure 8.4A** lowest panel). When stimulating the next higher contact (C3), ERNA could still be recorded from adjacent contacts, however, only at much higher DBS intensity (e.g. 4.5 mA for Patient 1 left hemisphere). Stimulation to any of the superior contacts in thalamus did not elicit ERNA recorded from surrounding contacts. The observed ERNA shows similar characteristics as reported before in PD: it starts as a high frequency oscillation at ~ 350 Hz and gradually decreases before reaching a steady state after about 1 min (Wiest et al., 2020).

ERNA has previously been suggested as a placement marker for STN. In support of this, ERNA amplitudes were extracted from the first 10 pulses of a DBS block at 130 Hz and 2 mA in the time domain (similar to **Figure 8.4B**). The average ERNA amplitudes of the first 10 pulses were largest in dorsolateral STN (**Figure 8.4C**) and dropped to all directions with increasing distance from that sweet spot (ERNA from 21 contacts and 11 hemispheres was included).

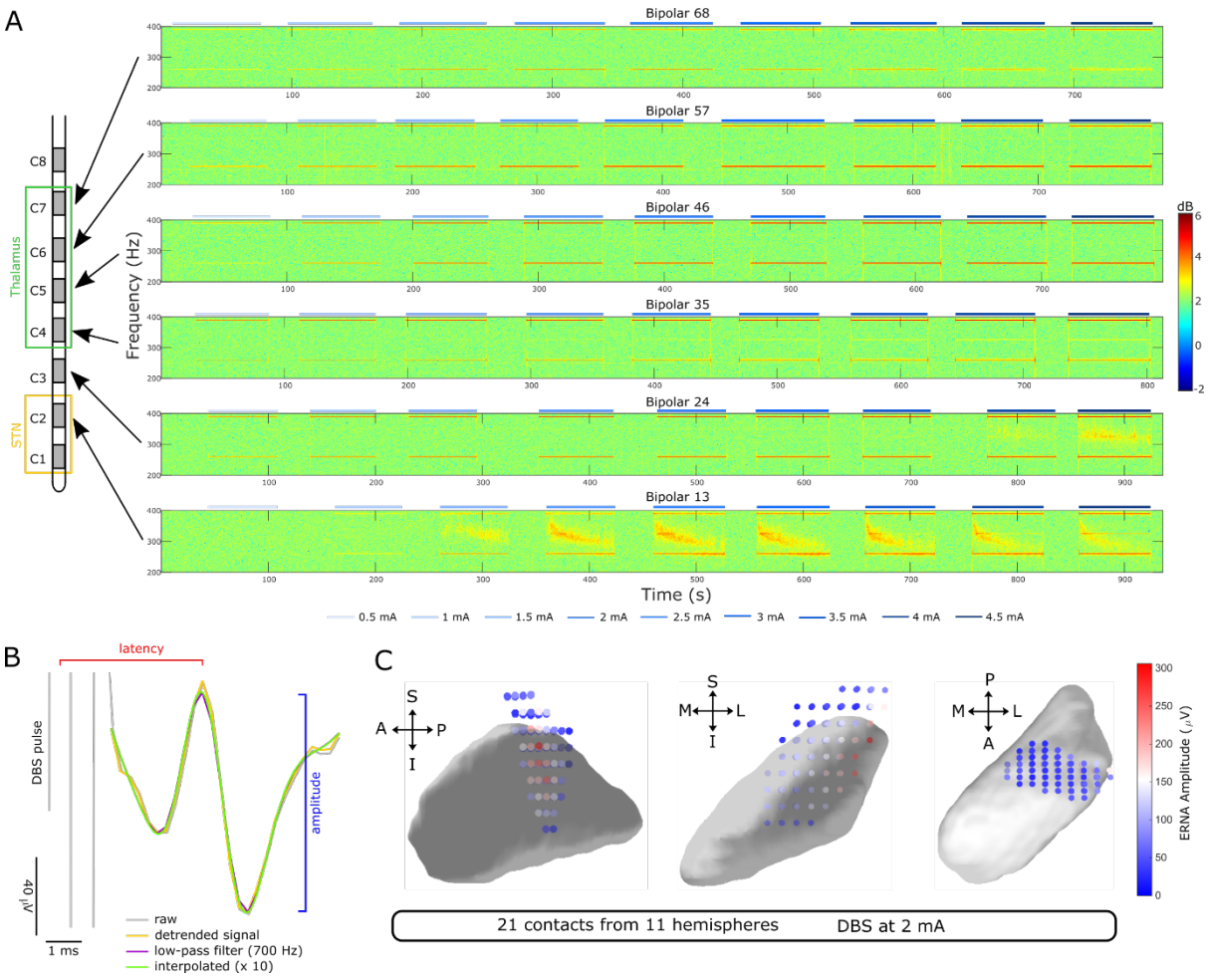


Figure 8.4. Evoked Resonant Neural Activity (ERNA) can be elicited by STN-DBS in dystonia. A. Stimulating contacts within or close to STN (C2) elicits ERNA recorded from adjacent contacts (C1-C3) with increasing DBS intensity (example spectrograms shown for Patient 1). Note that higher DBS intensity is required to elicit ERNA in contact levels that are further away from a sweet spot in STN (DBS to C3 and recording from C2-C4). Stimulation to any of the more superior contacts (in thalamus) did not elicit ERNA (C4-C7). **B.** Schematic of how ERNA latency and amplitude were calculated based on the time series waveform. The inter-pulse interval was linearly detrended, low-pass filtered at 700 Hz and upsampled using a spline interpolation. **C.** Average ERNA amplitudes of the first 10 pulses at 2 mA stimulation are largest within dorsolateral STN (n = 21; contacts from the right hemisphere were mirrored to the left, individual contact positions were interpolated in 3 D as in Horn et al., 2019). (S: superior, I: inferior, A: anterior, P: posterior, M: medial, L: lateral) The three subplots show the left STN viewed from lateral, anterior, superior, respectively.

8.3.4. Single pulse stimulation induces ENA and its parameters change with distance from the STN

To test if and to what extent STN-DBS will affect neurons in rZI and thalamus, we applied repetitive single pulse stimulation in Patients 5-7 (**Table 8.1**) to all 8 contact levels and recorded LFPs from the remaining 7 contacts in unipolar mode. When aligning and averaging the ENA over successive DBS pulses, we observed a clear ENA peak in all contacts when

stimulating the two most inferior contact levels in or close to STN (C1 and C2, **Figure 8.5A**). However, the pattern of the ENA changed across different recording contacts. In inferior contacts within or close to STN (C1 + C2), there was an 'oscillatory' pattern comprising a peak and a trough. In the remaining contacts (C3-C8), we only observed a peak whose latency increased with distance from STN (LME: estimate = 0.24, t = 24.92, $p < .001$). This process appeared to be non-linear with the sharpest rise between C3 and C4, which mirrors the transition from rZI to thalamus (**Figure 8.5B**). Furthermore, ENA amplitudes changed as a function of distance from STN. When stimulating the most inferior contact in STN (C1), ENA amplitudes (calculated as shown in **Figure 8.4B**) were largest in C2, dropped in C3 (LME: estimate = -71.23, t = -44.72, $p < .001$) before increasing again up to the C5 contact which is placed in thalamus (LME: estimate = 6.10, t = 9.18, $p < .001$) (**Figure 8.5B**). ENA amplitudes decreased again in any of the more superior contacts (C6-C8) (LME: estimate = -7.63, t = -24.72, $p < .001$). Changing DBS pulse polarity did not reverse the polarity of the ENA after each pulse. Single pulse stimulation in patients 6 and 7 had similar effects. In these patients, contacts C2 or C3 were placed in STN (as judged by lead reconstructions, see **Figure 8.5 C-F**). Again, ENA amplitudes were largest in contacts adjacent to stimulation (higher amplitudes in the superior neighbour), then dropped in the middle contacts (C4-C6) and increased again in contacts placed in thalamus (C7-8). ENA latencies were lowest in the middle contact levels (C4-C5) and rapidly increased between C5 and C6 (**Figure 8.5C, D and F**) or C4 and C5 (**Figure 8.5E**), a jump that mirrors the transition from rZI to thalamus.

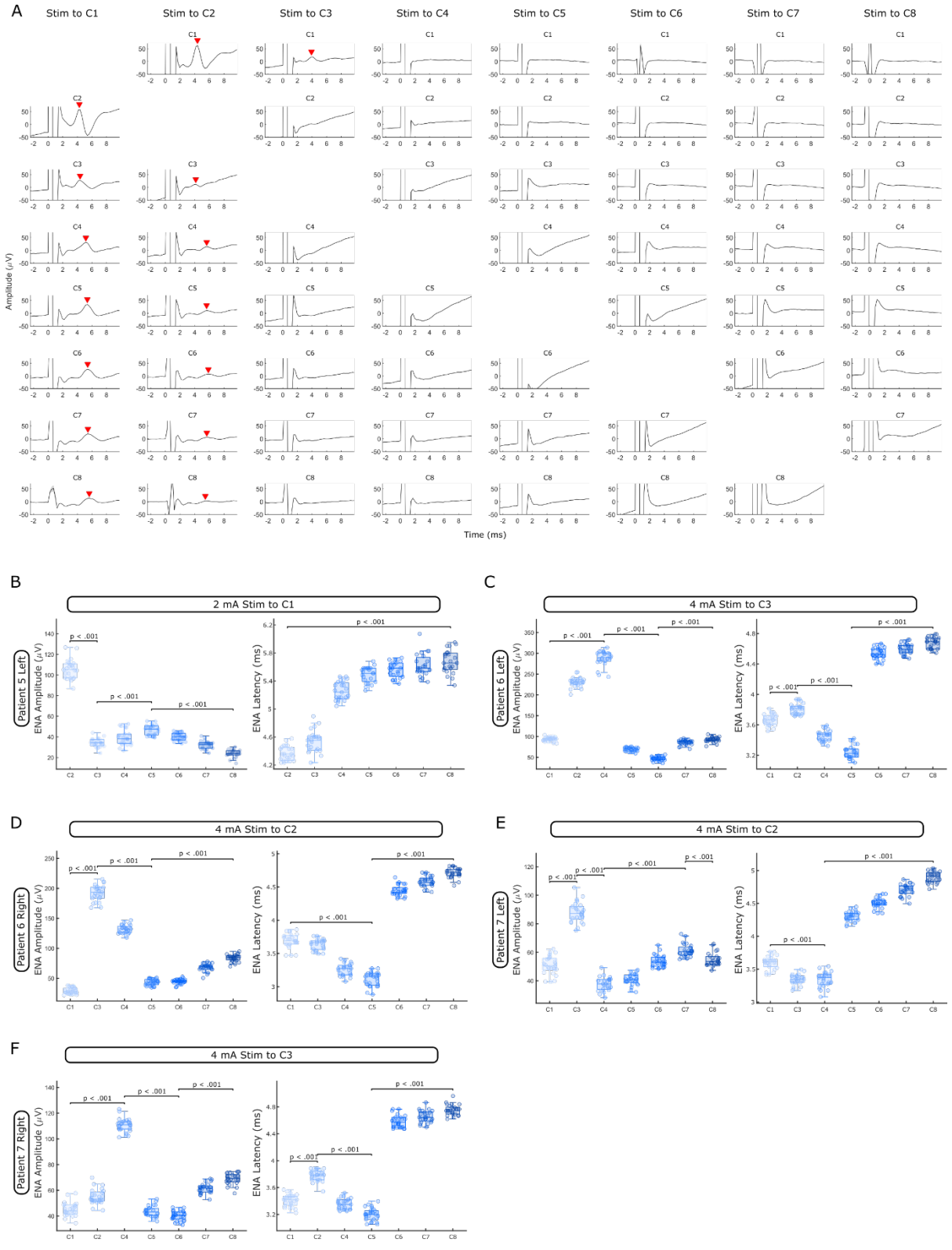


Figure 8.5. Single pulse STN stimulation elicits Evoked Neural Activity (ENA). A. Average ENA responses (mean ± SEM; n = 23 when Stim to C1 and n = 25 for all other columns) after single DBS pulses at 2 mA (ENA peaks are highlighted with red arrowheads, data from Patient 5 left lead). **B.-F.** When stimulating a contact in STN (C1 in B, C2 in D and E, C3 in C and F, as judged by Lead-DBS), ENA amplitudes were largest in the neighbouring contacts (in C-F: superior contact > inferior contact), dropped outside of STN and increased again in thalamus. ENA latencies were shortest in contacts adjacent to stimulation (B) or decreased initially with increasing distance (C-F). Latencies then

increased between C3-C4 (B), C5-C6 (C, D and F) and C4-C5 (E), a jump that mirrors the transition from Zona incerta to thalamus. (p-values of linear mixed-effect models are shown)

8.3.5. DBS induced FTG in the STN of dystonic patients when stimulation is switched off

Levodopa-induced FTG was suggested as a biomarker for dyskinesia in PD (Swann et al., 2016). Recently, we reported that FTG can also be induced in STN by DBS alone without dopaminergic medication or dyskinesia in PD patients (Wiest et al., 2021). Now, we observed the same phenomenon in two dystonic patients (**Figure 8.6A**). Unlike previous reports of FTG in dystonia (Kempf et al., 2009; Miocinovic et al., 2018b), this FTG activity is *de-novo* DBS-induced and not present at rest. In these patients, DBS-induced FTG appears when stimulation is switched off and decreases in frequency as reported before (Wiest et al., 2021). Furthermore, the amplitude of DBS-induced FTG increases with rising DBS intensity and it can also be observed at different DBS frequencies (such as 100, 150 and 180 Hz, **Figure 8.6B**). We observe DBS-induced FTG in 2 of 7 patients (3 of 12 hemispheres), a similar proportion compared to what was reported in PD (Wiest et al., 2021). DBS-induced FTG did not correlate with dystonic symptoms or the clinical effect of STN-DBS.

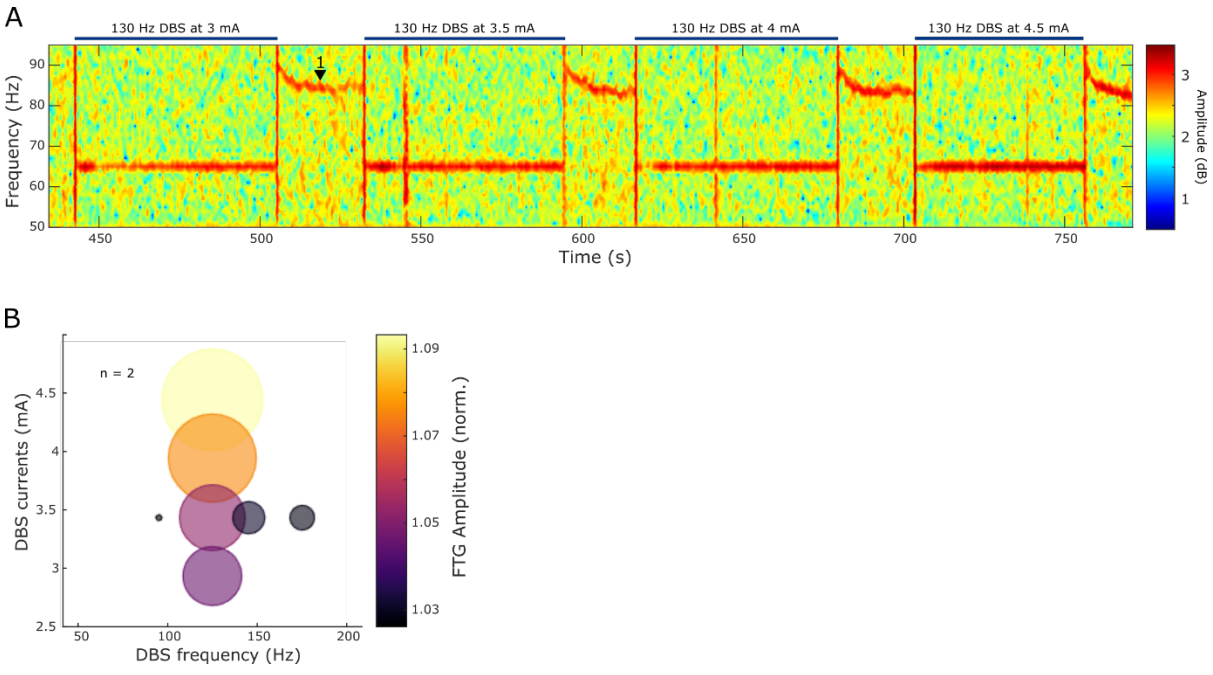


Figure 8.6. DBS-induced finely-tuned gamma (FTG) oscillations occur in the STN of dystonic patients when stimulation is switched off. A. Spectrogram with blocks of increasing DBS intensity (3-4.5 mA). DBS-induced FTG (label 1) occurs after the respective DBS blocks (2 of 7 hemispheres) when patients do not exhibit prominent dystonia due to the stun effect. **B.** The amplitude of DBS-induced FTG increases with rising DBS intensity and DBS-induced FTG can also be elicited when stimulating at different frequencies such as 100, 150 and 180 Hz. Size and colour code of the bubbles denote FTG amplitudes (n = 2 hemispheres).

8.4. Discussion

Here we report for the first time stimulation-induced spectral changes recorded from the STN of people with isolated dystonia. There was no prominent theta peak as has previously been reported in recordings from GPi. We found a range of robust stimulation-induced changes in our dystonia patients that have previously only been reported in PD including a broadband power suppression, ERNA and DBS-induced FTG. ERNA/ENA amplitudes and DBS-induced broadband suppression were largest in STN, supporting their usefulness as markers for lead placement in STN and contact selection in general. Finally, we showed that the aperiodic exponent of STN-LFPs changes with increasing DBS intensity in a way that is reconcilable with the E/I hypothesis. Taken together, these findings point to potential differences in network dynamics in dystonia between GPi and STN, which may be relevant to future work looking at correlations of spectral features with clinical symptoms for adaptive stimulation in dystonia. Furthermore, STN DBS-induced spectral changes reported here may reflect a transdiagnostic pattern of how STN-LFPs respond to high-frequency stimulation. Understanding the origin and temporal dynamics of these changes may open a door to understanding mechanisms underlying high-frequency STN stimulation in general, and therefore its potential application to treatment of other neurological and psychiatric disorders.

8.4.1. Spectral features of the dystonic STN and thalamus

Theta oscillations in GPi (C C Chen et al., 2006; Chiung Chu Chen et al., 2006c; Liu et al., 2008; Neumann et al., 2017a; Silberstein et al., 2003) and STN (Geng et al., 2017; Neumann

et al., 2012) have been associated with dystonic symptoms and, hence, suggested as a potential signal for adaptive stimulation in dystonia. Here, we did not observe a prominent peak in the theta frequency band of the STN-LFP, which differs from the studies mentioned above in GPi and STN (**Figure 2A**). Despite the post-operative stun effect as a potential confounder in this study, our results are backed up by a previous report that did not find increased theta power in the STN of dystonia patients, which could be due to differences in input between the GPi and STN (Wang et al., 2016). Another recent study indicates that dystonia-related spectral changes in the STN may be more prominent during voluntary movements, however, this study investigated dystonia as a motor sign of PD instead of isolated dystonia (Olson et al., 2022).

Contrary to the prominent beta peaks in STN that are a hallmark of PD (P Brown et al., 2001b; Kuhn et al., 2006), we did not observe a clear beta peak in the STN of dystonic patients (**Figure 8.2A**), despite other studies showing beta activity in the STN of dystonic patients at rest (Wang et al., 2016) and subthalamic beta peaks in patients with obsessive compulsive disorder (Rappel et al., 2018). However, we observed larger beta power in STN compared to thalamus. Two previous studies reported higher beta peaks in the GPi-LFP of PD compared to dystonia (Silberstein et al., 2003; Weinberger et al., 2012). These disease-specific spectral differences may be explained by the widespread neurodegeneration in PD, which affects basal ganglia neurophysiology and cements excessive beta synchronisation within the basal ganglia as a near pathognomonic marker of bradykinesia and rigidity in PD.

8.4.2. DBS-induced power suppression, ERNA and DBS-induced FTG are not specific to PD

Stimulation-induced changes in STN-LFPs in the beta and gamma range are well studied in PD (Andrea A. Kühn et al., 2008; Wiest et al., 2020). What is less clear is if these changes are specific to PD or common features of how the STN responds to high-frequency stimulation.

Our results support the latter. From the broad (25-80 Hz) subthalamic DBS-induced power suppression (**Figure 8.3A**), we can infer that excessive, pathological synchronisation in STN anywhere across a broad spectrum in a particular disease could be flattened by high-frequency DBS of that nucleus. Along with our finding of increasing aperiodic exponents as a function of DBS intensity, we could infer that high-frequency STN-DBS will overall have an inhibitory effect on STN neuronal activity. This might broaden the scope of DBS and make STN-DBS a viable option for other disorders with excessive oscillatory peaks in the STN power spectrum.

As in PD, we also observed ERNA in the STN of dystonic patients. Several attempts have been undertaken to find clinical correlates of the ERNA in PD (Awad et al., 2021; Schmidt et al., 2020; Sinclair et al., 2019b; Wiest et al., 2020). Our results show for the first time that ERNA can also be observed in the STN of dystonic patients with similar temporal dynamics to what has been described in PD, demonstrating that it is not a disease-specific phenomenon. While its origin is unclear, it is assumed that the ERNA originates from the effect of STN-DBS on reciprocal STN-GPe (external globus pallidus) connections (Schmidt et al., 2020). Here, we provide evidence that the ERNA is not reliant on PD-specific changes but can also be elicited in the brains of dystonic patients without the widespread neurodegeneration. However, it is still possible, that the ERNA is modulated in the dopamine-deficient brain similar to beta activity.
Levodopa-induced FTG has previously been recorded in PD and linked with the presence of dyskinesia (Swann et al., 2016). This link was recently challenged by a study showing that DBS-induced FTG can be observed in PD even without dyskinesia (C Wiest et al., 2022; Wiest et al., 2021). Previously, spontaneous FTG has also been reported in dystonic patients in both cortical and thalamic LFPs, when it was linked with hyperkinetic movements (Kempf et al., 2009; Miocinovic et al., 2018b). In our cohort, we recorded *de-novo* DBS-induced FTG in STN, which did not vary relative to dystonic postures but appeared reliably after DBS was

stopped. This challenges the direct link between DBS-induced FTG with both Parkinsonian and dystonic symptoms and it may rather present a signal of effective STN stimulation (C Wiest et al., 2022), be it epiphenomenal or not.

Rather than linking ERNA, DBS-induced FTG and broad DBS-induced power suppression with disease-specific symptoms, they might provide insights into the mechanisms underlying STN-DBS. Given the lack of synaptic interconnectivity in STN (Steiner et al., 2019), all of the above activities likely arise within the basal ganglia network, be it interactions between STN and GPe or other cortico-striato-thalamic loops. It is possible that the almost instantaneous broad power suppression in STN (Wiest et al., 2020) or the fast ERNA changes within the first 10 pulses (Schmidt et al., 2020) are due to the rapid synaptic depletion of glutamatergic synapses leading to functional separation of cortex and STN.

8.4.3. ERNA/ENA amplitudes and DBS-induced power suppression are largest within STN

Both ERNA (Sinclair et al., 2021, 2018a) and beta power (Darcy et al., 2022; Horn et al., 2017a) have been suggested as placement markers during surgery and as predictors for the best clinical contact. Our findings of the largest ERNA amplitudes and strongest beta/gamma power suppression in the dorsolateral part of STN (**Figure 8.3B** and **Figure 8.4C**) are in line with the above studies. Importantly, we show that amplitudes and latencies of ENAs after single DBS pulses are also localised to STN (**Figure 8.5**). It is, therefore, not necessary to apply longer bursts of stimulation. Single pulses, which can be applied in a fraction of a second, may be sufficient to optimise lead placement and accelerate contact selection. In general, ENA and ERNA represent the same activity but ERNA has the added component of resonance caused by repetitive DBS pulses at an inter-pulse interval (frequency) that enhances the amplitude and duration of the ENA (positive interference). Moreover, ENA amplitudes and latencies do not decrease linearly as a function of distance upon stimulation of STN (**Figure 8.5B**). ENA

amplitudes are largest in STN and second largest in contacts placed in the ventrolateral thalamus (**see Figure 8.5B+E**). This possibly reflects the thalamic region that receives most inputs from the basal ganglia output structures. ENA latencies initially decrease (**Figure 8.5C-F**) before increasing in a non-linear fashion with the strongest jump (C3 to C4 in **Figure 8.5B**, C4 to C5 in **Figure 8.5E** and C5 to C6 in **Figures 8.5C, D and F**) reflecting the border between rZI and thalamus.

Overall, our results confirm the utility of ERNA/ENA amplitudes and beta/gamma power suppression for both lead placement and contact selection, but challenge the specificity of these spectral changes for PD.

8.4.4. Aperiodic exponents of STN-LFPs and DBS-induced FTG are modulated by increasing DBS intensity

Long considered as noise, aperiodic exponents were often removed from the signal (1/F correction) to emphasise oscillatory components. Recently, the aperiodic exponent was shown to be modulated by age (Voytek et al., 2015), psychiatric disorders (Adelhöfer et al., 2021; Molina et al., 2020) and to reflect E/I balance (Gao et al., 2017). In this context, higher aperiodic exponents tally with states of more inhibition/less excitation and vice versa (Gao et al., 2017; Waschke et al., 2021; Christoph Wiest et al., 2022b). Our results show higher aperiodic exponents when larger DBS currents are applied (**Figure 8.3E**), in keeping with more inhibition/less excitation of STN. This finding is reconcilable with both the E/I hypothesis of the aperiodic exponent and the inactivation hypothesis of DBS.

We showed that DBS-induced FTG amplitudes increase with rising intensity of the previous DBS block. This is striking in so far as the FTG activity lasts for tens of seconds and this demonstrates a long-lasting effect of the previous DBS block. Although the mechanism underlying DBS-induced FTG is unclear, it is conceivable that a stronger impetus of an internal oscillator might explain this intensity-dependent effect (comparable to a stronger push to a

swing). Why the FTG only appears in a sub-set of patients is still unclear. It may be possible that the occurrence of DBS-induced FTG is related to lead placement and FTG may be specific to a much smaller sweet spot.

8.4.5. Limitations

Our results may have been confounded by postoperative stun effect, which obscured dystonic symptoms and is known to lower beta activity in PD (Chiung Chu Chen et al., 2006d). Furthermore, we have a relatively low sample size of 7 dystonic patients (12 hemispheres). This is mostly due to the scarcity of externalised DBS patients and externalised dystonic patients with leads in STN are even rarer.

8.5. Summarised Findings

- No theta peaks observed in the subthalamic nucleus (STN) of dystonic patients
- STN-DBS induces broad power suppression and resonant activity (ERNA) in dystonia
- Power suppression and ERNA localise to STN and may be used as placement markers
- STN-DBS flattens excessive oscillatory peaks and elicits finely-tuned gamma activity
- STN-DBS might be an option for other disorders with pathological STN activity

9. General Discussion

9.1. General summary of results 224
9.2. ERNA and FTG are not artefacts 227
9.2.1. The ERNA is not an artefact 227
9.2.2. FTG is not an artefact 228
9.3. Markers for lead placement and contact prediction 229
9.4. Mechanisms of deep brain stimulation 231
9.5. Open questions for future studies 232
9.6. Summary of Study limitations 233
9.7. Future of adaptive DBS: a thought experiment 235
9.8. Conclusions 236

As all projects were discussed separately at the end of each chapter, we focus here on a more holistic approach which we hope complements previous discussions.

9.1. General summary of results

In this thesis, we investigated high-frequency stimulation-induced spectral changes in the STN local field potential such as ERNA, FTG, power suppression and changes of the aperiodic component.

We refer to the evoked response after single pulses or the evoked response after the first pulse of a pulse train as ENA since ERNA, as its name suggests, requires resonance within the circuit that generates these oscillations, which in turn requires repetitive input to a system (namely a minimum of 2 pulses). Due to this, evoked responses after 2 or more pulses are referred to as ERNA. Having said that, we recognise that single pulse stimulation may elicit oscillatory activities for a limited period of time.

Other names were used in previous studies for the ERNA including DBS local evoked potentials (DLEP) or evoked compound activity (ECA). However, if our hypothesis on the origin of the ERNA proves to be true, the ERNA may not be generated local to the DBS target.

If the ERNA is triggered by antidromic activation of GPe terminals and its ringing feature by an interplay of synchronisation through auto-inhibition and the GPe's autonomous pacemaker properties, the ERNA may much rather be generated by the GPe-STN loop instead. This is supported by studies reporting ERNA in GPe (Bar-Gad et al., 2004; Schmidt et al., 2020). Since the term ECA does not capture the resonant properties of the ERNA to which we refer in several chapters in this thesis, we stick to our terminology choice.

The ERNA has recently been reported during subthalamic stimulation (Sinclair et al., 2018a), however, its first description may have been much earlier (Bar-Gad et al., 2004). In chapters 3 and 4, we study ERNA parameter dynamics with sustained stimulation in comparison to those of beta and gamma oscillations and probe the ERNA under different stimulation settings to assess how it is modulated. We report that ERNA modulation and beta/gamma power suppression during DBS happen at different time scales (~ 70 s vs. 0.5 s), which argues for different mechanisms underlying both activities. We further show that ERNA has a fast component in addition to the slow modulation, which may reflect synaptic depletion of fast glutamatergic neurons (hyperdirect pathway) during DBS. The slow ERNA dynamics (over the first ~ 70 s) may be caused by potentially slower synaptic depletion of the STN-GPe synapse, which modulates GABAergic input from prototypic GPe neurons to STN. Of note, fast ERNA dynamics happen at a similar time scale as DBS-induced power suppression in the beta and low-gamma power band (chapter 3+4), potentially hinting at a common cause.

In a series of complementary analyses, we found that both slow and fast ERNA dynamics were modulated by increasing DBS frequencies and intensities such that ERNA may be used as a marker of the optimal DBS frequency and lowest effective intensity. ERNA amplitudes and latencies differ with levodopa, which makes them a potential feedback signal for aDBS. This is complicated by the different ERNA parameter dynamics during cDBS and aDBS. While both stimulation methods elicit significant clinical improvement in a reaching task, ERNA does

not reach steady state during aDBS. On the one hand, that could mean that cDBS and aDBS have different underlying mechanisms and circuit states within the basal ganglia and could be explained within the framework of the synaptic depletion hypothesis. On the other hand, ERNA steady state may be completely detached from clinical efficacy, but ERNA parameters after single pulse stimulation may still aid for lead placement and contact and parameter selection.

We report the presence of *de-novo* DBS-induced FTG during and after stimulation in chapter 5. FTG has been referred to as narrowband gamma oscillations in previous studies. As there is no appreciable difference between the two, we stick to the terminology we used before. Our results demonstrate that FTG can be induced by DBS when patients are OFF levodopa and non-dyskinetic, in contrast to previous studies (Swann et al., 2018, 2016). We characterised DBS-induced FTG showing that its frequency changes within and across subsequent DBS blocks and that DBS-induced FTG is not entrained at half stimulation frequency, at least not during the first 2 minutes of stimulation. This is particularly interesting since cortical FTG has previously been shown to be entrained at a subharmonic of stimulation (Swann et al., 2016). In addition, we show that DBS-induced FTG is not specific to PD since it can be recorded from the STN of dystonic patients as well (chapter 8). While it is unlikely to be directly linked to symptoms of PD, the FTG may serve as a placement marker within STN. In chapter 6, we performed a literature review and compare the FTG, be it levodopa or DBS-induced, with movement-related gamma synchronisation and speculate on its usefulness in aDBS.

In chapter 7, we confirm the link between aperiodic exponents and the E/I ratio and show that higher aperiodic exponents of STN-LFPs tally with a balance tipped towards inhibition. In the next step, we report higher aperiodic exponents ON levodopa and ON stimulation, which is consistent with treated PD manifesting as increased inhibition and hypoactivity of STN. If it will be computationally feasible to parameterise power spectra in real-time in a miniaturised device, analysis of the aperiodic component may complement existing feedback markers for

aDBS in PD. The aperiodic component of the power spectrum has many other names (see chapter 7). Here, we stick to the term coined by the Voytek group who developed the FoooF toolbox.

9.2. ERNA and FTG are not artefacts

9.2.1. The ERNA is not an artefact

How can we be sure the ERNA is not a specious artefact of the stimulation and recording system? First, reversing the polarity of stimulation pulses is an established method of distinguishing neural activity from stimulation artefact (Brown and Abbas, 1990; Kent and Grill, 2013, 2012; Sinclair et al., 2019a; Walker et al., 2012). We replicated the experiments by Sinclair et al., 2019a and did not observe a change in the morphology of the ERNA upon pulse reversal suggesting that the ERNA is independent from artefact. Second, the ERNA is not present in a saline tank test (Sinclair et al., 2019 and our data). Similarly, we replicated experiments performed in Sinclair et al., 2019a, which show that DBS artefacts in saline solution subside within 1 ms. Using an amplifier with 83,333 Hz sampling rate, we did not see any stimulation artefact beyond 1 ms after the DBS pulse. The lack of stimulation artefact beyond 1 ms in a saline recording is indicative that the stimulation and recording system did not introduce prolonged artefacts. Third, as saline does not completely reflect recording conditions of an electrode in tissue, Sinclair et al. implanted a DBS electrode into the visual cortex of a feline model and did not observe any electrophysiological activity that resembles the ERNA (Sinclair et al., 2019a). Fourth, the ERNA is focal to STN, GPe and cortex and absent in white matter tracts adjacent to these regions (Ozturk et al., 2021; Schmidt et al., 2020; Walker et al., 2012) and in VIM of patients with essential tremor and dystonia (chapter 8 and Sinclair et al., 2019). This corroborates that the ERNA is localisable to certain brain regions and not an artefact. Fifth, in this thesis we describe levodopa-induced changes to ERNA

parameters over the first 10 pulses (chapter 4). If the ERNA was an artefact of stimulation, we would not expect it to be systematically modulated by dopaminergic medication across participants. Sixth, we observe an amplitude increase when the ERNA crosses a harmonic of stimulation. This transient activity increase, potentially signalling entrainment at a superharmonic of stimulation, initially increases with rising DBS intensity, but eventually decreases with further increasing DBS intensity; conditions that would be very untypical of an artefact. Seventh, the anti-aliasing filter cut-off frequency in our recording system is considerably higher than the ERNA frequency. We recorded the ERNA with different amplifiers, at different sampling rates and with different hardware anti-aliasing filters and therefore, the ERNA is very unlikely due to filter ringing artefacts. Finally, the ERNA has been consistently reported and replicated by many groups across the globe using different recording and stimulation systems (Awad et al., 2021; Ozturk et al., 2021; Schmidt et al., 2020; Sinclair et al., 2018a; Wiest et al., 2020).

9.2.2. FTG is not an artefact

As pointed out in chapter 5, *de-novo* DBS-induced FTG during and after stimulation is very unlikely artefactual. However there is more uncertainty about activity at exactly half stimulation frequency. This activity may reflect two different underlying processes. On the one hand, there is cortical 65 Hz activity recorded over many hours that comes and goes with dopaminergic medication, while DBS is consistently switched on (Swann et al., 2016) and outlasts 130 Hz STN-DBS (observations from the group of Philip Starr). Given the close link to changes in the medication state and their dissociation from the stimulation artefact at 130 Hz, this activity likely reflects physiological changes. On the other hand, there is subcortical 65 Hz activity in STN which appears immediately when stimulation is turned on, instantaneously locks to 65 Hz and stays locked to that value until DBS is switched off, mirroring the stimulation artefact at 130 Hz (see **Figure 8.6**). On anecdotal evidence, levodopa-

induced FTG can be observed before DBS at ~ 80 Hz and over the first few seconds of stimulation, it slowly drifts to 65 Hz until it becomes locked at that frequency. This activity at exactly half stimulation may be focal to STN and vary between contacts (our data and observations from the group of Andrea Kühn). These observations point towards a potential physiological mechanism such as 1:2 entrainment as underlying this activity (Sermon et al., 2022). In a saline tank test, we observed activity at half-harmonics at higher frequencies (see **Figure 2.2**). With increasing stimulation intensity, these half-harmonics also appeared at lower frequencies. Given differences in impedance and electrode-tissue interaction between a saline tank and the brain, it is possible that activity at half stimulation frequency that locks to that value immediately when stimulation is switched on, is artefactual. However, we cannot exclude the possibility of this being the lock-in entrainment at half stimulation frequency (also in **Figure 8.6A**) and it may be challenging to parse entrainment from artefact.

9.3. Markers for lead placement and contact prediction

Technical innovations in lead designs yielded DBS electrodes with more contacts, which increases the number of possible DBS settings exponentially, which in turn increases programming time (Ten Brinke et al., 2018). Consequently, there is a need for fast or automatic parameter selection. Previously, electrophysiological markers, such as beta activity at rest and during movement, and imaging-guided approaches were suggested to aid programming (Bour et al., 2015; Milosevic et al., 2020; Tinkhauser et al., 2018; Yoshida et al., 2010; Zaidel et al., 2010). In this thesis, we mapped DBS-induced beta power suppression onto subcortical space and confirmed that beta/gamma power suppression localise to dorsolateral STN (chapter 8), which is a prerequisite for contact selection.

Nevertheless, combining multiple electrophysiological markers has the potential to outperform beta-based contact selection, even more so when anatomical information is added to a model

(Shah et al., 2022). DBS-induced power suppression in the beta/gamma range can be recorded with commercial DBS devices with sensing features and, hence, this approach can be used clinically already.

As demonstrated in this thesis, the ERNA, which is also focal to STN, is another promising candidate for contact selection, but requires sampling rates that at the moment cannot be achieved by commercially available, chronically implanted pulse generators. Still, the ERNA can be probed intraoperatively, with the caveat that DBS leads were shown to rotate within the first 24 hours after implantation, and directional contacts that elicited largest ERNA amplitudes may shift (Rau et al., 2021). In a recent study, the ERNA outperformed beta activity and an imaging based approach with respect to predicting the clinician-chosen contact (Xu et al., 2022). However, it is possible that the anatomy approach was not fully exhausted in this study. Other studies used individual tractography to predict best clinical contacts in essential tremor and PD and suggested this approach as a way forward (Horn et al., 2017a; Lin et al., 2020; Petry-Schmelzer et al., 2020).

A general confounder in the search for predictors of contact selection is a subjective component in the choice of the best clinical contact. Clinical improvement may be similar in two contacts and potentially even better in a contact that was disregarded if different settings had been tested. At the moment, deciding the best contact is a time consuming game of trial and error. In chapter 7, we present a quick method to quickly screen all 8 contacts of a lead and extract ENA latencies and amplitudes. Testing single pulses at random intervals with different pulse widths, intensities, phase gaps and frequencies (paired pulses), will not add much time in theatres, but would accelerate the painstakingly slow process of contact selection afterwards.

9.4. Mechanisms of deep brain stimulation

Different hypotheses for the mechanisms underlying DBS were introduced in chapter 1. In this thesis, we add to this discussion and overall our findings support the inactivation hypothesis of STN-DBS. In chapter 8, we show that aperiodic exponents of the STN-LFP in rodents can be a proxy for excitatory and inhibitory input to STN where higher exponents tally with more inhibition and vice versa. This created a platform to speculate on the mechanism behind DBS. We found increased aperiodic exponents ON dopaminergic medication and ON stimulation, in keeping with more inhibition/less excitation of STN while symptoms improve. In addition, we speculate on the origin of the ERNA and suggest it to be a predominantly inhibitory signal (chapter 4). We and others put forward that the ERNA may be generated through orthodromic and antidromic activation of prototypic GPe terminals in STN and larger ERNA amplitudes may indicate more inhibitory input to STN. This links well with the larger ERNA amplitudes ON levodopa observed in chapter 4. While both projects support the inactivation hypothesis of STN-DBS, the underlying mechanism may be more complex. Site-specific and frequency-dependent neuronal effects may determine if a target structure is excited or inhibited (Milosevic et al., 2021). Some questions on the mechanism of DBS are yet unanswered, e.g. how may instantaneous inhibition of a brain nucleus explain clinical improvement in PD at different time scales (see chapter 1)? At first sight, the slow and fast temporal dynamics of the ERNA might have appeared as promising correlates of symptom improvement in PD at different speed. However, the same fast and slow ERNA dynamics are also present in dystonia and, hence, are unlikely to be only linked with PD-specific symptoms. Furthermore, the mechanism underlying adaptation to DBS (e.g. synaptic plasticity) in PD, essential tremor and dystonia remains speculative.

9.5. Open questions for future studies

In chapters 3 and 4 we investigated the ERNA, however, there are still many unknowns with respect to clinical correlates and its underlying mechanism. We show that ERNA is present in PD and CD, which shows that its sheer presence is not a direct reflection of parkinsonian symptoms. However, it is possible that ERNA parameters/dynamics are different in the dopamine-deficient state as our results suggest. Moreover, it is unclear if ERNA parameters are modulated by movement or different cognitive states that can be observed in PD, CD and, indeed, in health. In addition, we observed ERNA fluctuations at steady state at ~ 1.5 Hz (**Figure 9.S1**). These fluctuations are unlikely to be caused by sampling noise given their regularity and their absence at the start of stimulation. It is unclear what this activity represents. We also observed potential ERNA entrainment whenever it crosses a harmonic of stimulation (**Figure 9.S2**). More studies will be needed to show if ERNA entrainment is of clinical relevance and how it can be exploited for aDBS. If the ERNA is to become a valuable feedback signal for aDBS in the future, it will need to reflect symptoms of PD or CD in some way. One way of implementing ERNA-based aDBS would be in combination with a fast beta-triggered aDBS algorithm. Average ERNA latencies and frequencies could be calculated for all pulses in a stimulation burst. If mean ERNA values per burst would exceed a certain range, the beta threshold could be adapted or DBS intensity could be adapted proportionally. However, this would require sensing at a high sampling rate of ~ 4000 Hz to capture the ERNA's delicate changes at reasonable accuracy.

Furthermore, the ERNA's underlying mechanism is still speculative. We propose a mechanism, which builds on previous modelling work and suggests the ERNA may be primarily generated in GPe and captured in the inhibitory synaptic input to STN. We further suggest that glutamate has a modulatory effect on this mechanism (see chapter 4). While the kinetics of cortico-subthalamic synaptic depletion were described before (Steiner et al., 2019), the kinetics of

STN-GPe synapses to reach depletion are less clear. Essentially, although unlikely, we cannot rule out an STN-intrinsic mechanism underlying the ERNA. More studies will be needed to prove or disprove our hypothesis.

Even more uncertainties are emanating from the FTG. Again, clinical links and mechanistic understanding are elusive. Initially, levodopa-induced FTG was suggested as a readout of dyskinesia in PD, however, this link is more and more contested. Our results in chapter 5 show that FTG can also be DBS-induced in the absence of dyskineas and levodopa. We discussed the pros and cons of a link between FTG and dyskinesia in chapter 6 more in depth.

We showed in chapter 7 how aperiodic exponents of STN-LFPs reflect the E/I ratio of synaptic input to that structure and how aperiodic exponents change with medication and DBS in a way that is reconcilable with the inactivation hypothesis of DBS. This finding could be supported by studying aperiodic exponents of M1-LFPs picked up with ECoG during medication and stimulation. We hypothesise the impact of stimulation artefacts and, hence, the spectral plateau to be less in cortical signals. An even simpler prove of principle would be using non-invasive TACS and concomitant EEG recordings to excite cortical neurons and examine if changes in E/I are reflected in the aperiodic exponent.

9.6. Summary of Study limitations

Since most PD patients reported in the results here had electrodes implanted in STN and not GPi it is unclear to what extent results extend to GPi. In light of the matching presence of beta oscillations in both nuclei, the similarity in effect of clinical DBS and functional connectivity within the basal ganglia give reason for optimism (P Brown et al., 2001a).

PD patients that were uncomfortable withdrawing from antiparkinsonian medication overnight were excluded from some studies incorporated in this thesis. This may have led to a sampling bias towards less severely affected cases. Related to this, dopamine agonists and extended

release levodopa have prolonged half-lives and were not fully metabolised after overnight withdrawal. Hence, some patients were possibly not studied at the maximal possible dopamine deficient state. The off medication state was confirmed by clinical testing nevertheless this may have introduced variability across patients.

The timing of the recording in the immediate postoperative periods comes with another limitation. Lead implantation causes focal damage and tissue oedema which affects the physiology of the underlying network and results in clinical improvement (stun effect) (Chiung Chu Chen et al., 2006a). Despite this, beta oscillations were shown to be stable over 7 years compared with perioperative recordings which provides hope for a good correlation between the acute and chronic state (Giannicola et al., 2012). Another study found good correlation between acute localisation of beta oscillations and localisation of chronic stimulation contacts suggesting the link is robust (Yoshida et al., 2010).

Slightly different operative procedures across sites may increase variability. Lead mapping using pre- and post-operative imaging and clinical efficacy were used to assess contact placement and comparability. The effects of different amplifiers, recording systems, sampling rates and stimulators was reduced by normalisation of power spectral data within subjects and down-sampling to common sampling rates. Common mode rejection could theoretically suppress prominent oscillations that are present in multiple channels. Practically, this did not appear to be a significant problem given that low-amplitude signals (e.g. beta oscillations) or high-amplitude activity (e.g. ERNA) were found in the majority of patients off medication or during DBS respectively.

Time constraints, patient fatigue and patient compliance led to differences in the number of trials across participants. Data were analysed using LMEM to account for this heterogeneity. Other general limitations include the limited sample size potentially giving rise to type I and II

errors. Given the current level of knowledge it is up to speculation whether some of the described findings (e.g. FTG and ERNA) will be shared by other phenotypes or even healthy subjects and hence there is only limited if any causal inference possible.

9.7. Future of adaptive DBS: a thought experiment

In a way, aDBS where clinicians adjust DBS parameters between outpatient visits is already common practice. Nevertheless, this "very slow" aDBS approach cannot account for all the symptom fluctuations, which is why feedback signals are required, be it electrophysiological signals or inertial signals from wearables, as introduced in chapter 1. aDBS offers the possibility to optimise DBS by automatically adjusting the time and parameters of DBS in real-time, which has potential for significant innovation in movement disorders (Starr, 2018). Single biomarker approaches have the advantage of directly targeting pathophysiological mechanisms, whereas machine learning-based decoding at times derives correlates of symptoms indirectly through learning noisy correlations (Neumann et al., 2019). On the other hand, single biomarkers alone cannot account for the complex set of symptoms in PD such as gait, speech and tremor (Molina et al., 2021; Thenaisie et al., 2022). Advantages and disadvantages of feedback marker for aDBS that were investigated in this thesis are listed in **Table 9.S1**.

In a thought experiment, it is informative to speculate how optimal symptom control using aDBS may be achieved in the future disregarding all technological restraints. Taking into consideration how dramatically computers, tablets and smartphones changed over the past 20 years, a small skull-mounted device that is capable of tracking multiple feedback signals and integrating them in real-time may not be too far-fetched. The best stimulation contacts, lowest effective intensity and pulse width and the optimal DBS frequency may be chosen by analysing the ENA/ERNA after single and paired-pulse stimulation before patients are discharged after

IPG implantation. Due to the ever growing body of literature that links beta activity with bradykinesia and rigidity in PD (Little and Brown, 2020), this could become the main feedback signal. Slow and fast beta (or even more granular with many different smoothing windows from 200 ms to 1 min) will be extracted simultaneously, weighted, integrated and eventually a binary or proportional output will determine when DBS will be switched on/off or increased/decreased. In addition, every minute aperiodic exponents of cortical and subcortical LFPs will be calculated based on multiple fitting ranges and ERNA latencies and amplitudes will be extracted after every DBS pulse. Beta power, ERNA and aperiodic exponent changes will be integrated in real-time, which may lead to adjustments of the beta threshold to trigger stimulation and adjustments of DBS parameters. This includes for example stimulating both hemispheres at different frequencies to further desynchronise pathological circuits or automatic adjustments during sleep. Additional decoding improvement may be achieved if patients are implanted with subdural and subcortical leads (Merk et al., 2022).

However, even in this utopic description of future aDBS, symptom control would not be perfect. There is an urgent need for non-motor neural correlates in PD or other disorders. 40-50% of PD patients suffer from affective disorders which may require more DBS leads in different brain regions to identify electrophysiological correlates that may serve as feedback signals (Marsh, 2013).

9.8. Conclusions

Overall, this thesis provides a detailed characterisation of the ERNA, challenges FTG as a biomarker of dyskinesias, clarifies that ERNA, beta/gamma power suppression and DBS-induced FTG are not specific to PD and suggested the aperiodic exponent of STN-LFPs as a readout for E/I balance. All of the above can advance knowledge on feedback markers for aDBS and improve understanding of network effects of DBS.

10. References

Abdi, A., Mallet, N., Mohamed, F.Y., Sharott, A., Dodson, P.D., Nakamura, K.C., Suri, S., Avery, S. V, Larvin, J.T., Garas, F.N., Garas, S.N., Vinciati, F., Morin, S., Bezard, E., Baufreton, J., Magill, P.J., 2015a. Prototypic and arkypallidal neurons in the dopamine-intact external globus pallidus. J. Neurosci. 35, 6667–6688. https://doi.org/10.1523/JNEUROSCI.4662-14.2015

Abdi, A., Mallet, X.N., Mohamed, F.Y., Sharott, A., Dodson, X.P.D., Nakamura, X.K.C., Suri, S., Avery, S. V, Larvin, X.J.T., Garas, F.N., Garas, S.N., Vinciati, F., Bezard, X.E., Je, X., Magill, P.J., 2015b. Prototypic and Arkypallidal Neurons in the Dopamine-Intact External Globus Pallidus 35, 6667–6688. https://doi.org/10.1523/JNEUROSCI.4662-14.2015

Abosch, A., Lanctin, D., Onaran, I., Eberly, L., Spaniol, M., Ince, N.F., 2012. Long-term recordings of local field potentials from implanted deep brain stimulation electrodes. Neurosurgery 71, 804–814. https://doi.org/10.1227/NEU.0b013e3182676b91

Adams, J.R., van Netten, H., Schulzer, M., Mak, E., Mckenzie, J., Strongosky, A., Sossi, V., Ruth, T.J., Lee, C.S., Farrer, M., Gasser, T., Uitti, R.J., Calne, D.B., Wszolek, Z.K., Stoessl, A.J., 2005. PET in LRRK2 mutations: comparison to sporadic Parkinson's disease and evidence for presymptomatic compensation. Brain 128, 2777–2785. https://doi.org/10.1093/brain/awh607

Adelhöfer, N., Paulus, T., Mückschel, M., Bäumer, T., Bluschke, A., Takacs, A., Tóth-Fáber, E., Tárnok, Z., Roessner, V., Weissbach, A., Münchau, A., Beste, C., 2021. Increased scale-free and aperiodic neural activity during sensorimotor integration-a novel facet in Tourette syndrome. Brain Commun. 3, fcab250. https://doi.org/10.1093/braincomms/fcab250

Afshar, P., Khambhati, A., Stanslaski, S., Carlson, D., Jensen, R., Linde, D., Dani, S., Lazarewicz, M., Cong, P., Giftakis, J., Stypulkowski, P., Denison, T., 2012. A translational platform for prototyping closed-loop neuromodulation systems. Front. Neural Circuits 6, 117. https://doi.org/10.3389/fncir.2012.00117

Ahlskog, J.E., 2005. Challenging conventional wisdom: the etiologic role of dopamine oxidative stress in Parkinson's disease. Mov. Disord. 20, 271–282. https://doi.org/10.1002/mds.20362

Ahlskog, J.E., Muenter, M.D., 2001. Frequency of levodopa-related dyskinesias and motor fluctuations as estimated from the cumulative literature. Mov. Disord. 16, 448–458. https://doi.org/10.1002/mds.1090

Ajiboye, A.B., Willett, F.R., Young, D.R., Memberg, W.D., Murphy, B.A., Miller, J.P., Walter, B.L., Sweet, J.A., Hoyen, H.A., Keith, M.W., Peckham, P.H., Simeral, J.D., Donoghue, J.P., Hochberg, L.R., Kirsch, R.F., 2017. Restoration of reaching and grasping movements through brain-controlled muscle stimulation in a person with tetraplegia: a proof-of-concept demonstration. Lancet (London, England) 389, 1821–1830. https://doi.org/10.1016/S0140-6736(17)30601-3

Al-Fatly, B., Ewert, S., Kübler, D., Kroneberg, D., Horn, A., Kühn, A.A., 2019. Connectivity profile

of thalamic deep brain stimulation to effectively treat essential tremor. Brain 142, 3086–3098. https://doi.org/10.1093/brain/awz236

Albanese, A., Bhatia, K., Bressman, S.B., Delong, M.R., Fahn, S., Fung, V.S.C., Hallett, M., Jankovic, J., Jinnah, H.A., Klein, C., Lang, A.E., Mink, J.W., Teller, J.K., 2013. Phenomenology and classification of dystonia: a consensus update. Mov. Disord. 28, 863–873. https://doi.org/10.1002/mds.25475

Alberquilla, S., Gonzalez-Granillo, A., Martín, E.D., Moratalla, R., 2020. Dopamine regulates spine density in striatal projection neurons in a concentration-dependent manner. Neurobiol. Dis. 134, 104666. https://doi.org/10.1016/j.nbd.2019.104666

Albin, R.L., Young, A.B., Penney, J.B., 1989. The functional anatomy of basal ganglia disorders. Trends Neurosci. 12, 366–375. https://doi.org/10.1016/0166-2236(89)90074-x

Alegre, M., Alonso-Frech, F., Rodríguez-Oroz, M.C., Guridi, J., Zamarbide, I., Valencia, M., Manrique, M., Obeso, J.A., Artieda, J., 2005. Movement-related changes in oscillatory activity in the human subthalamic nucleus: ipsilateral vs. contralateral movements. Eur. J. Neurosci. 22, 2315–2324. https://doi.org/10.1111/j.1460-9568.2005.04409.x

Alegre, M., Lopez-Azcarate, J., Obeso, I., Wilkinson, L., Rodriguez-Oroz, M.C., Valencia, M., Garcia-Garcia, D., Guridi, J., Artieda, J., Jahanshahi, M., Obeso, J.A., 2013. The subthalamic nucleus is involved in successful inhibition in the stop-signal task: a local field potential study in Parkinson's disease. Exp. Neurol. 239, 1–12. https://doi.org/10.1016/j.expneurol.2012.08.027

Alonso-Frech, F., Zamarbide, I., Alegre, M., Rodríguez-Oroz, M.C., Guridi, J., Manrique, M., Valencia, M., Artieda, J., Obeso, J.A., 2006. Slow oscillatory activity and levodopa-induced dyskinesias in Parkinson's disease. Brain 129, 1748–1757. https://doi.org/10.1093/brain/awl103

Alterman, R.L., Miravite, J., Weisz, D., Shils, J.L., Bressman, S.B., Tagliati, M., 2007. Sixty hertz pallidal deep brain stimulation for primary torsion dystonia. Neurology 69, 681–688. https://doi.org/10.1212/01.wnl.0000267430.95106.ff

Alvarez, L., Macias, R., Pavón, N., López, G., Rodríguez-Oroz, M.C., Rodríguez, R., Alvarez, M., Pedroso, I., Teijeiro, J., Fernández, R., Casabona, E., Salazar, S., Maragoto, C., Carballo, M., García, I., Guridi, J., Juncos, J.L., DeLong, M.R., Obeso, J.A., 2009. Therapeutic efficacy of unilateral subthalamotomy in Parkinson's disease: results in 89 patients followed for up to 36 months. J. Neurol. Neurosurg. Psychiatry 80, 979–985. https://doi.org/10.1136/jnnp.2008.154948

Anderson, M.E., Postupna, N., Ruffo, M., 2003. Effects of high-frequency stimulation in the internal globus pallidus on the activity of thalamic neurons in the awake monkey. J. Neurophysiol. 89, 1150–1160. https://doi.org/10.1152/jn.00475.2002

Androulidakis, A.G., Doyle, L.M.F., Yarrow, K., Litvak, V., Gilbertson, T.P., Brown, P., 2007a. Anticipatory changes in beta synchrony in the human corticospinal system and associated improvements in task performance. Eur. J. Neurosci. 25, 3758–3765.

https://doi.org/10.1111/j.1460-9568.2007.05620.x

Androulidakis, A.G., Kühn, A.A., Chen, C.C., Blomstedt, P., Kempf, F., Kupsch, A., Schneider, G.-H., Doyle, L., Dowsey-Limousin, P., Hariz, M.I., Brown, P., 2007b. Dopaminergic therapy promotes lateralized motor activity in the subthalamic area in Parkinson's disease. Brain 130, 457–468. https://doi.org/10.1093/brain/awl358

Anzak, A., Gaynor, L., Beigi, M., Limousin, P., Hariz, M., Zrinzo, L., Foltynie, T., Brown, P., Jahanshahi, M., 2011. A gamma band specific role of the subthalamic nucleus in switching during verbal fluency tasks in Parkinson's disease. Exp. Neurol. 232, 136–142. https://doi.org/10.1016/j.expneurol.2011.07.010

Anzak, A., Tan, H., Pogosyan, A., Foltynie, T., Limousin, P., Zrinzo, L., Hariz, M., Ashkan, K., Bogdanovic, M., Green, A.L., Aziz, T., Brown, P., 2012. Subthalamic nucleus activity optimizes maximal effort motor responses in Parkinson's disease. Brain 135, 2766–2778. https://doi.org/10.1093/brain/aws183

Arlotti, M., Marceglia, S., Foffani, G., Volkmann, J., Lozano, A.M., Moro, E., Cogiamanian, F., Prenassi, M., Bocci, T., Cortese, F., Rampini, P., Barbieri, S., Priori, A., 2018. Eight-hours adaptive deep brain stimulation in patients with Parkinson disease. Neurology 90, e971–e976. https://doi.org/10.1212/WNL.0000000000005121

Arlotti, M., Rosa, M., Marceglia, S., Barbieri, S., Priori, A., 2016. The adaptive deep brain stimulation challenge. Parkinsonism Relat. Disord. 28, 12–17. https://doi.org/10.1016/j.parkreldis.2016.03.020

Aru, Juhan, Aru, Jaan, Priesemann, V., Wibral, M., Lana, L., Pipa, G., Singer, W., Vicente, R., 2015. Untangling cross-frequency coupling in neuroscience. Curr. Opin. Neurobiol. 31, 51–61. https://doi.org/10.1016/j.conb.2014.08.002

Ascherio, A., Chen, H., Weisskopf, M.G., O'Reilly, E., McCullough, M.L., Calle, E.E., Schwarzschild, M.A., Thun, M.J., 2006. Pesticide exposure and risk for Parkinson's disease. Ann. Neurol. 60, 197–203. https://doi.org/10.1002/ana.20904

Awad, M.Z., Vaden, R.J., Irwin, Z.T., Gonzalez, C.L., Black, S., Nakhmani, A., Jaeger, B.C., Bentley, J.N., Guthrie, B.L., Walker, H.C., 2021. Subcortical short-term plasticity elicited by deep brain stimulation. Ann. Clin. Transl. Neurol. 8, 1010–1023. https://doi.org/10.1002/acn3.51275

Aziz, T.Z., Peggs, D., Sambrook, M.A., Crossman, A.R., 1991. Lesion of the subthalamic nucleus for the alleviation of 1-methyl-4-phenyl-1,2,3,6-tetrahydropyridine (MPTP)-induced parkinsonism in the primate. Mov. Disord. 6, 288–292. https://doi.org/10.1002/mds.870060404

Baggio, H.C., Segura, B., Junque, C., 2015. Resting-state functional brain networks in Parkinson's disease. CNS Neurosci. Ther. 21, 793–801. https://doi.org/10.1111/cns.12417

Bai, S., Song, Y., Huang, X., Peng, L., Jia, J., Liu, Y., Lu, H., 2016. Statin Use and the Risk of Parkinson's Disease: An Updated Meta-Analysis. PLoS One 11, e0152564. https://doi.org/10.1371/journal.pone.0152564

Bamford, N.S., Robinson, S., Palmiter, R.D., Joyce, J.A., Moore, C., Meshul, C.K., 2004. Dopamine modulates release from corticostriatal terminals. J. Neurosci. 24, 9541–9552. https://doi.org/10.1523/JNEUROSCI.2891-04.2004

Bar-Gad, I., Elias, S., Vaadia, E., Bergman, H., 2004. Complex locking rather than complete cessation of neuronal activity in the globus pallidus of a 1-methyl-4-phenyl-1,2,3,6-tetrahydropyridine-treated primate in response to pallidal microstimulation. J. Neurosci. Off. J. Soc. Neurosci. 24, 7410–7419. https://doi.org/10.1523/JNEUROSCI.1691-04.2004

Baranauskas, G., Maggiolini, E., Vato, A., Angotzi, G., Bonfanti, A., Zambra, G., Spinelli, A., Fadiga, L., 2012. Origins of 1/f2 scaling in the power spectrum of intracortical local field potential. J. Neurophysiol. 107, 984–994. https://doi.org/10.1152/jn.00470.2011

Barbe, M.T., Liebhart, L., Runge, M., Pauls, K.A.M., Wojtecki, L., Schnitzler, A., Allert, N., Fink, G.R., Sturm, V., Maarouf, M., Timmermann, L., 2011. Deep brain stimulation in the nucleus ventralis intermedius in patients with essential tremor: habituation of tremor suppression. J. Neurol. 258, 434–439. https://doi.org/10.1007/s00415-010-5773-3

Barone, P., 2010. Neurotransmission in Parkinson's disease: beyond dopamine. Eur. J. Neurol. 17, 364–376. https://doi.org/10.1111/j.1468-1331.2009.02900.x

Barone, P., Antonini, A., Colosimo, C., Marconi, R., Morgante, L., Avarello, T.P., Bottacchi, E., Cannas, A., Ceravolo, G., Ceravolo, R., Cicarelli, G., Gaglio, R.M., Giglia, R.M., Iemolo, F., Manfredi, M., Meco, G., Nicoletti, A., Pederzoli, M., Petrone, A., Pisani, A., Pontieri, F.E., Quatrale, R., Ramat, S., Scala, R., Volpe, G., Zappulla, S., Bentivoglio, A.R., Stocchi, F., Trianni, G., Dotto, P. Del, 2009. The PRIAMO study: A multicenter assessment of nonmotor symptoms and their impact on quality of life in Parkinson's disease. Mov. Disord. 24, 1641–1649. https://doi.org/10.1002/mds.22643

Basu, I., Graupe, D., Tuninetti, D., Shukla, P., Slavin, K. V, Metman, L.V., Corcos, D.M., 2013. Pathological tremor prediction using surface electromyogram and acceleration: potential use in "ON-OFF" demand driven deep brain stimulator design. J. Neural Eng. 10, 36019. https://doi.org/10.1088/1741-2560/10/3/036019

Basu, I., Tuninetti, D., Graupe, D., Slavin, K. V, 2011. Adaptive control of deep brain stimulator for essential tremor: entropy-based tremor prediction using surface-EMG. Conf. Proc. ... Annu. Int. Conf. IEEE Eng. Med. Biol. Soc. IEEE Eng. Med. Biol. Soc. Annu. Conf. 2011, 7711–7714. https://doi.org/10.1109/IEMBS.2011.6091900

Belova, E.M., Semenova, U., Gamaleya, A.A., Tomskiy, A.A., Sedov, A., 2021. Voluntary movements cause beta oscillations increase and broadband slope decrease in the subthalamic nucleus of parkinsonian patients. Eur. J. Neurosci. 53, 2205–2213. https://doi.org/10.1111/ejn.14715

Benabid, A.L., Pollak, P., Gross, C., Hoffmann, D., Benazzouz, A., Gao, D.M., Laurent, A., Gentil, M., Perret, J., 1994. Acute and long-term effects of subthalamic nucleus stimulation in

Parkinson's disease. Stereotact. Funct. Neurosurg. 62, 76–84. https://doi.org/10.1159/000098600

Benabid, A.L., Pollak, P., Louveau, A., Henry, S., de Rougemont, J., 1987. Combined (thalamotomy and stimulation) stereotactic surgery of the VIM thalamic nucleus for bilateral Parkinson disease. Appl. Neurophysiol. 50, 344–346.

Benjamini, Y. Hochberg, Y., 1995. Controlling the false discovery rate: a practical and powerful approach to multiple testing. J R Stat Soc Ser. B 57:289–300.

Bergman, H., 2021. The Hidden Life of the Basal Ganglia, The Hidden Life of the Basal Ganglia. The MIT Press, Cambridge, Massachusetts. https://doi.org/10.7551/mitpress/14075.001.0001

Bergman, H., Wichmann, T., DeLong, M.R., 1990. Reversal of experimental parkinsonism by lesions of the subthalamic nucleus. Science 249, 1436–1438. https://doi.org/10.1126/science.2402638

Bergman, H., Wichmann, T., Karmon, B., DeLong, M.R., 1994. The primate subthalamic nucleus. II. Neuronal activity in the MPTP model of parkinsonism. J. Neurophysiol. 72, 507–520. https://doi.org/10.1152/jn.1994.72.2.507

Berman, B.D., Starr, P.A., Marks, W.J.J., Ostrem, J.L., 2009. Induction of bradykinesia with pallidal deep brain stimulation in patients with cranial-cervical dystonia. Stereotact. Funct. Neurosurg. 87, 37–44. https://doi.org/10.1159/000195718

Beudel, M., Oswal, A., Jha, A., Foltynie, T., Zrinzo, L., Hariz, M., Limousin, P., Litvak, V., 2017. Oscillatory Beta Power Correlates With Akinesia-Rigidity in the Parkinsonian Subthalamic Nucleus. Mov. Disord. https://doi.org/10.1002/mds.26860

Bevan, M.D., Hallworth, N.E., Baufreton, J., 2007. GABAergic control of the subthalamic nucleus. Prog. Brain Res. 160, 173–188. https://doi.org/10.1016/S0079-6123(06)60010-1

Bezard, E., Gross, C.E., Brotchie, J.M., 2003. Presymptomatic compensation in Parkinson's disease is not dopamine-mediated. Trends Neurosci. 26, 215–221. https://doi.org/10.1016/S0166-2236(03)00038-9

Bilyk, J.R., Yen, M.T., Bradley, E.A., Wladis, E.J., Mawn, L.A., 2018. Chemodenervation for the Treatment of Facial Dystonia: A Report by the American Academy of Ophthalmology. Ophthalmology 125, 1459–1467. https://doi.org/10.1016/j.ophtha.2018.03.013

Birdno, M.J., Grill, W.M., 2008. Mechanisms of deep brain stimulation in movement disorders as revealed by changes in stimulus frequency. Neurother. J. Am. Soc. Exp. Neurother. 5, 14–25. https://doi.org/10.1016/j.nurt.2007.10.067

Blahak, C., Bäzner, H., Capelle, H.-H., Wöhrle, J.C., Weigel, R., Hennerici, M.G., Krauss, J.K., 2009. Rapid response of parkinsonian tremor to STN-DBS changes: direct modulation of oscillatory basal ganglia activity? Mov. Disord. 24, 1221–1225. https://doi.org/10.1002/mds.22536

Blahak, C., Capelle, H.-H., Baezner, H., Kinfe, T.M., Hennerici, M.G., Krauss, J.K., 2011. Micrographia induced by pallidal DBS for segmental dystonia: a subtle sign of hypokinesia? J. Neural Transm. 118, 549–553. https://doi.org/10.1007/s00702-010-0544-y

Blainey, P., Krzywinski, M., Altman, N., 2014. Points of significance: replication. Nat. Methods 11, 879–880. https://doi.org/10.1038/nmeth.3091

Blomstedt, P., Hariz, M.I., 2005. Hardware-related complications of deep brain stimulation: a ten year experience. Acta Neurochir. (Wien). 147, 1061–4; discussion 1064. https://doi.org/10.1007/s00701-005-0576-5

Blomstedt, P., Sandvik, U., Fytagoridis, A., Tisch, S., 2009. The posterior subthalamic area in the treatment of movement disorders: past, present, and future. Neurosurgery 64, 1029–1042. https://doi.org/10.1227/01.NEU.0000345643.69486.BC

Bodner, R.A., Outeiro, T.F., Altmann, S., Maxwell, M.M., Cho, S.H., Hyman, B.T., McLean, P.J., Young, A.B., Housman, D.E., Kazantsev, A.G., 2006. Pharmacological promotion of inclusion formation: a therapeutic approach for Huntington's and Parkinson's diseases. Proc. Natl. Acad. Sci. U. S. A. 103, 4246–4251. https://doi.org/10.1073/pnas.0511256103

Bojanic, S., Sethi, H., Hyam, J., Yianni, J., Nandi, D., Joint, C., Carter, H., Gregory, R., Bain, P., Aziz, T.Z., 2004. Externalising deep brain electrodes: an increased risk of infection? J. Clin. Neurosci. Off. J. Neurosurg. Soc. Australas. 11, 732–734. https://doi.org/10.1016/j.jocn.2003.09.019

Bolam, J.P., Brown, M.T.C., Moss, J., Magill, P.J., 2009. Basal Ganglia : Internal Organization 97–104.

Börgers, C., Epstein, S., Kopell, N.J., 2005. Background gamma rhythmicity and attention in cortical local circuits: a computational study. Proc. Natl. Acad. Sci. U. S. A. 102, 7002–7007. https://doi.org/10.1073/pnas.0502366102

Bour, L.J., Lourens, M.A.J., Verhagen, R., de Bie, R.M.A., van den Munckhof, P., Schuurman, P.R., Contarino, M.F., 2015. Directional Recording of Subthalamic Spectral Power Densities in Parkinson's Disease and the Effect of Steering Deep Brain Stimulation. Brain Stimul. 8, 730–741. https://doi.org/10.1016/j.brs.2015.02.002

Bouthour, W., Mégevand, P., Donoghue, J., Lüscher, C., Birbaumer, N., Krack, P., 2019. Biomarkers for closed-loop deep brain stimulation in Parkinson disease and beyond. Nat. Rev. Neurol. 15, 343–352. https://doi.org/10.1038/s41582-019-0166-4

Bouton, C.E., Shaikhouni, A., Annetta, N. V, Bockbrader, M.A., Friedenberg, D.A., Nielson, D.M., Sharma, G., Sederberg, P.B., Glenn, B.C., Mysiw, W.J., Morgan, A.G., Deogaonkar, M., Rezai, A.R., 2016. Restoring cortical control of functional movement in a human with quadriplegia. Nature 533, 247–250. https://doi.org/10.1038/nature17435

Bresadola, M., 2008. Animal electricity at the end of the eighteenth century: the many facets of a great scientific controversy. J. Hist. Neurosci. 17, 8–32. https://doi.org/10.1080/09647040600764787

Brittain, J.-S., Probert-Smith, P., Aziz, T.Z., Brown, P., 2013. Tremor suppression by rhythmic transcranial current stimulation. Curr. Biol. 23, 436–440.

https://doi.org/10.1016/j.cub.2013.01.068

Brittain, J.-S., Watkins, K.E., Joundi, R.A., Ray, N.J., Holland, P., Green, A.L., Aziz, T.Z., Jenkinson, N., 2012. A role for the subthalamic nucleus in response inhibition during conflict. J. Neurosci. Off. J. Soc. Neurosci. 32, 13396–13401. https://doi.org/10.1523/JNEUROSCI.2259-12.2012

Broca, P., 1861. Perte de la parole, ramollissement chronique et destruction partielle du lobe antérieur gauche du cerveau. Bull Soc Anthr. 2:235-238.

Broen, M.P.G., Narayen, N.E., Kuijf, M.L., Dissanayaka, N.N.W., Leentjens, A.F.G., 2016. Prevalence of anxiety in Parkinson's disease: A systematic review and meta-analysis. Mov. Disord. 31, 1125–1133. https://doi.org/10.1002/mds.26643

Bronstein, J.M., Tagliati, M., Alterman, R.L., Lozano, A.M., Volkmann, J., Stefani, A., Horak, F.B., Okun, M.S., Foote, K.D., Krack, P., Pahwa, R., Henderson, J.M., Hariz, M.I., Bakay, R.A., Rezai, A., Marks, W.J.J., Moro, E., Vitek, J.L., Weaver, F.M., Gross, R.E., DeLong, M.R., 2011. Deep brain stimulation for Parkinson disease: an expert consensus and review of key issues. Arch. Neurol. 68, 165. https://doi.org/10.1001/archneurol.2010.260

Bronte-Stewart, H., Barberini, C., Koop, M.M., Hill, B.C., Henderson, J.M., Wingeier, B., 2009. The STN beta-band profile in Parkinson's disease is stationary and shows prolonged attenuation after deep brain stimulation. Exp. Neurol. 215, 20–28. https://doi.org/10.1016/j.expneurol.2008.09.008

Brown, C.J., Abbas, P.J., 1990. Electrically evoked whole-nerve action potentials: parametric data from the cat. J. Acoust. Soc. Am. 88, 2205–2210. https://doi.org/10.1121/1.400117

Brown, P., 2003. Oscillatory nature of human basal ganglia activity: relationship to the pathophysiology of Parkinson's disease. Mov. Disord. 18, 357–363. https://doi.org/10.1002/mds.10358

Brown, P., Eusebio, A., 2008. Paradoxes of functional neurosurgery: clues from basal ganglia recordings. Mov. Disord. 23, 12–20; quiz 158. https://doi.org/10.1002/mds.21796

Brown, P, Oliviero, A., Mazzone, P., Insola, A., Tonali, P., Di Lazzaro, V., 2001a. Dopamine dependency of oscillations between subthalamic nucleus and pallidum in Parkinson's disease. J. Neurosci. 21, 1033–1038. https://doi.org/10.1523/JNEUROSCI.21-03-01033.2001

Brown, P, Oliviero, A., Mazzone, P., Insola, A., Tonali, P., Di Lazzaro, V., 2001b. Dopamine dependency of oscillations between subthalamic nucleus and pallidum in Parkinson's disease. J. Neurosci. 21, 1033–1038. https://doi.org/10.1523/JNEUROSCI.21-03-01033.2001

Brown, Peter, Oliviero, A., Mazzone, P., Insola, A., Tonali, P., Lazzaro, V. Di, 2001. Dopamine Dependency of Oscillations between Subthalamic Nucleus and Pallidum in Parkinson ' s Disease 21, 1033–1038.

Brown, P., Salenius, S., Rothwell, J.C., Hari, R., 1998. Cortical correlate of the Piper rhythm in humans. J. Neurophysiol. 80, 2911–2917. https://doi.org/10.1152/jn.1998.80.6.2911

Brown, P., Williams, D., 2005. Basal ganglia local field potential activity: character and functional

significance in the human. Clin. Neurophysiol. Off. J. Int. Fed. Clin. Neurophysiol. 116, 2510–2519. https://doi.org/10.1016/j.clinph.2005.05.009

Brücke, C., Bock, A., Huebl, J., Krauss, J.K., Schönecker, T., Schneider, G.-H., Brown, P., Kühn, A.A., 2013. Thalamic gamma oscillations correlate with reaction time in a Go/noGo task in patients with essential tremor. Neuroimage 75, 36–45. https://doi.org/10.1016/j.neuroimage.2013.02.038

Brücke, C., Huebl, J., Schönecker, T., Neumann, W.-J., Yarrow, K., Kupsch, A., Blahak, C., Lütjens, G., Brown, P., Krauss, J.K., Schneider, G.-H., Kühn, A.A., 2012. Scaling of movement is related to pallidal γ oscillations in patients with dystonia. J. Neurosci. 32, 1008–1019. https://doi.org/10.1523/JNEUROSCI.3860-11.2012

Brücke, C., Kempf, F., Kupsch, A., Schneider, G.-H., Krauss, J.K., Aziz, T., Yarrow, K., Pogosyan, A., Brown, P., Kühn, A.A., 2008. Movement-related synchronization of gamma activity is lateralized in patients with dystonia. Eur. J. Neurosci. 27, 2322–2329. https://doi.org/10.1111/j.1460-9568.2008.06203.x

Bruns, A., 2004. Fourier-, Hilbert- and wavelet-based signal analysis: are they really different approaches? J. Neurosci. Methods 137, 321–332. https://doi.org/10.1016/j.jneumeth.2004.03.002

Brys, I., Halje, P., Scheffer-Teixeira, R., Varney, M., Newman-Tancredi, A., Petersson, P., 2018. Neurophysiological effects in cortico-basal ganglia-thalamic circuits of antidyskinetic treatment with 5-HT(1A) receptor biased agonists. Exp. Neurol. 302, 155–168. https://doi.org/10.1016/j.expneurol.2018.01.010

Burke, R.E., Fahn, S., Marsden, C.D., 1986. Torsion dystonia: a double-blind, prospective trial of high-dosage trihexyphenidyl. Neurology 36, 160–164. https://doi.org/10.1212/wnl.36.2.160

Buzsáki, G., Anastassiou, C.A., Koch, C., 2012. The origin of extracellular fields and currents — EEG, ECoG, LFP and spikes. Nat. Rev. Neurosci. 13, 407.

Buzsáki, G., Wang, X.-J., 2012. Mechanisms of gamma oscillations. Annu. Rev. Neurosci. 35, 203–225. https://doi.org/10.1146/annurev-neuro-062111-150444

Cagnan, H., Brittain, J.-S., Little, S., Foltynie, T., Limousin, P., Zrinzo, L., Hariz, M., Joint, C., Fitzgerald, J., Green, A.L., Aziz, T., Brown, P., 2013. Phase dependent modulation of tremor amplitude in essential tremor through thalamic stimulation. Brain 136, 3062–3075. https://doi.org/10.1093/brain/awt239

Cagnan, H., Brown, P., Bourget, D., Denison, T., 2015. Inertial-Based Control System Concepts for the Treatment of Movement Disorders. Int. Solid-State Sensors, Actuators Microsystems Conf. [proceedings]. Int. Conf. Solid-State Sensors, Actuators, Microsystems 18, 70–73. https://doi.org/10.1109/TRANSDUCERS.2015.7180863

Cagnan, H., Little, S., Foltynie, T., Limousin, P., Zrinzo, L., Hariz, M., Cheeran, B., Fitzgerald, J., Green, A.L., Aziz, T., Brown, P., 2014. The nature of tremor circuits in parkinsonian and

essential tremor. Brain 137, 3223–3234. https://doi.org/10.1093/brain/awu250

Cagnan, H., Pedrosa, D., Little, S., Pogosyan, A., Cheeran, B., Aziz, T., Green, A., Fitzgerald, J., Foltynie, T., Limousin, P., Zrinzo, L., Hariz, M., Friston, K.J., Denison, T., Brown, P., 2017. Stimulating at the right time: phase-specific deep brain stimulation. Brain 140, 132–145. https://doi.org/10.1093/brain/aww286

Calabresi, P., Centonze, D., Bernardi, G., 2000. Electrophysiology of dopamine in normal and denervated striatal neurons. Trends Neurosci. 23, S57-63. https://doi.org/10.1016/s1471-1931(00)00017-3

Calabresi, P., Picconi, B., Tozzi, A., Ghiglieri, V., Filippo, M. Di, 2014. review Direct and indirect pathways of basal ganglia : a critical reappraisal. Nat. Publ. Gr. 17. https://doi.org/10.1038/nn.3743

Canolty, R.T., Knight, R.T., 2010. The functional role of cross-frequency coupling. Trends Cogn. Sci. 14, 506–515. https://doi.org/10.1016/j.tics.2010.09.001

Cantero, J.L., Atienza, M., Salas, R.M., 2002. Human alpha oscillations in wakefulness, drowsiness period, and REM sleep: different electroencephalographic phenomena within the alpha band. Neurophysiol. Clin. 32, 54–71. https://doi.org/10.1016/s0987-7053(01)00289-1

Carbon, M., Su, S., Dhawan, V., Raymond, D., Bressman, S., Eidelberg, D., 2004. Regional metabolism in primary torsion dystonia: effects of penetrance and genotype. Neurology 62, 1384–1390. https://doi.org/10.1212/01.wnl.0000120541.97467.fe

Cassidy, M., Mazzone, P., Oliviero, A., Insola, A., Tonali, P., Di Lazzaro, V., Brown, P., 2002. Movement-related changes in synchronization in the human basal ganglia. Brain 125, 1235–1246. https://doi.org/10.1093/brain/awf135

Castelão, M., Marques, R.E., Duarte, G.S., Rodrigues, F.B., Ferreira, J., Sampaio, C., Moore, A.P., Costa, J., 2017. Botulinum toxin type A therapy for cervical dystonia. Cochrane database Syst. Rev. 12, CD003633. https://doi.org/10.1002/14651858.CD003633.pub3

Cenci, M.A., Konradi, C., 2010. Maladaptive striatal plasticity in L-DOPA-induced dyskinesia. Prog. Brain Res. 183, 209–233. https://doi.org/10.1016/S0079-6123(10)83011-0

Chan, J., Brin, M.F., Fahn, S., 1991. Idiopathic cervical dystonia: clinical characteristics. Mov. Disord. 6, 119–126. https://doi.org/10.1002/mds.870060206

Chen, Chiung Chu, Brücke, C., Kempf, F., Kupsch, A., Lu, C.S., Lee, S.T., Tisch, S., Limousin, P., Hariz, M., Brown, P., 2006a. Deep brain stimulation of the subthalamic nucleus: a two-edged sword. Curr. Biol. https://doi.org/10.1016/j.cub.2006.10.013

Chen, Chiung Chu, Brücke, C., Kempf, F., Kupsch, A., Lu, C.S., Lee, S.T., Tisch, S., Limousin, P., Hariz, M., Brown, P., 2006b. Deep brain stimulation of the subthalamic nucleus: a two-edged sword. Curr. Biol. 16, R952–R953. https://doi.org/10.1016/j.cub.2006.10.013

Chen, C C, Kühn, A.A., Hoffmann, K.-T., Kupsch, A., Schneider, G.-H., Trottenberg, T., Krauss, J.K., Wöhrle, J.C., Bardinet, E., Yelnik, J., Brown, P., 2006. Oscillatory pallidal local field

potential activity correlates with involuntary EMG in dystonia. Neurology 66, 418–420. https://doi.org/10.1212/01.wnl.0000196470.00165.7d

Chen, Chiung Chu, Kühn, A.A., Trottenberg, T., Kupsch, A., Schneider, G.-H., Brown, P., 2006c. Neuronal activity in globus pallidus interna can be synchronized to local field potential activity over 3-12 Hz in patients with dystonia. Exp. Neurol. 202, 480–486. https://doi.org/10.1016/j.expneurol.2006.07.011

Chen, Chiung Chu, Pogosyan, A., Zrinzo, L.U., Tisch, S., Limousin, P., Ashkan, K., Yousry, T., Hariz, M.I., Brown, P., 2006d. Intra-operative recordings of local field potentials can help localize the subthalamic nucleus in Parkinson's disease surgery. Exp. Neurol. 198, 214–221. https://doi.org/10.1016/j.expneurol.2005.11.019

Chen, H., Huang, X., Guo, X., Mailman, R.B., Park, Y., Kamel, F., Umbach, D.M., Xu, Q., Hollenbeck, A., Schatzkin, A., Blair, A., 2010. Smoking duration, intensity, and risk of Parkinson disease. Neurology 74, 878–884. https://doi.org/10.1212/WNL.0b013e3181d55f38

Chestek, C.A., Gilja, V., Nuyujukian, P., Foster, J.D., Fan, J.M., Kaufman, M.T., Churchland, M.M., Rivera-Alvidrez, Z., Cunningham, J.P., Ryu, S.I., Shenoy, K. V, 2011. Long-term stability of neural prosthetic control signals from silicon cortical arrays in rhesus macaque motor cortex. J. Neural Eng. 8, 45005. https://doi.org/10.1088/1741-2560/8/4/045005

Cheyne, D., Bells, S., Ferrari, P., Gaetz, W., Bostan, A.C., 2008. Self-paced movements induce high-frequency gamma oscillations in primary motor cortex. Neuroimage 42, 332–342. https://doi.org/10.1016/j.neuroimage.2008.04.178

Cheyne, D., Ferrari, P., 2013. MEG studies of motor cortex gamma oscillations: evidence for a gamma "fingerprint" in the brain? Front. Hum. Neurosci. 7, 575. https://doi.org/10.3389/fnhum.2013.00575

Chiken, S., Nambu, A., 2016. Mechanism of Deep Brain Stimulation: Inhibition, Excitation, or Disruption? Neurosci. a Rev. J. bringing Neurobiol. Neurol. psychiatry 22, 313–322. https://doi.org/10.1177/1073858415581986

Chiken, S., Nambu, A., 2013. High-frequency pallidal stimulation disrupts information flow through the pallidum by GABAergic inhibition. J. Neurosci. 33, 2268–2280. https://doi.org/10.1523/JNEUROSCI.4144-11.2013

Chini, M., Pfeffer, T., Hanganu-Opatz, I., 2022. An increase of inhibition drives the developmental decorrelation of neural activity. Elife 11. https://doi.org/10.7554/eLife.78811

Cif, L., Vasques, X., Gonzalez, V., Ravel, P., Biolsi, B., Collod-Beroud, G., Tuffery-Giraud, S., Elfertit, H., Claustres, M., Coubes, P., 2010. Long-term follow-up of DYT1 dystonia patients treated by deep brain stimulation: an open-label study. Mov. Disord. 25, 289–299. https://doi.org/10.1002/mds.22802

Cohen, M.X., Grafman, J., 2014. Analyzing Neural Time Series Data : Theory and Practice. MIT Press, Cambridge, UNITED STATES.

Colombo, M.A., Napolitani, M., Boly, M., Gosseries, O., Casarotto, S., Rosanova, M., Brichant, J.-F., Boveroux, P., Rex, S., Laureys, S., Massimini, M., Chieregato, A., Sarasso, S., 2019. The spectral exponent of the resting EEG indexes the presence of consciousness during unresponsiveness induced by propofol, xenon, and ketamine. Neuroimage 189, 631–644. https://doi.org/10.1016/j.neuroimage.2019.01.024

Connolly, A.T., Jensen, A.L., Bello, E.M., Netoff, T.I., Baker, K.B., Johnson, M.D., Vitek, J.L., 2015. Modulations in oscillatory frequency and coupling in globus pallidus with increasing parkinsonian severity. J. Neurosci. 35, 6231–6240. https://doi.org/10.1523/JNEUROSCI.4137-14.2015

Connolly, A.T., Vetter, R.J., Hetke, J.F., Teplitzky, B.A., Kipke, D.R., Pellinen, D.S., Anderson, D.J., Baker, K.B., Vitek, J.L., Johnson, M.D., 2016. A Novel Lead Design for Modulation and Sensing of Deep Brain Structures. IEEE Trans. Biomed. Eng. 63, 148–157. https://doi.org/10.1109/TBME.2015.2492921

Cooper, I.S., 1953. Ligation of the anterior choroidal artery for involuntary movements; parkinsonism. Psychiatr. Q. 27, 317–319. https://doi.org/10.1007/BF01562492

Corp, D.T., Joutsa, J., Darby, R.R., Delnooz, C.C.S., van de Warrenburg, B.P.C., Cooke, D., Prudente, C.N., Ren, J., Reich, M.M., Batla, A., Bhatia, K.P., Jinnah, H.A., Liu, H., Fox, M.D., 2019. Network localization of cervical dystonia based on causal brain lesions. Brain 142, 1660–1674. https://doi.org/10.1093/brain/awz112

Corvol, J.-C., Artaud, F., Cormier-Dequaire, F., Rascol, O., Durif, F., Derkinderen, P., Marques, A.-R., Bourdain, F., Brandel, J.-P., Pico, F., Lacomblez, L., Bonnet, C., Brefel-Courbon, C., Ory-Magne, F., Grabli, D., Klebe, S., Mangone, G., You, H., Mesnage, V., Lee, P.-C., Brice, A., Vidailhet, M., Elbaz, A., 2018. Longitudinal analysis of impulse control disorders in Parkinson disease. Neurology 91, e189–e201. https://doi.org/10.1212/WNL.0000000000005816

Crone, N.E., Miglioretti, D.L., Gordon, B., Lesser, R.P., 1998. Functional mapping of human sensorimotor cortex with electrocorticographic spectral analysis. II. Event-related synchronization in the gamma band. Brain 121 (Pt 1, 2301–2315. https://doi.org/10.1093/brain/121.12.2301

Cui, G., Jun, S.B., Jin, X., Pham, M.D., Vogel, S.S., Lovinger, D.M., Costa, R.M., 2013. Concurrent activation of striatal direct and indirect pathways during action initiation. Nature 494, 238–242. https://doi.org/10.1038/nature11846

Danish, S.F., Moyer, J.T., Finkel, L.H., Baltuch, G.H., Jaggi, J.L., Priori, A., Foffani, G., 2007. High-frequency oscillations (>200 Hz) in the human non-parkinsonian subthalamic nucleus. Brain Res. Bull. 74, 84–90. https://doi.org/10.1016/j.brainresbull.2007.05.006

Darcy, N., Lofredi, R., Al-Fatly, B., Neumann, W.-J., Hübl, J., Brücke, C., Krause, P., Schneider, G.-H., Kühn, A., 2022. Spectral and spatial distribution of subthalamic beta peak activity in Parkinson's disease patients. Exp. Neurol. 114150.

https://doi.org/10.1016/j.expneurol.2022.114150

Davis, G.C., Williams, A.C., Markey, S.P., Ebert, M.H., Caine, E.D., Reichert, C.M., Kopin, I.J., 1979. Chronic Parkinsonism secondary to intravenous injection of meperidine analogues. Psychiatry Res. 1, 249–254. https://doi.org/10.1016/0165-1781(79)90006-4

de Bie, R.M.A., de Haan, R.J., Schuurman, P.R., Esselink, R.A.J., Bosch, D.A., Speelman, J.D., 2002. Morbidity and mortality following pallidotomy in Parkinson's disease: a systematic review. Neurology 58, 1008–1012. https://doi.org/10.1212/wnl.58.7.1008

de Hemptinne, C., Swann, N.C., Ostrem, J.L., Ryapolova-Webb, E.S., San Luciano, M., Galifianakis, N.B., Starr, P.A., 2015. Therapeutic deep brain stimulation reduces cortical phase-amplitude coupling in Parkinson's disease. Nat. Neurosci. 18, 779–786. https://doi.org/10.1038/nn.3997

de Hemptinne, C., Wang, D.D., Miocinovic, S., Chen, W., Ostrem, J.L., Starr, P.A., 2019. Pallidal thermolesion unleashes gamma oscillations in the motor cortex in Parkinson's disease. Mov. Disord. 34, 903–911. https://doi.org/10.1002/mds.27658

De Pablo-Fernandez, E., Goldacre, R., Pakpoor, J., Noyce, A.J., Warner, T.T., 2018. Association between diabetes and subsequent Parkinson disease: A record-linkage cohort study. Neurology 91, e139–e142. https://doi.org/10.1212/WNL.0000000000005771

Debarros, J., Gaignon, L., He, S., Pogosyan, A., Benjaber, M., Denison, T., Brown, P., Tan, H., 2020. Artefact-free recording of local field potentials with simultaneous stimulation for closed-loop Deep-Brain Stimulation. Annu. Int. Conf. IEEE Eng. Med. Biol. Soc. IEEE Eng. Med. Biol. Soc. Annu. Int. Conf. 2020, 3367–3370. https://doi.org/10.1109/EMBC44109.2020.9176665

Defazio, G., Hallett, M., Jinnah, H.A., Berardelli, A., 2013. Development and validation of a clinical guideline for diagnosing blepharospasm. Neurology 81, 236–240. https://doi.org/10.1212/WNL.0b013e31829bfdf6

Deffains, M., Iskhakova, L., Bergman, H., 2016. Previews Stop and Think about Basal Ganglia Functional Organization : The Pallido-Striatal '" Stop "' Route 237–239. https://doi.org/10.1016/j.neuron.2016.01.003

Deffains, M., Iskhakova, L., Katabi, S., Israel, Z., Bergman, H., 2018. Longer β oscillatory episodes reliably identify pathological subthalamic activity in Parkinsonism. Mov. Disord. 33, 1609–1618. https://doi.org/10.1002/mds.27418

Degos, B., Deniau, J.-M., Chavez, M., Maurice, N., 2013. Subthalamic nucleus high-frequency stimulation restores altered electrophysiological properties of cortical neurons in parkinsonian rat. PLoS One 8, e83608. https://doi.org/10.1371/journal.pone.0083608

Delaville, C., McCoy, A.J., Gerber, C.M., Cruz, A. V, Walters, J.R., 2015. Subthalamic nucleus activity in the awake hemiparkinsonian rat: relationships with motor and cognitive networks. J. Neurosci. 35, 6918–6930. https://doi.org/10.1523/JNEUROSCI.0587-15.2015

DeLong, M.R., 1990. Primate models of movement disorders of basal ganglia origin. Trends Neurosci. 13, 281–285. https://doi.org/10.1016/0166-2236(90)90110-v

Dembek, T., Asendorf, A., Wirths, J., Barbe, M., Visser-Vandewalle, V., Treuer, H., 2020. Temporal Stability of Lead Orientation in Directional Deep Brain Stimulation.

Dembek, T.A., Hoevels, M., Hellerbach, A., Horn, A., Petry-Schmelzer, J.N., Borggrefe, J., Wirths, J., Dafsari, H.S., Barbe, M.T., Visser-Vandewalle, V., Treuer, H., 2019. Directional DBS leads show large deviations from their intended implantation orientation. Parkinsonism Relat. Disord. 67, 117–121. https://doi.org/10.1016/j.parkreldis.2019.08.017

Deniau, J.-M., Degos, B., Bosch, C., Maurice, N., 2010. Deep brain stimulation mechanisms: beyond the concept of local functional inhibition. Eur. J. Neurosci. 32, 1080–1091. https://doi.org/10.1111/j.1460-9568.2010.07413.x

Denker, A., Rizzoli, S.O., 2010. Synaptic vesicle pools: An update. Front. Synaptic Neurosci. 2, 1–12. https://doi.org/10.3389/fnsyn.2010.00135

Deo, R.C., 2015. Machine Learning in Medicine. Circulation 132, 1920–1930. https://doi.org/10.1161/CIRCULATIONAHA.115.001593

Deuschl, G., Bain, P., Brin, M., 1998. Consensus statement of the Movement Disorder Society on Tremor. Ad Hoc Scientific Committee. Mov. Disord. 13 Suppl 3, 2–23. https://doi.org/10.1002/mds.870131303

Deuschl, G., Herzog, J., Kleiner-Fisman, G., Kubu, C., Lozano, A.M., Lyons, K.E., Rodriguez-Oroz, M.C., Tamma, F., Tröster, A.I., Vitek, J.L., Volkmann, J., Voon, V., 2006. Deep brain stimulation: postoperative issues. Mov. Disord. 21 Suppl 1, S219-37. https://doi.org/10.1002/mds.20957

Donaldson, N.D., Donaldson, P.E., 1986. When are actively balanced biphasic ('Lilly') stimulating pulses necessary in a neurological prosthesis? I. Historical background; Pt resting potential; Q studies. Med. Biol. Eng. Comput. 24, 41–49. https://doi.org/10.1007/BF02441604

Donoghue, T., Haller, M., Peterson, E.J., Varma, P., Sebastian, P., Gao, R., Noto, T., Lara, A.H., Wallis, J.D., Knight, R.T., Shestyuk, A., Voytek, B., 2020. Parameterizing neural power spectra into periodic and aperiodic components. Nat. Neurosci. 23, 1655–1665. https://doi.org/10.1038/s41593-020-00744-x

Dostrovsky, J.O., Levy, R., Wu, J.P., Hutchison, W.D., Tasker, R.R., Lozano, A.M., 2000. Microstimulation-induced inhibition of neuronal firing in human globus pallidus. J. Neurophysiol. 84, 570–574. https://doi.org/10.1152/jn.2000.84.1.570

Duchet, B., Ghezzi, F., Weerasinghe, G., Tinkhauser, G., Kühn, A.A., Brown, P., Bick, C., Bogacz, R., 2021. Average beta burst duration profiles provide a signature of dynamical changes between the ON and OFF medication states in Parkinson's disease. PLoS Comput. Biol. 17, e1009116. https://doi.org/10.1371/journal.pcbi.1009116

Dupre, K.B., Cruz, A. V, McCoy, A.J., Delaville, C., Gerber, C.M., Eyring, K.W., Walters, J.R., 2016. Effects of L-dopa priming on cortical high beta and high gamma oscillatory activity in a rodent model of Parkinson's disease. Neurobiol. Dis. 86, 1–15.

https://doi.org/10.1016/j.nbd.2015.11.009

Eidelberg, D., Moeller, J.R., Antonini, A., Kazumata, K., Nakamura, T., Dhawan, V., Spetsieris, P., deLeon, D., Bressman, S.B., Fahn, S., 1998. Functional brain networks in DYT1 dystonia. Ann. Neurol. 44, 303–312. https://doi.org/10.1002/ana.410440304

Eltahawy, H.A., Saint-Cyr, J., Giladi, N., Lang, A.E., Lozano, A.M., 2004. Primary dystonia is more responsive than secondary dystonia to pallidal interventions: outcome after pallidotomy or pallidal deep brain stimulation. Neurosurgery 54, 613–621. https://doi.org/10.1227/01.neu.0000108643.94730.21

Endo, T., Okuno, R., Yokoe, M., Akazawa, K., Sakoda, S., 2009. A novel method for systematic analysis of rigidity in Parkinson's disease. Mov. Disord. 24, 2218–2224. https://doi.org/10.1002/mds.22752

Escobar Sanabria, D., Johnson, L.A., Nebeck, S.D., Zhang, J., Johnson, M.D., Baker, K.B., Molnar, G.F., Vitek, J.L., 2017. Parkinsonism and vigilance: alteration in neural oscillatory activity and phase-amplitude coupling in the basal ganglia and motor cortex. J. Neurophysiol. 118, 2654–2669. https://doi.org/10.1152/jn.00388.2017

Espay, A.J., Morgante, F., Merola, A., Fasano, A., Marsili, L., Fox, S.H., Bezard, E., Picconi, B., Calabresi, P., Lang, A.E., 2018. Levodopa-induced dyskinesia in Parkinson disease: Current and evolving concepts. Ann. Neurol. 84, 797–811. https://doi.org/10.1002/ana.25364

Etz, A., 2018. Introduction to the Concept of Likelihood and Its Applications. https://doi.org/10.1177/2515245917744314

Eusebio, A., Thevathasan, W., Doyle Gaynor, L., Pogosyan, A., Bye, E., Foltynie, T., Zrinzo, L., Ashkan, K., Aziz, T., Brown, P., 2011a. Deep brain stimulation can suppress pathological synchronisation in parkinsonian patients. J. Neurol. Neurosurg. Psychiatry 82, 569–573. https://doi.org/10.1136/jnnp.2010.217489

Eusebio, A., Thevathasan, W., Doyle Gaynor, L., Pogosyan, A., Bye, E., Foltynie, T., Zrinzo, L., Ashkan, K., Aziz, T., Brown, P., 2011b. Deep brain stimulation can suppress pathological synchronisation in parkinsonian patients. J. Neurol. Neurosurg. Psychiatry 82, 569–573. https://doi.org/10.1136/jnnp.2010.217489

Fasano, A., Aquino, C.C., Krauss, J.K., Honey, C.R., Bloem, B.R., 2015. Axial disability and deep brain stimulation in patients with Parkinson disease. Nat. Rev. Neurol. 11, 98–110. https://doi.org/10.1038/nrneurol.2014.252

Feany, M.B., 2004. New genetic insights into Parkinson's disease. N. Engl. J. Med. 351, 1937–1940. https://doi.org/10.1056/NEJMp048263

Feldman, R.P., Goodrich, J.T., 2001. Psychosurgery: a historical overview. Neurosurgery 48, 647–649. https://doi.org/10.1097/00006123-200103000-00041

Fénelon, G., Mahieux, F., Huon, R., Ziégler, M., 2000. Hallucinations in Parkinson's disease: prevalence, phenomenology and risk factors. Brain 123 (Pt 4, 733–745.

https://doi.org/10.1093/brain/123.4.733

Ferguson, M.A., Lim, C., Cooke, D., Darby, R.R., Wu, O., Rost, N.S., Corbetta, M., Grafman, J., Fox, M.D., 2019. A human memory circuit derived from brain lesions causing amnesia. Nat. Commun. 10, 3497. https://doi.org/10.1038/s41467-019-11353-z

Ferrier, D., 1874. On the Localisation of the Functions of the Brain. Br. Med. J. 2, 766–767. https://doi.org/10.1136/bmj.2.729.766

Filali, M., Hutchison, W.D., Palter, V.N., Lozano, A.M., Dostrovsky, J.O., 2004. Stimulation-induced inhibition of neuronal firing in human subthalamic nucleus. Exp. brain Res. 156, 274–281. https://doi.org/10.1007/s00221-003-1784-y

Findley, L.J., Gresty, M.A., Halmagyi, G.M., 1981. Tremor, the cogwheel phenomenon and clonus in Parkinson's disease. J. Neurol. Neurosurg. Psychiatry 44, 534–546. https://doi.org/10.1136/jnnp.44.6.534

Fischer, M., Gemende, I., Marsch, W.C., Fischer, P.A., 2001. Skin function and skin disorders in Parkinson's disease. J. Neural Transm. 108, 205–213. https://doi.org/10.1007/s007020170088

Fischer, P., 2021. Mechanisms of network interactions for flexible cortico-basal ganglia-mediated action control. eNeuro 8. https://doi.org/10.1523/ENEURO.0009-21.2021

Fischer, P., Pogosyan, A., Herz, D.M., Cheeran, B., Green, A.L., Fitzgerald, J., Aziz, T.Z., Hyam, J., Little, S., Foltynie, T., Limousin, P., Zrinzo, L., Brown, P., Tan, H., 2017. Subthalamic nucleus gamma activity increases not only during movement but also during movement inhibition. Elife 6. https://doi.org/10.7554/eLife.23947

Fisher, R., Salanova, V., Witt, T., Worth, R., Henry, T., Gross, R., Oommen, K., Osorio, I., Nazzaro, J., Labar, D., Kaplitt, M., Sperling, M., Sandok, E., Neal, J., Handforth, A., Stern, J., DeSalles, A., Chung, S., Shetter, A., Bergen, D., Bakay, R., Henderson, J., French, J., Baltuch, G., Rosenfeld, W., Youkilis, A., Marks, W., Garcia, P., Barbaro, N., Fountain, N., Bazil, C., Goodman, R., McKhann, G., Babu Krishnamurthy, K., Papavassiliou, S., Epstein, C., Pollard, J., Tonder, L., Grebin, J., Coffey, R., Graves, N., 2010. Electrical stimulation of the anterior nucleus of thalamus for treatment of refractory epilepsy. Epilepsia 51, 899–908. https://doi.org/10.1111/j.1528-1167.2010.02536.x

Foffani, G., Ardolino, G., Egidi, M., Caputo, E., Bossi, B., Priori, A., 2006. Subthalamic oscillatory activities at beta or higher frequency do not change after high-frequency DBS in Parkinson's disease. Brain Res. Bull. 69, 123–130. https://doi.org/10.1016/j.brainresbull.2005.11.012

Foffani, G., Bianchi, A.M., Baselli, G., Priori, A., 2005. Movement-related frequency modulation of beta oscillatory activity in the human subthalamic nucleus. J. Physiol. 568, 699–711. https://doi.org/10.1113/jphysiol.2005.089722

Foffani, G., Priori, A., Egidi, M., Rampini, P., Tamma, F., Caputo, E., Moxon, K.A., Cerutti, S., Barbieri, S., 2003. 300-Hz subthalamic oscillations in Parkinson's disease. Brain 126, 2153–2163. https://doi.org/10.1093/brain/awg229

Fogelson, N., Pogosyan, A., Kühn, A.A., Kupsch, A., van Bruggen, G., Speelman, H., Tijssen, M., Quartarone, A., Insola, A., Mazzone, P., Di Lazzaro, V., Limousin, P., Brown, P., 2005. Reciprocal interactions between oscillatory activities of different frequencies in the subthalamic region of patients with Parkinson's disease. Eur. J. Neurosci. 22, 257–266. https://doi.org/10.1111/j.1460-9568.2005.04179.x

Fogelson, N., Williams, D., Tijssen, M., van Bruggen, G., Speelman, H., Brown, P., 2006. Different functional loops between cerebral cortex and the subthalmic area in Parkinson's disease. Cereb. Cortex 16, 64–75. https://doi.org/10.1093/cercor/bhi084

Follett, K.A., Weaver, F.M., Stern, M., Hur, K., Harris, C.L., Luo, P., Marks, W.J.J., Rothlind, J., Sagher, O., Moy, C., Pahwa, R., Burchiel, K., Hogarth, P., Lai, E.C., Duda, J.E., Holloway, K., Samii, A., Horn, S., Bronstein, J.M., Stoner, G., Starr, P.A., Simpson, R., Baltuch, G., De Salles, A., Huang, G.D., Reda, D.J., 2010. Pallidal versus subthalamic deep-brain stimulation for Parkinson's disease. N. Engl. J. Med. 362, 2077–2091. https://doi.org/10.1056/NEJMoa0907083

Foltynie, T., Hariz, M.I., 2010. Surgical management of Parkinson's disease. Expert Rev. Neurother. 10, 903–914. https://doi.org/10.1586/ern.10.68

Fox, M.D., 2018. Mapping Symptoms to Brain Networks with the Human Connectome. N. Engl. J. Med. 379, 2237–2245. https://doi.org/10.1056/NEJMra1706158

Freedman, D., Diaconis, P., 1981. On the histogram as a density estimator:L2 theory. Zeitschrift für Wahrscheinlichkeitstheorie und Verwandte Gebiete 57, 453–476. https://doi.org/10.1007/BF01025868

Fries, P., 2015. Rhythms for Cognition: Communication through Coherence. Neuron 88, 220–235. https://doi.org/10.1016/j.neuron.2015.09.034

Fujimoto, K., Kita, H., 1993. Response characteristics of subthalamic neurons to the stimulation of the sensorimotor cortex in the rat. Brain Res. 609, 185–192. https://doi.org/10.1016/0006-8993(93)90872-k

Galati, S., Mazzone, P., Fedele, E., Pisani, A., Peppe, A., Pierantozzi, M., Brusa, L., Tropepi, D., Moschella, V., Raiteri, M., Stanzione, P., Bernardi, G., Stefani, A., 2006. Biochemical and electrophysiological changes of substantia nigra pars reticulata driven by subthalamic stimulation in patients with Parkinson's disease. Eur. J. Neurosci. 23, 2923–2928. https://doi.org/10.1111/j.1460-9568.2006.04816.x

Galvan, A., Hu, X., Rommelfanger, K.S., Pare, J.-F., Khan, Z.U., Smith, Y., Wichmann, T., 2014. Localization and function of dopamine receptors in the subthalamic nucleus of normal and parkinsonian monkeys. J. Neurophysiol. 112, 467–479. https://doi.org/10.1152/jn.00849.2013

Gao, R., Peterson, E.J., Voytek, B., 2017. Inferring synaptic excitation/inhibition balance from field potentials. Neuroimage 158, 70–78. https://doi.org/10.1016/j.neuroimage.2017.06.078

Geng, X., Zhang, J., Jiang, Y., Ashkan, K., Foltynie, T., Limousin, P., Zrinzo, L., Green, A., Aziz, T., Brown, P., Wang, S., 2017. Comparison of oscillatory activity in subthalamic nucleus in

Parkinson's disease and dystonia. Neurobiol. Dis. 98, 100–107. https://doi.org/10.1016/j.nbd.2016.12.006

German, D.C., Schlusselberg, D.S., Woodward, D.J., 1983. Three-dimensional computer reconstruction of midbrain dopaminergic neuronal populations: from mouse to man. J. Neural Transm. 57, 243–254. https://doi.org/10.1007/bf01248996

Gerster, M., Waterstraat, G., Litvak, V., Lehnertz, K., Schnitzler, A., Florin, E., Curio, G., Nikulin, V., 2022. Separating Neural Oscillations from Aperiodic 1/f Activity: Challenges and Recommendations. Neuroinformatics. https://doi.org/10.1007/s12021-022-09581-8

Ghanouni, P., Pauly, K.B., Elias, W.J., Henderson, J., Sheehan, J., Monteith, S., Wintermark, M., 2015. Transcranial MRI-Guided Focused Ultrasound: A Review of the Technologic and Neurologic Applications. AJR. Am. J. Roentgenol. 205, 150–159. https://doi.org/10.2214/AJR.14.13632

Giannicola, G., Marceglia, S., Rossi, L., Mrakic-Sposta, S., Rampini, P., Tamma, F., Cogiamanian, F., Barbieri, S., Priori, A., 2010. The effects of levodopa and ongoing deep brain stimulation on subthalamic beta oscillations in Parkinson's disease. Exp. Neurol. 226, 120–127. https://doi.org/10.1016/j.expneurol.2010.08.011

Giannicola, G., Rosa, M., Servello, D., Menghetti, C., Carrabba, G., Pacchetti, C., Zangaglia, R., Cogiamanian, F., Scelzo, E., Marceglia, S., Rossi, L., Priori, A., 2012. Subthalamic local field potentials after seven-year deep brain stimulation in Parkinson's disease. Exp. Neurol. 237, 312–317. https://doi.org/10.1016/j.expneurol.2012.06.012

Gilron, R., Little, S., Perrone, R., Wilt, R., de Hemptinne, C., Yaroshinsky, M.S., Racine, C.A., Wang, S.S., Ostrem, J.L., Larson, P.S., Wang, D.D., Galifianakis, N.B., Bledsoe, I.O., San Luciano, M., Dawes, H.E., Worrell, G.A., Kremen, V., Borton, D.A., Denison, T., Starr, P.A., 2021. Long-term wireless streaming of neural recordings for circuit discovery and adaptive stimulation in individuals with Parkinson's disease. Nat. Biotechnol. https://doi.org/10.1038/s41587-021-00897-5

Giovannoni, G., Van Schalkwyk, J., Fritz, V.U., Lees, A.J., 1999. Bradykinesia akinesia inco-ordination test (BRAIN TEST): An objective computerised assessment of upper limb motor function. J. Neurol. Neurosurg. Psychiatry 67, 624–629. https://doi.org/10.1136/jnnp.67.5.624

Global, regional, and national burden of Parkinson's disease, 1990-2016: a systematic analysis for the Global Burden of Disease Study 2016., 2018. . Lancet. Neurol. 17, 939–953. https://doi.org/10.1016/S1474-4422(18)30295-3

Gmel, G.E., Hamilton, T.J., Obradovic, M., Gorman, R.B., Single, P.S., Chenery, H.J., Coyne, T., Silburn, P.A., Parker, J.L., 2015. A new biomarker for subthalamic deep brain stimulation for patients with advanced Parkinson's disease--a pilot study. J. Neural Eng. 12, 66013. https://doi.org/10.1088/1741-2560/12/6/066013

Goedert, M., Spillantini, M.G., Del Tredici, K., Braak, H., 2013. 100 years of Lewy pathology. Nat.

Rev. Neurol. 9, 13–24. https://doi.org/10.1038/nrneurol.2012.242

Goetz, C.G., Tilley, B.C., Shaftman, S.R., Stebbins, G.T., Fahn, S., Martinez-Martin, P., Poewe, W., Sampaio, C., Stern, M.B., Dodel, R., Dubois, B., Holloway, R., Jankovic, J., Kulisevsky, J., Lang, A.E., Lees, A., Leurgans, S., LeWitt, P.A., Nyenhuis, D., Olanow, C.W., Rascol, O., Schrag, A., Teresi, J.A., van Hilten, J.J., LaPelle, N., 2008. Movement Disorder Society-sponsored revision of the Unified Parkinson's Disease Rating Scale (MDS-UPDRS): scale presentation and clinimetric testing results. Mov. Disord. 23, 2129–2170. https://doi.org/10.1002/mds.22340

Grahn, P.J., Mallory, G.W., Khurram, O.U., Berry, B.M., Hachmann, J.T., Bieber, A.J., Bennet, K.E., Min, H.-K., Chang, S.-Y., Lee, K.H., Lujan, J.L., 2014. A neurochemical closed-loop controller for deep brain stimulation: toward individualized smart neuromodulation therapies. Front. Neurosci. 8, 169. https://doi.org/10.3389/fnins.2014.00169

Graupe, D., Basu, I., Tuninetti, D., Vannemreddy, P., Slavin, K. V, 2010. Adaptively controlling deep brain stimulation in essential tremor patient via surface electromyography. Neurol. Res. 32, 899–904. https://doi.org/10.1179/016164110X12767786356354

Greene, P., Kang, U.J., Fahn, S., 1995. Spread of symptoms in idiopathic torsion dystonia. Mov. Disord. 10, 143–152. https://doi.org/10.1002/mds.870100204

Greene, P., Shale, H., Fahn, S., 1988. Experience with high dosages of anticholinergic and other drugs in the treatment of torsion dystonia. Adv. Neurol. 50, 547–556.

Greene, P.E., Bressman, S., 1998. Exteroceptive and interoceptive stimuli in dystonia. Mov. Disord. 13, 549–551. https://doi.org/10.1002/mds.870130329

Groppe, D., 2022a. mult_comp_perm_t1(data,n_perm,tail,alpha_level,mu,reports,seed_state) [WWW Document]. MATLAB Cent. File Exch. URL https://uk.mathworks.com/matlabcentral/fileexchange/29782-mult_comp_perm_t1-data-n_perm-tail-alpha_level-mu-reports-seed_state

Groppe, D., 2022b. mult_comp_perm_t1(data,n_perm,tail,alpha_level,mu,reports,seed_state) [WWW Document]. MATLAB Cent. File Exch. URL https://www.mathworks.com/matlabcentral/fileexchange/29782-mult_comp_perm_t1-data-n_perm-tail-alpha_level-mu-reports-seed_state (accessed 11.8.22).

Gross, D.W., Gotman, J., 1999. Correlation of high-frequency oscillations with the sleep-wake cycle and cognitive activity in humans. Neuroscience 94, 1005–1018. https://doi.org/10.1016/s0306-4522(99)00343-7

Gross, R.E., Stern, M.A., 2018. Magnetic resonance-guided stereotactic laser pallidotomy for dystonia. Mov. Disord. https://doi.org/10.1002/mds.27400

Gustafsson, H., Nordström, A., Nordström, P., 2015. Depression and subsequent risk of Parkinson disease: A nationwide cohort study. Neurology 84, 2422–2429. https://doi.org/10.1212/WNL.0000000000001684

Güttler, C., Altschüler, J., Tanev, K., Böckmann, S., Haumesser, J.K., Nikulin, V. V, Kühn, A.A., van Riesen, C., 2020. Levodopa-Induced Dyskinesia Are Mediated by Cortical Gamma Oscillations in Experimental Parkinsonism. Mov. Disord. https://doi.org/10.1002/mds.28403

Haider, B., Schulz, D.P.A., Häusser, M., Carandini, M., 2016. Millisecond Coupling of Local Field Potentials to Synaptic Currents in the Awake Visual Cortex. Neuron 90, 35–42. https://doi.org/10.1016/j.neuron.2016.02.034

Halgren, M., Kang, R., Voytek, B., Ulbert, I., Fabo, D., Eross, L., Wittner, L., Madsen, J., Doyle, W.K., Devinsky, O., Halgren, E., Harnett, M.T., Cash, S.S., 2021. The timescale and magnitude of 1/f aperiodic activity decrease with cortical depth in humans, macaques, and mice. bioRxiv. https://doi.org/10.1101/2021.07.28.454235

Halje, P., Tamtè, M., Richter, U., Mohammed, M., Cenci, M.A., Petersson, P., 2012. Levodopa-induced dyskinesia is strongly associated with resonant cortical oscillations. J. Neurosci. 32, 16541–16551. https://doi.org/10.1523/JNEUROSCI.3047-12.2012

Hallett, M., 2006. Pathophysiology of writer's cramp. Hum. Mov. Sci. 25, 454–463. https://doi.org/10.1016/j.humov.2006.05.004

Halliday, D.M., Rosenberg, J.R., Amjad, A.M., Breeze, P., Conway, B.A., Farmer, S.F., 1995. A framework for the analysis of mixed time series/point process data--theory and application to the study of physiological tremor, single motor unit discharges and electromyograms. Prog. Biophys. Mol. Biol. 64, 237–278. https://doi.org/10.1016/s0079-6107(96)00009-0

Hammond, C., Ammari, R., Bioulac, B., Garcia, L., 2008. Latest view on the mechanism of action of deep brain stimulation. Mov. Disord. 23, 2111–2121. https://doi.org/10.1002/mds.22120

Harlow, J.M., 1993. Recovery from the passage of an iron bar through the head. Hist. Psychiatry 4, 274–281. https://doi.org/10.1177/0957154X9300401407

Hashimoto, T., Elder, C.M., Okun, M.S., Patrick, S.K., Vitek, J.L., 2003. Stimulation of the subthalamic nucleus changes the firing pattern of pallidal neurons. J. Neurosci. 23, 1916–1923. https://doi.org/10.1523/JNEUROSCI.23-05-01916.2003

Hassler, R., 1959. "Anatomy of the Thalamus," in Introduction to Stereotaxic Operations With an Atlas of the Human Brain, eds G. Schaltenbrand and P. Bailey. Stuttgart; New York, NY: Georg Thieme Verlag, pp. 230–290.

Hauptmann, C., Tass, P.A., 2007. Therapeutic rewiring by means of desynchronizing brain stimulation. Biosystems. 89, 173–181. https://doi.org/10.1016/j.biosystems.2006.04.015

He, B.J., 2014. Scale-free brain activity: past, present, and future. Trends Cogn. Sci. 18, 480–487. https://doi.org/10.1016/j.tics.2014.04.003

He, B.J., Zempel, J.M., Snyder, A.Z., Raichle, M.E., 2010. The temporal structures and functional significance of scale-free brain activity. Neuron 66, 353–369. https://doi.org/10.1016/j.neuron.2010.04.020

He, S., Baig, F., Merla, A., Torrecillos, F., Perera, A., Wiest, C., Debarros, J., Benjaber, M., Hart,

M.G., Morgante, F., Hasegawa, H., Samuel, M., Edwards, M., Denison, T., Pogosyan, A., Ashkan, K., Pereira, E., Tan, H., 2022. Beta-triggered adaptive deep brain stimulation during reaching movement in Parkinson's disease. medRxiv 2022.12.20.22283430. https://doi.org/10.1101/2022.12.20.22283430

He, S., Baig, F., Mostofi, A., Pogosyan, A., Debarros, J., Green, A.L., Aziz, T.Z., Pereira, E., Brown, P., Tan, H., 2021. Closed-Loop Deep Brain Stimulation for Essential Tremor Based on Thalamic Local Field Potentials. Mov. Disord. 36, 863–873. https://doi.org/10.1002/mds.28513

He, W., Donoghue, T., Sowman, P.F., Seymour, R.A., Brock, J., Crain, S., Voytek, B., Hillebrand, A., 2019. Co-Increasing Neuronal Noise and Beta Power in the Developing Brain. bioRxiv. https://doi.org/10.1101/839258

Herrington, T.M., Cheng, J.J., Eskandar, E.N., 2016. Mechanisms of deep brain stimulation. J. Neurophysiol. 115, 19–38. https://doi.org/10.1152/jn.00281.2015

Herron, J., Chizeck, H.J., 2014. Prototype closed-loop deep brain stimulation systems inspired by Norbert Wiener, in: 2014 IEEE Conference on Norbert Wiener in the 21st Century (21CW). pp. 1–6. https://doi.org/10.1109/NORBERT.2014.6893922

Herz, D.M., Little, S., Pedrosa, D.J., Tinkhauser, G., Cheeran, B., Foltynie, T., Bogacz, R., Brown, P., 2018. Mechanisms Underlying Decision-Making as Revealed by Deep-Brain Stimulation in Patients with Parkinson's Disease. Curr. Biol. 28, 1169-1178.e6. https://doi.org/10.1016/j.cub.2018.02.057

Herzog, J., Pinsker, M., Wasner, M., Steigerwald, F., Wailke, S., Deuschl, G., Volkmann, J., 2007. Stimulation of subthalamic fibre tracts reduces dyskinesias in STN-DBS. Mov. Disord. 22, 679–684. https://doi.org/10.1002/mds.21387

Hirsch, E.C., Hunot, S., 2009. Neuroinflammation in Parkinson's disease: a target for neuroprotection? Lancet. Neurol. 8, 382–397. https://doi.org/10.1016/S1474-4422(09)70062-6

Hirschmann, J., Butz, M., Hartmann, C.J., Hoogenboom, N., Özkurt, T.E., Vesper, J., Wojtecki, L., Schnitzler, A., 2016. Parkinsonian Rest Tremor Is Associated With Modulations of Subthalamic High-Frequency Oscillations. Mov. Disord. 31, 1551–1559. https://doi.org/10.1002/mds.26663

Hochberg, L.R., Bacher, D., Jarosiewicz, B., Masse, N.Y., Simeral, J.D., Vogel, J., Haddadin, S., Liu, J., Cash, S.S., van der Smagt, P., Donoghue, J.P., 2012. Reach and grasp by people with tetraplegia using a neurally controlled robotic arm. Nature 485, 372–375. https://doi.org/10.1038/nature11076

Hoehn, M.M., Yahr, M.D., 1967. Parkinsonism: onset, progression and mortality. Neurology 17, 427–442. https://doi.org/10.1212/wnl.17.5.427

Holt, A.B., Kormann, E., Gulberti, A., Pötter-Nerger, M., McNamara, C.G., Cagnan, H., Baaske, M.K., Little, S., Köppen, J.A., Buhmann, C., Westphal, M., Gerloff, C., Engel, A.K., Brown, P., Hamel, W., Moll, C.K.E., Sharott, A., 2019. Phase-Dependent Suppression of Beta Oscillations in Parkinson's Disease Patients. J. Neurosci. 39, 1119–1134.

https://doi.org/10.1523/JNEUROSCI.1913-18.2018

Horn, A., Li, N., Dembek, T.A., Kappel, A., Boulay, C., Ewert, S., Tietze, A., Husch, A., Perera, T., Neumann, W.-J., Reisert, M., Si, H., Oostenveld, R., Rorden, C., Yeh, F.-C., Fang, Q., Herrington, T.M., Vorwerk, J., Kühn, A.A., 2019. Lead-DBS v2: Towards a comprehensive pipeline for deep brain stimulation imaging. Neuroimage 184, 293–316. https://doi.org/10.1016/j.neuroimage.2018.08.068

Horn, A., Neumann, W.-J., Degen, K., Schneider, G.-H., Kühn, A.A., 2017a. Toward an electrophysiological "sweet spot" for deep brain stimulation in the subthalamic nucleus. Hum. Brain Mapp. 38, 3377–3390. https://doi.org/10.1002/hbm.23594

Horn, A., Reich, M., Vorwerk, J., Li, N., Wenzel, G., Fang, Q., Schmitz-Hübsch, T., Nickl, R., Kupsch, A., Volkmann, J., Kühn, A.A., Fox, M.D., 2017b. Connectivity Predicts deep brain stimulation outcome in Parkinson disease. Ann. Neurol. 82, 67–78. https://doi.org/10.1002/ana.24974

Hornykiewicz, O., 2006. The discovery of dopamine deficiency in the parkinsonian brain. J. Neural Transm. Suppl. 9–15. https://doi.org/10.1007/978-3-211-45295-0_3

Horsley, V., Clarke, R.H., 1908. THE STRUCTURE AND FUNCTIONS OF THE CEREBELLUM EXAMINED BY A NEW METHOD. Brain 31, 45–124. https://doi.org/10.1093/brain/31.1.45

Huang, Y., Hu, K., Green, A.L., Ma, X., Gillies, M.J., Wang, S., Fitzgerald, J.J., Pan, Y., Martin, S., Huang, P., Zhan, S., Li, D., Tan, H., Aziz, T.Z., Sun, B., 2020. Dynamic changes in rhythmic and arrhythmic neural signatures in the subthalamic nucleus induced by anaesthesia and tracheal intubation. Br. J. Anaesth. 125, 67–76. https://doi.org/10.1016/j.bja.2020.03.014

Huebl, J., Brücke, C., Schneider, G.-H., Blahak, C., Krauss, J.K., Kühn, A.A., 2015. Bradykinesia induced by frequency-specific pallidal stimulation in patients with cervical and segmental dystonia. Parkinsonism Relat. Disord. 21, 800–803. https://doi.org/10.1016/j.parkreldis.2015.04.023

Hughes, A.J., Daniel, S.E., Kilford, L., Lees, A.J., 1992. Accuracy of clinical diagnosis of idiopathic Parkinson's disease: a clinico-pathological study of 100 cases. J. Neurol. Neurosurg. Psychiatry 55, 181–184. https://doi.org/10.1136/jnnp.55.3.181

Huot, P., Parent, A., 2007. Dopaminergic neurons intrinsic to the striatum. J. Neurochem. 101, 1441–1447. https://doi.org/10.1111/j.1471-4159.2006.04430.x

Ince, N.F., Gupte, A., Wichmann, T., Ashe, J., Henry, T., Bebler, M., Eberly, L., Abosch, A., 2010. Selection of optimal programming contacts based on local field potential recordings from subthalamic nucleus in patients with Parkinson's disease. Neurosurgery 67, 390–397. https://doi.org/10.1227/01.NEU.0000372091.64824.63

Iturrate, I., Martin, S., Chavarriaga, R., Orset, B., Leeb, R., Sobolewski, A., Pralong, E., Castro-Jiménez, M., Benninger, D., Bloch, J., Millán, J. del R., 2019. Beta-driven closed-loop deep brain stimulation can compromise human motor behavior in Parkinson's Disease. bioRxiv

696385. https://doi.org/10.1101/696385

Jafari, S., Etminan, M., Aminzadeh, F., Samii, A., 2013. Head injury and risk of Parkinson disease: a systematic review and meta-analysis. Mov. Disord. 28, 1222–1229. https://doi.org/10.1002/mds.25458

Jankovic, J., Beach, J., 1997. Long-term effects of tetrabenazine in hyperkinetic movement disorders. Neurology 48, 358–362. https://doi.org/10.1212/wnl.48.2.358

Jarosiewicz, B., Sarma, A.A., Bacher, D., Masse, N.Y., Simeral, J.D., Sorice, B., Oakley, E.M., Blabe, C., Pandarinath, C., Gilja, V., Cash, S.S., Eskandar, E.N., Friehs, G., Henderson, J.M., Shenoy, K. V, Donoghue, J.P., Hochberg, L.R., 2015. Virtual typing by people with tetraplegia using a self-calibrating intracortical brain-computer interface. Sci. Transl. Med. 7, 313ra179. https://doi.org/10.1126/scitranslmed.aac7328

Javidan, M., Elek, J., Prochazka, A., 1992. Attenuation of pathological tremors by functional electrical stimulation. II: Clinical evaluation. Ann. Biomed. Eng. 20, 225–236. https://doi.org/10.1007/BF02368522

Jenkinson, N., Kühn, A.A., Brown, P., 2013. γ oscillations in the human basal ganglia. Exp. Neurol. 245, 72–76. https://doi.org/10.1016/j.expneurol.2012.07.005

Jiang, W., Ju, C., Jiang, H., Zhang, D., 2014. Dairy foods intake and risk of Parkinson's disease: a dose-response meta-analysis of prospective cohort studies. Eur. J. Epidemiol. 29, 613–619. https://doi.org/10.1007/s10654-014-9921-4

Jobbágy, A., Harcos, P., Karoly, R., Fazekas, G., 2005. Analysis of finger-tapping movement. J. Neurosci. Methods 141, 29–39. https://doi.org/10.1016/j.jneumeth.2004.05.009

Jobst, B.C., Darcey, T.M., Thadani, V.M., Roberts, D.W., 2010. Brain stimulation for the treatment of epilepsy. Epilepsia 51 Suppl 3, 88–92. https://doi.org/10.1111/j.1528-1167.2010.02618.x

Johnson, L.A., Nebeck, S.D., Muralidharan, A., Johnson, M.D., Baker, K.B., Vitek, J.L., 2016. Closed-Loop Deep Brain Stimulation Effects on Parkinsonian Motor Symptoms in a Non-Human Primate - Is Beta Enough? Brain Stimul. 9, 892–896. https://doi.org/10.1016/j.brs.2016.06.051

Johnson, L.A., Wang, J., Nebeck, S.D., Zhang, J., Johnson, M.D., Vitek, J.L., 2020. Direct activation of primary motor cortex during subthalamic but not pallidal deep brain stimulation. J. Neurosci. 40, 2480–19. https://doi.org/10.1523/jneurosci.2480-19.2020

Johnson, M.D., McIntyre, C.C., 2008. Quantifying the neural elements activated and inhibited by globus pallidus deep brain stimulation. J. Neurophysiol. 100, 2549–2563. https://doi.org/10.1152/jn.90372.2008

Joundi, R.A., Brittain, J.-S., Green, A.L., Aziz, T.Z., Brown, P., Jenkinson, N., 2013. Persistent suppression of subthalamic beta-band activity during rhythmic finger tapping in Parkinson's disease. Clin. Neurophysiol. Off. J. Int. Fed. Clin. Neurophysiol. 124, 565–573. https://doi.org/10.1016/j.clinph.2012.07.029

Joundi, R.A., Brittain, J.-S., Green, A.L., Aziz, T.Z., Brown, P., Jenkinson, N., 2012. Oscillatory activity in the subthalamic nucleus during arm reaching in Parkinson's disease. Exp. Neurol. 236, 319–326. https://doi.org/10.1016/j.expneurol.2012.05.013

Katzenschlager, R., Evans, A., Manson, A., Patsalos, P.N., Ratnaraj, N., Watt, H., Timmermann, L., Van der Giessen, R., Lees, A.J., 2004. Mucuna pruriens in Parkinson's disease: a double blind clinical and pharmacological study. J. Neurol. Neurosurg. Psychiatry 75, 1672–1677. https://doi.org/10.1136/jnnp.2003.028761

Katzenschlager, R., Poewe, W., Rascol, O., Trenkwalder, C., Deuschl, G., Chaudhuri, K.R., Henriksen, T., van Laar, T., Spivey, K., Vel, S., Staines, H., Lees, A., 2018. Apomorphine subcutaneous infusion in patients with Parkinson's disease with persistent motor fluctuations (TOLEDO): a multicentre, double-blind, randomised, placebo-controlled trial. Lancet. Neurol. 17, 749–759. https://doi.org/10.1016/S1474-4422(18)30239-4

Kempf, F., Brücke, C., Salih, F., Trottenberg, T., Kupsch, A., Schneider, G.-H., Doyle Gaynor, L.M.F., Hoffmann, K.-T., Vesper, J., Wöhrle, J., Altenmüller, D.-M., Krauss, J.K., Mazzone, P., Di Lazzaro, V., Yelnik, J., Kühn, A.A., Brown, P., 2009. Gamma activity and reactivity in human thalamic local field potentials. Eur. J. Neurosci. 29, 943–953. https://doi.org/10.1111/j.1460-9568.2009.06655.x

Kent, A.R., Grill, W.M., 2013. Neural origin of evoked potentials during thalamic deep brain stimulation. J. Neurophysiol. 110, 826–843. https://doi.org/10.1152/jn.00074.2013

Kent, A.R., Grill, W.M., 2012. Recording evoked potentials during deep brain stimulation: development and validation of instrumentation to suppress the stimulus artefact. J. Neural Eng. 9, 36004. https://doi.org/10.1088/1741-2560/9/3/036004

Kerr, P.B., Caputy, A.J., Horwitz, N.H., 2005. A history of cerebral localization. Neurosurg. Focus 18, e1. https://doi.org/10.3171/foc.2005.18.4.2

Khawaldeh, S., Tinkhauser, G., Shah, S.A., Peterman, K., Debove, I., Nguyen, T.A.K., Nowacki, A., Lachenmayer, M.L., Schuepbach, M., Pollo, C., Krack, P., Woolrich, M., Brown, P., 2020. Subthalamic nucleus activity dynamics and limb movement prediction in Parkinson's disease. Brain 143, 582–596. https://doi.org/10.1093/brain/awz417

Kilpatrick, M., Church, E., Danish, S., Stiefel, M., Jaggi, J., Halpern, C., Kerr, M., Maloney, E., Robinson, M., Lucki, I., Krizman-Grenda, E., Baltuch, G., 2010. Intracerebral microdialysis during deep brain stimulation surgery. J. Neurosci. Methods 190, 106–111. https://doi.org/10.1016/j.jneumeth.2010.04.013

Kim, J.-W., Lee, J.-H., Kwon, Y., Kim, C.-S., Eom, G.-M., Koh, S.-B., Kwon, D.-Y., Park, K.-W., 2011. Quantification of bradykinesia during clinical finger taps using a gyrosensor in patients with Parkinson's disease. Med. Biol. Eng. Comput. 49, 365–371. https://doi.org/10.1007/s11517-010-0697-8

Kim, J., Lee, J., Kim, E., Choi, J.H., Rah, J.-C., Choi, J.-W., 2022. Dopamine depletion can be

predicted by the aperiodic component of subthalamic local field potentials. Neurobiol. Dis. 168, 105692. https://doi.org/10.1016/j.nbd.2022.105692

Kishida, K.T., Sandberg, S.G., Lohrenz, T., Comair, Y.G., Sáez, I., Phillips, P.E.M., Montague, P.R., 2011. Sub-second dopamine detection in human striatum. PLoS One 6, e23291. https://doi.org/10.1371/journal.pone.0023291

Kiss, Z.H.T., Doig-Beyaert, K., Eliasziw, M., Tsui, J., Haffenden, A., Suchowersky, O., 2007. The Canadian multicentre study of deep brain stimulation for cervical dystonia. Brain 130, 2879–2886. https://doi.org/10.1093/brain/awm229

Kita, T., Shigematsu, N., Kita, H., 2016. Intralaminar and tectal projections to the subthalamus in the rat. Eur. J. Neurosci. 44, 2899–2908. https://doi.org/10.1111/ejn.13413

Kleiner-Fisman, G., Liang, G.S.L., Moberg, P.J., Ruocco, A.C., Hurtig, H.I., Baltuch, G.H., Jaggi, J.L., Stern, M.B., 2007. Subthalamic nucleus deep brain stimulation for severe idiopathic dystonia: impact on severity, neuropsychological status, and quality of life. J. Neurosurg. 107, 29–36. https://doi.org/10.3171/JNS-07/07/0029

Koller, W.C., Glatt, S., Vetere-Overfield, B., Hassanein, R., 1989. Falls and Parkinson's disease. Clin. Neuropharmacol. 12, 98–105. https://doi.org/10.1097/00002826-198904000-00003

Koop, M.M., Andrzejewski, A., Hill, B.C., Heit, G., Bronte-Stewart, H.M., 2006. Improvement in a quantitative measure of bradykinesia after microelectrode recording in patients with Parkinson's disease during deep brain stimulation surgery. Mov. Disord. 21, 673–678. https://doi.org/10.1002/mds.20796

Krack, P., Pollak, P., Limousin, P., Benazzouz, A., Deuschl, G., Benabid, A.L., 1999. From off-period dystonia to peak-dose chorea. The clinical spectrum of varying subthalamic nucleus activity. Brain 122 (Pt 6, 1133–1146. https://doi.org/10.1093/brain/122.6.1133

Kress, G.J., Yamawaki, N., Wokosin, D.L., Wickersham, I.R., Shepherd, G.M.G., Surmeier, D.J., 2013. B r i e f c o m m u n i c at i o n s Convergent cortical innervation of striatal projection neurons. Nat. Publ. Gr. 16, 665–668. https://doi.org/10.1038/nn.3397

Kühn, Andrea A., Kempf, F., Brücke, C., Doyle, L.G., Martinez-Torres, I., Pogosyan, A., Trottenberg, T., Kupsch, A., Schneider, G.H., Hariz, M.I., Vandenberghe, W., Nuttin, B., Brown, P., 2008. High-frequency stimulation of the subthalamic nucleus suppresses oscillatory β activity in patients with Parkinson's disease in parallel with improvement in motor performance. J. Neurosci. 28, 6165–6173. https://doi.org/10.1523/JNEUROSCI.0282-08.2008

Kuhn, A.A., Kempf, F., Brucke, C., Gaynor Doyle, L., Martinez-Torres, I., Pogosyan, A., Trottenberg, T., Kupsch, A., Schneider, G.-H., Hariz, M.I., Vandenberghe, W., Nuttin, B., Brown, P., 2008. High-frequency stimulation of the subthalamic nucleus suppresses oscillatory beta activity in patients with Parkinson's disease in parallel with improvement in motor performance. J. Neurosci. 28, 6165–6173. https://doi.org/10.1523/JNEUROSCI.0282-08.2008

Kühn, Andrea A, Kempf, F., Brücke, C., Gaynor Doyle, L., Martinez-Torres, I., Pogosyan, A.,

Trottenberg, T., Kupsch, A., Schneider, G.-H., Hariz, M.I., Vandenberghe, W., Nuttin, B., Brown, P., 2008. High-frequency stimulation of the subthalamic nucleus suppresses oscillatory beta activity in patients with Parkinson's disease in parallel with improvement in motor performance. J. Neurosci. 28, 6165–6173. https://doi.org/10.1523/JNEUROSCI.0282-08.2008

Kuhn, A.A., Kupsch, A., Schneider, G.-H., Brown, P., 2006. Reduction in subthalamic 8-35 Hz oscillatory activity correlates with clinical improvement in Parkinson's disease. Eur. J. Neurosci. 23, 1956–1960. https://doi.org/10.1111/j.1460-9568.2006.04717.x

Kühn, Andrea A, Kupsch, A., Schneider, G.-H., Brown, P., 2006. Reduction in subthalamic 8-35 Hz oscillatory activity correlates with clinical improvement in Parkinson's disease. Eur. J. Neurosci. 23, 1956–1960. https://doi.org/10.1111/j.1460-9568.2006.04717.x

Kühn, Andrea A., Kupsch, A., Schneider, G.H., Brown, P., 2006. Reduction in subthalamic 8-35 Hz oscillatory activity correlates with clinical improvement in Parkinson's disease. Eur. J. Neurosci. 23, 1956–1960. https://doi.org/10.1111/j.1460-9568.2006.04717.x

Kühn, A.A., Trottenberg, T., Kivi, A., Kupsch, A., Schneider, G.-H., Brown, P., 2005. The relationship between local field potential and neuronal discharge in the subthalamic nucleus of patients with Parkinson's disease. Exp. Neurol. 194, 212–220. https://doi.org/10.1016/j.expneurol.2005.02.010

Kühn, A.A., Tsui, A., Aziz, T., Ray, N., Brücke, C., Kupsch, A., Schneider, G.-H., Brown, P., 2009. Pathological synchronisation in the subthalamic nucleus of patients with Parkinson's disease relates to both bradykinesia and rigidity. Exp. Neurol. 215, 380–387. https://doi.org/10.1016/j.expneurol.2008.11.008

Kuncel, A.M., Turner, D.A., Ozelius, L.J., Greene, P.E., Grill, W.M., Stacy, M.A., 2009. Myoclonus and tremor response to thalamic deep brain stimulation parameters in a patient with inherited myoclonus-dystonia syndrome. Clin. Neurol. Neurosurg. 111, 303–306. https://doi.org/10.1016/j.clineuro.2008.10.015

Kupsch, A., Benecke, R., Müller, J., Trottenberg, T., Schneider, G.-H., Poewe, W., Eisner, W., Wolters, A., Müller, J.-U., Deuschl, G., Pinsker, M.O., Skogseid, I.M., Roeste, G.K., Vollmer-Haase, J., Brentrup, A., Krause, M., Tronnier, V., Schnitzler, A., Voges, J., Nikkhah, G., Vesper, J., Naumann, M., Volkmann, J., 2006. Pallidal deep-brain stimulation in primary generalized or segmental dystonia. N. Engl. J. Med. 355, 1978–1990. https://doi.org/10.1056/NEJMoa063618

Lai, E.C., Jankovic, J., Krauss, J.K., Ondo, W.G., Grossman, R.G., 2000. Long-term efficacy of posteroventral pallidotomy in the treatment of Parkinson's disease. Neurology 55, 1218–1222. https://doi.org/10.1212/wnl.55.8.1218

Lalo, E., Thobois, S., Sharott, A., Polo, G., Mertens, P., Pogosyan, A., Brown, P., 2008. Patterns of bidirectional communication between cortex and basal ganglia during movement in patients with Parkinson disease. J. Neurosci. 28, 3008–3016. https://doi.org/10.1523/JNEUROSCI.5295-07.2008

Lange, O., Bigalke, H., Dengler, R., Wegner, F., deGroot, M., Wohlfarth, K., 2009. Neutralizing antibodies and secondary therapy failure after treatment with botulinum toxin type A: much ado about nothing? Clin. Neuropharmacol. 32, 213–218. https://doi.org/10.1097/WNF.0b013e3181914d0a

Langston, J.W., 2006. The Parkinson's complex: parkinsonism is just the tip of the iceberg. Ann. Neurol. 59, 591–596. https://doi.org/10.1002/ana.20834

Langston, J.W., Ballard, P., Tetrud, J.W., Irwin, I., 1983. Chronic Parkinsonism in humans due to a product of meperidine-analog synthesis. Science 219, 979–980. https://doi.org/10.1126/science.6823561

Langston, J.W., Forno, L.S., Tetrud, J., Reeves, A.G., Kaplan, J.A., Karluk, D., 1999. Evidence of active nerve cell degeneration in the substantia nigra of humans years after 1-methyl-4-phenyl-1,2,3,6-tetrahydropyridine exposure. Ann. Neurol. 46, 598–605. https://doi.org/10.1002/1531-8249(199910)46:4<598::aid-ana7>3.0.co;2-f

Le Van Quyen, M., Foucher, J., Lachaux, J., Rodriguez, E., Lutz, A., Martinerie, J., Varela, F.J., 2001. Comparison of Hilbert transform and wavelet methods for the analysis of neuronal synchrony. J. Neurosci. Methods 111, 83–98. https://doi.org/10.1016/s0165-0270(01)00372-7

Lee, K.H., Blaha, C.D., Garris, P.A., Mohseni, P., Horne, A.E., Bennet, K.E., Agnesi, F., Bledsoe, J.M., Lester, D.B., Kimble, C., Min, H.-K., Kim, Y.-B., Cho, Z.-H., 2009. Evolution of Deep Brain Stimulation: Human Electrometer and Smart Devices Supporting the Next Generation of Therapy. Neuromodulation 12, 85–103. https://doi.org/10.1111/j.1525-1403.2009.00199.x

Lee, S., Jones, S.R., 2013. Distinguishing mechanisms of gamma frequency oscillations in human current source signals using a computational model of a laminar neocortical network. Front. Hum. Neurosci. 7, 869. https://doi.org/10.3389/fnhum.2013.00869

Leksell, L., 1951. The stereotaxic method and radiosurgery of the brain. Acta Chir. Scand. 102, 316–319.

Leksell, L., Backlund, E.O., 1978. [Radiosurgical capsulotomy--a closed surgical method for psychiatric surgery]. Lakartidningen 75, 546–547.

Lendner, J.D., Helfrich, R.F., Mander, B.A., Romundstad, L., Lin, J.J., Walker, M.P., Larsson, P.G., Knight, R.T., 2020. An electrophysiological marker of arousal level in humans. Elife 9. https://doi.org/10.7554/eLife.55092

Levin, J., Krafczyk, S., Valkovic, P., Eggert, T., Claassen, J., Bötzel, K., 2009. Objective measurement of muscle rigidity in Parkinsonian patients treated with subthalamic stimulation. Mov. Disord. 24, 57–63. https://doi.org/10.1002/mds.22291

Levy, R., Ashby, P., Hutchison, W.D., Lang, A.E., Lozano, A.M., Dostrovsky, J.O., 2002. Dependence of subthalamic nucleus oscillations on movement and dopamine in Parkinson's disease. Brain 125, 1196–1209.

Levy, R., Dostrovsky, J.O., Lang, A.E., Sime, E., Hutchison, W.D., Lozano, A.M., 2001. Effects of

apomorphine on subthalamic nucleus and globus pallidus internus neurons in patients with Parkinson's disease. J. Neurophysiol. 86, 249–260. https://doi.org/10.1152/jn.2001.86.1.249

Levy, R., Hutchison, W.D., Lozano, A.M., Dostrovsky, J.O., 2000. High-frequency synchronization of neuronal activity in the subthalamic nucleus of parkinsonian patients with limb tremor. J. Neurosci. 20, 7766–7775. https://doi.org/10.1523/JNEUROSCI.20-20-07766.2000

Lhommée, E., Wojtecki, L., Czernecki, V., Witt, K., Maier, F., Tonder, L., Timmermann, L., Hälbig, T.D., Pineau, F., Durif, F., Witjas, T., Pinsker, M., Mehdorn, M., Sixel-Döring, F., Kupsch, A., Krüger, R., Elben, S., Chabardès, S., Thobois, S., Brefel-Courbon, C., Ory-Magne, F., Regis, J.-M., Maltête, D., Sauvaget, A., Rau, J., Schnitzler, A., Schüpbach, M., Schade-Brittinger, C., Deuschl, G., Houeto, J.-L., Krack, P., 2018. Behavioural outcomes of subthalamic stimulation and medical therapy versus medical therapy alone for Parkinson's disease with early motor complications (EARLYSTIM trial): secondary analysis of an open-label randomised trial. Lancet. Neurol. 17, 223–231. https://doi.org/10.1016/S1474-4422(18)30035-8

Li, N., Baldermann, J.C., Kibleur, A., Treu, S., Akram, H., Elias, G.J.B., Boutet, A., Lozano, A.M., Al-Fatly, B., Strange, B., Barcia, J.A., Zrinzo, L., Joyce, E., Chabardes, S., Visser-Vandewalle, V., Polosan, M., Kuhn, J., Kühn, A.A., Horn, A., 2020. A unified connectomic target for deep brain stimulation in obsessive-compulsive disorder. Nat. Commun. 11, 3364. https://doi.org/10.1038/s41467-020-16734-3

Limousin, P., Pollak, P., Benazzouz, A., Hoffmann, D., Le Bas, J.F., Broussolle, E., Perret, J.E., Benabid, A.L., 1995. Effect of parkinsonian signs and symptoms of bilateral subthalamic nucleus stimulation. Lancet (London, England) 345, 91–95. https://doi.org/10.1016/s0140-6736(95)90062-4

Lin, H., Na, P., Zhang, D., Liu, J., Cai, X., Li, W., 2020. Brain connectivity markers for the identification of effective contacts in subthalamic nucleus deep brain stimulation. Hum. Brain Mapp. 41, 2028–2036. https://doi.org/10.1002/hbm.24927

Little, S., Beudel, M., Zrinzo, L., Foltynie, T., Limousin, P., Hariz, M., Neal, S., Cheeran, B., Cagnan, H., Gratwicke, J., Aziz, T.Z., Pogosyan, A., Brown, P., 2016a. Bilateral adaptive deep brain stimulation is effective in Parkinson's disease. J. Neurol. Neurosurg. Psychiatry 87, 717–721. https://doi.org/10.1136/jnnp-2015-310972

Little, S., Brown, P., 2020. Debugging Adaptive Deep Brain Stimulation for Parkinson's Disease. Mov. Disord. 35, 555–561. https://doi.org/10.1002/mds.27996

Little, S., Pogosyan, A., Neal, S., Zavala, B., Zrinzo, L., Hariz, M., Foltynie, T., Limousin, P., Ashkan, K., FitzGerald, J., Green, A.L., Aziz, T.Z., Brown, P., 2013. Adaptive deep brain stimulation in advanced Parkinson disease. Ann. Neurol. 74, 449–457. https://doi.org/10.1002/ana.23951

Little, S., Tripoliti, E., Beudel, M., Pogosyan, A., Cagnan, H., Herz, D., Bestmann, S., Aziz, T., Cheeran, B., Zrinzo, L., Hariz, M., Hyam, J., Limousin, P., Foltynie, T., Brown, P., 2016b.

Adaptive deep brain stimulation for Parkinson's disease demonstrates reduced speech side effects compared to conventional stimulation in the acute setting. J. Neurol. Neurosurg. Psychiatry. https://doi.org/10.1136/jnnp-2016-313518

Litvak, V., Eusebio, A., Jha, A., Oostenveld, R., Barnes, G., Foltynie, T., Limousin, P., Zrinzo, L., Hariz, M.I., Friston, K., Brown, P., 2012. Movement-related changes in local and long-range synchronization in Parkinson's disease revealed by simultaneous magnetoencephalography and intracranial recordings. J. Neurosci. 32, 10541–10553. https://doi.org/10.1523/JNEUROSCI.0767-12.2012

Liu, R., Guo, X., Park, Y., Huang, X., Sinha, R., Freedman, N.D., Hollenbeck, A.R., Blair, A., Chen, H., 2012. Caffeine intake, smoking, and risk of Parkinson disease in men and women. Am. J. Epidemiol. 175, 1200–1207. https://doi.org/10.1093/aje/kwr451

Liu, X., Wang, S., Yianni, J., Nandi, D., Bain, P.G., Gregory, R., Stein, J.F., Aziz, T.Z., 2008. The sensory and motor representation of synchronized oscillations in the globus pallidus in patients with primary dystonia. Brain 131, 1562–1573. https://doi.org/10.1093/brain/awn083

Lofredi, R., Neumann, W.-J., Bock, A., Horn, A., Huebl, J., Siegert, S., Schneider, G.-H., Krauss, J.K., Kühn, A.A., 2018. Dopamine-dependent scaling of subthalamic gamma bursts with movement velocity in patients with Parkinson's disease. Elife 7. https://doi.org/10.7554/eLife.31895

Lofredi, R., Tan, H., Neumann, W.-J., Yeh, C.-H., Schneider, G.-H., Kühn, A.A., Brown, P., 2019. Beta bursts during continuous movements accompany the velocity decrement in Parkinson's disease patients. Neurobiol. Dis. 127, 462–471. https://doi.org/10.1016/j.nbd.2019.03.013

Logroscino, G., Sesso, H.D., Paffenbarger, R.S.J., Lee, I.-M., 2006. Physical activity and risk of Parkinson's disease: a prospective cohort study. J. Neurol. Neurosurg. Psychiatry 77, 1318–1322. https://doi.org/10.1136/jnnp.2006.097170

López-Azcárate, J., Tainta, M., Rodríguez-Oroz, M.C., Valencia, M., González, R., Guridi, J., Iriarte, J., Obeso, J.A., Artieda, J., Alegre, M., 2010a. Coupling between beta and high-frequency activity in the human subthalamic nucleus may be a pathophysiological mechanism in Parkinson's disease. J. Neurosci. 30, 6667–6677. https://doi.org/10.1523/JNEUROSCI.5459-09.2010

López-Azcárate, J., Tainta, M., Rodríguez-Oroz, M.C., Valencia, M., González, R., Guridi, J., Iriarte, J., Obeso, J.A., Artieda, J., Alegre, M., 2010b. Coupling between beta and high-frequency activity in the human subthalamic nucleus may be a pathophysiological mechanism in Parkinson's disease. J. Neurosci. 30, 6667–6677. https://doi.org/10.1523/JNEUROSCI.5459-09.2010

Louis, E.D., 2016. Treatment of Medically Refractory Essential Tremor. N. Engl. J. Med. https://doi.org/10.1056/NEJMe1606517

Lozano, A.M., Kumar, R., Gross, R.E., Giladi, N., Hutchison, W.D., Dostrovsky, J.O., Lang, A.E.,

1997. Globus pallidus internus pallidotomy for generalized dystonia. Mov. Disord. 12, 865–870. https://doi.org/10.1002/mds.870120606

Lozano, A.M., Lipsman, N., Bergman, H., Brown, P., Chabardes, S., Chang, J.W., Matthews, K., McIntyre, C.C., Schlaepfer, T.E., Schulder, M., Temel, Y., Volkmann, J., Krauss, J.K., 2019. Deep brain stimulation: current challenges and future directions. Nat. Rev. Neurol. 15, 148–160. https://doi.org/10.1038/s41582-018-0128-2

Lv, Z., Qi, H., Wang, L., Fan, X., Han, F., Wang, H., Bi, S., 2014. Vitamin D status and Parkinson's disease: a systematic review and meta-analysis. Neurol. Sci. Off. J. Ital. Neurol. Soc. Ital. Soc. Clin. Neurophysiol. 35, 1723–1730. https://doi.org/10.1007/s10072-014-1821-6

Ly, T.T., Weinzimer, S.A., Maahs, D.M., Sherr, J.L., Roy, A., Grosman, B., Cantwell, M., Kurtz, N., Carria, L., Messer, L., von Eyben, R., Buckingham, B.A., 2017. Automated hybrid closed-loop control with a proportional-integral-derivative based system in adolescents and adults with type 1 diabetes: individualizing settings for optimal performance. Pediatr. Diabetes 18, 348–355. https://doi.org/10.1111/pedi.12399

Magariños-Ascone, C., Pazo, J.H., Macadar, O., Buño, W., 2002. High-frequency stimulation of the subthalamic nucleus silences subthalamic neurons: a possible cellular mechanism in Parkinson's disease. Neuroscience 115, 1109–1117. https://doi.org/10.1016/s0306-4522(02)00538-9

Magill, P.J., Bolam, J.P., Bevan, M.D., 2001. Dopamine regulates the impact of the cerebral cortex on the subthalamic nucleus-globus pallidus network. Neuroscience 106, 313–330. https://doi.org/10.1016/s0306-4522(01)00281-0

Magill, P.J., Pogosyan, A., Sharott, A., Csicsvari, J., Bolam, J.P., Brown, P., 2006. Changes in functional connectivity within the rat striatopallidal axis during global brain activation in vivo. J. Neurosci. 26, 6318–6329. https://doi.org/10.1523/JNEUROSCI.0620-06.2006

Magill, P.J., Sharott, A., Bevan, M.D., Brown, P., Bolam, J.P., 2004. Synchronous unit activity and local field potentials evoked in the subthalamic nucleus by cortical stimulation. J. Neurophysiol. 92, 700–714. https://doi.org/10.1152/jn.00134.2004

Makeig, S., 1993. Auditory event-related dynamics of the EEG spectrum and effects of exposure to tones. Electroencephalogr. Clin. Neurophysiol. 86, 283–293. https://doi.org/10.1016/0013-4694(93)90110-h

Mallet, N., Micklem, B.R., Henny, P., Brown, M.T., Williams, C., Bolam, J.P., Nakamura, K.C., Magill, P.J., 2012a. Article Dichotomous Organization of the External Globus Pallidus. Neuron 74, 1075–1086. https://doi.org/10.1016/j.neuron.2012.04.027

Mallet, N., Micklem, B.R., Henny, P., Brown, M.T., Williams, C., Bolam, J.P., Nakamura, K.C., Magill, P.J., 2012b. Dichotomous organization of the external globus pallidus. Neuron 74, 1075–1086. https://doi.org/10.1016/j.neuron.2012.04.027

Mallet, N., Pogosyan, A., Márton, L.F., Bolam, J.P., Brown, P., Magill, P.J., 2008a. Parkinsonian beta

oscillations in the external globus pallidus and their relationship with subthalamic nucleus activity. J. Neurosci. 28, 14245–14258. https://doi.org/10.1523/JNEUROSCI.4199-08.2008

Mallet, N., Pogosyan, A., Sharott, A., Csicsvari, J., Bolam, J.P., Brown, P., Magill, P.J., 2008b. Disrupted dopamine transmission and the emergence of exaggerated beta oscillations in subthalamic nucleus and cerebral cortex. J. Neurosci. 28, 4795–4806. https://doi.org/10.1523/JNEUROSCI.0123-08.2008

Mann, J.M., Foote, K.D., Garvan, C.W., Fernandez, H.H., Jacobson, C.E. 4th, Rodriguez, R.L., Haq, I.U., Siddiqui, M.S., Malaty, I.A., Morishita, T., Hass, C.J., Okun, M.S., 2009. Brain penetration effects of microelectrodes and DBS leads in STN or GPi. J. Neurol. Neurosurg. Psychiatry 80, 794–797. https://doi.org/10.1136/jnnp.2008.159558

Manning, J.R., Jacobs, J., Fried, I., Kahana, M.J., 2009. Broadband shifts in local field potential power spectra are correlated with single-neuron spiking in humans. J. Neurosci. 29, 13613–13620. https://doi.org/10.1523/JNEUROSCI.2041-09.2009

Manyam, B. V, 1990. Paralysis agitans and levodopa in "Ayurveda": ancient Indian medical treatise. Mov. Disord. 5, 47–48. https://doi.org/10.1002/mds.870050112

Marceglia, S., Guidetti, M., Harmsen, I.E., Loh, A., Meoni, S., Foffani, G., Lozano, A.M., Volkmann, J., Moro, E., Priori, A., 2021. Deep brain stimulation: is it time to change gears by closing the loop? J. Neural Eng. 18, 061001. https://doi.org/10.1088/1741-2552/ac3267

Marsden, C.D., Obeso, J.A., 1994. The functions of the basal ganglia and the paradox of stereotaxic surgery in Parkinson's disease. Brain 117 (Pt 4, 877–897. https://doi.org/10.1093/brain/117.4.877

Marsh, L., 2013. Depression and Parkinson's disease: current knowledge. Curr. Neurol. Neurosci. Rep. 13, 409. https://doi.org/10.1007/s11910-013-0409-5

Maurice, N., Thierry, A.-M., Glowinski, J., Deniau, J.-M., 2003. Spontaneous and evoked activity of substantia nigra pars reticulata neurons during high-frequency stimulation of the subthalamic nucleus. J. Neurosci. 23, 9929–9936. https://doi.org/10.1523/JNEUROSCI.23-30-09929.2003

McIntyre, C.C., Savasta, M., Walter, B.L., Vitek, J.L., 2004. How does deep brain stimulation work? Present understanding and future questions. J. Clin. Neurophysiol. Off. Publ. Am. Electroencephalogr. Soc. 21, 40–50. https://doi.org/10.1097/00004691-200401000-00006

Meidahl, A.C., Moll, C.K.E., van Wijk, B.C.M., Gulberti, A., Tinkhauser, G., Westphal, M., Engel, A.K., Hamel, W., Brown, P., Sharott, A., 2019. Synchronised spiking activity underlies phase amplitude coupling in the subthalamic nucleus of Parkinson's disease patients. Neurobiol. Dis. 127, 101–113. https://doi.org/10.1016/j.nbd.2019.02.005

Meidahl, A.C., Tinkhauser, G., Herz, D.M., Cagnan, H., Debarros, J., Brown, P., 2017. Adaptive Deep Brain Stimulation for Movement Disorders: The Long Road to Clinical Therapy. Mov. Disord. 32, 810–819. https://doi.org/10.1002/mds.27022

Meissner, W., Leblois, A., Hansel, D., Bioulac, B., Gross, C.E., Benazzouz, A., Boraud, T., 2005.

Subthalamic high frequency stimulation resets subthalamic firing and reduces abnormal oscillations. Brain 128, 2372–2382. https://doi.org/10.1093/brain/awh616

Merello, M., Tenca, E., Pérez Lloret, S., Martín, M.E., Bruno, V., Cavanagh, S., Antico, J., Cerquetti, D., Leiguarda, R., 2008. Prospective randomized 1-year follow-up comparison of bilateral subthalamotomy versus bilateral subthalamic stimulation and the combination of both in Parkinson's disease patients: a pilot study. Br. J. Neurosurg. 22, 415–422. https://doi.org/10.1080/02688690801971667

Merk, T., Peterson, V., Lipski, W., Blankertz, B., Turner, R.S., Li, N., Horn, A., Kühn, A.A., Richardson, R.M., Neumann, W.-J., 2021. Electrocorticography is superior to subthalamic local field potentials for movement decoding in Parkinson{\textquoteright}s disease. bioRxiv. https://doi.org/10.1101/2021.04.24.441207

Merk, T., Peterson, V., Lipski, W.J., Blankertz, B., Turner, R.S., Li, N., Horn, A., Richardson, R.M., Neumann, W.-J., 2022. Electrocorticography is superior to subthalamic local field potentials for movement decoding in Parkinson's disease. Elife 11. https://doi.org/10.7554/eLife.75126

Merrill, D.R., Bikson, M., Jefferys, J.G.R., 2005. Electrical stimulation of excitable tissue: design of efficacious and safe protocols. J. Neurosci. Methods 141, 171–198. https://doi.org/10.1016/j.jneumeth.2004.10.020

Mestre, T.A., Lang, A.E., Okun, M.S., 2016. Factors influencing the outcome of deep brain stimulation: Placebo, nocebo, lessebo, and lesion effects. Mov. Disord. 31, 290–296. https://doi.org/10.1002/mds.26500

Meyers, R., 1942. The modification of alternating tremors, rigidity, and festination of surgery of the basal ganglia. Res. Publ. Assoc. Res. Nerv. Ment. Dis. 21, 602–665.

Middlebrooks, E.H., Grewal, S.S., Stead, M., Lundstrom, B.N., Worrell, G.A., Van Gompel, J.J., 2018. Differences in functional connectivity profiles as a predictor of response to anterior thalamic nucleus deep brain stimulation for epilepsy: a hypothesis for the mechanism of action and a potential biomarker for outcomes. Neurosurg. Focus 45, E7. https://doi.org/10.3171/2018.5.FOCUS18151

Miller, K.J., Leuthardt, E.C., Schalk, G., Rao, R.P.N., Anderson, N.R., Moran, D.W., Miller, J.W., Ojemann, J.G., 2007. Spectral changes in cortical surface potentials during motor movement. J. Neurosci. 27, 2424–2432. https://doi.org/10.1523/JNEUROSCI.3886-06.2007

Milosevic, L., Kalia, S.K., Hodaie, M., Lozano, A.M., Fasano, A., Popovic, M.R., Hutchison, W.D., 2018. Neuronal inhibition and synaptic plasticity of basal ganglia neurons in Parkinson's disease. Brain 141, 177–190. https://doi.org/10.1093/brain/awx296

Milosevic, L., Kalia, S.K., Hodaie, M., Lozano, A.M., Popovic, M.R., Hutchison, W.D., Lankarany, M., 2021. A theoretical framework for the site-specific and frequency-dependent neuronal effects of deep brain stimulation. Brain Stimul. 14, 807–821. https://doi.org/10.1016/j.brs.2021.04.022

Milosevic, L., Scherer, M., Cebi, I., Guggenberger, R., Machetanz, K., Naros, G., Weiss, D., Gharabaghi, A., 2020. Online Mapping With the Deep Brain Stimulation Lead: A Novel Targeting Tool in Parkinson's Disease. Mov. Disord. 35, 1574–1586. https://doi.org/10.1002/mds.28093

Miocinovic, S., de Hemptinne, C., Chen, W., Isbaine, F., Willie, J.T., Ostrem, J.L., Starr, P.A., 2018a. Cortical Potentials Evoked by Subthalamic Stimulation Demonstrate a Short Latency Hyperdirect Pathway in Humans. J. Neurosci. 38, 9129–9141. https://doi.org/10.1523/JNEUROSCI.1327-18.2018

Miocinovic, S., Swann, N.C., de Hemptinne, C., Miller, A., Ostrem, J.L., Starr, P.A., 2018b. Cortical gamma oscillations in isolated dystonia. Parkinsonism Relat. Disord. 49, 104–105. https://doi.org/10.1016/j.parkreldis.2018.01.017

Miskovic, V., MacDonald, K.J., Rhodes, L.J., Cote, K.A., 2019. Changes in EEG multiscale entropy and power-law frequency scaling during the human sleep cycle. Hum. Brain Mapp. 40, 538–551. https://doi.org/10.1002/hbm.24393

Mohammed, A., Zamani, M., Bayford, R., Demosthenous, A., 2017. Toward On-Demand Deep Brain Stimulation Using Online Parkinson's Disease Prediction Driven by Dynamic Detection. IEEE Trans. neural Syst. Rehabil. Eng. a Publ. IEEE Eng. Med. Biol. Soc. 25, 2441–2452. https://doi.org/10.1109/TNSRE.2017.2722986

Molina, J.L., Voytek, B., Thomas, M.L., Joshi, Y.B., Bhakta, S.G., Talledo, J.A., Swerdlow, N.R., Light, G.A., 2020. Memantine Effects on Electroencephalographic Measures of Putative Excitatory/Inhibitory Balance in Schizophrenia. Biol. psychiatry. Cogn. Neurosci. neuroimaging 5, 562–568. https://doi.org/10.1016/j.bpsc.2020.02.004

Molina, R., Hass, C.J., Cernera, S., Sowalsky, K., Schmitt, A.C., Roper, J.A., Martinez-Ramirez, D., Opri, E., Hess, C.W., Eisinger, R.S., Foote, K.D., Gunduz, A., Okun, M.S., 2021. Closed-Loop Deep Brain Stimulation to Treat Medication-Refractory Freezing of Gait in Parkinson's Disease. Front. Hum. Neurosci. 15, 633655. https://doi.org/10.3389/fnhum.2021.633655

Monakow, K.H., Akert, K., Künzle, H., 1978. Projections of the precentral motor cortex and other cortical areas of the frontal lobe to the subthalamic nucleus in the monkey. Exp. brain Res. 33, 395–403. https://doi.org/10.1007/BF00235561

Montgomery, E.B.J., 2006. Effects of GPi stimulation on human thalamic neuronal activity. Clin. Neurophysiol. Off. J. Int. Fed. Clin. Neurophysiol. 117, 2691–2702. https://doi.org/10.1016/j.clinph.2006.08.011

Montgomery, E.B.J., Gale, J.T., 2008. Mechanisms of action of deep brain stimulation(DBS) . Neurosci. Biobehav. Rev. 32, 388–407. https://doi.org/10.1016/j.neubiorev.2007.06.003

Moore, H., Grace, A.A., 2002. A role for electrotonic coupling in the striatum in the expression of dopamine receptor-mediated stereotypies. Neuropsychopharmacol. Off. Publ. Am. Coll. Neuropsychopharmacol. 27, 980–992. https://doi.org/10.1016/S0893-133X(02)00383-4

Moran, A., Stein, E., Tischler, H., Belelovsky, K., Bar-Gad, I., 2011. Dynamic stereotypic responses of Basal Ganglia neurons to subthalamic nucleus high-frequency stimulation in the parkinsonian primate. Front. Syst. Neurosci. 5, 21. https://doi.org/10.3389/fnsys.2011.00021

Morgan, J.P., 1982. The first reported case of electrical stimulation of the human brain. J. Hist. Med. Allied Sci. 37, 51–64. https://doi.org/10.1093/jhmas/xxxvii.1.51

Morishita, T., Hilliard, J.D., Okun, M.S., Neal, D., Nestor, K.A., Peace, D., Hozouri, A.A., Davidson, M.R., Bova, F.J., Sporrer, J.M., Oyama, G., Foote, K.D., 2017. Postoperative lead migration in deep brain stimulation surgery: Incidence, risk factors, and clinical impact. PLoS One 12, e0183711. https://doi.org/10.1371/journal.pone.0183711

Morrell, M.J., 2011. Responsive cortical stimulation for the treatment of medically intractable partial epilepsy. Neurology 77, 1295–1304. https://doi.org/10.1212/WNL.0b013e3182302056

Mostile, G., Giuliano, L., Dibilio, V., Luca, A., Cicero, C.E., Sofia, V., Nicoletti, A., Zappia, M., 2019. Complexity of electrocortical activity as potential biomarker in untreated Parkinson's disease. J. Neural Transm. 126, 167–172. https://doi.org/10.1007/s00702-018-1961-6

Murakami, T., Shoji, M., Imai, Y., Inoue, H., Kawarabayashi, T., Matsubara, E., Harigaya, Y., Sasaki, A., Takahashi, R., Abe, K., 2004. Pael-R is accumulated in Lewy bodies of Parkinson's disease. Ann. Neurol. 55, 439–442. https://doi.org/10.1002/ana.20064

Muth, C., Bales, K.L., Hinde, K., Maninger, N., Mendoza, S.P., Ferrer, E., 2016. Alternative Models for Small Samples in Psychological Research: Applying Linear Mixed Effects Models and Generalized Estimating Equations to Repeated Measures Data. Educ. Psychol. Meas. 76, 64–87. https://doi.org/10.1177/0013164415580432

Muthukumaraswamy, S.D., 2010. Functional properties of human primary motor cortex gamma oscillations. J. Neurophysiol. 104, 2873–2885. https://doi.org/10.1152/jn.00607.2010

Muthuraman, M., Bange, M., Koirala, N., Ciolac, D., Pintea, B., Glaser, M., Tinkhauser, G., Brown, P., Deuschl, G., Groppa, S., 2020. Cross-frequency coupling between gamma oscillations and deep brain stimulation frequency in Parkinson's disease. Brain. https://doi.org/10.1093/brain/awaa297

Muthuraman, M., Koirala, N., Ciolac, D., Pintea, B., Glaser, M., Groppa, Stanislav, Tamás, G., Groppa, Sergiu, 2018. Deep Brain Stimulation and L-DOPA Therapy: Concepts of Action and Clinical Applications in Parkinson's Disease. Front. Neurol. 9, 711. https://doi.org/10.3389/fneur.2018.00711

Nambu, A., Tokuno, H., Takada, M., 2002. Functional significance of the cortico-subthalamo-pallidal "hyperdirect" pathway. Neurosci. Res. 43, 111–117. https://doi.org/10.1016/s0168-0102(02)00027-5

Nelson, A.B., Kreitzer, A.C., 2014. Reassessing models of basal ganglia function and dysfunction. Annu. Rev. Neurosci. 37, 117–135. https://doi.org/10.1146/annurev-neuro-071013-013916

Neumann, W.-J., Degen, K., Schneider, G.-H., Brücke, C., Huebl, J., Brown, P., Kühn, A.A., 2016a.

Subthalamic synchronized oscillatory activity correlates with motor impairment in patients with Parkinson's disease. Mov. Disord. 31, 1748–1751. https://doi.org/10.1002/mds.26759

Neumann, W.-J., Horn, A., Ewert, S., Huebl, J., Brücke, C., Slentz, C., Schneider, G.-H., Kühn, A.A., 2017a. A localized pallidal physiomarker in cervical dystonia. Ann. Neurol. 82, 912–924. https://doi.org/10.1002/ana.25095

Neumann, W.-J., Huebl, J., Brücke, C., Ruiz, M.H., Kupsch, A., Schneider, G.-H., Kühn, A.A., 2012. Enhanced low-frequency oscillatory activity of the subthalamic nucleus in a patient with dystonia. Mov. Disord. 27, 1063–1066. https://doi.org/10.1002/mds.25078

Neumann, W.-J., Staub-Bartelt, F., Horn, A., Schanda, J., Schneider, G.-H., Brown, P., Kühn, A.A., 2017b. Long term correlation of subthalamic beta band activity with motor impairment in patients with Parkinson's disease. Clin. Neurophysiol. Off. J. Int. Fed. Clin. Neurophysiol. 128, 2286–2291. https://doi.org/10.1016/j.clinph.2017.08.028

Neumann, W.-J., Staub, F., Horn, A., Schanda, J., Mueller, J., Schneider, G.-H., Brown, P., Kühn, A.A., 2016b. Deep Brain Recordings Using an Implanted Pulse Generator in Parkinson's Disease. Neuromodulation 19, 20–24. https://doi.org/10.1111/ner.12348

Neumann, W.-J., Turner, R.S., Blankertz, B., Mitchell, T., Kühn, A.A., Richardson, R.M., 2019. Toward Electrophysiology-Based Intelligent Adaptive Deep Brain Stimulation for Movement Disorders. Neurother. J. Am. Soc. Exp. Neurother. 16, 105–118. https://doi.org/10.1007/s13311-018-00705-0

Neychev, V.K., Gross, R.E., Lehéricy, S., Hess, E.J., Jinnah, H.A., 2011. The functional neuroanatomy of dystonia. Neurobiol. Dis. 42, 185–201. https://doi.org/10.1016/j.nbd.2011.01.026

NICE, 2006. Parkinson's Disease: National clinical guideline for diagnosis and management in primary and secondary care. Natl. Collab. Cent. Chronic Cond. Appendix F.

Niethard, N., Hasegawa, M., Itokazu, T., Oyanedel, C.N., Born, J., Sato, T.R., 2016. Sleep-Stage-Specific Regulation of Cortical Excitation and Inhibition. Curr. Biol. 26, 2739–2749. https://doi.org/10.1016/j.cub.2016.08.035

Niranjan, A., Kondziolka, D., Baser, S., Heyman, R., Lunsford, L.D., 2000. Functional outcomes after gamma knife thalamotomy for essential tremor and MS-related tremor. Neurology 55, 443–446. https://doi.org/10.1212/wnl.55.3.443

Noyce, A.J., Bestwick, J.P., Silveira-Moriyama, L., Hawkes, C.H., Giovannoni, G., Lees, A.J., Schrag, A., 2012. Meta-analysis of early nonmotor features and risk factors for Parkinson disease. Ann. Neurol. 72, 893–901. https://doi.org/10.1002/ana.23687

Nutt, J.G., Hammerstad, J.P., deGarmo, P., Carter, J., 1984. Cranial dystonia: double-blind crossover study of anticholinergics. Neurology 34, 215–217. https://doi.org/10.1212/wnl.34.2.215

Nygaard, T.G., Trugman, J.M., de Yebenes, J.G., Fahn, S., 1990. Dopa-responsive dystonia: the spectrum of clinical manifestations in a large North American family. Neurology 40, 66–69.

https://doi.org/10.1212/wnl.40.1.66

Oakley, A.E., Collingwood, J.F., Dobson, J., Love, G., Perrott, H.R., Edwardson, J.A., Elstner, M., Morris, C.M., 2007. Individual dopaminergic neurons show raised iron levels in Parkinson disease. Neurology 68, 1820–1825. https://doi.org/10.1212/01.wnl.0000262033.01945.9a

Odekerken, V.J.J., van Laar, T., Staal, M.J., Mosch, A., Hoffmann, C.F.E., Nijssen, P.C.G., Beute, G.N., van Vugt, J.P.P., Lenders, M.W.P.M., Contarino, M.F., Mink, M.S.J., Bour, L.J., van den Munckhof, P., Schmand, B.A., de Haan, R.J., Schuurman, P.R., de Bie, R.M.A., 2013. Subthalamic nucleus versus globus pallidus bilateral deep brain stimulation for advanced Parkinson's disease (NSTAPS study): a randomised controlled trial. Lancet. Neurol. 12, 37–44. https://doi.org/10.1016/S1474-4422(12)70264-8

Oh, M.Y., Abosch, A., Kim, S.H., Lang, A.E., Lozano, A.M., 2002. Long-term hardware-related complications of deep brain stimulation. Neurosurgery 50, 1266–1268. https://doi.org/10.1097/00006123-200206000-00017

Okun, M.S., 2012. Deep-brain stimulation for Parkinson's disease. N. Engl. J. Med. 367, 1529–1538. https://doi.org/10.1056/NEJMct1208070

Olanow, C.W., Watts, R.L., Koller, W.C., 2001. An algorithm (decision tree) for the management of Parkinson's disease (2001): treatment guidelines. Neurology 56, S1–S88. https://doi.org/10.1212/wnl.56.suppl_5.s1

Oliveria, S.F., 2018. The dark history of early deep brain stimulation. Lancet Neurol. 17, 748. https://doi.org/10.1016/S1474-4422(18)30237-0

Olson, J.W., Nakhmani, A., Irwin, Z.T., Edwards, L.J., Gonzalez, C.L., Wade, M.H., Black, S.D., Awad, M.Z., Kuhman, D.J., Hurt, C.P., Guthrie, B.L., Walker, H.C., 2022. Cortical and Subthalamic Nucleus Spectral Changes During Limb Movements in Parkinson's Disease Patients with and Without Dystonia. Mov. Disord. 37, 1683–1692. https://doi.org/10.1002/mds.29057

Oostenveld, R., Fries, P., Maris, E., Schoffelen, J., 2011. FieldTrip : Open Source Software for Advanced Analysis of MEG , EEG , and Invasive Electrophysiological Data. Comput Intell Neurosci 2011. https://doi.org/10.1155/2011/156869

Opri, E., Cernera, S., Molina, R., Eisinger, R.S., Cagle, J.N., Almeida, L., Denison, T., Okun, M.S., Foote, K.D., Gunduz, A., 2020. Chronic embedded cortico-thalamic closed-loop deep brain stimulation for the treatment of essential tremor. Sci. Transl. Med. 12. https://doi.org/10.1126/scitranslmed.aay7680

Ostrem, J.L., Racine, C.A., Glass, G.A., Grace, J.K., Volz, M.M., Heath, S.L., Starr, P.A., 2011. Subthalamic nucleus deep brain stimulation in primary cervical dystonia. Neurology 76, 870–878. https://doi.org/10.1212/WNL.0b013e31820f2e4f

Ostrem, J.L., San Luciano, M., Dodenhoff, K.A., Ziman, N., Markun, L.C., Racine, C.A., de Hemptinne, C., Volz, M.M., Heath, S.L., Starr, P.A., 2017. Subthalamic nucleus deep brain

stimulation in isolated dystonia: A 3-year follow-up study. Neurology 88, 25–35. https://doi.org/10.1212/WNL.0000000000003451

Oswal, A., Beudel, M., Zrinzo, L., Limousin, P., Hariz, M., Foltynie, T., Litvak, V., Brown, P., 2016. Deep brain stimulation modulates synchrony within spatially and spectrally distinct resting state networks in Parkinson's disease. Brain 139, 1482–1496. https://doi.org/10.1093/brain/aww048

Oswal, A., Brown, P., Litvak, V., 2013. Synchronized neural oscillations and the pathophysiology of Parkinson's disease. Curr. Opin. Neurol. 26, 662–670. https://doi.org/10.1097/WCO.0000000000000034

Özkurt, T.E., Butz, M., Homburger, M., Elben, S., Vesper, J., Wojtecki, L., Schnitzler, A., 2011. High frequency oscillations in the subthalamic nucleus: a neurophysiological marker of the motor state in Parkinson's disease. Exp. Neurol. 229, 324–331. https://doi.org/10.1016/j.expneurol.2011.02.015

Ozturk, M., Kaku, H., Jimenez-Shahed, J., Viswanathan, A., Sheth, S.A., Kumar, S., Ince, N.F., 2020. Subthalamic Single Cell and Oscillatory Neural Dynamics of a Dyskinetic Medicated Patient With Parkinson's Disease. Front. Neurosci. 14, 391. https://doi.org/10.3389/fnins.2020.00391

Ozturk, M., Viswanathan, A., Sheth, S.A., Ince, N.F., 2021. Electroceutically induced subthalamic high-frequency oscillations and evoked compound activity may explain the mechanism of therapeutic stimulation in Parkinson's disease. Commun. Biol. 4, 393. https://doi.org/10.1038/s42003-021-01915-7

Padmanabhan, J.L., Cooke, D., Joutsa, J., Siddiqi, S.H., Ferguson, M., Darby, R.R., Soussand, L., Horn, A., Kim, N.Y., Voss, J.L., Naidech, A.M., Brodtmann, A., Egorova, N., Gozzi, S., Phan, T.G., Corbetta, M., Grafman, J., Fox, M.D., 2019. A Human Depression Circuit Derived From Focal Brain Lesions. Biol. Psychiatry 86, 749–758. https://doi.org/10.1016/j.biopsych.2019.07.023

Pagano, G., Ferrara, N., Brooks, D.J., Pavese, N., 2016. Age at onset and Parkinson disease phenotype. Neurology 86, 1400–1407. https://doi.org/10.1212/WNL.0000000000002461

Panov, F., Levin, E., de Hemptinne, C., Swann, N.C., Qasim, S., Miocinovic, S., Ostrem, J.L., Starr, P.A., 2017. Intraoperative electrocorticography for physiological research in movement disorders: principles and experience in 200 cases. J. Neurosurg. 126, 122–131. https://doi.org/10.3171/2015.11.JNS151341

Park, B.K., Kwon, Y., Kim, J.-W., Lee, J.-H., Eom, G.-M., Koh, S.-B., Jun, J.-H., Hong, J., 2011. Analysis of viscoelastic properties of wrist joint for quantification of parkinsonian rigidity. IEEE Trans. neural Syst. Rehabil. Eng. a Publ. IEEE Eng. Med. Biol. Soc. 19, 167–176. https://doi.org/10.1109/TNSRE.2010.2091149

Parkinson, J., 1817. An essay on the shaking palsy. Sherwood, Neely and Jones, London. https://doi.org/10.1176/jnp.14.2.223

Parr-Brownlie, L.C., Poloskey, S.L., Flanagan, K.K., Eisenhofer, G., Bergstrom, D.A., Walters, J.R.,

2007. Dopamine lesion-induced changes in subthalamic nucleus activity are not associated with alterations in firing rate or pattern in layer V neurons of the anterior cingulate cortex in anesthetized rats. Eur. J. Neurosci. 26, 1925–1939. https://doi.org/10.1111/j.1460-9568.2007.05814.x

Parr, J.R., Green, A.L., Joint, C., Andrew, M., Gregory, R.P., Scott, R.B., McShane, M.A., Aziz, T.Z., 2007. Deep brain stimulation in childhood: an effective treatment for early onset idiopathic generalised dystonia. Arch. Dis. Child. 92, 708–711. https://doi.org/10.1136/adc.2006.095380

Parsons, T.D., Rogers, S.A., Braaten, A.J., Woods, S.P., Tröster, A.I., 2006. Cognitive sequelae of subthalamic nucleus deep brain stimulation in Parkinson's disease: a meta-analysis. Lancet. Neurol. 5, 578–588. https://doi.org/10.1016/S1474-4422(06)70475-6

Peckham, P.H., Knutson, J.S., 2005. Functional electrical stimulation for neuromuscular applications. Annu. Rev. Biomed. Eng. 7, 327–360. https://doi.org/10.1146/annurev.bioeng.6.040803.140103

Petry-Schmelzer, J.N., Dembek, T.A., Steffen, J.K., Jergas, H., Dafsari, H.S., Fink, G.R., Visser-Vandewalle, V., Barbe, M.T., 2020. Selecting the Most Effective DBS Contact in Essential Tremor Patients Based on Individual Tractography. Brain Sci. 10. https://doi.org/10.3390/brainsci10121015

Phukan, J., Albanese, A., Gasser, T., Warner, T., 2011. Primary dystonia and dystonia-plus syndromes: clinical characteristics, diagnosis, and pathogenesis. Lancet. Neurol. 10, 1074–1085. https://doi.org/10.1016/S1474-4422(11)70232-0

Picillo, M., Lozano, A.M., Kou, N., Puppi Munhoz, R., Fasano, A., 2016. Programming Deep Brain Stimulation for Parkinson's Disease: The Toronto Western Hospital Algorithms. Brain Stimul. 9, 425–437. https://doi.org/10.1016/j.brs.2016.02.004

Piña-Fuentes, D., Beudel, M., Little, S., Brown, P., Oterdoom, D.L.M., van Dijk, J.M.C., 2019. Adaptive deep brain stimulation as advanced Parkinson's disease treatment (ADAPT study): protocol for a pseudo-randomised clinical study. BMJ Open 9, e029652. https://doi.org/10.1136/bmjopen-2019-029652

Piper, H., 1907. Über den willkürlichen Muskeltetanus. Arch. für die gesamte Physiol. des Menschen und der Tiere 119, 301–338. https://doi.org/10.1007/BF01678075

Pisani, A., Bernardi, G., Ding, J., Surmeier, D.J., 2007. Re-emergence of striatal cholinergic interneurons in movement disorders. Trends Neurosci. 30, 545–553. https://doi.org/10.1016/j.tins.2007.07.008

Plaha, P., Khan, S., Gill, S.S., 2008. Bilateral stimulation of the caudal zona incerta nucleus for tremor control. J. Neurol. Neurosurg. Psychiatry 79, 504–513. https://doi.org/10.1136/jnnp.2006.112334

Pogosyan, A., Kühn, A.A., Trottenberg, T., Schneider, G.-H., Kupsch, A., Brown, P., 2006. Elevations in local gamma activity are accompanied by changes in the firing rate and information coding capacity of neurons in the region of the subthalamic nucleus in Parkinson's

disease. Exp. Neurol. 202, 271–279. https://doi.org/10.1016/j.expneurol.2006.06.014

Porritt, M., Stanic, D., Finkelstein, D., Batchelor, P., Lockhart, S., Hughes, A., Kalnins, R., Howells, D., 2005. Dopaminergic innervation of the human striatum in Parkinson's disease. Mov. Disord. 20, 810–818. https://doi.org/10.1002/mds.20399

Pralong, E., Debatisse, D., Maeder, M., Vingerhoets, F., Ghika, J., Villemure, J.-G., 2003. Effect of deep brain stimulation of GPI on neuronal activity of the thalamic nucleus ventralis oralis in a dystonic patient. Neurophysiol. Clin. 33, 169–173. https://doi.org/10.1016/j.neucli.2003.07.001

Pringsheim, T., Jette, N., Frolkis, A., Steeves, T.D.L., 2014. The prevalence of Parkinson's disease: a systematic review and meta-analysis. Mov. Disord. 29, 1583–1590. https://doi.org/10.1002/mds.25945

Priori, A., Foffani, G., Pesenti, A., Tamma, F., Bianchi, A.M., Pellegrini, M., Locatelli, M., Moxon, K.A., Villani, R.M., 2004. Rhythm-specific pharmacological modulation of subthalamic activity in Parkinson's disease. Exp. Neurol. 189, 369–379. https://doi.org/10.1016/j.expneurol.2004.06.001

Pritchard, W.S., 1992. The brain in fractal time: 1/f-like power spectrum scaling of the human electroencephalogram. Int. J. Neurosci. 66, 119–129. https://doi.org/10.3109/00207459208999796

Przedborski, S., Tieu, K., Perier, C., Vila, M., 2004. MPTP as a mitochondrial neurotoxic model of Parkinson's disease. J. Bioenerg. Biomembr. 36, 375–379. https://doi.org/10.1023/B:JOBB.0000041771.66775.d5

Quinn, E.J., Blumenfeld, Z., Velisar, A., Koop, M.M., Shreve, L.A., Trager, M.H., Hill, B.C., Kilbane, C., Henderson, J.M., Brontë-Stewart, H., 2015. Beta oscillations in freely moving Parkinson's subjects are attenuated during deep brain stimulation. Mov. Disord. 30, 1750–1758. https://doi.org/10.1002/mds.26376

Rajput, A.H., Gibb, W.R., Zhong, X.H., Shannak, K.S., Kish, S., Chang, L.G., Hornykiewicz, O., 1994. Dopa-responsive dystonia: pathological and biochemical observations in a case. Ann. Neurol. 35, 396–402. https://doi.org/10.1002/ana.410350405

Ramaker, C., Marinus, J., Stiggelbout, A.M., Van Hilten, B.J., 2002. Systematic evaluation of rating scales for impairment and disability in Parkinson's disease. Mov. Disord. 17, 867–876. https://doi.org/10.1002/mds.10248

Ramirez-Zamora, A., Giordano, J., Gunduz, A., Alcantara, J., Cagle, J.N., Cernera, S., Difuntorum, P., Eisinger, R.S., Gomez, J., Long, S., Parks, B., Wong, J.K., Chiu, S., Patel, B., Grill, W.M., Walker, H.C., Little, S.J., Gilron, R., Tinkhauser, G., Thevathasan, W., Sinclair, N.C., Lozano, A.M., Foltynie, T., Fasano, A., Sheth, S.A., Scangos, K., Sanger, T.D., Miller, J., Brumback, A.C., Rajasethupathy, P., McIntyre, C., Schlachter, L., Suthana, N., Kubu, C., Sankary, L.R., Herrera-Ferrá, K., Goetz, S., Cheeran, B., Steinke, G.K., Hess, C., Almeida, L., Deeb, W., Foote, K.D., Okun, M.S., 2020. Proceedings of the Seventh Annual Deep Brain Stimulation

Think Tank: Advances in Neurophysiology, Adaptive DBS, Virtual Reality, Neuroethics and Technology. Front. Hum. Neurosci. 14, 54. https://doi.org/10.3389/fnhum.2020.00054

Rappel, P., Marmor, O., Bick, A.S., Arkadir, D., Linetsky, E., Castrioto, A., Tamir, I., Freedman, S.A., Mevorach, T., Gilad, M., Bergman, H., Israel, Z., Eitan, R., 2018. Subthalamic theta activity: a novel human subcortical biomarker for obsessive compulsive disorder. Transl. Psychiatry 8, 118. https://doi.org/10.1038/s41398-018-0165-z

Rau, A., Urbach, H., Coenen, V.A., Egger, K., Reinacher, P.C., 2021. Deep brain stimulation electrodes may rotate after implantation-an animal study. Neurosurg. Rev. 44, 2349–2353. https://doi.org/10.1007/s10143-020-01429-6

Ray, N.J., Brittain, J.-S., Holland, P., Joundi, R.A., Stein, J.F., Aziz, T.Z., Jenkinson, N., 2012. The role of the subthalamic nucleus in response inhibition: evidence from local field potential recordings in the human subthalamic nucleus. Neuroimage 60, 271–278. https://doi.org/10.1016/j.neuroimage.2011.12.035

Ray, N.J., Jenkinson, N., Brittain, J., Holland, P., Joint, C., Nandi, D., Bain, P.G., Yousif, N., Green, A., Stein, J.S., Aziz, T.Z., 2009. The role of the subthalamic nucleus in response inhibition: evidence from deep brain stimulation for Parkinson's disease. Neuropsychologia 47, 2828–2834. https://doi.org/10.1016/j.neuropsychologia.2009.06.011

Ray, N.J., Jenkinson, N., Wang, S., Holland, P., Brittain, J.S., Joint, C., Stein, J.F., Aziz, T., 2008. Local field potential beta activity in the subthalamic nucleus of patients with Parkinson's disease is associated with improvements in bradykinesia after dopamine and deep brain stimulation. Exp. Neurol. 213, 108–113. https://doi.org/10.1016/j.expneurol.2008.05.008

Ray, S., Maunsell, J.H.R., 2011. Different origins of gamma rhythm and high-gamma activity in macaque visual cortex. PLoS Biol. 9, e1000610. https://doi.org/10.1371/journal.pbio.1000610

Rizzoli, S.O., Betz, W.J., 2005a. SYNAPTIC VESICLE POOLS 6. https://doi.org/10.1038/nrn1583

Rizzoli, S.O., Betz, W.J., 2005b. Synaptic vesicle pools. Nat. Rev. Neurosci. 6, 57–69. https://doi.org/10.1038/nrn1583

Robertson, M.M., Furlong, S., Voytek, B., Donoghue, T., Boettiger, C.A., Sheridan, M.A., 2019. EEG power spectral slope differs by ADHD status and stimulant medication exposure in early childhood. J. Neurophysiol. 122, 2427–2437. https://doi.org/10.1152/jn.00388.2019

Rosa, M., Arlotti, M., Marceglia, S., Cogiamanian, F., Ardolino, G., Fonzo, A. Di, Lopiano, L., Scelzo, E., Merola, A., Locatelli, M., Rampini, P.M., Priori, A., 2017a. Adaptive deep brain stimulation controls levodopa-induced side effects in Parkinsonian patients. Mov. Disord. https://doi.org/10.1002/mds.26953

Rosa, M., Marceglia, S., Servello, D., Foffani, G., Rossi, L., Sassi, M., Mrakic-Sposta, S., Zangaglia, R., Pacchetti, C., Porta, M., Priori, A., 2010. Time dependent subthalamic local field potential changes after DBS surgery in Parkinson's disease. Exp. Neurol. 222, 184–190. https://doi.org/10.1016/j.expneurol.2009.12.013

Rosa, M., Scelzo, E., Locatelli, M., Carrabba, G., Levi, V., Arlotti, M., Barbieri, S., Rampini, P., Priori, A., 2017b. Risk of Infection After Local Field Potential Recording from Externalized Deep Brain Stimulation Leads in Parkinson's Disease. World Neurosurg. 97, 64–69. https://doi.org/10.1016/j.wneu.2016.09.069

Rosenbaum, R., Zimnik, A., Zheng, F., Turner, R.S., Alzheimer, C., Doiron, B., Rubin, J.E., 2014. Axonal and synaptic failure suppress the transfer of firing rate oscillations, synchrony and information during high frequency deep brain stimulation. Neurobiol. Dis. 62, 86–99. https://doi.org/10.1016/j.nbd.2013.09.006

Rosin, B., Slovik, M., Mitelman, R., Rivlin-Etzion, M., Haber, S.N., Israel, Z., Vaadia, E., Bergman, H., 2011. Closed-loop deep brain stimulation is superior in ameliorating parkinsonism. Neuron 72, 370–384. https://doi.org/10.1016/j.neuron.2011.08.023

Ryapolova-Webb, E., Afshar, P., Stanslaski, S., Denison, T., de Hemptinne, C., Bankiewicz, K., Starr, P.A., 2014. Chronic cortical and electromyographic recordings from a fully implantable device: preclinical experience in a nonhuman primate. J. Neural Eng. 11, 16009. https://doi.org/10.1088/1741-2560/11/1/016009

Samii, A., Etminan, M., Wiens, M.O., Jafari, S., 2009. NSAID use and the risk of Parkinson's disease: systematic review and meta-analysis of observational studies. Drugs Aging 26, 769–779. https://doi.org/10.2165/11316780-000000000-00000

Sanders, T.H., 2016. Phase-amplitude coupling, an indication of bursting in parkinsonism, is masked by periodic pulses. J. Neurophysiol. 115, 1587–1595. https://doi.org/10.1152/jn.00801.2015

Santamaria, J., Chiappa, K.H., 1987. The EEG of drowsiness in normal adults. J. Clin. Neurophysiol. Off. Publ. Am. Electroencephalogr. Soc. 4, 327–382. https://doi.org/10.1097/00004691-198710000-00002

Schaworonkow, N., Voytek, B., 2021. Longitudinal changes in aperiodic and periodic activity in electrophysiological recordings in the first seven months of life. Dev. Cogn. Neurosci. 47, 100895. https://doi.org/10.1016/j.dcn.2020.100895

Schiff, S.J., 2005. Dangerous phase. Neuroinformatics 3, 315–318. https://doi.org/10.1385/NI:3:4:315

Schjerling, L., Hjermind, L.E., Jespersen, B., Madsen, F.F., Brennum, J., Jensen, S.R., Løkkegaard, A., Karlsborg, M., 2013. A randomized double-blind crossover trial comparing subthalamic and pallidal deep brain stimulation for dystonia. J. Neurosurg. 119, 1537–1545. https://doi.org/10.3171/2013.8.JNS13844

Schmidt, S.L., Brocker, D.T., Swan, B.D., Turner, D.A., Grill, W.M., 2020. Evoked potentials reveal neural circuits engaged by human deep brain stimulation. Brain Stimul. 13, 1706–1718. https://doi.org/10.1016/j.brs.2020.09.028

Schneggenburger, R., Sakaba, T., Neher, E., 2002. Vesicle pools and short-term synaptic depression: Lessons from a large synapse. Trends Neurosci. 25, 206–212. https://doi.org/10.1016/S0166-2236(02)02139-2

Schoffelen, J.-M., Oostenveld, R., Fries, P., 2005. Neuronal coherence as a mechanism of effective corticospinal interaction. Science 308, 111–113. https://doi.org/10.1126/science.1107027

Schrader, C., Capelle, H.-H., Kinfe, T.M., Blahak, C., Bäzner, H., Lütjens, G., Dressler, D., Krauss, J.K., 2011. GPi-DBS may induce a hypokinetic gait disorder with freezing of gait in patients with dystonia. Neurology 77, 483–488. https://doi.org/10.1212/WNL.0b013e318227b19e

Schwalb, J.M., Hamani, C., 2008. The history and future of deep brain stimulation. Neurother. J. Am. Soc. Exp. Neurother. 5, 3–13. https://doi.org/10.1016/j.nurt.2007.11.003

Schwartz, A.B., Cui, X.T., Weber, D.J., Moran, D.W., 2006. Brain-controlled interfaces: movement restoration with neural prosthetics. Neuron 52, 205–220. https://doi.org/10.1016/j.neuron.2006.09.019

Sermon, J.J., Olaru, M., Anso, J., Little, S., Bogacz, R., Starr, P.A., Denison, T., Duchet, B., 2022. Sub-harmonic Entrainment of Cortical Gamma Oscillations to Deep Brain Stimulation in Parkinson{\textquoteright}s Disease: Predictions and Validation of a Patient-Specific Nonlinear Model. bioRxiv. https://doi.org/10.1101/2022.03.01.482549

Seymour, R.A., Rippon, G., Kessler, K., 2017. The Detection of Phase Amplitude Coupling during Sensory Processing. Front. Neurosci. 11, 487. https://doi.org/10.3389/fnins.2017.00487

Shah, A., Nguyen, T.-A.K., Peterman, K., Khawaldeh, S., Debove, I., Shah, S.A., Torrecillos, F., Tan, H., Pogosyan, A., Lachenmayer, M.L., Michelis, J., Brown, P., Pollo, C., Krack, P., Nowacki, A., Tinkhauser, G., 2022. Combining Multimodal Biomarkers to Guide Deep Brain Stimulation Programming in Parkinson Disease. Neuromodulation. https://doi.org/10.1016/j.neurom.2022.01.017

Shallop, J.K., Facer, G.W., Peterson, A., 1999. Neural response telemetry with the nucleus CI24M cochlear implant. Laryngoscope 109, 1755–1759. https://doi.org/10.1097/00005537-199911000-00006

Sharott, A., Gulberti, A., Hamel, W., Köppen, J.A., Münchau, A., Buhmann, C., Pötter-Nerger, M., Westphal, M., Gerloff, C., Moll, C.K.E., Engel, A.K., 2018. Spatio-temporal dynamics of cortical drive to human subthalamic nucleus neurons in Parkinson's disease. Neurobiol. Dis. 112, 49–62. https://doi.org/10.1016/j.nbd.2018.01.001

Sherer, T.B., Betarbet, R., Testa, C.M., Seo, B.B., Richardson, J.R., Kim, J.H., Miller, G.W., Yagi, T., Matsuno-Yagi, A., Greenamyre, J.T., 2003. Mechanism of toxicity in rotenone models of Parkinson's disease. J. Neurosci. 23, 10756–10764. https://doi.org/10.1523/JNEUROSCI.23-34-10756.2003

Shi, L.-H., Luo, F., Woodward, D.J., Chang, J.-Y., 2006. Basal ganglia neural responses during behaviorally effective deep brain stimulation of the subthalamic nucleus in rats performing a treadmill locomotion test. Synapse 59, 445–457. https://doi.org/10.1002/syn.20261

Shih, L.C., LaFaver, K., Lim, C., Papavassiliou, E., Tarsy, D., 2013. Loss of benefit in VIM thalamic deep brain stimulation (DBS) for essential tremor (ET): how prevalent is it? Parkinsonism

Relat. Disord. 19, 676–679. https://doi.org/10.1016/j.parkreldis.2013.03.006

Shimamoto, S.A., Ryapolova-Webb, E.S., Ostrem, J.L., Galifianakis, N.B., Miller, K.J., Starr, P.A., 2013. Subthalamic nucleus neurons are synchronized to primary motor cortex local field potentials in Parkinson's disease. J. Neurosci. 33, 7220–7233. https://doi.org/10.1523/JNEUROSCI.4676-12.2013

Shin, D.S., Samoilova, M., Cotic, M., Zhang, L., Brotchie, J.M., Carlen, P.L., 2007. High frequency stimulation or elevated K+ depresses neuronal activity in the rat entopeduncular nucleus. Neuroscience 149, 68–86. https://doi.org/10.1016/j.neuroscience.2007.06.055

Shivitz, N., Koop, M.M., Fahimi, J., Heit, G., Bronte-Stewart, H.M., 2006. Bilateral subthalamic nucleus deep brain stimulation improves certain aspects of postural control in Parkinson's disease, whereas medication does not. Mov. Disord. 21, 1088–1097. https://doi.org/10.1002/mds.20905

Shon, Y.-M., Lee, K.H., Goerss, S.J., Kim, I.Y., Kimble, C., Van Gompel, J.J., Bennet, K., Blaha, C.D., Chang, S.-Y., 2010. High frequency stimulation of the subthalamic nucleus evokes striatal dopamine release in a large animal model of human DBS neurosurgery. Neurosci. Lett. 475, 136–140. https://doi.org/10.1016/j.neulet.2010.03.060

Silberstein, P., Kühn, A.A., Kupsch, A., Trottenberg, T., Krauss, J.K., Wöhrle, J.C., Mazzone, P., Insola, A., Di Lazzaro, V., Oliviero, A., Aziz, T., Brown, P., 2003. Patterning of globus pallidus local field potentials differs between Parkinson's disease and dystonia. Brain 126, 2597–2608. https://doi.org/10.1093/brain/awg267

Sinclair, N.C., Fallon, J.B., Bulluss, K.J., Thevathasan, W., 2019a. On the neural basis of deep brain stimulation evoked resonant activity On the neural basis of deep brain stimulation evoked resonant activity.

Sinclair, N.C., McDermott, H.J., Bulluss, K.J., Fallon, J.B., Perera, T., Xu, S.S., Brown, P., Thevathasan, W., 2018a. Subthalamic nucleus deep brain stimulation evokes resonant neural activity. Ann. Neurol. 83, 1027–1031. https://doi.org/10.1002/ana.25234

Sinclair, N.C., McDermott, H.J., Bulluss, K.J., Fallon, J.B., Perera, T., Xu, S.S., Brown, P., Thevathasan, W., 2018b. Subthalamic nucleus deep brain stimulation evokes resonant neural activity. Ann. Neurol. 83, 1027–1031. https://doi.org/10.1002/ana.25234

Sinclair, N.C., McDermott, H.J., Fallon, J.B., Perera, T., Brown, P., Bulluss, K.J., Thevathasan, W., 2019b. Deep brain stimulation for Parkinson's disease modulates high-frequency evoked and spontaneous neural activity. Neurobiol. Dis. 130, 104522. https://doi.org/10.1016/j.nbd.2019.104522

Sinclair, N.C., McDermott, H.J., Lee, W.-L., Xu, S.S., Acevedo, N., Begg, A., Perera, T., Thevathasan, W., Bulluss, K.J., 2021. Electrically evoked and spontaneous neural activity in the subthalamic nucleus under general anesthesia. J. Neurosurg. 1–10. https://doi.org/10.3171/2021.8.JNS204225

Singleton, A.B., Farrer, M.J., Bonifati, V., 2013. The genetics of Parkinson's disease: progress and therapeutic implications. Mov. Disord. 28, 14–23. https://doi.org/10.1002/mds.25249

Sisterson, N.D., Carlson, A.A., Rutishauser, U., Mamelak, A.N., Flagg, M., Pouratian, N., Salimpour, Y., Anderson, W.S., Richardson, R.M., 2021. Electrocorticography During Deep Brain Stimulation Surgery: Safety Experience From 4 Centers Within the National Institute of Neurological Disorders and Stroke Research Opportunities in Human Consortium. Neurosurgery. https://doi.org/10.1093/neuros/nyaa592

Slater, K.D., Sinclair, N.C., Nelson, T.S., Blamey, P.J., McDermott, H.J., 2015. neuroBi: A Highly Configurable Neurostimulator for a Retinal Prosthesis and Other Applications. IEEE J. Transl. Eng. Heal. Med. 3, 3800111. https://doi.org/10.1109/JTEHM.2015.2455507

Smith, Y., Bevan, M.D., Shink, E., Bolam, J.P., 1998. Microcircuitry of the direct and indirect pathways of the basal ganglia. Neuroscience 86, 353–387. https://doi.org/10.1016/s0306-4522(98)00004-9

Smith, Y., Villalba, R.M., Raju, D. V, 2009. Striatal spine plasticity in Parkinson's disease: pathological or not? Parkinsonism Relat. Disord. 15 Suppl 3, S156-61. https://doi.org/10.1016/S1353-8020(09)70805-3

Spiegel, E.A., Wycis, H.T., Marks, M., Lee, A.J., 1947. Stereotaxic Apparatus for Operations on the Human Brain. Science 106, 349–350. https://doi.org/10.1126/science.106.2754.349

Stanslaski, S., Cong, P., Carlson, D., Santa, W., Jensen, R., Molnar, G., Marks, W.J.J., Shafquat, A., Denison, T., 2009. An implantable bi-directional brain-machine interface system for chronic neuroprosthesis research. Conf. Proc. ... Annu. Int. Conf. IEEE Eng. Med. Biol. Soc. IEEE Eng. Med. Biol. Soc. Annu. Conf. 2009, 5494–5497. https://doi.org/10.1109/IEMBS.2009.5334562

Starr, P.A., 2018. Totally Implantable Bidirectional Neural Prostheses: A Flexible Platform for Innovation in Neuromodulation. Front. Neurosci. 12, 619. https://doi.org/10.3389/fnins.2018.00619

Steeves, T.D., Day, L., Dykeman, J., Jette, N., Pringsheim, T., 2012. The prevalence of primary dystonia: a systematic review and meta-analysis. Mov. Disord. 27, 1789–1796. https://doi.org/10.1002/mds.25244

Steiner, L.A., Barreda Tomás, F.J., Planert, H., Alle, H., Vida, I., Geiger, J.R.P., 2019. Connectivity and Dynamics Underlying Synaptic Control of the Subthalamic Nucleus. J. Neurosci. 39, 2470–2481. https://doi.org/10.1523/JNEUROSCI.1642-18.2019

Steriade, M., 2000. Corticothalamic resonance, states of vigilance and mentation. Neuroscience 101, 243–276. https://doi.org/10.1016/s0306-4522(00)00353-5

Svenningsson, P., Westman, E., Ballard, C., Aarsland, D., 2012. Cognitive impairment in patients with Parkinson's disease: diagnosis, biomarkers, and treatment. Lancet. Neurol. 11, 697–707. https://doi.org/10.1016/S1474-4422(12)70152-7

Swann, N.C., de Hemptinne, C., Miocinovic, S., Qasim, S., Wang, S.S., Ziman, N., Ostrem, J.L., San Luciano, M., Galifianakis, N.B., Starr, P.A., 2016. Gamma Oscillations in the Hyperkinetic State Detected with Chronic Human Brain Recordings in Parkinson's Disease. J. Neurosci. 36, 6445–6458. https://doi.org/10.1523/JNEUROSCI.1128-16.2016

Swann, N.C., de Hemptinne, C., Thompson, M.C., Miocinovic, S., Miller, A.M., Gilron, R., Ostrem, J.L., Chizeck, H.J., Starr, P.A., 2018. Adaptive deep brain stimulation for Parkinson's disease using motor cortex sensing. J. Neural Eng. 15, 46006. https://doi.org/10.1088/1741-2552/aabc9b

Tan, H., Debarros, J., He, S., Pogosyan, A., Aziz, T.Z., Huang, Y., Wang, S., Timmermann, L., Visser-Vandewalle, V., Pedrosa, D.J., Green, A.L., Brown, P., 2019. Decoding voluntary movements and postural tremor based on thalamic LFPs as a basis for closed-loop stimulation for essential tremor. Brain Stimul. 12, 858–867. https://doi.org/10.1016/j.brs.2019.02.011

Tan, H., Pogosyan, A., Anzak, A., Ashkan, K., Bogdanovic, M., Green, A.L., Aziz, T., Foltynie, T., Limousin, P., Zrinzo, L., Brown, P., 2013. Complementary roles of different oscillatory activities in the subthalamic nucleus in coding motor effort in Parkinsonism. Exp. Neurol. 248, 187–195. https://doi.org/10.1016/j.expneurol.2013.06.010

Tan, M.M.X., Malek, N., Lawton, M.A., Hubbard, L., Pittman, A.M., Joseph, T., Hehir, J., Swallow, D.M.A., Grosset, K.A., Marrinan, S.L., Bajaj, N., Barker, R.A., Burn, D.J., Bresner, C., Foltynie, T., Hardy, J., Wood, N., Ben-Shlomo, Y., Grosset, D.G., Williams, N.M., Morris, H.R., 2019. Genetic analysis of Mendelian mutations in a large UK population-based Parkinson's disease study. Brain 142, 2828–2844. https://doi.org/10.1093/brain/awz191

Tandberg, E., Larsen, J.P., Karlsen, K., 1998. A community-based study of sleep disorders in patients with Parkinson's disease. Mov. Disord. 13, 895–899. https://doi.org/10.1002/mds.870130606

Tanner, C.M., 1992. Epidemiology of Parkinson's disease. Neurol. Clin. 10, 317–329.

Tarsy, D., 2009. Does subthalamotomy have a place in the treatment of Parkinson's disease? J. Neurol. Neurosurg. Psychiatry. https://doi.org/10.1136/jnnp.2008.163949

Tass, P.A., 2003. A model of desynchronizing deep brain stimulation with a demand-controlled coordinated reset of neural subpopulations. Biol. Cybern. https://doi.org/10.1007/s00422-003-0425-7

Temperli, P., Ghika, J., Villemure, J.-G., Burkhard, P.R., Bogousslavsky, J., Vingerhoets, F.J.G., 2003. How do parkinsonian signs return after discontinuation of subthalamic DBS? Neurology 60, 78–81. https://doi.org/10.1212/wnl.60.1.78

Ten Brinke, T.R., Odekerken, V.J.J., Dijk, J.M., van den Munckhof, P., Schuurman, P.R., de Bie, R.M.A., 2018. Directional Deep Brain Stimulation: First experiences in centers across the globe. Brain Stimul. https://doi.org/10.1016/j.brs.2018.04.008

Thenaisie, Y., Lee, K., Moerman, C., Scafa, S., Gálvez, A., Pirondini, E., Burri, M., Ravier, J., Puiatti, A., Accolla, E., Wicki, B., Zacharia, A., Castro Jiménez, M., Bally, J.F., Courtine, G., Bloch, J., Moraud, E.M., 2022. Principles of gait encoding in the subthalamic nucleus of people with

Parkinson's disease. Sci. Transl. Med. 14, eabo1800. https://doi.org/10.1126/scitranslmed.abo1800

Thevathasan, W., Sinclair, N.C., Bulluss, K.J., McDermott, H.J., 2020. Tailoring Subthalamic Nucleus Deep Brain Stimulation for Parkinson's Disease Using Evoked Resonant Neural Activity. Front. Hum. Neurosci. 14, 71. https://doi.org/10.3389/fnhum.2020.00071

Thompson, S.M., Gähwiler, B.H., 1989. Activity-dependent disinhibition. III. Desensitization and GABAB receptor-mediated presynaptic inhibition in the hippocampus in vitro. J. Neurophysiol. 61, 524–533. https://doi.org/10.1152/jn.1989.61.3.524

Timmermann, L., Schüpbach, M., Hertel, F., Wolf, E., Eleopra, R., Franzini, A., Servello, D., Skogseid, I.-M., Rumia, J., Aliaga, A.S., Barbe, M.T., Pauls, K.A.M., Lin, J.-P., Moro, E., Lloyd, A., Maarouf, M., 2013. A new rechargeable device for deep brain stimulation: a prospective patient satisfaction survey. Eur. Neurol. 69, 193–199. https://doi.org/10.1159/000342236

Tinkhauser, G., Pogosyan, A., Debove, I., Nowacki, A., Shah, S.A., Seidel, K., Tan, H., Brittain, J., Petermann, K., di Biase, L., Oertel, M., Pollo, C., Brown, P., Schuepbach, M., 2018. Directional local field potentials: A tool to optimize deep brain stimulation. Mov. Disord. 33, 159–164. https://doi.org/10.1002/mds.27215

Tinkhauser, G., Pogosyan, A., Little, S., Beudel, M., Herz, D.M., Tan, H., Brown, P., 2017a. The modulatory effect of adaptive deep brain stimulation on beta bursts in Parkinson ' s disease 1053–1067. https://doi.org/10.1093/brain/awx010

Tinkhauser, G., Pogosyan, A., Tan, H., Herz, D.M., Kuhn, A.A., Brown, P., 2017b. Beta burst dynamics in Parkinson's disease OFF and ON dopaminergic medication. Brain 140, 2968–2981. https://doi.org/10.1093/brain/awx252

Tinkhauser, G., Torrecillos, F., Pogosyan, A., Mostofi, A., Bange, M., Fischer, P., Tan, H., Hasegawa, H., Glaser, M., Muthuraman, M., Groppa, S., Ashkan, K., Pereira, E.A., Brown, P., 2020. The Cumulative Effect of Transient Synchrony States on Motor Performance in Parkinson's Disease. J. Neurosci. 40, 1571–1580. https://doi.org/10.1523/JNEUROSCI.1975-19.2019

Torrecillos, F., Tinkhauser, G., Fischer, P., Green, A.L., Aziz, T.Z., Foltynie, T., Limousin, P., Zrinzo, L., Ashkan, K., Brown, P., Tan, H., 2018. Modulation of Beta Bursts in the Subthalamic Nucleus Predicts Motor Performance. J. Neurosci. 38, 8905–8917. https://doi.org/10.1523/JNEUROSCI.1314-18.2018

Tort, A.B.L., Komorowski, R.W., Manns, J.R., Kopell, N.J., Eichenbaum, H., 2009. Theta-gamma coupling increases during the learning of item-context associations. Proc. Natl. Acad. Sci. U. S. A. 106, 20942–20947. https://doi.org/10.1073/pnas.0911331106

Trager, M.H., Koop, M.M., Velisar, A., Blumenfeld, Z., Nikolau, J.S., Quinn, E.J., Martin, T., Bronte-Stewart, H., 2016. Subthalamic beta oscillations are attenuated after withdrawal of chronic high frequency neurostimulation in Parkinson's disease. Neurobiol. Dis. 96, 22–30.

https://doi.org/10.1016/j.nbd.2016.08.003

Trakoshis, S., Martínez-Cañada, P., Rocchi, F., Canella, C., You, W., Chakrabarti, B., Ruigrok, A.N., Bullmore, E.T., Suckling, J., Markicevic, M., Zerbi, V., Baron-Cohen, S., Gozzi, A., Lai, M.-C., Panzeri, S., Lombardo, M. V, 2020. Intrinsic excitation-inhibition imbalance affects medial prefrontal cortex differently in autistic men versus women. Elife 9. https://doi.org/10.7554/eLife.55684

Trottenberg, T., Fogelson, N., Kühn, A.A., Kivi, A., Kupsch, A., Schneider, G.-H., Brown, P., 2006. Subthalamic gamma activity in patients with Parkinson's disease. Exp. Neurol. 200, 56–65. https://doi.org/10.1016/j.expneurol.2006.01.012

Trottenberg, T., Kupsch, A., Schneider, G.-H., Brown, P., Kühn, A.A., 2007. Frequency-dependent distribution of local field potential activity within the subthalamic nucleus in Parkinson's disease. Exp. Neurol. 205, 287–291. https://doi.org/10.1016/j.expneurol.2007.01.028

Troung, D.D., Rontal, M., Rolnick, M., Aronson, A.E., Mistura, K., 1991. Double-blind controlled study of botulinum toxin in adductor spasmodic dysphonia. Laryngoscope 101, 630–634. https://doi.org/10.1288/00005537-199106000-00010

Truong, D., Brodsky, M., Lew, M., Brashear, A., Jankovic, J., Molho, E., Orlova, O., Timerbaeva, S., 2010. Long-term efficacy and safety of botulinum toxin type A (Dysport) in cervical dystonia. Parkinsonism Relat. Disord. 16, 316–323. https://doi.org/10.1016/j.parkreldis.2010.03.002

Tsang, Eric W, Hamani, C., Moro, E., Mazzella, F., Lozano, A.M., Hodaie, M., Yeh, I.-J., Chen, R., 2012. Movement related potentials and oscillatory activities in the human internal globus pallidus during voluntary movements. J. Neurol. Neurosurg. Psychiatry 83, 91–97. https://doi.org/10.1136/jnnp.2011.243857

Tsang, E W, Hamani, C., Moro, E., Mazzella, F., Saha, U., Lozano, A.M., Hodaie, M., Chuang, R., Steeves, T., Lim, S.Y., Neagu, B., Chen, R., 2012. Subthalamic deep brain stimulation at individualized frequencies for Parkinson disease. Neurology 78, 1930–1938. https://doi.org/10.1212/WNL.0b013e318259e183

Urrestarazu, E., Iriarte, J., Alegre, M., Clavero, P., Rodriguez-Oroz, M.C., Guridi, J., Obeso, J.A., Artieda, J., 2009. Beta activity in the subthalamic nucleus during sleep in patients with Parkinson's disease. Mov. Disord. 24, 254–260. https://doi.org/10.1002/mds.22351

Vaillancourt, D.E., Prodoehl, J., Sturman, M.M., Bakay, R.A.E., Metman, L.V., Corcos, D.M., 2006. Effects of deep brain stimulation and medication on strength, bradykinesia, and electromyographic patterns of the ankle joint in Parkinson's disease. Mov. Disord. 21, 50–58. https://doi.org/10.1002/mds.20672

Van Camp, G., Flamez, A., Cosyns, B., Weytjens, C., Muyldermans, L., Van Zandijcke, M., De Sutter, J., Santens, P., Decoodt, P., Moerman, C., Schoors, D., 2004. Treatment of Parkinson's disease with pergolide and relation to restrictive valvular heart disease. Lancet (London, England) 363, 1179–1183. https://doi.org/10.1016/S0140-6736(04)15945-X

van Hilten, J.J., Weggeman, M., van der Velde, E.A., Kerkhof, G.A., van Dijk, J.G., Roos, R.A., 1993. Sleep, excessive daytime sleepiness and fatigue in Parkinson's disease. J. Neural Transm. Park. Dis. Dement. Sect. 5, 235–244. https://doi.org/10.1007/bf02257678

van Rheede, J.J., Feldmann, L.K., Busch, J.L., Fleming, J.E., Mathiopoulou, V., Denison, T., Sharott, A., Kühn, A.A., 2022. Diurnal modulation of subthalamic beta oscillatory power in Parkinson's disease patients during deep brain stimulation. NPJ Park. Dis. 8, 88. https://doi.org/10.1038/s41531-022-00350-7

van Wijk, B.C.M., Beudel, M., Jha, A., Oswal, A., Foltynie, T., Hariz, M.I., Limousin, P., Zrinzo, L., Aziz, T.Z., Green, A.L., Brown, P., Litvak, V., 2016. Subthalamic nucleus phase-amplitude coupling correlates with motor impairment in Parkinson's disease. Clin. Neurophysiol. Off. J. Int. Fed. Clin. Neurophysiol. 127, 2010–2019. https://doi.org/10.1016/j.clinph.2016.01.015

Vancea, R., Simonyan, K., Petracca, M., Brys, M., Di Rocco, A., Ghilardi, M.F., Inglese, M., 2019. Cognitive performance in mid-stage Parkinson's disease: functional connectivity under chronic antiparkinson treatment. Brain Imaging Behav. 13, 200–209. https://doi.org/10.1007/s11682-017-9765-0

Vayssiere, N., van der Gaag, N., Cif, L., Hemm, S., Verdier, R., Frerebeau, P., Coubes, P., 2004. Deep brain stimulation for dystonia confirming a somatotopic organization in the globus pallidus internus. J. Neurosurg. 101, 181–188. https://doi.org/10.3171/jns.2004.101.2.0181

Veerakumar, A., Tiruvadi, V., Howell, B., Waters, A.C., Crowell, A.L., Voytek, B., Riva-Posse, P., Denison, L., Rajendra, J.K., Edwards, J.A., Bijanki, K.R., Choi, K.S., Mayberg, H.S., 2019. Field potential 1/f activity in the subcallosal cingulate region as a candidate signal for monitoring deep brain stimulation for treatment-resistant depression. J. Neurophysiol. 122, 1023–1035. https://doi.org/10.1152/jn.00875.2018

Velisar, A., Syrkin-Nikolau, J., Blumenfeld, Z., Trager, M.H., Afzal, M.F., Prabhakar, V., Bronte-Stewart, H., 2019. Dual threshold neural closed loop deep brain stimulation in Parkinson disease patients. Brain Stimul. 12, 868–876. https://doi.org/10.1016/j.brs.2019.02.020

Vilensky, J.A., Gilman, S., 2002. Horsley was the first to use electrical stimulation of the human cerebral cortex intraoperatively. Surg. Neurol. 58, 425–426. https://doi.org/10.1016/s0090-3019(02)00920-5

Vitek, J.L., 2002a. Pathophysiology of dystonia: a neuronal model. Mov. Disord. 17 Suppl 3, S49-62. https://doi.org/10.1002/mds.10142

Vitek, J.L., 2002b. Mechanisms of Deep Brain Stimulation : Excitation or Inhibition 17, 3–6. https://doi.org/10.1002/mds.10144

Vitek, J.L., Bakay, R.A., Hashimoto, T., Kaneoke, Y., Mewes, K., Zhang, J.Y., Rye, D., Starr, P., Baron, M., Turner, R., DeLong, M.R., 1998. Microelectrode-guided pallidotomy: technical approach and its application in medically intractable Parkinson's disease. J. Neurosurg. 88, 1027–1043. https://doi.org/10.3171/jns.1998.88.6.1027

Vitek, J.L., Bakay, R.A.E., Freeman, A., Evatt, M., Green, J., McDonald, W., Haber, M., Barnhart, H., Wahlay, N., Triche, S., Mewes, K., Chockkan, V., Zhang, J.-Y., DeLong, M.R., 2003. Randomized trial of pallidotomy versus medical therapy for Parkinson's disease. Ann. Neurol. 53, 558–569. https://doi.org/10.1002/ana.10517

Vitek, J.L., Hashimoto, T., Peoples, J., DeLong, M.R., Bakay, R.A.E., 2004. Acute stimulation in the external segment of the globus pallidus improves parkinsonian motor signs. Mov. Disord. 19, 907–915. https://doi.org/10.1002/mds.20137

Voges, J., Waerzeggers, Y., Maarouf, M., Lehrke, R., Koulousakis, A., Lenartz, D., Sturm, V., 2006. Deep-brain stimulation: long-term analysis of complications caused by hardware and surgery--experiences from a single centre. J. Neurol. Neurosurg. Psychiatry 77, 868–872. https://doi.org/10.1136/jnnp.2005.081232

Volkmann, J., Wolters, A., Kupsch, A., Müller, J., Kühn, A.A., Schneider, G.-H., Poewe, W., Hering, S., Eisner, W., Müller, J.-U., Deuschl, G., Pinsker, M.O., Skogseid, I.-M., Roeste, G.K., Krause, M., Tronnier, V., Schnitzler, A., Voges, J., Nikkhah, G., Vesper, J., Classen, J., Naumann, M., Benecke, R., 2012. Pallidal deep brain stimulation in patients with primary generalised or segmental dystonia: 5-year follow-up of a randomised trial. Lancet. Neurol. 11, 1029–1038. https://doi.org/10.1016/S1474-4422(12)70257-0

Voytek, B., Kramer, M.A., Case, J., Lepage, K.Q., Tempesta, Z.R., Knight, R.T., Gazzaley, A., 2015. Age-Related Changes in 1/f Neural Electrophysiological Noise. J. Neurosci. 35, 13257–13265. https://doi.org/10.1523/JNEUROSCI.2332-14.2015

Wakabayashi, K., Tanji, K., Mori, F., Takahashi, H., 2007. The Lewy body in Parkinson's disease: molecules implicated in the formation and degradation of alpha-synuclein aggregates. Neuropathology 27, 494–506. https://doi.org/10.1111/j.1440-1789.2007.00803.x

Waldvogel, D., Baumann-Vogel, H., Stieglitz, L., Hänggi-Schickli, R., Baumann, C.R., 2020. Beware of deep water after subthalamic deep brain stimulation. Neurology 94, 39–41. https://doi.org/10.1212/WNL.0000000000008664

Walker, H.C., Huang, H., Gonzalez, C.L., Bryant, J.E., Killen, J., Cutter, G.R., Knowlton, R.C., Montgomery, E.B., Guthrie, B.L., Watts, R.L., 2012. Short latency activation of cortex during clinically effective subthalamic deep brain stimulation for Parkinson's disease. Mov. Disord. 27, 864–873. https://doi.org/10.1002/mds.25025

Wang, D.D., de Hemptinne, C., Miocinovic, S., Qasim, S.E., Miller, A.M., Ostrem, J.L., Galifianakis, N.B., San Luciano, M., Starr, P.A., 2016. Subthalamic local field potentials in Parkinson's disease and isolated dystonia: An evaluation of potential biomarkers. Neurobiol. Dis. 89, 213–222. https://doi.org/10.1016/j.nbd.2016.02.015

Wang, J., Hirschmann, J., Elben, S., Hartmann, C.J., Vesper, J., Wojtecki, L., Schnitzler, A., 2014. High-frequency oscillations in Parkinson's disease: spatial distribution and clinical relevance. Mov. Disord. 29, 1265–1272. https://doi.org/10.1002/mds.25962

Wang, S.-Y., Aziz, T.Z., Stein, J.F., Liu, X., 2005. Time-frequency analysis of transient neuromuscular events: dynamic changes in activity of the subthalamic nucleus and forearm muscles related to the intermittent resting tremor. J. Neurosci. Methods 145, 151–158. https://doi.org/10.1016/j.jneumeth.2004.12.009

Wang, S., Chen, Y., Ding, M., Feng, J., Stein, J.F., Aziz, T.Z., Liu, X., 2007. Revealing the dynamic causal interdependence between neural and muscular signals in Parkinsonian tremor 344, 180–195. https://doi.org/10.1016/j.jfranklin.2006.06.003

Waschke, L., Donoghue, T., Fiedler, L., Smith, S., Garrett, D.D., Voytek, B., Obleser, J., 2021. Modality-specific tracking of attention and sensory statistics in the human electrophysiological spectral exponent. Elife 10. https://doi.org/10.7554/eLife.70068

Weinberger, M., Hutchison, W.D., Alavi, M., Hodaie, M., Lozano, A.M., Moro, E., Dostrovsky, J.O., 2012. Oscillatory activity in the globus pallidus internus: comparison between Parkinson's disease and dystonia. Clin. Neurophysiol. Off. J. Int. Fed. Clin. Neurophysiol. 123, 358–368. https://doi.org/10.1016/j.clinph.2011.07.029

Weinberger, M., Hutchison, W.D., Lozano, A.M., Hodaie, M., Dostrovsky, J.O., 2009. Increased gamma oscillatory activity in the subthalamic nucleus during tremor in Parkinson's disease patients. J. Neurophysiol. 101, 789–802. https://doi.org/10.1152/jn.90837.2008

Weinberger, M., Mahant, N., Hutchison, W.D., Lozano, A.M., Moro, E., Hodaie, M., Lang, A.E., Dostrovsky, J.O., 2006. Beta oscillatory activity in the subthalamic nucleus and its relation to dopaminergic response in Parkinson's disease. J. Neurophysiol. 96, 3248–3256. https://doi.org/10.1152/jn.00697.2006

Welch, P., 1967. The use of fast Fourier transform for the estimation of power spectra: A method based on time averaging over short, modified periodograms. IEEE Trans. Audio Electroacoust. 15, 70–73. https://doi.org/10.1109/TAU.1967.1161901

Wessel, J.R., Jenkinson, N., Brittain, J.-S., Voets, S.H.E.M., Aziz, T.Z., Aron, A.R., 2016. Surprise disrupts cognition via a fronto-basal ganglia suppressive mechanism. Nat. Commun. 7, 11195. https://doi.org/10.1038/ncomms11195

Whitmer, D., de Solages, C., Hill, B., Yu, H., Henderson, J.M., Bronte-Stewart, H., 2012. High frequency deep brain stimulation attenuates subthalamic and cortical rhythms in Parkinson's disease. Front. Hum. Neurosci. 6, 155. https://doi.org/10.3389/fnhum.2012.00155

Wiest, C., He, S., Duchet, B., Pogosyan, A., Benjaber, M., Denison, T., Hasegawa, H., Ashkan, K., Baig, F., Bertaina, I., Morgante, F., Pereira, E.A., Torrecillos, F., Tan, H., 2023a. Evoked resonant neural activity in subthalamic local field potentials reflects basal ganglia network dynamics. Neurobiol. Dis. 106019. https://doi.org/https://doi.org/10.1016/j.nbd.2023.106019

Wiest, Christoph, Morgante, F., Torrecillos, F., Pogosyan, A., He, S., Baig, F., Bertaina, I., Hart, M.G., Edwards, M.J., Pereira, E.A., Tan, H., 2022a. Subthalamic Nucleus Stimulation-Induced Local Field Potential Changes in Dystonia. Mov. Disord. https://doi.org/10.1002/mds.29302

Wiest, C., Tinkhauser, G., Pogosyan, A., Bange, M., Muthuraman, M., Groppa, S., Baig, F., Mostofi, A., Pereira, E.A., Tan, H., Brown, P., Torrecillos, F., 2020. Local field potential activity dynamics in response to deep brain stimulation of the subthalamic nucleus in Parkinson's disease. Neurobiol. Dis. 143, 105019. https://doi.org/10.1016/j.nbd.2020.105019

Wiest, C., Tinkhauser, G., Pogosyan, A., He, S., Baig, F., Morgante, F., Mostofi, A., Pereira, E.A., Tan, H., Brown, P., Torrecillos, F., 2021. Subthalamic deep brain stimulation induces finely-tuned gamma oscillations in the absence of levodopa. Neurobiol. Dis. 152, 105287. https://doi.org/10.1016/j.nbd.2021.105287

Wiest, Christoph, Torrecillos, F., Pogosyan, A., Bange, M., Muthuraman, M., Groppa, S., Hulse, N., Hasegawa, H., Ashkan, K., Baig, F., Morgante, F., Pereira, E., Mallet, N., Magill, P., Brown, P., Sharott, A., Tan, H., 2022b. The aperiodic exponent of subthalamic field potentials reflects excitation/inhibition balance in Parkinsonism: a cross-species study in vivo. bioRxiv 2022.08.23.504923. https://doi.org/10.1101/2022.08.23.504923

Wiest, C., Torrecillos, F., Pogosyan, A., Bange, M., Muthuraman, M., Groppa, S., Hulse, N., Hasegawa, H., Ashkan, K., Baig, F., Morgante, F., Pereira, E.A., Mallet, N., Magill, P.J., Brown, P., Sharott, A., Tan, H., 2023b. The aperiodic exponent of subthalamic field potentials reflects excitation/inhibition balance in Parkinsonism. Elife 12, e82467. https://doi.org/10.7554/eLife.82467

Wiest, C, Torrecillos, F., Tinkhauser, G., Pogosyan, A., Morgante, F., Pereira, E.A., Tan, H., 2022. Finely-tuned gamma oscillations: Spectral characteristics and links to dyskinesia. Exp. Neurol. 351, 113999. https://doi.org/10.1016/j.expneurol.2022.113999

Williams, D., Tijssen, M., Van Bruggen, G., Bosch, A., Insola, A., Di Lazzaro, V., Mazzone, P., Oliviero, A., Quartarone, A., Speelman, H., Brown, P., 2002. Dopamine-dependent changes in the functional connectivity between basal ganglia and cerebral cortex in humans. Brain 125, 1558–1569. https://doi.org/10.1093/brain/awf156

Willis, A.W., Evanoff, B.A., Lian, M., Galarza, A., Wegrzyn, A., Schootman, M., Racette, B.A., 2010. Metal emissions and urban incident Parkinson disease: a community health study of Medicare beneficiaries by using geographic information systems. Am. J. Epidemiol. 172, 1357–1363. https://doi.org/10.1093/aje/kwq303

Wilson, C.J., Beverlin, B. 2nd, Netoff, T., 2011. Chaotic desynchronization as the therapeutic mechanism of deep brain stimulation. Front. Syst. Neurosci. 5, 50. https://doi.org/10.3389/fnsys.2011.00050

Windels, F., Bruet, N., Poupard, A., Urbain, N., Chouvet, G., Feuerstein, C., Savasta, M., 2000. Effects of high frequency stimulation of subthalamic nucleus on extracellular glutamate and GABA in substantia nigra and globus pallidus in the normal rat. Eur. J. Neurosci. 12, 4141–4146. https://doi.org/10.1046/j.1460-9568.2000.00296.x

Wolf, M.E., Capelle, H.H., Bäzner, H., Hennerici, M.G., Krauss, J.K., Blahak, C., 2016. Hypokinetic

gait changes induced by bilateral pallidal deep brain stimulation for segmental dystonia. Gait Posture 49, 358–363. https://doi.org/10.1016/j.gaitpost.2016.07.301

Xiong, H., Wang, D., Chen, L., Choo, Y.S., Ma, H., Tang, C., Xia, K., Jiang, W., Ronai, Z., Zhuang, X., Zhang, Z., 2009. Parkin, PINK1, and DJ-1 form a ubiquitin E3 ligase complex promoting unfolded protein degradation. J. Clin. Invest. 119, 650–660. https://doi.org/10.1172/JCI37617

Xu, S.S., Lee, W.-L., Perera, T., Sinclair, N.C., Bulluss, K.J., McDermott, H.J., Thevathasan, W., 2022. Can brain signals and anatomy refine contact choice for deep brain stimulation in Parkinson's disease? J. Neurol. Neurosurg. Psychiatry. https://doi.org/10.1136/jnnp-2021-327708

Yamamoto, T., Katayama, Y., Ushiba, J., Yoshino, H., Obuchi, T., Kobayashi, K., Oshima, H., Fukaya, C., 2013. On-demand control system for deep brain stimulation for treatment of intention tremor. Neuromodulation 16, 230–5; discussion 235. https://doi.org/10.1111/j.1525-1403.2012.00521.x

Ye, T., Bartlett, M.J., Sherman, S.J., Falk, T., Cowen, S.L., 2021. Spectral signatures of L-DOPA-induced dyskinesia depend on L-DOPA dose and are suppressed by ketamine. Exp. Neurol. 340, 113670. https://doi.org/10.1016/j.expneurol.2021.113670

Yelnik, J., Damier, P., Bejjani, B.P., Francois, C., Gervais, D., Dormont, D., Arnulf, I., M Bonnet, A., Cornu, P., Pidoux, B., Agid, Y., 2000. Functional mapping of the human globus pallidus: contrasting effect of stimulation in the internal and external pallidum in Parkinson's disease. Neuroscience 101, 77–87. https://doi.org/10.1016/s0306-4522(00)00364-x

Yelnik, J., Percheron, G., 1979. Subthalamic neurons in primates: a quantitative and comparative analysis. Neuroscience 4, 1717–1743. https://doi.org/10.1016/0306-4522(79)90030-7

Yoshida, F., Martinez-Torres, I., Pogosyan, A., Holl, E., Petersen, E., Chen, C.C., Foltynie, T., Limousin, P., Zrinzo, L.U., Hariz, M.I., Brown, P., 2010. Value of subthalamic nucleus local field potentials recordings in predicting stimulation parameters for deep brain stimulation in Parkinson's disease. J. Neurol. Neurosurg. Psychiatry 81, 885–889. https://doi.org/10.1136/jnnp.2009.190918

Zaidel, A., Spivak, A., Grieb, B., Bergman, H., Israel, Z., 2010. Subthalamic span of beta oscillations predicts deep brain stimulation efficacy for patients with Parkinson's disease. Brain 133, 2007–2021. https://doi.org/10.1093/brain/awq144

Zaidel, A., Spivak, A., Shpigelman, L., Bergman, H., Israel, Z., 2009. Delimiting subterritories of the human subthalamic nucleus by means of microelectrode recordings and a Hidden Markov Model. Mov. Disord. 24, 1785–1793. https://doi.org/10.1002/mds.22674

Zesiewicz, T.A., Elble, R., Louis, E.D., Hauser, R.A., Sullivan, K.L., Dewey, R.B.J., Ondo, W.G., Gronseth, G.S., Weiner, W.J., 2005. Practice parameter: therapies for essential tremor: report of the Quality Standards Subcommittee of the American Academy of Neurology. Neurology 64, 2008–2020. https://doi.org/10.1212/01.WNL.0000163769.28552.CD

Zetusky, W.J., Jankovic, J., Pirozzolo, F.J., 1985. The heterogeneity of Parkinson's disease: clinical and prognostic implications. Neurology 35, 522–526. https://doi.org/10.1212/wnl.35.4.522

Zhang, Z.X., Román, G.C., 1993. Worldwide occurrence of Parkinson's disease: an updated review. Neuroepidemiology 12, 195–208. https://doi.org/10.1159/000110318

Zucker, R.S., 1989. Short-term synaptic plasticity. Annu. Rev. Neurosci. 12, 13–31. https://doi.org/10.1146/annurev.ne.12.030189.000305

11. Supplementary Figures and Tables

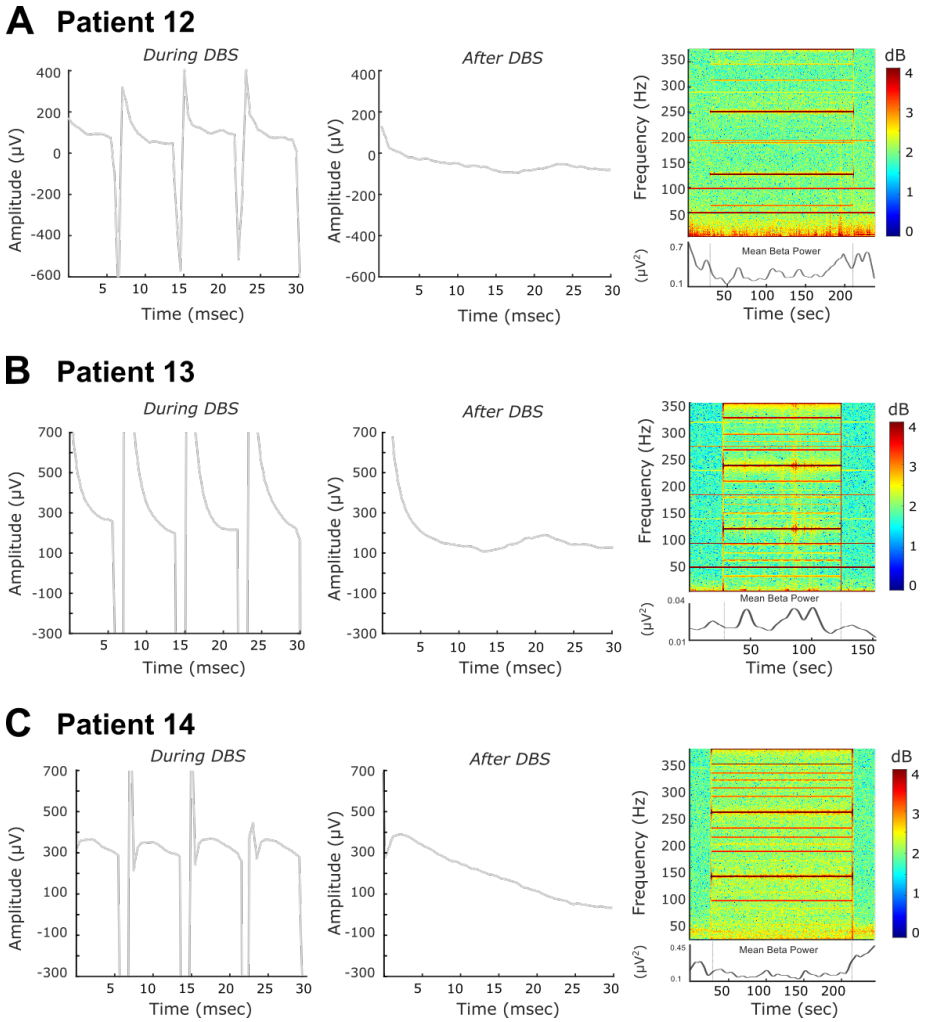


Figure 3.S1. STNs showing absence of an ERNA in response to 130 Hz stimulation in three cases. A-C; In these three patients, the time domain analysis revealed no evoked response between consecutive pulses during DBS (l*eft*), or after the last pulse of stimulation (*middle*). The absence of ERNA in the time domain is accompanied by an absence of ERNA in the spectral domain (*right*). Mean beta power is shown below respective DBS blocks. Vertical lines correspond to start and end of DBS.

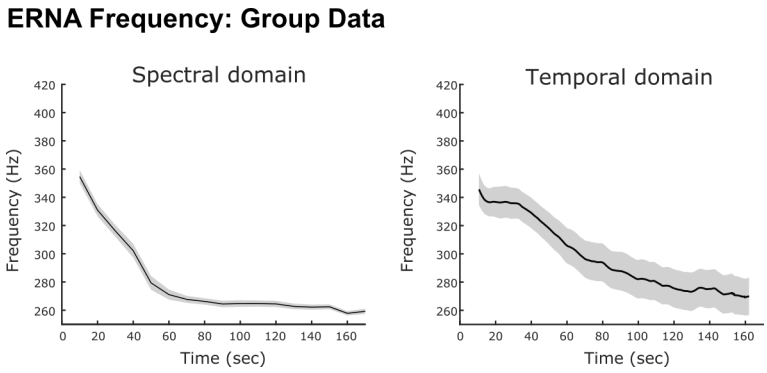


Figure 3.S2. Comparison of spectral and time domain analysis in group data. *Left:* Change in the ERNA frequency based on spectral analysis of consecutive 10s windows in each long duration stimulation block, averaged for each STN (similar to Figure 2Aiii), and then averaged across STNs. *Right:* Change in ERNA frequency based on temporal analysis. The frequency is computed as the inverse of the latency between the previous artefact and the first peak of the evoked response and repeated for the duration of the long stimulation blocks. Data were averaged across stimulation blocks and then STNs (mean ± SEM). Note that the frequency computed from the temporal analysis has greater variability, in part because of the relatively low sampling frequency (2048 Hz).

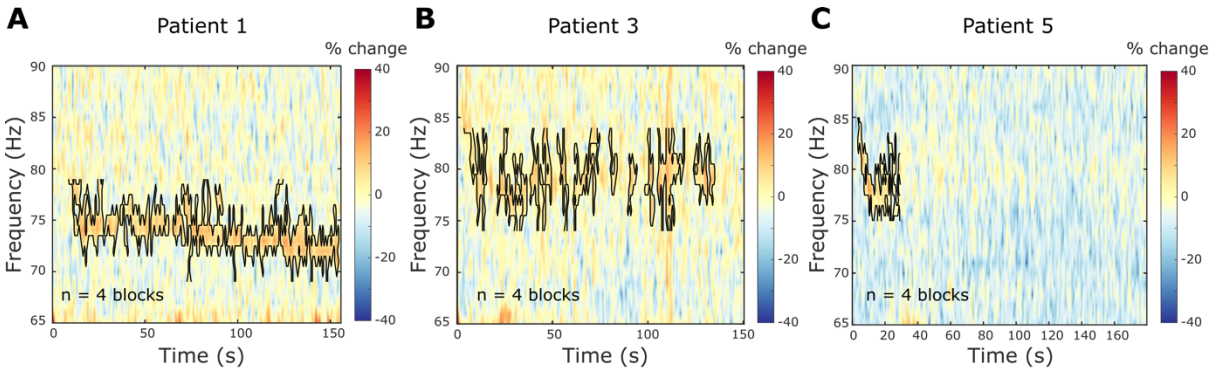


Figure 5.S1. Promotion of FTG during DBS is greater than the promotion of broadband gamma activity. Averaged percentage change of power estimates between 65 and 90 Hz during DBS blocks with respect to a 50-second baseline period prior to DBS start. 4 DBS blocks of slightly different durations were recorded in each patient. Power changes were averaged across blocks and spectrograms are shown for the duration of the shortest block. The FTG feature is surrounded by a black contour (see Methods).

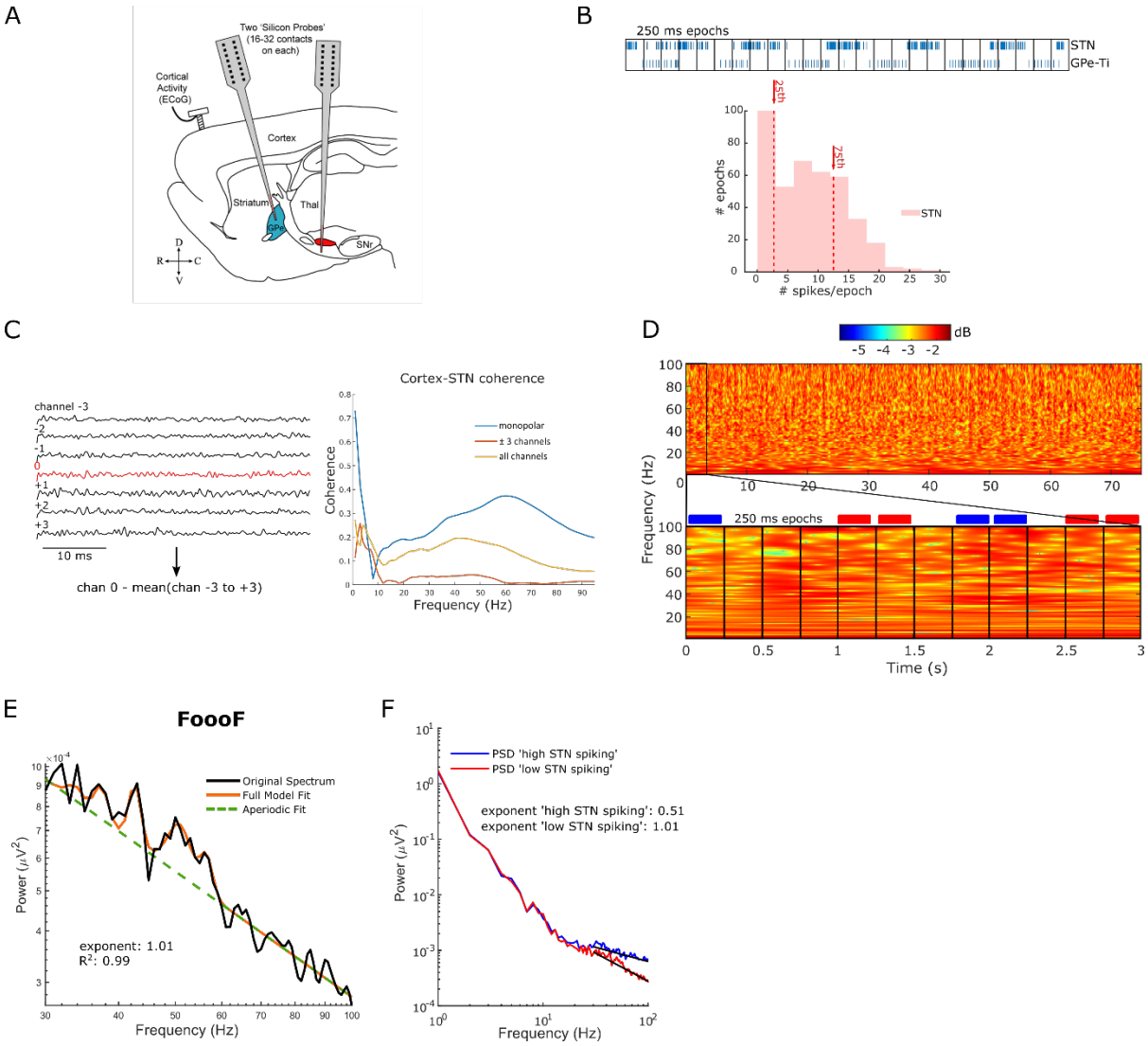


Figure 7.S1. Signal processing of the electrophysiological data recorded in animals. A. Parasagittal cross section of the rat brain. Multi-contact electrode arrays ('silicon probes') were used to record wideband signals (incorporating LFPs and single-unit activities) from the subthalamic nucleus (STN, in red) in eight 6-OHDA-lesioned rats during cortical slow-wave activity (SWA). GPe: external globus pallidus, SNr: substantia nigra pars reticulata, Thal: thalamus, ECoG: electrocorticogram, D: dorsal, V: ventral, R: rostral, C: caudal. **B.** Spikes were isolated from the wideband signal using standard spike sorting procedures as in Mallet et al., 2008[25]. *Top:* Spike events per 250-ms epoch were calculated for probe channels within STN (GPe-Ti spikes are shown for comparison). *Bottom:* The spike distribution is shown for an example STN channel. Epochs above the 75th percentile were considered high spiking. Epochs below the 25th percentile were considered low spiking. **C.** *Left:* LFP was re-referenced by subtracting the mean of the 6 neighbouring LFP channels. *Right:* This approach was chosen to control volume conduction since coherence between the re-referenced LFP channel and ECoG recorded from a steel screw over the frontal cortex (red) was lower compared to no re-referencing (blue) and subtracting the mean of all channels (yellow). **D.** Complex Morlet Wavelet Transforms (50 cycles) were used for time-frequency decomposition of the full LFP time series. Afterwards, average power spectral densities (PSDs) were computed for non-overlapping 250-ms epochs. PSDs of all high spiking epochs (blue boxes) and low spiking epochs (red boxes) were averaged. **E.** Periodic and aperiodic components of the PSD were separated using the FoooF parameterisation (see Methods). The original PSD of all low spiking epochs (black) is shown for one example LFP channel with the FoooF model fit (orange) and the aperiodic fit (dashed green). The aperiodic exponent and goodness of fit metric for this example are shown. **F.** Example analysis of the aperiodic exponent for one STN-LFP channel in one subject.

The blue and red lines show the average PSDs of ‘high STN spiking’ epochs and ‘low STN spiking’ epochs respectively. The black lines denote the aperiodic fit in the selected fitting range (30-100 Hz). Note the PSD is roughly linear across this frequency range in log-log space.

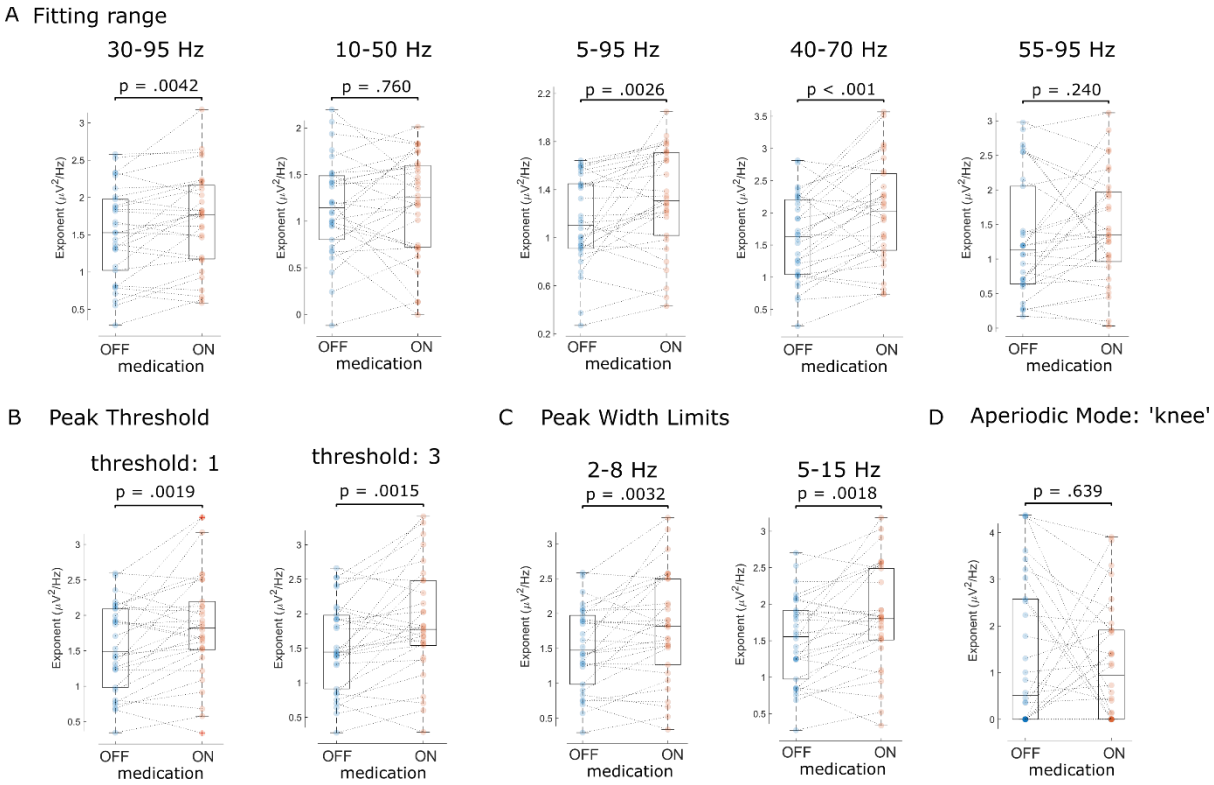


Figure 7.S2. Sensitivity analysis of FoooF parameterisation. We tested different fitting ranges (A), peak thresholds (B), peak width limits (C) and a different aperiodic mode (D) for FoooF parameterisation of patients LFPs in both medication states. Dots denote individual hemispheres.

.

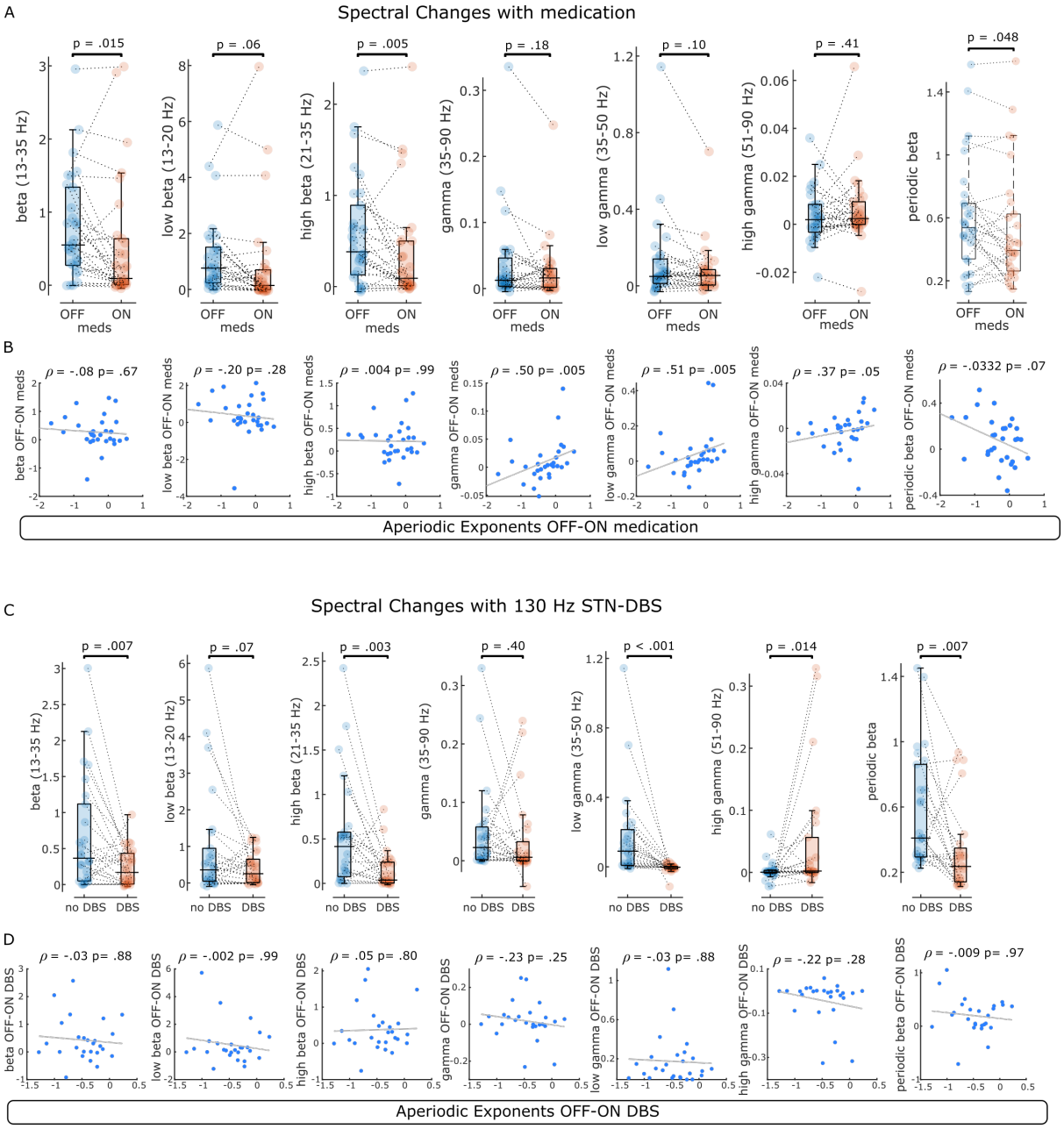


Figure 7.S3. Spectral changes with levodopa and STN-DBS. A. Average power of 6 different frequency bands and periodic beta power were compared between OFF and ON levodopa. Changes in beta power distinguished medication states. **B.** For the same frequency bands, changes between medication states were correlated with aperiodic exponent changes. Note that correlations with beta power were not significant, while there was a weak positive correlation between aperiodic exponents at 40-90 Hz and power changes in the gamma range. **C.** Average power of the same frequency bands and periodic beta power were compared before and during 130 Hz STN-DBS. Primarily high beta and low gamma power separated ON and OFF stimulation conditions. Note the power increase of the high gamma band ON DBS, which is driven by artefacts of stimulation in this frequency band. **D.** Spectral changes with DBS were not correlated with changes of the aperiodic exponent at 10-50 Hz.

.

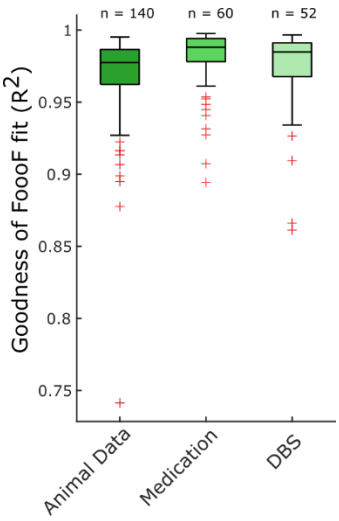


Figure 7.S4. Goodness of FoooF parameterisation. R^2 values are shown for all FoooF parameterisations used to analyse animal data in Figure 1 (n = 140; 70 LFP channels in both STN spiking states), human LFP data ON and OFF medication in Figure 2 (n = 60; 30 hemispheres in both conditions) and human LFP data ON and OFF DBS in Figure 3 (n = 52; 26 hemispheres in both conditions).

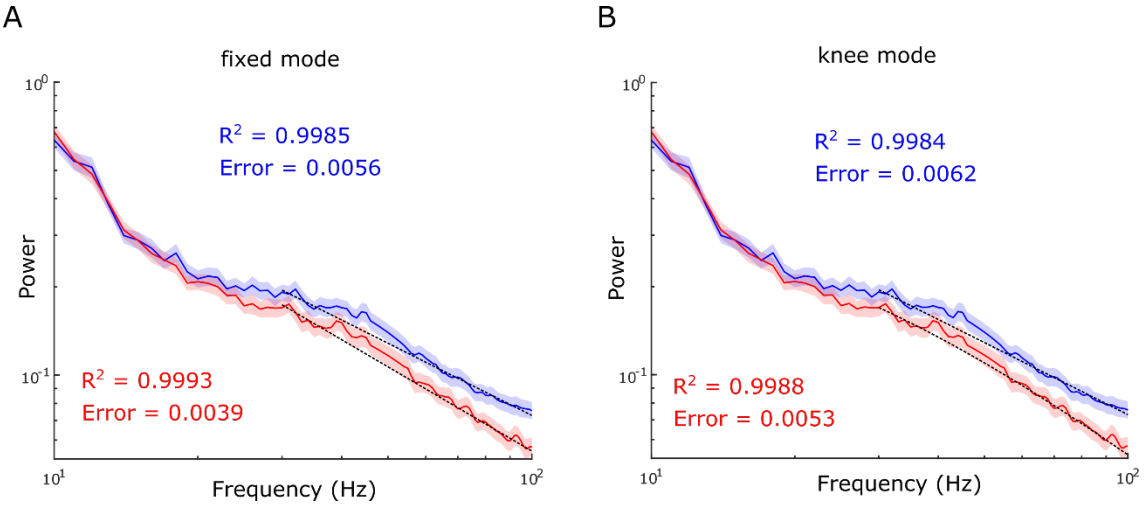


Figure 7.S5. Knee parameterisation of animal data. Power spectra from Figure 1C were parameterised using the fixed (A) and knee (B) mode. Goodness of fit and fitting errors are colour-coded. The dashed black line denotes the aperiodic fit from 30 to 100 Hz.

Study	Location	Disorder	Medication	Dyskinesia	Methods	Main Findings
Gilron et al., 2021	M1, STN	PD	ON	yes	Welch's method (250 ms window, 50% overlap)	an implanted, bidirectional neural interface was used to stream data over long periods of daily living, STN-M1 coherence in beta and gamma bands distinguished mobile and immobile states, sleep suppresses subthalamic beta and cortical gamma as well as STN-M1 coherence in both bands
Ozturk et al., 2020	STN	PD	ON	yes	FFT (1 s Hamming window, 50% overlap)	FTG power is strongest superior of STN (>10 mm above, likely thalamus)
de Hemptinne et al., 2019	M1	PD	OFF	no	Welch's method (~0.5 s Hann window, 50% overlap, 0.95 Hz resolution) and short-time FFT (~0.5 s window, ~90% overlap)	FTG appeared with effective thermolesion of the pallidum in 3 patients
Swann et al., 2018	M1	PD	ON	yes	method unclear	proof of principle study leveraging cortical FTG as a biomarker for dyskinesias in 2 patients
Miocinovic et al., 2018	M1	dystonia	n.a.	no	method unclear	cortical FTG during dystonic postures in 2 patients
Swann et al., 2016	M1, STN	PD	ON	yes	Welch's method (512 ms window, FFT length: 1024 points)	dyskinesia is associated with FTG in M1 and STN and coherence between the two, dyskinesia-related oscillations are minimally affected by voluntary movements, FTG is entrained at half stimulation frequency
Cagnan et al., 2014	STN	PD	ON	no	short-time FFT (1 s Hann window, 75% overlap)	FTG oscillations in the STN of both hemispheres are co-modulated
Lopez-Azcarate et al., 2010	STN	PD	ON	no	short-time FFT (~2 s Hann window, 75% overlap, ~0.5 Hz resolution)	levodopa induces STN-FTG in 3/13 patients
Kempf et al., 2009	ventral intermediate or centromedian nucleus of the thalamus	PD, ET, dystonia, myoclonic epilepsy	ON (if PD)	no	short-time FFT (0.5 s windows, 90% overlap 2 Hz resolution)	all patients presented an FTG peak which is modulated by movement and varied over the sleep-wake cycle, FTG is enhanced by statle-eliciting stimuli, sharply-tuned coherence at ~70 Hz between thalamus and GP
Alonso-Frech et al., 2006	STN	PD	ON	yes	short-time FFT (~1.28 s windows, 0% overlap)	low frequency power (4-10 Hz) may have a stronger link to levodopa-induced dyskinesias than FTG (60-80 Hz) power
Trottenberg et al., 2006	STN	PD	OFF	no	short-time FFT (~0.82 s windows)	gamma increase in 8/15 hemispheres 2 mm above the dorsal border of STN, gamma dropped 3 mm below the dorsal STN border, gamma LFP likely represents synchronous population activity in the upper STN/Zona incerta
Pogosyan et al., 2006	STN, Zona incerta	PD	OFF	no	short-time FFT	FTG activity has a major effect on neuron firing rate and information carrying capacity
Fogelson et al., 2005	STN	PD	ON	yes	short-time FFT (1 s Hann windows, 0% overlap, 1 Hz resolution)	negative correlation between low frequencies (5-32 Hz) and FTG (65-85 Hz) with contralateral levodopa-induced dyskinesias
Alegre et al., 2005	STN	PD	ON + OFF	no	Gabor transform	FTG power is modulated by movements, movement-related averages show an FTG amplitude and/or frequency increase at movement onset
Williams et al., 2002	STN, GPi, cortex	PD	ON	no	short-time FFT (1.28 s windows, 0.78 Hz resolution)	STN and GPi phase lead cortex in the 70-85 Hz band
Cassidy et al., 2002	STN, GPi	PD	ON	no	FFT	power within STN and STN-GPi coherence are dominated by FTG activity, coherence at FTG frequency increases with movement
Brown et al., 2001	STN, GPi	PD	ON	no	short-time FFT (1.024 s windows, 0% overlap 0.98 Hz resolution)	levodopa induces a fine gamma peak at ~70 Hz in STN, GPi and coherence between the two

Table 6.S1. Levodopa-induced FTG in humans. Studies presented in chronological order. M1: primary motor cortex; STN: subthalamic nucleus; GPi: internal segment of the globus pallidum; ET: essential tremor; PD: Parkinson's disease; ON: on dopaminergic medication; OFF: off dopaminergic medication; FFT: fast fourier transform.

Study	Location	Disorder	Medication	Methods	Main Findings
Güttler et al., 2021	M1	6-OHDA lesioned rats	levodopa	complex Morlet wavelet convolution (6 cycles)	levodopa-induced dyskinesias (LID) appear with a concomitant increase in cortical FTG activity
Ye et al., 2021	M1, striatum	6-OHDA lesioned rats	levodopa	short-time FFT (10s Hann window, 0.5 Hz resolution)	80 Hz oscillations are not exclusive for LID, sub-anaesthetic ketamine has anti-dyskinetic effects
Brys et al., 2018	RFA, M1, DMS, DLS, GP, thal, STN, SNr	6-OHDA lesioned rats	levodopa	Method unclear (8 s windows, 50% overlap, 0.12 Hz resolution, frequency range: 0-250 Hz)	dyskinetic symptoms are associated with 80 Hz oscillations and are suppressed by serotonin agonists
Dupre et al., 2016	M1	6-OHDA lesioned rats	levodopa	FFT (no further details)	cortical high-gamma (70-110 Hz) LFP activity is associated with the development of LID
Belic et al., 2016	M1, striatum	6-OHDA lesioned rats	levodopa	short-time FFT (no further details)	the dyskinetic state is related to increased coherence between M1 and striatum at ~80 Hz
Salvade et al., 2016	GP, frontal cortex	6-OHDA lesioned rats	levodopa	no details given	the development of LID was accompanied by a large gamma increase (60-80 Hz)
Delaville et al., 2015	STN, M1, mPFC	6-OHDA lesioned rats	levodopa, apomorphine	FFT (1 Hz resolution)	apomorphine and levodopa induce high-gamma activity in STN and cortex along with dyskinesias
Halje et al., 2012	M1, striatum	6-OHDA lesioned rats	levodopa	Welch's method (8 s Hann window, 50% overlap)	LID is strongly associated with 80 Hz LFP oscillations
Brown et al., 2002	STN	healthy rats	quinpirole	Method unclear (1 Hz resolution)	FTG is present in healthy rats at rest and increases with movement and dopaminergic medication

Table 6.S2. Levodopa-induced FTG in animal studies. Studies presented in chronological order. M1: primary motor cortex; GP: globus pallidum; STN: subthalamic nucleus; mPFC: medial prefrontal cortex; RFA: rostral forelimb area; DMS: dorsomedial striatum; DLS: dorsolateral striatum; thal: ventrolateral/ventroanterior nuclei of the thalamus; SNr: substantia nigra pars reticulate; FFT: fast fourier transform.

	Movement-related gamma ERS	DBS-induced FTG	Levodopa-induced FTG
duration (after MO or DBS stop in sec)	1.33 [1.27 - 1.39]	24.98 [7.67 - 53.96]	n.a.
amplitude (% change from baseline)	27.07 [25.51 - 28.64]	88.94 [44.78 - 198.41]	n.a.
frequency (Hz)	59.54 [58.67 - 60.42]	78.79 [74.90 - 82.71]	76.03 [68.15 - 84.55]
mean peak width (half-prominence in Hz)	7.89 [7.09 - 8.70]	4.09 [3.68 - 4.96]	5.41 [3.90 - 7.24]

Table 6.S3. Comparison of different gamma activities. Estimates for movement-related gamma ERS are based on the average of two PD patients performing a joystick task with 345 and 368 repetitions respectively. Estimates for DBS-induced FTG are based on 5 subjects with 3-6 stimulation blocks. If FTG was detected during and after stimulation (2 subjects), estimates of both instances were averaged. Estimates for levodopa-induced FTG are based on 6 PD patients performing a joystick task on dopaminergic medication. Different to movement-related gamma ERS, a narrowband FTG feature was present at rest. Spectrograms were divided into segments of 20-30 s and averaged to cancel out movement effects. Durations correspond to the extent of the contour in Figure 1. Amplitude, frequency and half-prominence width were computed based on the power spectrum of every time point using the

findpeaks function and averaged for every subject (see details in Methods). All values are presented as mean [range]. MO: movement onset; ERS: event-related synchronisation.

Study	Location	Disorder	Medication	Methods	Main Findings
Wiest et al., 2021	STN	PD	OFF	short-time FFT (1 s Hamming window, 25% overlap, 1 Hz resolution)	DBS induces FTG during and/or after stimulation without detectable dyskinesias, FTG is not entrained at half stimulation frequency
Muthuraman et al., 2020	M1, SMA, PMC, STN, cerebellum	PD	OFF	multitaper method (seven orthogonal tapers were used)	cross-frequency coupling of FTG power to the power of clinically effective DBS frequency

Table 6.S4. DBS-induced FTG in humans. Studies presented in chronological order. In both studies, DBS induces FTG off dopaminergic medication and without dyskinesias. M1: primary motor cortex; SMA: supplementary motor area; PMC: premotor cortex; STN: subthalamic nucleus; PD: Parkinson's disease, OFF: off dopaminergic medication; FFT: fast fourier spectrum.

Study	Location	Disorder	Medication	Methods	Main Findings
Lofredi et al., 2018	STN	PD	ON + OFF	complex Morlet wavelet convolution (7 cycles, from 1-100 Hz, 1 Hz resolution)	broad STN gamma positively correlates with maximal velocity and negatively with symptom severity, gamma bursts correlate with average power and increase with larger movements,
Fischer et al., 2017	STN	PD	ON	Filter Hilbert method (from 50-120 Hz, bandpass filtering the data in 10 Hz wide bands shifted by 2 Hz)	broad STN gamma increases when finger taps are successfully stopped
Brücke et al., 2013	ventral intermediate nucleus (thalamus)	ET	OFF	short-time FFT (~0.41 s Hann windows, ~25% overlap, 2.4 Hz resolution)	movement-related gamnma activity is lateralised to the contralateral thalamus, baseline gamma activity correlates with reaction times suggesting pre-cue gamma may relate to arousal
Tan et al., 2013a	STN	PD	ON	complex Morlet wavelet convolution	broad power increase in the gamma band (55-90 Hz), gamma power was further enhanced during grips with greater effort
Tan et al., 2013b	STN	PD	ON + OFF	complex Morlet wavelet convolution	broad gamma (55-375 Hz) was reduced concomitant with decreasing grip force
Brücke et al., 2012	GPi	dystonia	OFF	short-time FFT (0.512 s Hann windows, ~80% overlap, ~1.95 Hz resolution)	pallidal LFPs were recorded during a choice-reaction-time task, broad contralateral gamma band (35-105 Hz) ERS occurred at movement onset, the larger and faster the movement, the stronger the gamma ERS
Anzak et al., 2012	STN	PD	ON + OFF	method unclear	broad gamma activity (55-375 Hz) and grip force are correlated, broad gamma increases with activities encoding maximal effort grips but gamma increases only have a trivial contribution to reaction time shortening
Litvak et al., 2012	STN, M1	PD	ON + OFF	multitaper method (0.4 s windows, ~87.5% overlap, 5 Hz resolution, 3 tapers used for gamma)	broad gamma peaks (60-90 Hz) in M1, STN and coherence between the two, gamma power increased with movement and levodopa, STN gamma drives cortical gamma
Ray et al., 2012	STN	PD	ON	Hermite functions analysis (3 s windows aligned to movement onset, time-frequency area A/2 = 5, from 6-100 Hz, resolution: 10 ms x 0.33 Hz)	gamma oscillations (60-100 Hz) respond robustly to stop-signals as well as go-signals
Joundi et al., 2012	STN	PD	ON	Hermite functions analysis (time-frequency area A/2 = 5, resolution: 167 ms x 2.7 Hz)	gamma ERS is more pronounced during fast arm reaching movements
Anzak et al., 2011	STN	PD	ON	short-time FFT (1 s windows, 1 Hz resolution)	broad gamma increase (30-95 Hz) during verbal fluency tasks after controlling for motor output
Huo et al., 2011	M1	healthy children	OFF	complex Morlet wavelet convolution	broadband gamma increase (65-150 Hz) contralateral and ipsilateral to finger movements
Brücke et al., 2008	GPi	dystonia	OFF	short-time FFT (0.41 s Hann windows, ~25% overlap, 2.4 Hz resolution)	prominent, perimovement increase in 60-80 Hz activity contralateral to movement
Cheyne et al., 2008	M1	healthy adults	OFF	complex Morlet wavelet transform (7 cycles, from 2-110 Hz, 21 Hz resolution)	broad gamma oscillations (65-80 Hz) were localised to the contralateral M1 during self-paced movements, high gamma activity increased only during movement, gamma activity is task-dependent
Ball et al., 2008	M1, SMA (ECoG, EEG)	epilepsy, healthy adults	OFF	multitaper method (0.32 s window, ~87.5% overlap, 2 tapers)	broad gamma increase (60-90 Hz) over the sensorimotor cortex contralateral to the side of arm movement, gamma activity started at movement onset and became more pronounced at movement end
Androulidakis et al., 2007	STN	PD, ET	ON + OFF	short-time FFT (~1 s Hann windows, ~99% overlap, ~1 Hz resolution)	bilateral, symmetrical broad gamma band increase occurred around movement onset and was more pronounced on levodopa

Table 6.S5. Broad movement-related gamma ERS. These studies represent a non-systematic selection of relevant studies that are presented in chronological order. GPi: internal segment of the globus pallidum; STN: subthalamic nucleus; M1: primary motor cortex; SMA: supplementary motor area; ECoG: electrocorticography; EEG: electroencephalography; ET: essential tremor; PD: Parkinson's disease; OFF: off dopaminergic medication; ON: on dopaminergic medication; FFTL fast fourier transform; ERS: event-related synchronisation.

	Pros	Cons
Beta	excessive beta synchronisation is PD specific good evidence for the link between beta activity and bradykinesia and rigidity in PD beta-triggerd aDBS has been tested in several studies multiple slow and fast feedback algorithms available commercial device available that can perform beta-triggered aDBS	beta activity is not correlated with tremor or FOG beta activity is susceptible to movement artefacts not all patients have prominent beta peaks that are medication and stimulation responsive beta is a low-amplitude signal
ERNA	high-amplitude signal recordable during general anaesthesia from macroelectrodes also useful as a placement marker and potentially for selection of more DBS parameters varies with levodopa potential readout of the STN-GPe circuit	high sampling rate required for real-time feedback unclear clinical correlations not disease-specific unclear if modulated by movement
Aperiodic Exponent	potentially complementary to beta varies with levodopa (could be used to track medication states and adjust the beta threshold)	unfeasable for fast aDBS computational load for real-time analysis is unclear complicated by the spectral plateau during DBS
FTG	potentially localisable to a sweet spot in dorsolateral STN originally suggested as reflecting dyskinesia (link is increasingly contested)	unclear clinical correlations only present in a subset of patients can be induced by DBS without dyskinesias as well

Table 9.S1. Advantages and disadvantages of biomarkers for aDBS. FOG: freezing of gait, STN: subthalamic nucleus, GPe: external segment of the globus pallidum, PD: Parkinson's disease, aDBS: adaptive deep brain stimulation.

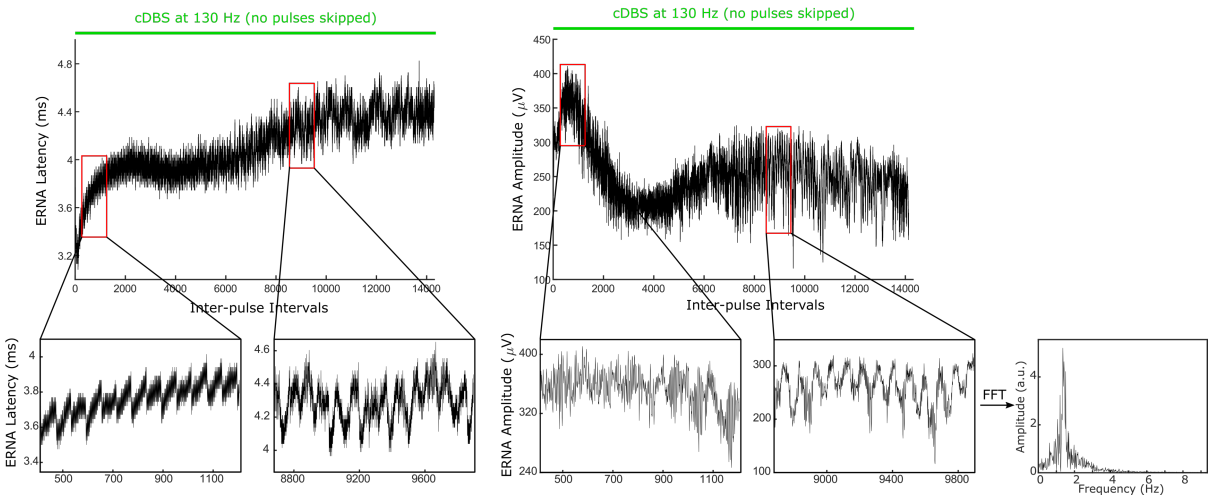


Figure 9.S1. ERNA fluctuations during steady state. Even without skipping pulses, ERNA parameters are fluctuating during steady state. ERNA amplitudes during steady state oscillate at ~ 1.5 Hz (data shown from 1 example hemisphere).

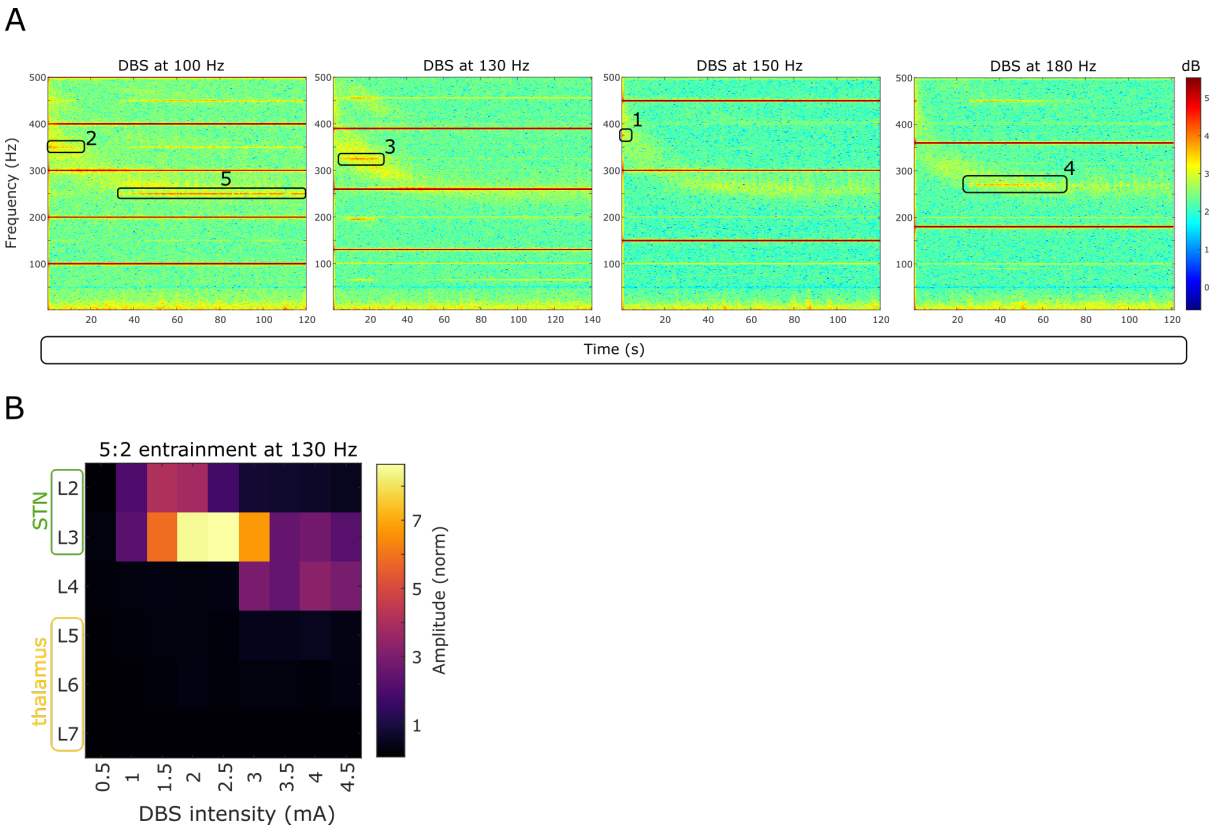


Figure 9.S2. ERNA is entrained when it crosses a harmonic of stimulation. A. The ERNA is entrained at harmonics of 100, 150 and 180 Hz DBS. (labels 1-5 show the sequence in which the ERNA passes through harmonics of respective DBS frequencies, data shown for one example hemisphere) **B.** 5:2 entrainment at 130 Hz DBS localises to STN and its amplitude decreases with increasing DBS intensity (data shown for one example hemisphere).